Cyclodextrins as the Basis of Molecular Devices

A thesis submitted for admission to the degree of

Doctor of Philosophy

by

Ryan Edward Dawson

Research School of Chemistry
Canberra, Australia

January 2007

Author's Statement

This is to declare that the work presented herein represents original work that I have carried out during my Ph.D candidature from February 2003 to January 2007. To the best of my knowledge, this thesis does not contain material that has been accepted for the award of any other degree or diploma in any university or other tertiary institution. Established results and methodologies published or written by another person are acknowledged by citation of the original work

I give consent for a copy of my thesis to be deposited in the University library and be available for loan and photocopying.

Ryan Dawson
January 2007

Acknowledgments

Firstly I would like to thank my supervisor Chris Easton for all his support, guidance and knowledge, all of which I could not have completed this thesis without. Furthermore, I would like to thank Chris for all of his proof reading of my writings, even when I am sure he could have thought of more interesting things he could be doing with his time. Also I would like to thank the members of the Easton group past and present who welcomed me with open arms from the moment I arrived in Canberra. Namely, thankyou to the following people and to any of those who I have missed; Adam Wright, Jamie Simpson, Amy Philbrook, Adam Mortimer, Zac Watts, Lorna Barr, Brendon Barratt, Satish Chand, Alex Buchan, Candace Tsai, Iris Li, Dave Brittain, Jim Hennessy, Roger Coulston, Subashani Maniam, Saara Bowen, Dharshana Padmakshan and Georgie Statham. The social atmosphere of the group has always been good and group weekends have been a highlight. Extra special mentions should go out to Hideki Onagi and Marta Cieslinksi for all their help in the field of cyclodextrins throughout my studies and to Tony Herlt who without his technical knowledge I do not know if I would be anywhere near this point today. I should also thank those who decided to hold the RSC Christmas party on the day I visited at the end of 2002. The party certainly gave me a good impression of the RSC in my first short visit. How did they know my propensity for beer and a BBQ?

While everyone at the Research School of Chemistry have made my time during my Ph.D enjoyable, I must also thank all those involved with the ANU volleyball teams past and present. I believe having an outside release from my work has been important in keeping my sanity at times. The guys and girls at the club have been great friends and team mates and I will remember those Unigames' as some the best times of my life. Also thankyou to the numerous friends I have made whilst living in Canberra. Without naming them individually they have made my stay in Canberra thoroughly enjoyable. Coming to Canberra proved to be one of the best decisions I could have made.

I guess I would not be here without the love and support of my family. My Mum and Dad have been there for me my entire life and are pillars of strength. They have always encouraged me to do what I wanted to do in life, but I bet at times they have wondered if I was ever going to finish school. Also to Jasmine, who is been a great sister and friend. Finally to Roanna. Over the past year or so you have seen the best and worse of me. You were always there to help me forget my troubles with your energy and your sense of fun. Above all thankyou for your love.

Abstract

The stilbene based CD [2]-rotaxanes **2.12** and **2.13** have been synthesised using trinitrophenyl blocking groups. Using 2D NMR spectroscopy it was determined that the [2]-rotaxanes **2.12** and **2.13** are orientational isomers. The [2]-rotaxanes **2.12** and **2.13** possess ditopic axles and have the potential to act as molecular shuttles upon isomerisation of the stilbene unit from the *trans* conformation to the *cis*-isomer.

Irradiation with UV light failed to isomerise the stilbene units of the [2]-rotaxanes **2.12** and **2.13**. It appears that the trinitrophenyl blocking groups disrupt the isomerisation pathway between the *trans* conformations and the *cis*-isomers. The addition of acid and base and consequent deprotonation and neutralisation of the secondary amines of the [2]-rotaxane **2.12** also failed to cause the CD to move along the axle. Thus the [2]-rotaxanes **2.12** and **2.13** failed to fulfil their roles as molecular shuttles.

Mesityl nitrile oxide (**4.3**) was used in attempts to form the [2]-rotaxanes **4.4** and **4.9** by cycloaddition with the acrylamides **4.2** and **4.7**. Instead cycloaddition of the acrylamide **4.2** with mesityl nitrile oxide (**4.3**) ~~and~~ only formed the 2-isoxazoline **4.5**. Treatment of the acrylamide **4.7** with mesityl nitrile oxide (**4.3**) also failed to give the hermaphroditic [2]-rotaxane **4.9**.

An hermaphroditic CD molecular switch was constructed that is powered through photochemical energy. The acetamide **5.5(E)** is converted to the *cis*-isomer **5.5(Z)** by irradiation with light of wavelength 350 nm. The reaction is reversible by irradiation of the *cis*-isomer **5.5(Z)** with light of wavelength 254 nm. The acetamides **5.5(E)** and **5.5(Z)** can act as molecular transports for the carriage of methyl orange (**5.8**) along an HPLC column. The *trans*-isomer **5.5(E)** was revealed to have a transport coefficient (*K*) of 2800 $dm^3\ mol^{-1}$, the *cis*-isomer **5.5(Z)** had a value of 30300 $dm^3\ mol^{-1}$ and αCD (**1.15**) a value of 7900 $dm^3\ mol^{-1}$. It was determined that the acetamide **5.5(E)** forms the dimeric inclusion complex **5.7** to hinder the transport of the dye **5.8** while the *cis*-isomer **5.5(Z)** allows the dye **5.8** to include facilitating its transport.

The [2]-rotaxanes **6.7**, **6.8** and **6.10** were synthesised using triazine blocking groups. The synthesis provides a means to produce a [2]-rotaxane with an alternative blocking group to the trinitrophenyl systems. The structures were assigned using 2D NMR spectroscopy.

The ditopic [2]-rotaxanes **7.1**, **7.2**, **7.6** and **7.7** were synthesised using the triazine blocking reagent **6.9**. Using 2D NMR spectroscopy, the [2]-rotaxanes **7.1** and **7.2** along with the [2]-rotaxanes **7.6** and **7.7** were determined to be pairs of orientational isomers with the CD situated on the stilbene unit of the axle. Each of the [2]-rotaxanes **7.1**, **7.2**, **7.6** and **7.7** was then determined to be a molecular shuttle. Irradiation with light of the wavelength 350 nm or 370 nm produced their *cis*-isomers. Irradiation with 254 nm light reformed the [2]-rotaxanes **7.1**, **7.2**, **7.6** and **7.7**. The [2]-rotaxanes **7.1(Z)** and **7.2(Z)** were able to be isolated and 2D NMR spectroscopy was used to determine that the isomerisation of the stilbene unit caused the CD to shuttle to a different part of the axle.

The hermaphroditic [2]-rotaxane **8.5(E,E)** was successfully synthesised using the triazine based blocking reagent **6.9**. The structural assignment of the hermaphroditic [2]-rotaxane **8.5(E,E)** was conducted using 2D NMR spectroscopy. Irradiation of the hermaphroditic [2]-rotaxane **8.5(E,E)** with light of wavelength 350 nm formed the *trans,cis*-isomer **8.5(E,Z)**. Irradiation for a longer period of time formed the *cis,cis*-isomer **8.5(Z,Z)**. The irradiation of the isomer mixture with 254 nm light reformed the hermaphroditic [2]-rotaxane **8.5(E,E)**. The system can therefore be considered a molecular muscle.

Glossary

aq	aqueous
anhyd	anhydrous
AU	absorbance units
AZO	azobenzene
BOC	*tert*-butoxycarbonyl
BOC-ON	2-(*tert*-butoxycarbonyloxyimino)-2-phenylacetonitrile
BOP	benzotriazol-1-yloxy-tris(dimethylamino)phosphonium hexafluorophosphate
br	broad
Bu_3N	tributylamine
°C	degrees Celcius
CD	cyclodextrin
CD-CX-Y	cyclodextrin carbon, X (carbon number) = 1-6, Y (glucopyranose unit) = A-F
CD-HX-Y	cyclodextrin proton, X (proton number) = 1-6, Y (glucopyranose unit) = A-F
CD-OHX	cyclodextrin hydroxyl proton, X (proton number) = 1-6
d	days
DCM	dichloromethane
DMF	*N*,*N*-dimethylformamide
DMSO	dimethyl sulfoxide
DMT-MM	4-(4,6-dimethoxy-1,3,5-triazin-2-yl)-4-methylmorpholinium chloride
DQCOSY	correlation spectroscopy
EDC	1-ethyl-3-(3'-dimethylaminopropyl)carbodiimide hydrochloride
EI	electron impact
eq	equivalent
en	1,2-diaminoethane
ESI	electrospray ionisation
et al.	*et alia*

EtOAc	ethyl acetate
EtOH	ethanol
g	gram
h	hour
HI-RES	high resolution
HMQC	heteronuclear multiple quantum correlation
HPLC	high performance liquid chromatography
hν	photon of light
Hz	hertz
I_2	iodine
i.d.	internal diameter
i-Pr_2NEt	*N,N*-diisopropylethylamine
J	coupling constant
K	molecular transport coefficient
K_a	association constant
lit.	literature
m	minute
M	moles per litre
$M^{+\cdot}$	molecular ion
MALDI	matrix-assisted laser desorption-ionisation
MeCN	acetonitrile
MeOH	methanol
MHz	megahertz
mm	millimetre
MQ	Milli-Q®
ms	millisecond
m/z	mass-to-charge ratio
nm	nanometre
NMP	*N*-methylpyrrolidinone
NMR	nuclear magnetic resonance
NOE	nuclear Overhauser effect

NOESY	nuclear Overhauser effect spectroscopy
OMe	methoxy
ppm	parts per million
$\bar{r}$	molar ratio
R_f	retention factor
ROESY	rotating-frame Overhauser effect spectroscopy
rt	room temperature
s	second
T	Tesla
TEA	triethylamine
tert	tertiary
TFA	trifluoroacetic acid
TfOH	trifluoromethanesulphonic acid
TLC	thin layer chromatography
TOCSY	total correlation spectroscopy
t_R	retention time
UV	ultraviolet
v	volume
w	weight
W	watts
1°	primary
2°	secondary
δ	chemical shift
ε	molar extinction coefficient
λ_{max}	wavelength absorption maximum
µl	microlitre
µm	micrometre

Contents

Chapter 1: Introduction

The association of molecules has been studied since the mid 1930s when the association of higher order entities was given the name "*Übermoleküle*", which literally means supermolecule.[1-3] Supramolecular chemistry was born out of the receptor concept conceived by Paul Ehlrich.[4,5] This concept stated that in the relationship of biological receptors for their substrates, the molecules would not act to perform their function unless bound.[4] Alfred Werner's coordination theory and Emil Fischer's lock and key image were also important in the development of the supramolecular chemistry concept.[5]

Molecular chemistry is a term that can be put to the mastering of rules associated with the properties of covalent bonds and their transformation.[4,6] In the same sense, supramolecular chemistry may be associated with the desire to master the rules governing intermolecular bonds.[5,6] Supramolecular chemistry has therefore been defined as "*chemistry beyond the molecule*" and is concerned with intermolecular interactions like electrostatic interactions, hydrogen bonding and van der Waals forces within a definite molecular structure.[4]

The field of supramolecular chemistry is now undergoing a change from structure towards the development of the function of assemblies.[7] This development is due to an awareness of the approaching impracticality of the scaling down of devices beyond a lower limit of 1 μm.[8] A "*bottom up*" approach manipulating systems at the molecular level to formulate devices is seen to be the bridge between these limits.[8] The molecular recognition of a substrate to its receptor with reactive functions forms a supermolecule that may act as a supramolecular reagent or catalyst.[4] Increasing the binding units creates more complex functions in what could be seen as molecular devices.[4] Research into this area has lead to new applications in the development of molecular electronics, artificial photosynthesis, construction of ion channels and the control of molecular motion.[7]

[2]-Rotaxanes **1.3** are considered ideal for the potential construction of molecular devices.[9] [2]-Rotaxanes **1.3** are a series of species consisting of a macrocycle threaded on an axle that has end groups that prevent the disassociation of the components.[9-11] The structure of a [2]-rotaxane **1.3** is shown on the right hand side of Figure 1.1 along with its components, the dumbbell **1.2** and macrocycle **1.1**, on the left. The name [2]-rotaxane

was suggested by Schill and Zollenkopf.[12] and is derived from the Latin terms, *rota* for wheel and *axis* for axle. Even before the first synthesis of a [2]-rotaxane, the possibility for its formation was pointed out in the discussion on chemical topology by Frisch and Wasserman[13] in 1961. Topology is concerned with interlocked structures that remain linked despite the distortion of bond lengths or angles.[13] In this paper, it was pointed out that [2]-rotaxanes could not be strictly classified as topological isomers.[13] Their existence is indebted to the "*...limited flexibility, extension and compression possible with molecular entities.*"[13] The expansion of the macrocycle of the [2]-rotaxane **1.3** would allow the disassociation of the molecule. A [2]-rotaxane, however, has much in common with topological isomers as their synthesis requires the specific arrangement of their components.[10]

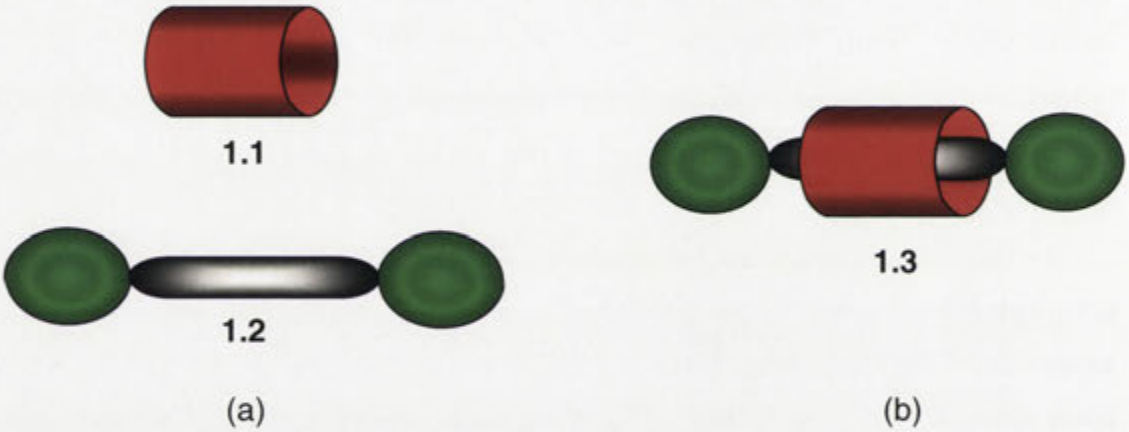

Figure 1.1. (a) The components of a [2]-rotaxane, and (b) a [2]-rotaxane **1.3**.

It is accepted that the construction of a [2]-rotaxane can proceed via the three different methods of "*clipping*", "*threading*" and "*slippage*".[8,14-16] These are illustrated in Scheme 1.1. The "*clipping*" method requires the open ended macrocycle **1.4** to enclose a dumbbell **1.2**. The clipping of the open ended macrocycle **1.4** then affords the [2]-rotaxane **1.3**. The "*threading*" method firstly involves the encapsulation of an axle **1.6** by a macrocycle **1.1**. The addition of large blocking groups **1.8** to the ends of the encapsulated axle **1.7** gives rise to the [2]-rotaxane **1.3**. The final method is the "*slippage*" method and involves the slipping of a macrocycle **1.1** over a blocking group of a dumbbell **1.2** using an external energy source to form a [2]-rotaxane **1.3**.

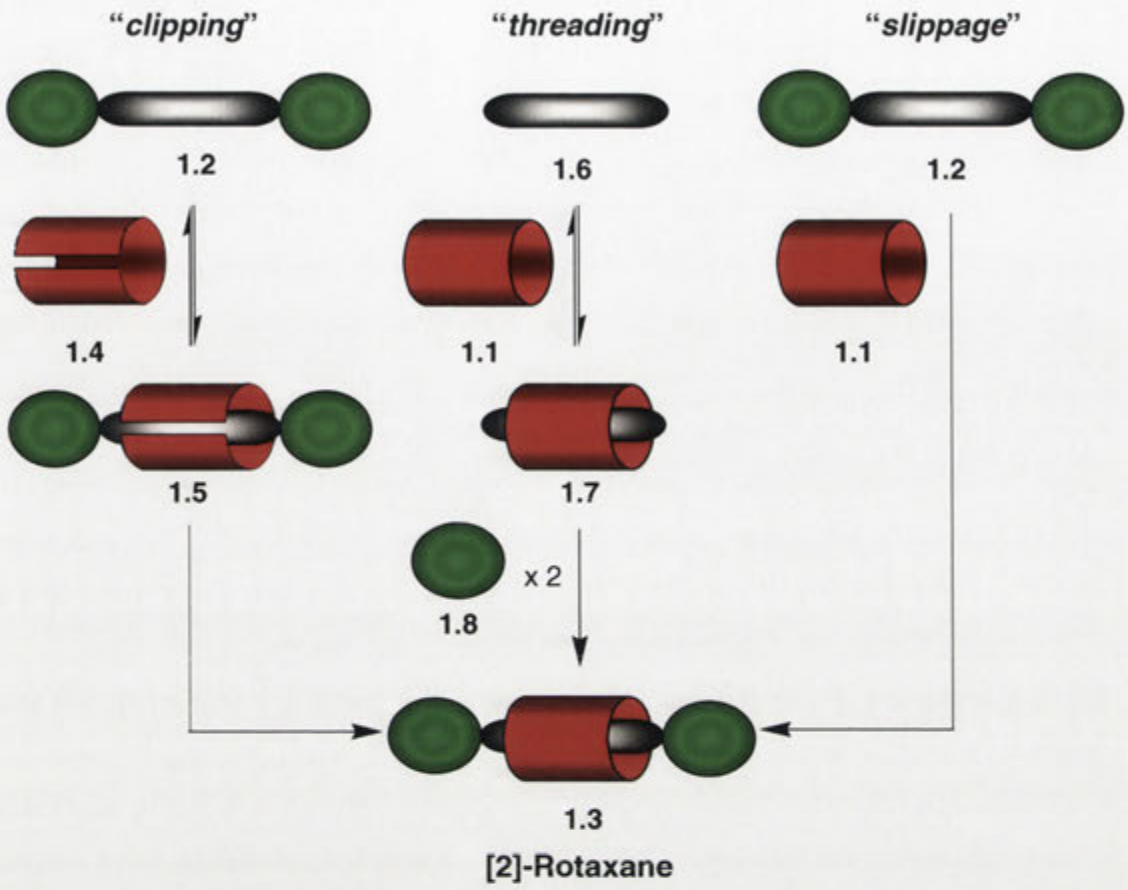

Scheme 1.1. Strategies for the synthesis of [2]-rotaxanes: "*clipping*", "*threading*" and "*slippage*".

The formation of the first [2]-rotaxane was reported by Harrison and Harrison,[17] in 1967. Using a statistical approach, a resin bound alkyl macrocycle was treated with the axle decane-1,10-diol and the blocking group triphenylmethyl chloride. The treatment was repeated 70 times after which a [2]-rotaxane was hydrolysed from the resin in 6% yield.[17] To improve the yield of the formation of a [2]-rotaxane it was suggested that the components had to be "*...positioned to each other in some way.*"[10] Schill and Zollenkopf[12] used a directed synthesis to position the building blocks for the formation of a [2]-rotaxane. Covalent bonds were used to bind a macrocycle to a dumbbell which improved the yield of the [2]-rotaxane forming reaction to 81%.[12] The synthesis, however, was long and required 15 steps for the preparation and cleavage of the ring to produce the final product.[12] A non-covalently bound method therefore seemed necessary to template the formation of a [2]-rotaxane in high yields.[10]

Macrocycles, depending on the make-up of the ring structure are able to bind a wide variety of molecules using non-covalent bonds. Sauvage *et al.*,[18-21] used the co-ordination of copper(I) with specifically designed terpyridine macrocyclic ligands to produce [2]-rotaxanes with yields of up to 59%.[20] Electrostatic interactions like π-stacking between electron rich and electron poor groups have been used by Stoddart and co-workers[22-26] to form [2]-rotaxanes. A variety of [2]-rotaxanes were able to be formed using the templating interaction between π-acceptor cyclophanes and π-donating tetrathiafulvalene or various aromatic ethers.[22-26] Leigh *et al.*[27-33] has in the past used hydrogen bonding interactions to form various [2]-rotaxanes by a clipping method. The templation of an aromatic diacid chloride and benzylic diamines with dipeptide dumbells followed by their condensation formed [2]-rotaxanes in up to 97% yield.[28] Cyclodextrins (CDs) have also been used to template the synthesis of [2]-rotaxanes. The process for the formation of CD [2]-rotaxanes is commented on later in this chapter.

Macrocycles that are functionalised with directly attached binding groups are able to form another set of [2]-rotaxanes. These macrocycles are also known as hermaphrodites **1.9** as they possess both a host and guest component.[34] The products able to be synthesised upon capping the hermaphrodite **1.9** with a suitable blocking reagent **1.8** are summarised in Scheme 1.2. If the linker between the binding group and the macrocycle is flexible, a cyclic [1]-rotaxane **1.10** may result from the capping.[35,36] Depending on the size and geometry of the binding group acyclic [n]-rotaxanes **1.11** can form. These molecules can also be viewed as supramolecular daisy chains.[37] It is also possible for a daisy chain to "*...bite its own tail...*"[37] to form cyclic [n]-rotaxanes **1.12**.[38] The cyclic [2]-rotaxane where n = 1 has been synthesised and is also known as an hermaphroditic [2]-rotaxane.[39]

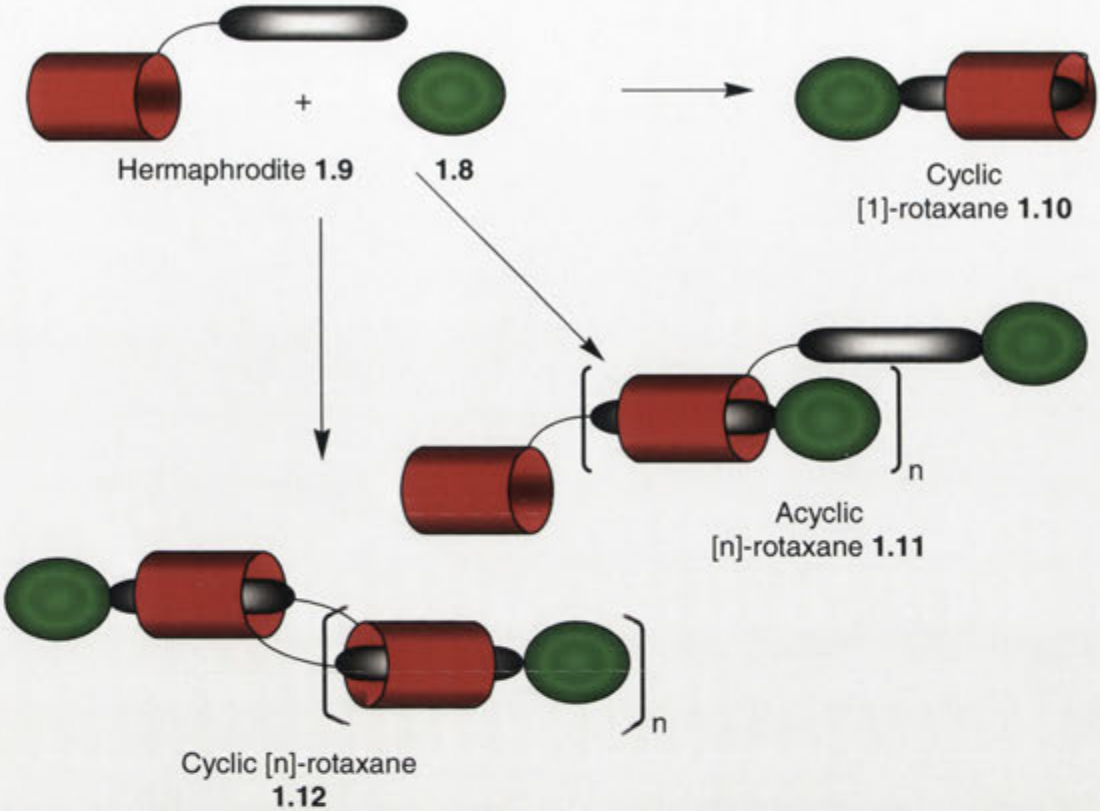

Scheme 1.2. Strategies for the synthesis of a cyclic [1]-rotaxane **1.10**, an acyclic [n]-rotaxane **1.11** and a cyclic [n]-rotaxane **1.12**.

An example of an hermaphroditic [2]-rotaxane, synthesised by Sauvage *et al.*,[40] is shown in Scheme 1.3. The [2]-rotaxane **1.13** was synthesised using copper(I) co-ordination of the terpyridine macrocyclic ligands of two hermaphrodites. As mentioned above, [2]-rotaxanes are considered ideal for the potential construction of molecular devices.[9] A molecular device is a chemical structure that upon the appropriate stimuli performs a mechanical movement.[41] The hermaphroditic [2]-rotaxane synthesised by Sauvage *et al.*,[40] can also be considered a molecular device. The removal of the copper(I) ions followed by the addition of zinc(II) causes complexation between a terpyridine and a phenanthroline unit to form the [2]-rotaxane **1.14**. This causes the length of the molecule to contract. Addition of copper(I) ions displaces the zinc(II) ions to reform the [2]-rotaxane **1.13**. By analogy, the contraction and expansion of the [2]-rotaxane **1.13** can be viewed as a molecular muscle. This process is a mimic of what occurs in the sarcomere where the myosin containing thick filament moves forwards and backwards along the actin polymer to induce contraction or relaxation of a muscle fibre.[42]

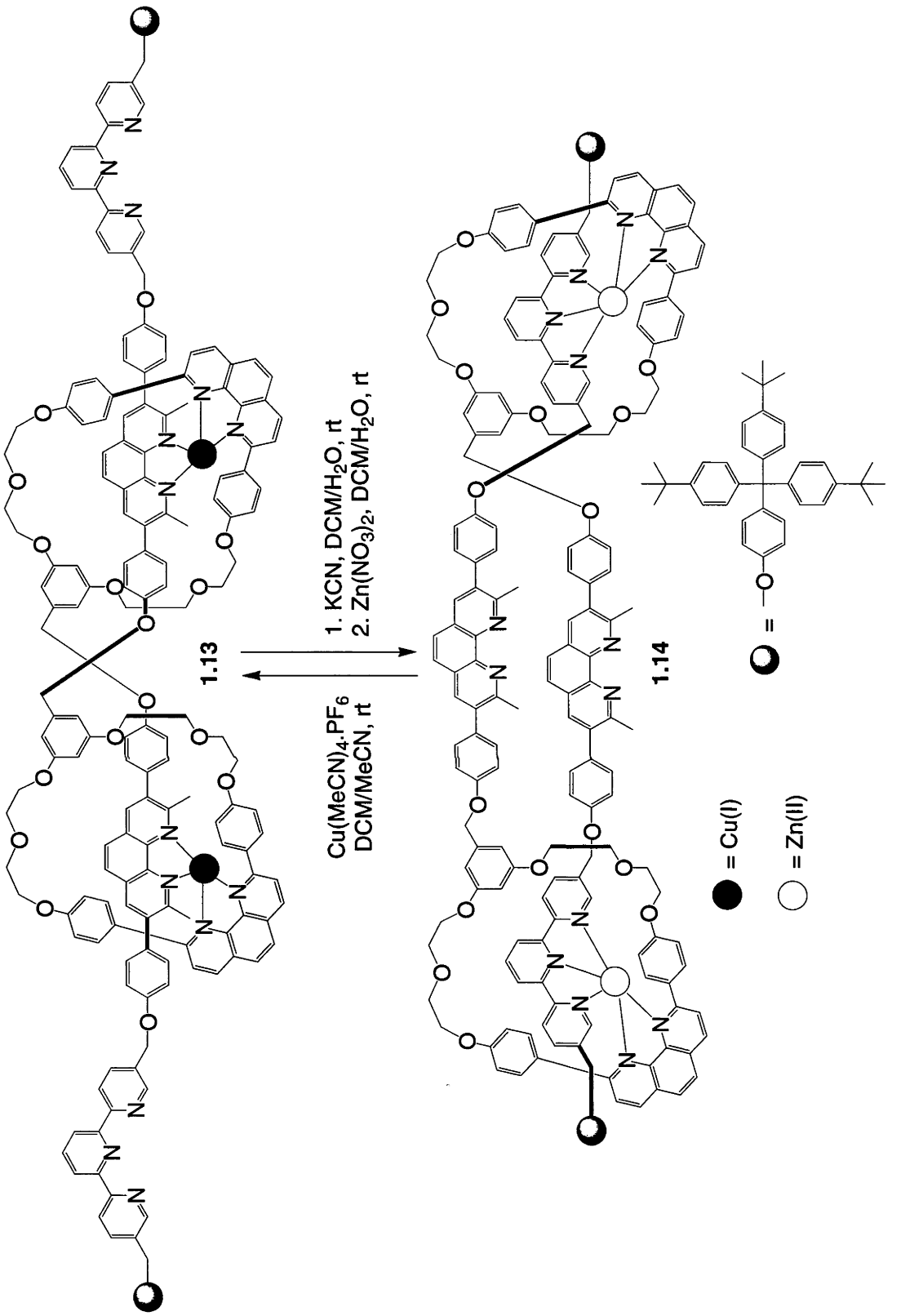

Scheme 1.3. A molecular muscle synthesised by Sauvage *et al.*[40]

In this project CDs were used as the macrocycles to construct similar molecular devices as that synthesised by Sauvage *et al.*[40] CDs, as they are known today, were discovered in the late nineteenth century by Villiers[43] through the digestion of starch with *Bacillus amylobacter.* It was not until 1936, however, that the structure of the CDs was postulated by Fruendenburg[44] and co-workers to be cyclic, comprising of α-1,4-glycosidic linkages. Extensive X-ray crystallography has since been conducted on the CDs to determine their precise structures.[45-47]

The structure and atom numbering of a CD can be represented as shown in Figure 1.2.[48,49] CDs are comprised of multiple α-1,4-glucopyranose units with the most commonly occurring αCD (**1.15**), βCD (**1.16**) and γCD (**1.17**) made up of 6, 7 and 8 units respectively. One face of the CD is slightly larger than the other which is why the structure is often represented as a truncated cone as shown on the right in Figure 1.2. Each of the glucopyranose units is aligned in a $^4C_1$ chair configuration which structures the CD so that each of the primary hydroxyls lines the smaller face while the secondary hydroxy groups line the larger face of the CD. The peripheral hydroxy groups render the CD soluble in water. The CD-H3, CD-H5 and CD-H6 hydrophobic protons line the cavity of the CD giving the annulus a hydrophobic nature.[48,49]

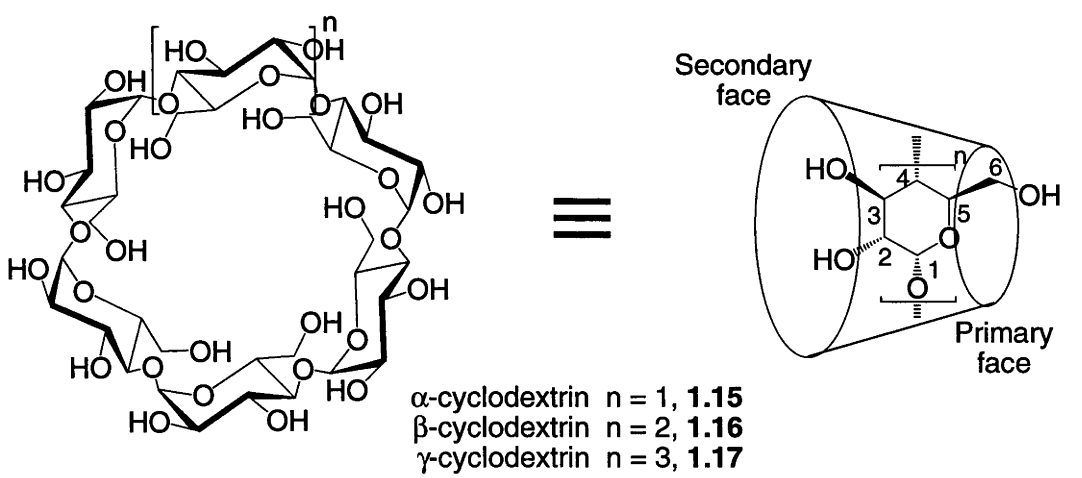

Figure 1.2. Illustration of a cyclodextrin (left) and its schematic representation as a truncated cone (right).

Even before the exact structure of the CDs had been resolved, the properties of CDs were studied which showed their ability to complex many organic compounds.[50,51]

The ability of CDs to complex organic molecules rests with the unique attributes of their structure. The hydrophobic nature of the annulus favours the inclusion of non-polar guest molecules in an aqueous solution. The complexation is favoured by the removal of non-polar guest molecules from a polar aqueous solution and the expulsion from the non-polar cavity of polar water molecules.[49,52]

The modification of natural CDs is also possible and allows the shape, size and other physical properties of CDs to be altered.[49] This modification has been performed for a variety of reasons which include improving their solubility or for the catalysis of reactions.[53] Modifications of CDs at their primary (CD-OH6) and secondary (CD-OH2 and CD-OH3) hydroxy groups are the most straightforward. The CD-OH6 groups are the most nucleophilic of the hydroxy groups and are able to be selectively modified with electrophilic species like *p*-toluenesulfonyl chloride (**1.18**).[49] The synthesis of the sulfonate **1.19**, shown in Scheme 1.4, has been extensively studied and provides a platform for further modification by nucleophilic substitution.[54-57] In Scheme 1.4, the synthetic procedure to form the amine **1.21** via the azide **1.20** is shown.[54,55,57]

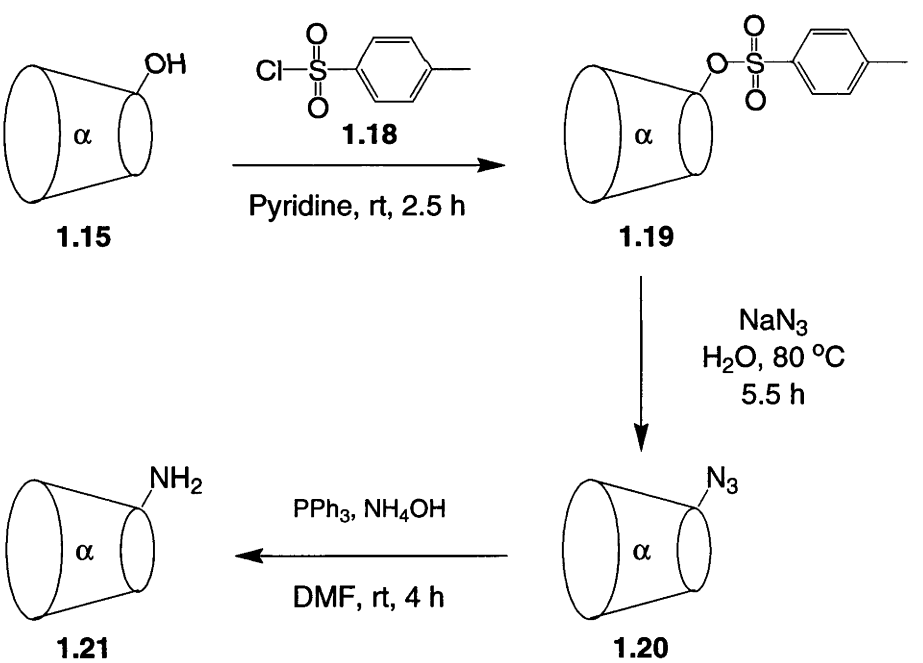

Scheme 1.4. Formation of the amine **1.21** according to the experimental conditions of Onagi.[57]

The complexation of guest molecules by CDs has been used in the formation of many [2]-rotaxanes. Of the three conceivable methods for the formation of a [2]-rotaxane described above, only the "*threading*" method has been utilised for the formation of CD [2]-rotaxanes. The "*clipping*" method is not realistic in the formation of a [2]-rotaxane of this type as this would negate the driving force of a CD's ability to form complexes.[16] An example of the utilisation of the slippage method with CDs was reported by Macartney[58] and is illustrated in Figure 1.3. The size of the *tert*-butylpyridinium groups is similar to the cavity of αCD (**1.15**). The rate constant for the inclusion is faster than the rate constant for the disassociation which extends the lifetime of the included species **1.22**. However, the included species **1.22** could not be considered a [2]-rotaxane as the *tert*-butylpyridinium groups do not prevent the disassociation of the CD.[58] Such included species are called [2]-pseudorotaxanes as they are not mechanically interlocked.[59]

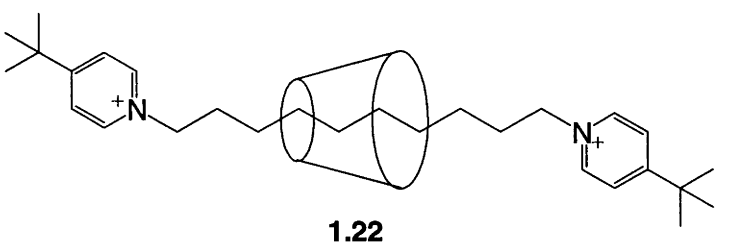

1.22

Figure 1.3. A cyclodextrin [2]-pseudorotaxane **1.22** reported by Macartney.[58]

The first record of the formation of a CD [2]-rotaxane using the "*threading*" method was reported by Ogino.[60,61] Transition metal complexes were used as blocking groups to form the [2]-rotaxanes **1.26** and **1.27** as shown in Scheme 1.5.

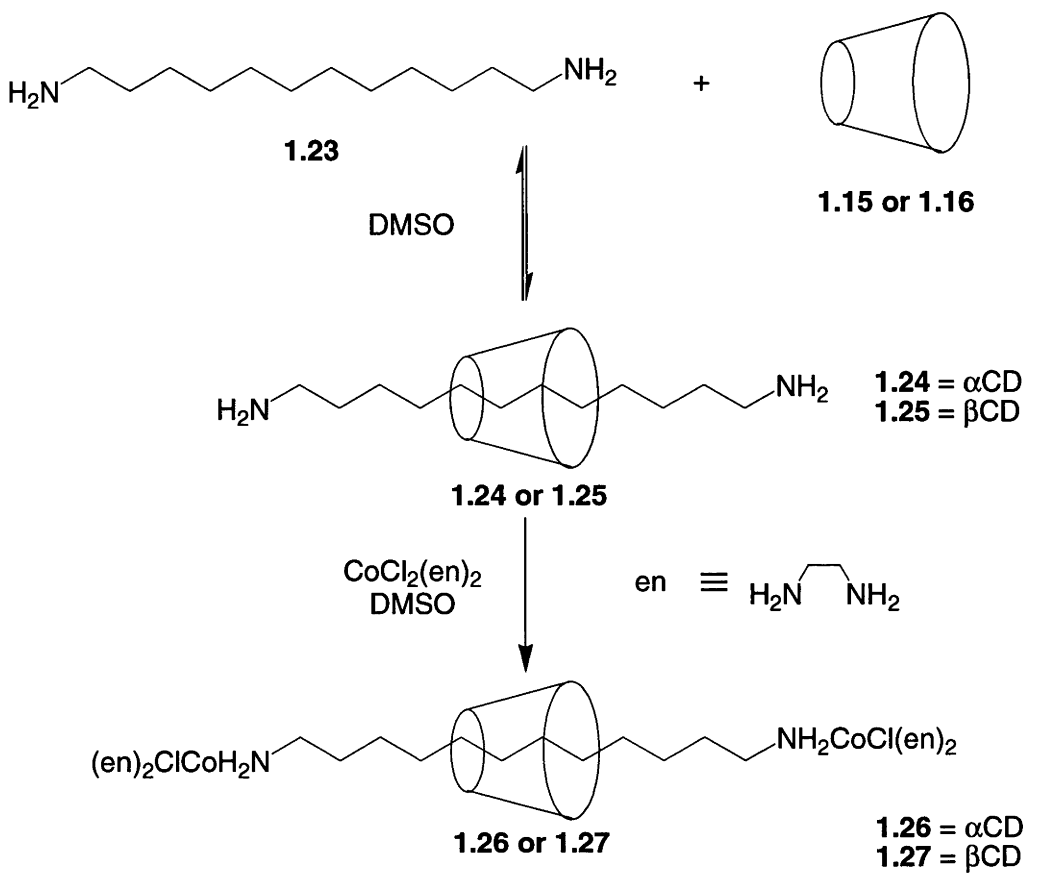

Scheme 1.5. Formation of the first cyclodextrin [2]-rotaxanes **1.26** and **1.27** reported by Ogino.[60]

Since then, the synthesis of [2]-rotaxanes using covalently linked blocking groups has been developed. Some examples are shown in Figure 1.4. The [2]-rotaxane **1.28** synthesised by Harada *et al.*[62] used covalently linked trinitrophenyl groups to block the CD from disassociating from the alkyl chain. Wenz *et al.*[63] used covalently linked triphenylmethyl groups in the synthesis of the [2]-rotaxane **1.29**. Recently, a review by Wenz *et al.*[64] detailed the synthesis of a range of new CD [2]-rotaxanes. Many of these possess the ability to act as molecular devices.

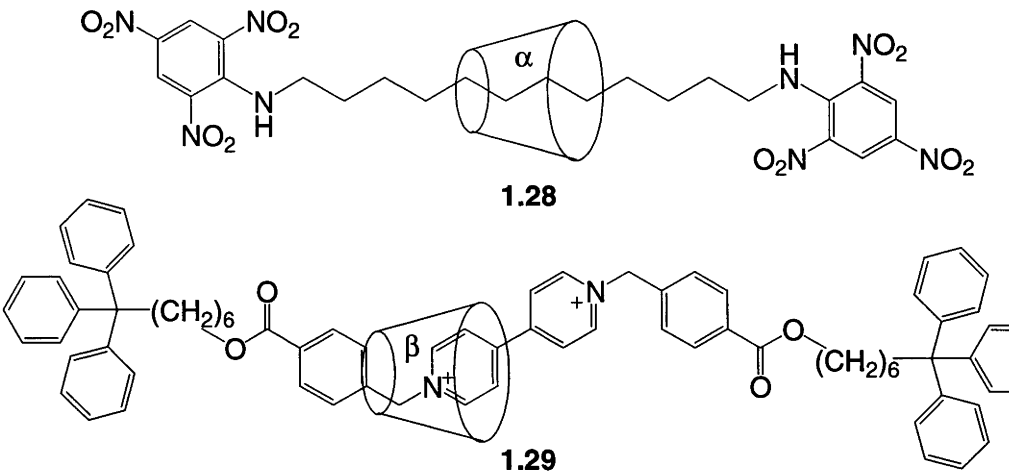

Figure 1.4. Examples of cyclodextrin [2]-rotaxanes reported by Harada *et al.*,[62] and Wenz *et al.*[63]

Stilbenes were chosen in this research project to form [2]-rotaxanes as various stilbene-CD [2]-rotaxanes had been previously synthesised. Illustrated in Scheme 1.6 is the stilbene based [2]-rotaxane **1.32** that was synthesised by Easton *et al.*[65] The synthesis uses 4,4'-diaminostilbene (**1.30**) as the non-polar guest to complex with αCD (**1.15**) in carbonate buffer at pH 10. This pH is used to maintain the stilbene **1.30** as the free amine for reaction with the blocking reagent 2,4,6-trinitrobenzene-1-sulfonic acid sodium salt (**1.31**). A nucleophilic aromatic substitution occurs to give the [2]-rotaxane **1.32**.

Hermaphroditic [2]-rotaxanes have also been formed using stilbenes and CDs. The reaction scheme for the formation of the hermaphroditic [2]-rotaxane **1.34** by Onagi *et al.*,[39] is shown in Scheme 1.7. Sulfonation of the CD-OH6 groups of αCD (**1.15**) as described above provides an avenue for CD modification. Addition of the stilbene **1.30** through nucleophilic substitution of the sulfonate group enables the formation of the hermaphroditic CD **1.33**. The hermaphroditic [2]-rotaxane **1.34** was isolated from the reaction of the hermaphroditic CD **1.33** with the trinitrophenyl blocking reagent **1.31**.

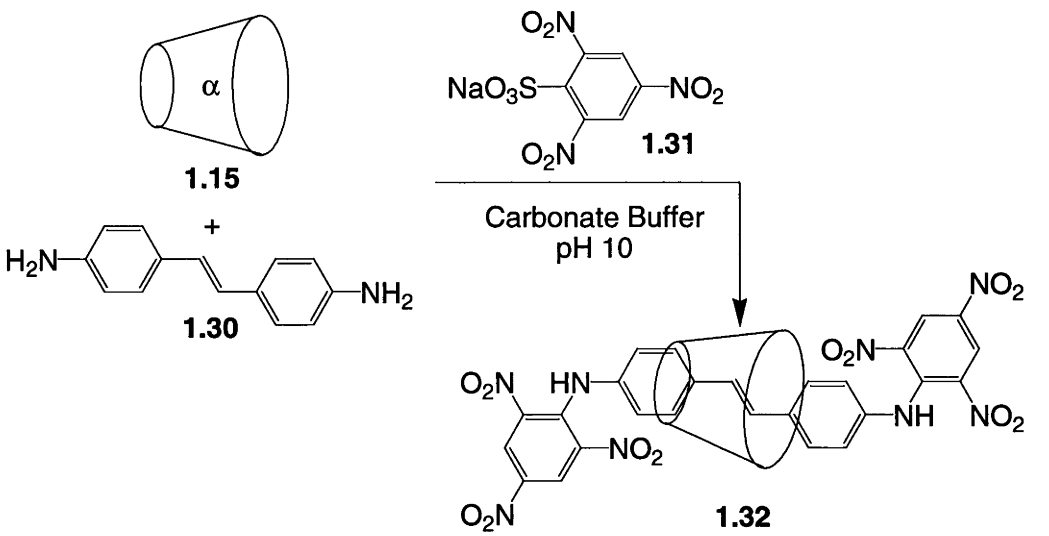

Scheme 1.6. Formation of the stilbene-based cyclodextrin [2]-rotaxane **1.32** by Easton *et al.*[65]

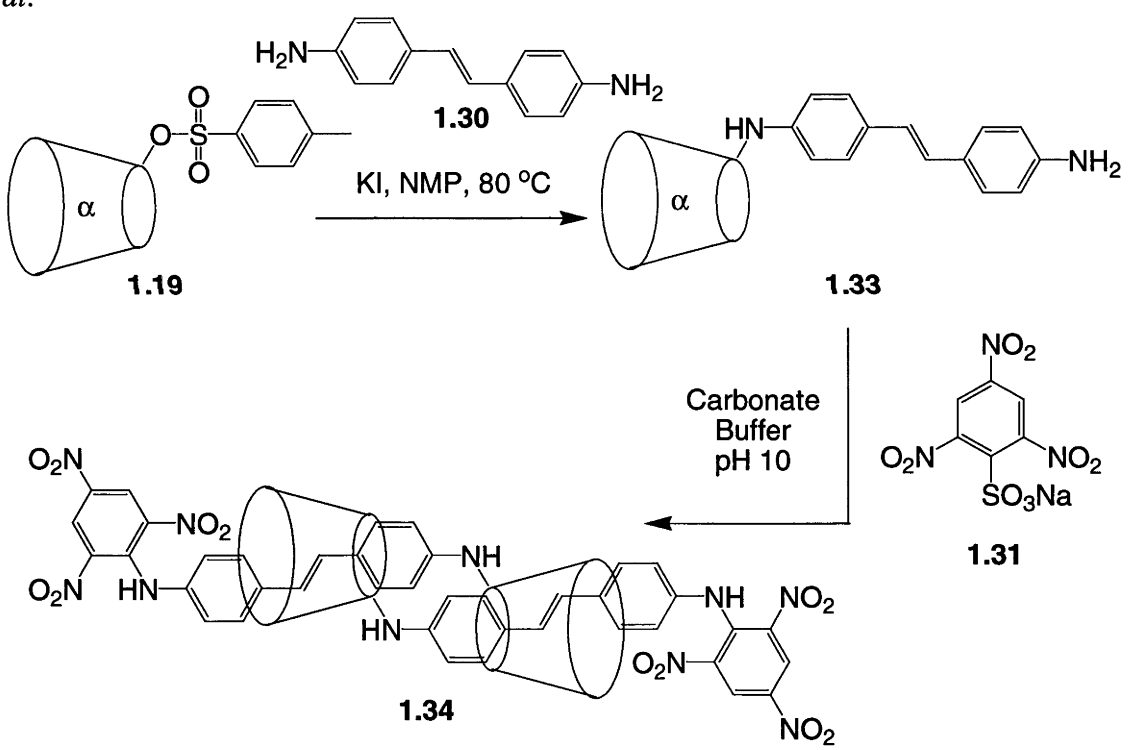

Scheme 1.7. Formation of the stilbene and cyclodextrin-based hermaphroditic [2]-rotaxane **1.34** by Onagi *et al.*[39]

The photochemistry of stilbenes was another important factor in the selection of them as the guests for the formation of CD [2]-rotaxanes. The photochemistry of the stilbene **1.35** is summarised in Scheme 1.8. The stilbene **1.35** which contains a *trans*-

olefinic bond can be isomerised to its *cis*-isomer **1.36** upon excitation with light. This isomerisation process is reversible to reform the *trans*-isomer **1.35**. There are also several competing reactions that can occur during the photoisomerisation process. One reaction is a cyclodimerisation reaction of two *trans*-stilbenes to form the isomeric cyclic dimers **1.37** and **1.38**. The *cis*-stilbene **1.36** can also undergo a cyclisation reaction to form the dihydrophenanthrene **1.39**. Further oxidation leads to the phenanthrene **1.40**.[66] It is the change in conformation of the stilbene unit upon isomerisation that is of interest for the formation of molecular shuttles and muscles.

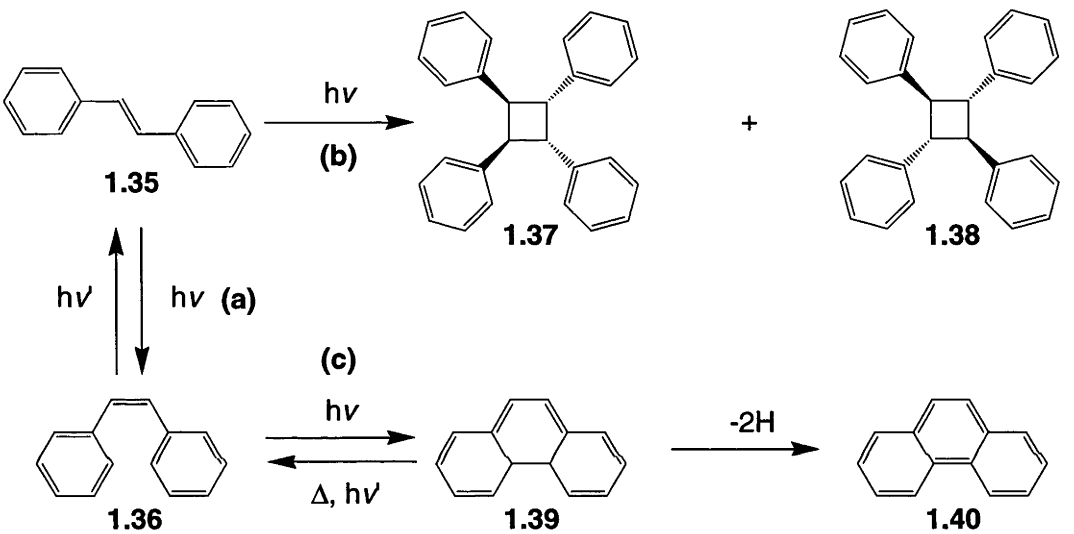

Scheme 1.8. Photochemistry of the stilbene **1.35**: (a) isomerisation, (b) cyclodimerisation, and (c) cyclisation.[66]

One stilbene based CD-[2]-rotaxane that can be viewed as a molecular shuttle is that synthesised by Stainer *et al.*,[67] shown in Scheme 1.9. Irradiation of the *trans*-isomer **1.41** at a wavelength of 347 nm produces the *cis*-isomer **1.42** and causes the CD to shuttle along the axle from the double bond at the centre to one side. The reverse reaction occurs when the *cis*-isomer **1.42** is irradiated at a wavelength of 265 nm. One perceived flaw in the molecular shuttle shown in Scheme 1.9 is the lack of a defined second CD binding unit. Consequently the CD does not move entirely off the stilbene unit when it is in its *cis* form.

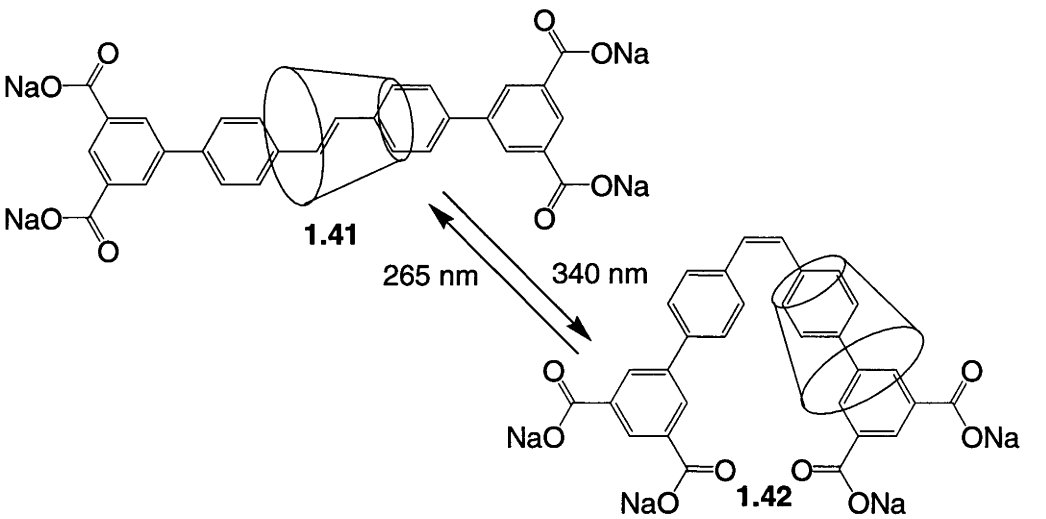

Scheme 1.9. A molecular shuttle synthesised by Stainer *et al.*[67]

The aim of this project was therefore to use the stable complex formed between stilbenes and CDs, to form alternative [2]-rotaxanes. A different [2]-rotaxane was sought with a second CD binding unit that would allow the CD to move completely off the stilbene unit after isomerisation. The construction of hermaphroditic [2]-rotaxanes using stilbenes and CDs that would act as molecular muscles like that synthesised by Sauvage *et al.*, [40] was also sought.

Chapter 2: Synthesis and Conformational Analysis of α-Cyclodextrin [2]-Rotaxanes with Trinitrophenyl Blocking Groups

In the previous chapter, it was described how the formation of a [2]-rotaxane could be undertaken using various means. The "*threading*" method has been used extensively in our research group and was selected to synthesise the [2]-rotaxanes in this work.

As shown in Scheme 2.1, a suitable sized non-polar guest **2.2** and CD **2.1** when placed in water are in equilibrium with the CD-guest complex **2.3**. The use of a suitable reagent **2.4** to add a bulky group to either end of the guest molecule **2.2** prevents the guest **2.2** from dissociating from the CD **2.1** thus forming the [2]-rotaxane **2.5**.

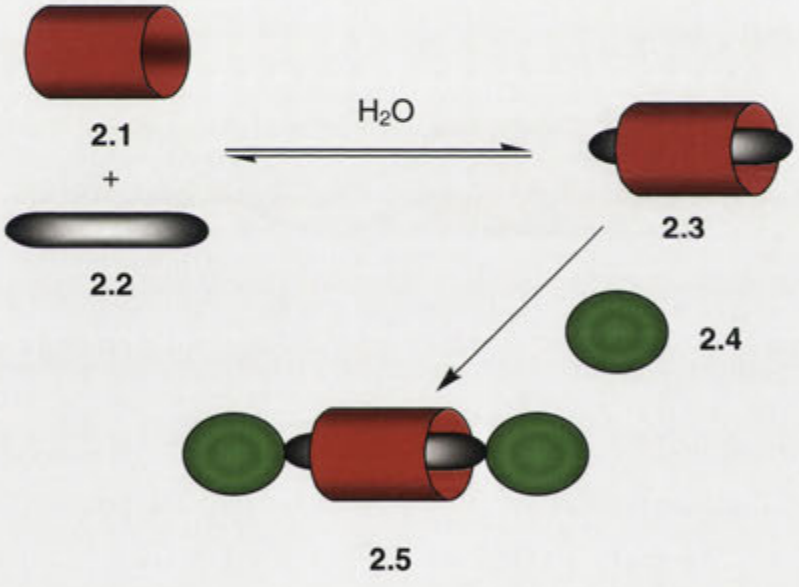

Scheme 2.1. Schematic diagram of the formation of the cyclodextrin [2]-rotaxane **2.5** using the "*threading*" method.

As described in Chapter 1, stilbenes have been used to form [2]-rotaxanes with CDs. Shown in Scheme 1.6 is the stilbene based [2]-rotaxane **1.32** that was previously synthesised by Easton *et al.*[65] Stilbenes also have the ability to photochemically interconvert between their *cis*- and *trans*-isomers. It has been previously reported that *trans*-stilbenes have higher affinity for αCD (**1.15**) than *cis*-stilbenes.[68] Therefore if a

second CD binding unit was selected that had a stronger binding with αCD (**1.15**) than a *cis*-stilbene, but weaker than with its *trans* counterpart, it could be attached to the stilbene and capped with a suitable blocking reagent to form a [2]-rotaxane with the potential to act as a molecular shuttle. This is shown in Scheme 2.2 where the isomerisation of the stilbene from the *trans* form **2.6** to the *cis* **2.7** would cause the CD to shuttle along the axle towards the second CD binding unit.

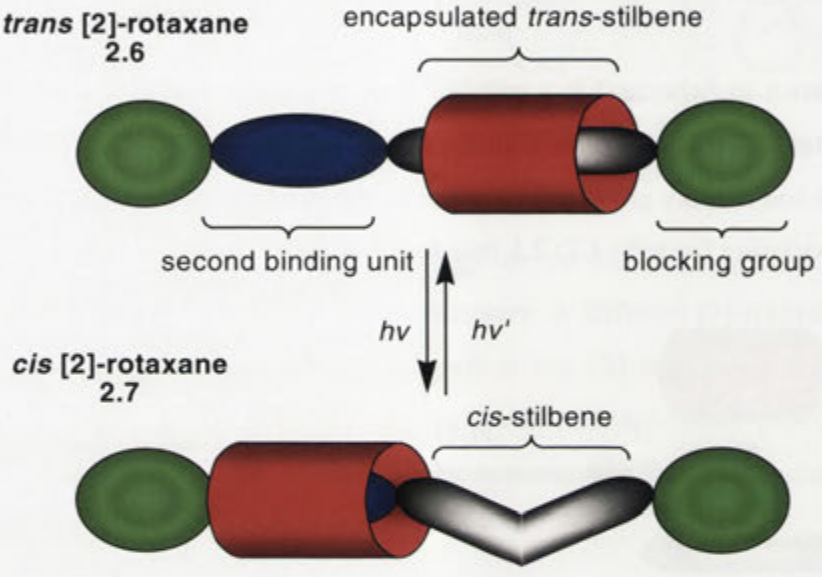

Scheme 2.2. Expected photochemical isomerisation of the stilbene unit of a *trans*-stilbene based [2]-rotaxane **2.6** to produce a *cis*-[2]-rotaxane **2.7** that would cause the cyclodextrin to shuttle to the second cyclodextrin binding unit.

As described in Chapter 1, a species that can be viewed as a molecular shuttle is that synthesised by Stainer *et al.*,[67] shown in Scheme 1.9. One perceived flaw in the molecular shuttle, however, is the lack of a defined second CD binding unit. Consequently the CD does not move entirely off the stilbene unit when it is in its *cis* form. A different [2]-rotaxane was sought with a second CD binding unit that would allow the CD to move completely off the stilbene unit after isomerisation.

In the synthesis of an alternative [2]-rotaxane molecular shuttle, 4-aminophenylacetic acid (**2.8**) was chosen as the source of a second CD binding unit. This was thought to be a suitable reagent as it could be coupled to the stilbene **1.30** through an amide bond. It was believed that the amide bond would provide suitable separation to

allow the CD to move completely away from the stilbene when isomerised. Phenyl groups are also rigid and were thought likely to provide a good linear axle for the formation of a [2]-rotaxane. In the synthesis shown in Scheme 2.3, the amine **2.8** was protected using BOC-ON under anhydrous conditions in DMF and TEA to form the carbamate **2.9** as had been previously reported in the literature.[69-72] Excess of the stilbene **1.30** was then coupled to the carbamate **2.9** using the amide coupling agent BOP in DMF with TEA. The crude product was purified by preparative HPLC to give the amide **2.10** in 44% yield. This was followed by deprotection of the amino group by dissolving in DCM for the addition of TFA to afford the diamine **2.11** in a yield of 87%. The diamine **2.11** was equilibrated in carbonate buffer of pH 10 with αCD (**1.15**) for 24 hours and then allowed to react with the sulfonate **1.31**. TLC showed the existence of a species with an R_f different to any starting material that absorbed UV light and on exposure to naphthalene-1,3-diol gave a pink colouration characteristic of a CD as was expected for a [2]-rotaxane.[65] The material was applied to a Diaion HP-20 column and the excess αCD (**1.15**) was eluted with MQ H_2O before the product of interest was removed with MeOH. It was then subjected to reverse phase HPLC where two components were revealed and isolated. The formation of two [2]-rotaxanes was confirmed by ESI mass spectrometry which gave an M^- ion of *m/z* 1736.4 for the first [2]-rotaxane **2.12**, and a HI-RES $M+Na^+$ ion of *m/z* 1760.4464 for the second [2]-rotaxane **2.13**. These species were found to be in a ratio of about 1:1 from the HPLC analysis and they were isolated in yields of 2.2% for the [2]-rotaxane **2.12** and 2.1% for the [2]-rotaxane **2.13**.

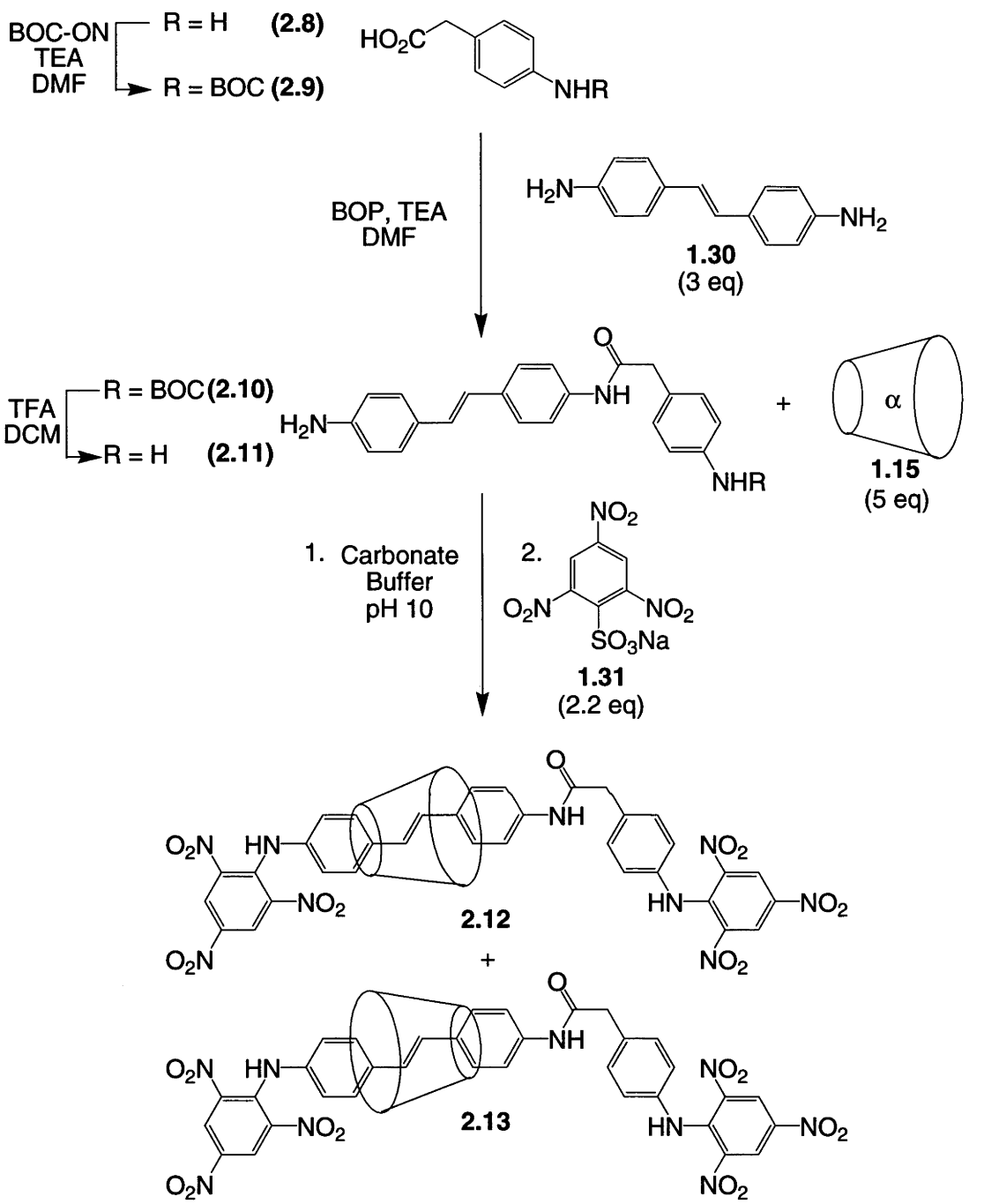

Scheme 2.3. Formation of the [2]-rotaxanes **2.12** and **2.13**.

The two apparently different [2]-rotaxanes **2.12** and **2.13** are formed due to the asymmetric nature of both αCD (**1.15**) and the axle species **2.11** creating two different possible orientations for the CD to reside over the axle. The formation of isomeric [2]-

rotaxanes has been identified on a number of previous occasions. Isnin and Kaifer[73] were the first to encounter this phenomenon. Upon reaction of the acid **2.14** and the amine **2.15** with the aqueous-stable amide coupling agent EDC in water in the presence of αCD (**1.15**), a mixture of the isomeric [2]-rotaxanes **2.16** and **2.17** was obtained as seen in Scheme 2.4. These [2]-rotaxanes were observed for an alkyl chain length of 7 and 11 and was verified by NOESY 2D NMR spectroscopy. The ^{1}H NMR spectrum showed two different amide proton signals that correlated through space with the CD primary and secondary hydroxyl groups, respectively. This indicated that the CD had two different orientations on the axle.

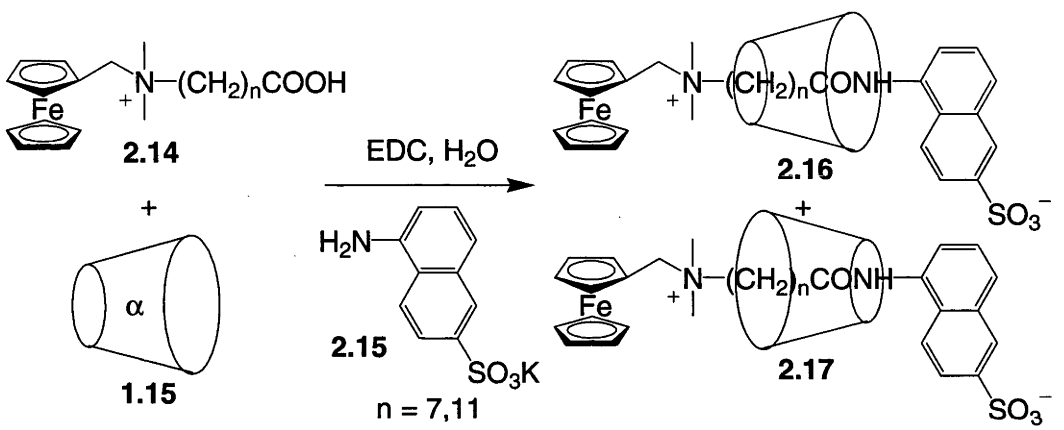

Scheme 2.4. Formation of the isomeric [2]-rotaxanes **2.16** and **2.17** reported by Isnin and Kaifer.[73]

Buston *et al.*[74] also encountered this phenomenon. In their approach to synthesise [2]-rotaxanes based on cyanine dyes they allowed the aldehyde **2.18** to react with the pyridinium chloride **2.19** and αCD (**1.15**) in aqueous sodium hydroxide as shown in Scheme 2.5. The isomeric [2]-rotaxanes **2.20** and **2.21** were formed in a 1:2 mixture as measured by ^{1}H NMR spectroscopy and were isolated and characterised along with the free dye **2.22**. NOESY 2D NMR spectroscopy was used to identify the position of the CD in each case. For the [2]-rotaxane **2.20** there were interactions between the CD-H3 protons and the julolidine stopper and between the CD-H5 protons and the adamantyl group. The reverse interactions were observed for the isomer **2.21**.

In another case, isomeric CD [2]-rotaxanes were synthesised by Park and Song.[75] Upon reaction of the bromide **2.24** with an equilibrated mixture of the aliphatic chain-linked carbazole viologen **2.23** and αCD (**1.15**), a mixture of the two isomers **2.25** and

2.26 was isolated in a yield of 27%. Fractional precipitation was used to separate the isomers and 2D NMR spectroscopy to verify that they were isomeric [2]-rotaxanes. From the ROESY spectra the isomer **2.25** showed NOE interactions between the CD-H3 and carbazole protons. The isomer **2.26** had NOE interactions between the CD-H6 and carbazole protons. Thus the orientation of the CD was as shown in Scheme 2.6.

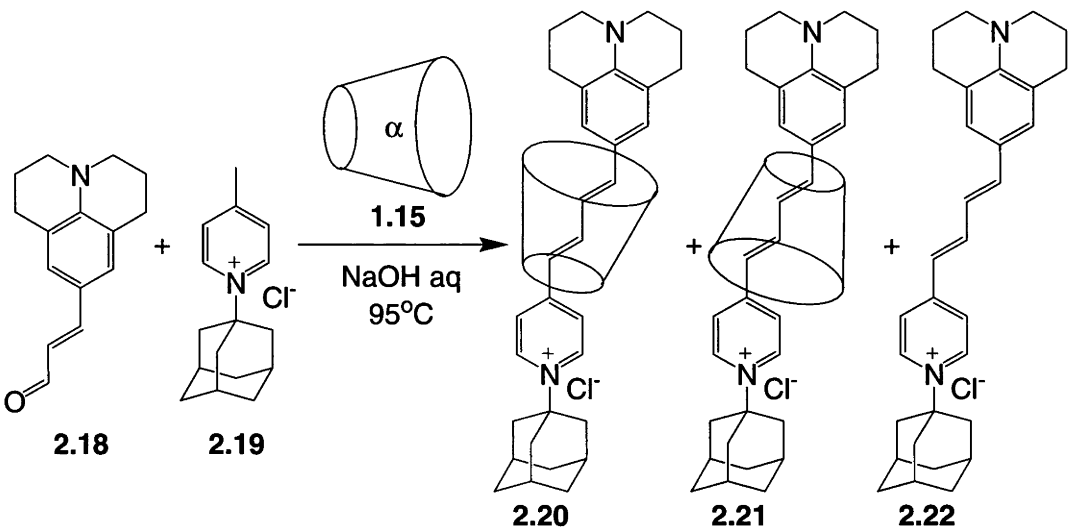

Scheme 2.5. Formation of the isomeric [2]-rotaxanes **2.20** and **2.21** reported by Buston *et al.*[74]

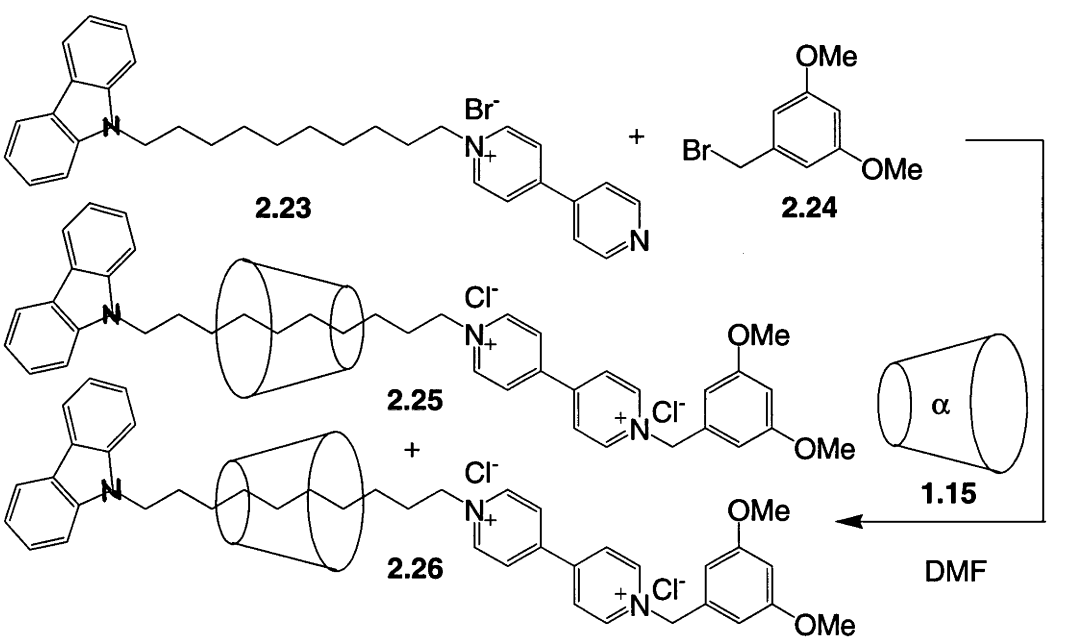

Scheme 2.6. Formation of the isomeric [2]-rotaxanes **2.25** and **2.26** reported by Park and Song.[75]

With the knowledge of the previous examples of isomeric CD [2]-rotaxanes it was then the objective to determine the exact orientation and positioning of the CD in the [2]-rotaxanes obtained in the present work (Scheme 2.3). This was mapped using a combination of ^{1}H DQCOSY and ^{1}H ROESY NMR techniques. From the ^{1}H DQCOSY spectrum each of the CD proton signals was firstly assigned to sets of protons within the [2]-rotaxane structure. The CD-H1 proton signals characteristically appear furthest downfield near 5 ppm. From this signal the CD-H2, CD-H3, CD-H4 and CD-H5 signals were assigned from their sequential DQCOSY interactions as shown in Figure 2.1. The remaining signals were allotted to the CD-H6^{A} and CD-H6^{B} protons that have a strong DQCOSY interaction with each other.

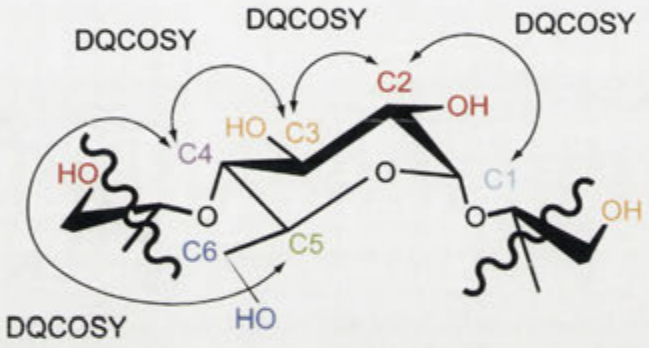

Figure 2.1. DQCOSY interactions of the cyclodextrin protons in a glucose sub-unit.

In looking at the CD region of the DQCOSY spectrum of the [2]-rotaxane **2.12** as shown in Figure 2.2, the CD-H1 proton signals are found at 4.92 ppm as they are the furthest downfield. The CD-H1 proton signals have one interaction with a set of signals at 3.42 ppm that can be concluded to be due to the CD-H2 protons. These in turn show an interaction with a signal at 3.90 ppm corresponding to the CD-H3 protons. The CD-H3 protons show an interaction with the CD-H4 protons for which signals are found at 3.57 ppm which in turn show an interaction with the CD-H5 protons with signals at 3.89 ppm. The two final strong crosspeaks of the CD-H6^{A} and CD-H6^{B} signals are found at 3.53 and 3.74 ppm.

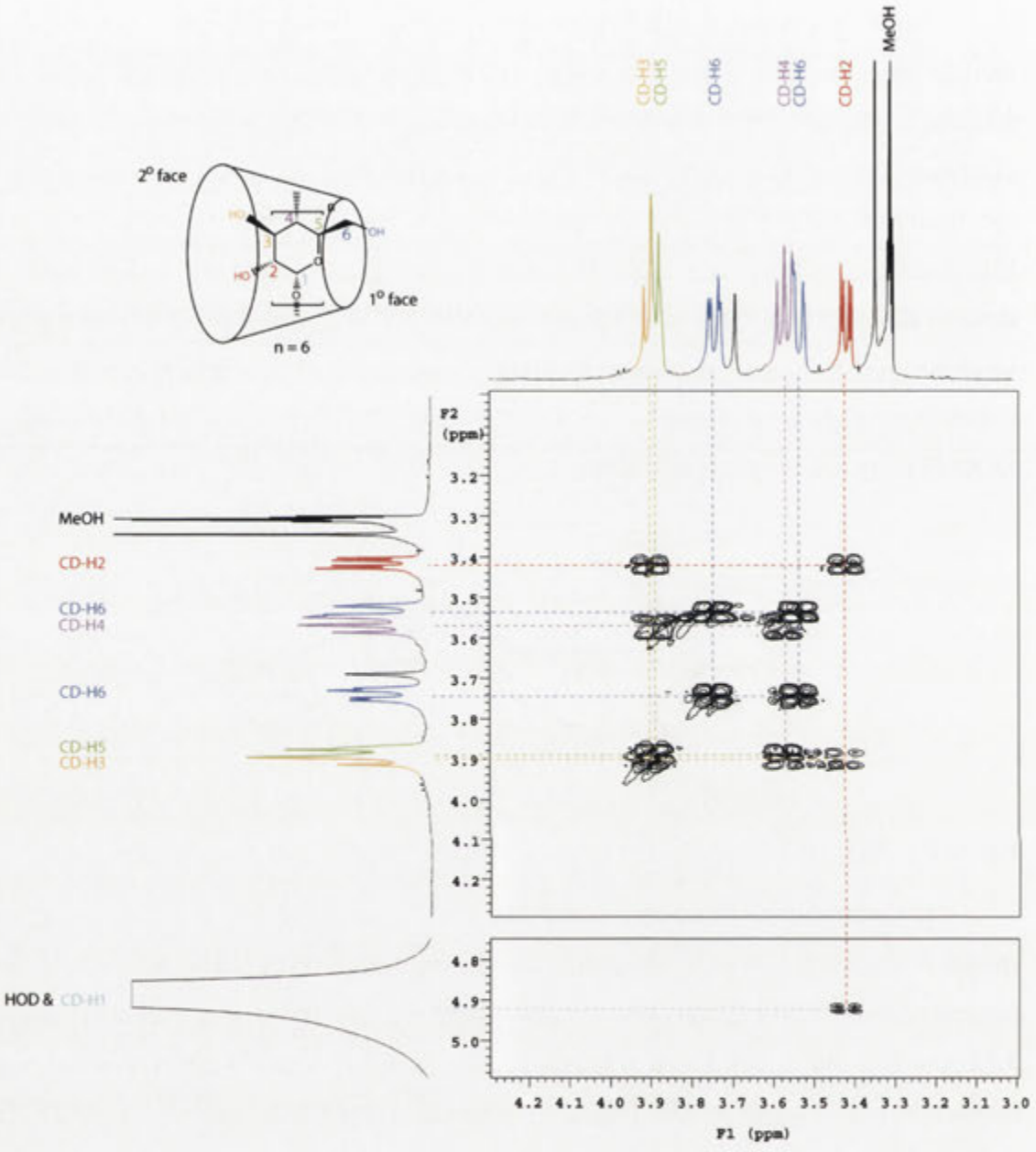

Figure 2.2. A section of the 500 MHz DQCOSY spectrum of the [2]-rotaxane **2.12** in d_4-methanol at 25 °C of the region where crosspeaks are observed between cyclodextrin proton signals.

For the purpose of assignment of the axle proton signals of the [2]-rotaxanes **2.12** and **2.13**, the designations shown in Figure 2.3 were used.

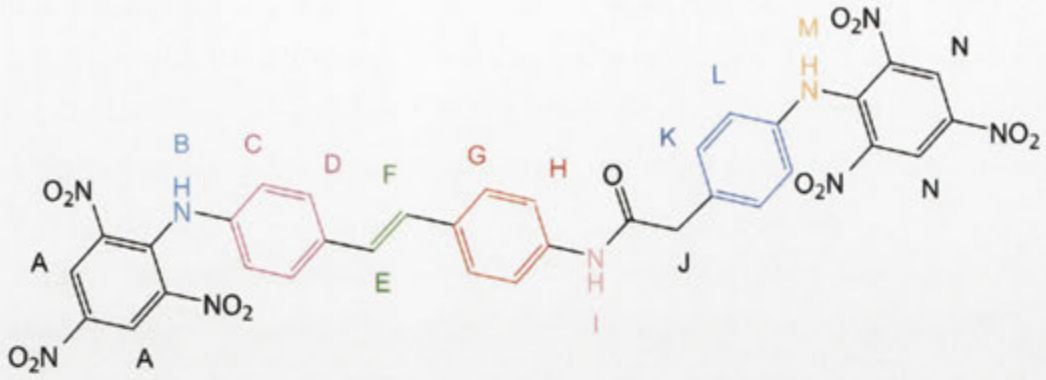

Figure 2.3. Proton designations of the axle of the [2]-rotaxanes **2.12** and **2.13.**

To assign signals to the axle protons, a combination of ^{1}H ROESY and ^{1}H DQCOSY NMR spectra was used as shown in Figure 2.4. In the stilbene moiety, the signals of the olefinic protons E and F are easily assigned due to their larger coupling. These signals should also show DQCOSY crosspeaks with each other. The signal due to protons D should have a stronger NOE ROESY interaction, and hence a larger crosspeak, with the signal of the olefinic proton F than that of E. This is because proton F would be closer in space than proton E. The larger crosspeak is due to the inverse relationship of the distance between two protons and the strength of their NOE interaction. Protons D should also have a DQCOSY and NOE interaction with C placing them next to D in the axle. Protons G should also show an interaction with the olefinic protons with a stronger NOE interaction with E than F as again E is closer in space.

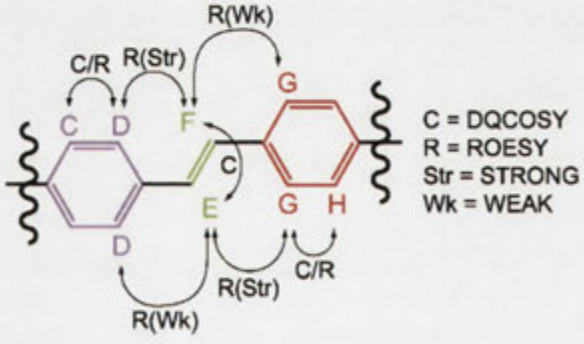

Figure 2.4. Method for assignment of the stilbene proton signals due to likely DQCOSY and ROESY interactions.

The ^{1}H DQCOSY NMR spectrum of the aromatic region for the [2]-rotaxane **2.12** is shown in Figure 2.5. The signals for the olefinic protons E and F at 7.01 and 7.12 ppm,

which were assigned on the basis of their large coupling constant, show a strong DQCOSY interaction. This coupling was calculated to be 16 Hz, consistent with that of a *trans*-olefinic bond.[76] The other aromatic proton signals also show DQCOSY interactions. The signal due to protons C at 7.66 ppm shows an interaction with the signal at 7.35 ppm corresponding to protons D. The signal due to protons G at 7.84 ppm shows an interaction with that of protons H at 7.11 ppm. In addition the protons K signal at 7.33 ppm shows an interaction with the protons L signal at 7.07 ppm. From this information, the signals due to the protons of the three *para*-substituted aromatic rings and the *trans*-olefinic bond from the product **2.12** were identified.

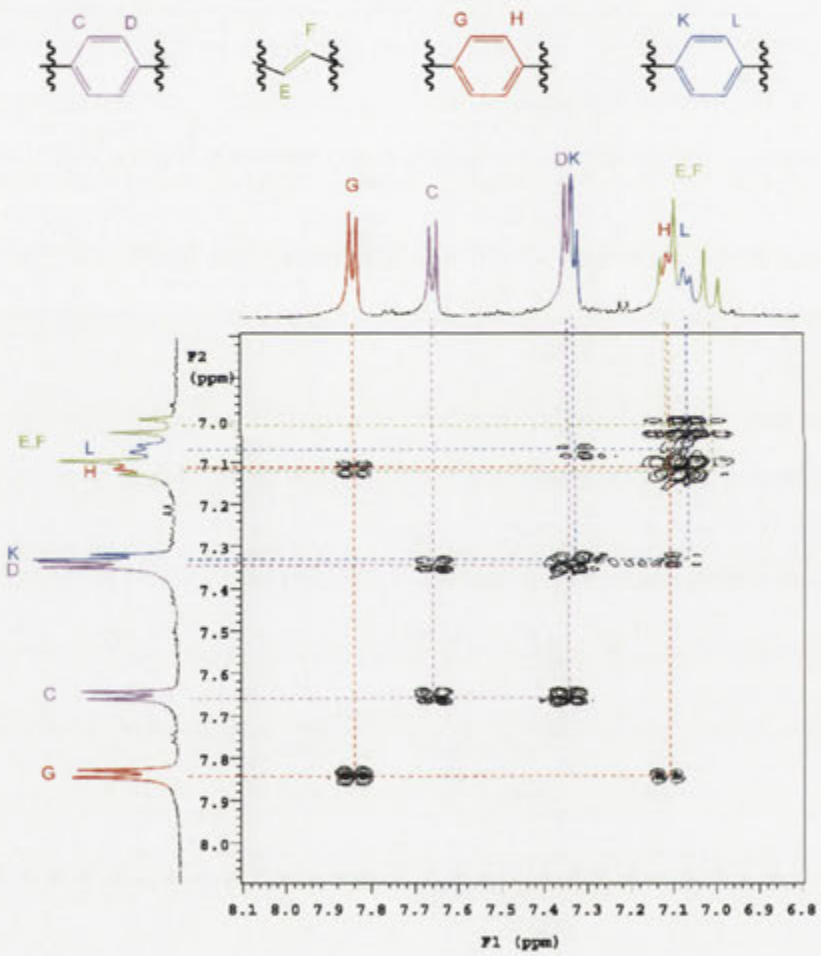

Figure 2.5. A section of the 500 MHz DQCOSY spectrum of the [2]-rotaxane **2.12** in d_4-methanol at 25 °C of the region where crosspeaks are observed between axle proton signals.

The ^{1}H ROESY NMR spectrum of the same aromatic region was next to be examined. The contour plot of interest is shown in Figure 2.6. From the spectrum all proton resonance assignments of the stilbene unit can be deduced. An NOE interaction is seen between the signals of aromatic protons D and G and those of the *trans*-olefinic bond. It is not possible to measure the relative strengths of the interactions because of the overlap between the interactions of protons G and H and those of K and L so the assignments for protons E and F could be the reverse of that shown. This is of no consequence, however, in the following analysis of the position of the CD on the axle. As in the previous DQCOSY spectrum, crosspeaks are observable between the C and D aromatic protons signals. As the protons K and L show no interactions with the olefinic protons, they are not part of the stilbene unit and must make up the *para*-substituted phenyl group of the second CD binding unit.

The section of the ^{1}H ROESY contour plot that shows crosspeaks between the axle and proton signals can be seen in Figure 2.7. On the y-axis the signals corresponding to the protons of the axle can be found while the x-axis shows those of the protons of the CD. The signal of protons C shows crosspeaks with the CD-H6^A and CD-H6^B proton signals and a very minor interaction with the CD-H5 proton signal placing them at the primary face of the CD. The signal of protons D shows both strong interactions with the CD-H6^A and CD-H6^B proton signals and either or both of the CD-H5 and CD-H3 proton signals. This fits with them residing next to C in the axle and towards the primary face of the CD. The olefinic signal at 7.02 ppm has strong crosspeaks with either or both those of the CD-H3 and CD-H5 annular protons and must sit centrally within the CD. The olefinic proton signal at 7.12 ppm is part of a multiplet that results from the overlapping signal of aromatic protons H. Due to the multiplet, it can only be deduced that either one or both of these axle proton types interacts with either or both of the CD-H3 and CD-H5 protons. The signal due to protons G shows NOE interactions with both the CD-H3 and CD-H5 proton signals and therefore protons G must be centrally located inside the CD annulus. The aromatic proton K shows no interactions with any of the CD annular protons. There is only a crosspeak with the signal due to the alkyl protons J. The K and J proton interaction is only seen through 2D ROESY NOE interactions. The signal of aromatic protons L shows no NOE interactions with the CD. This shows that the phenyl subunit of

the axle is not encapsulated by the CD. Therefore in its *trans* form, the CD is located on the stilbene of the axle in the [2]-rotaxane **2.12**.

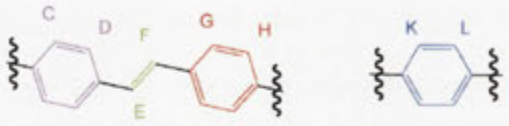

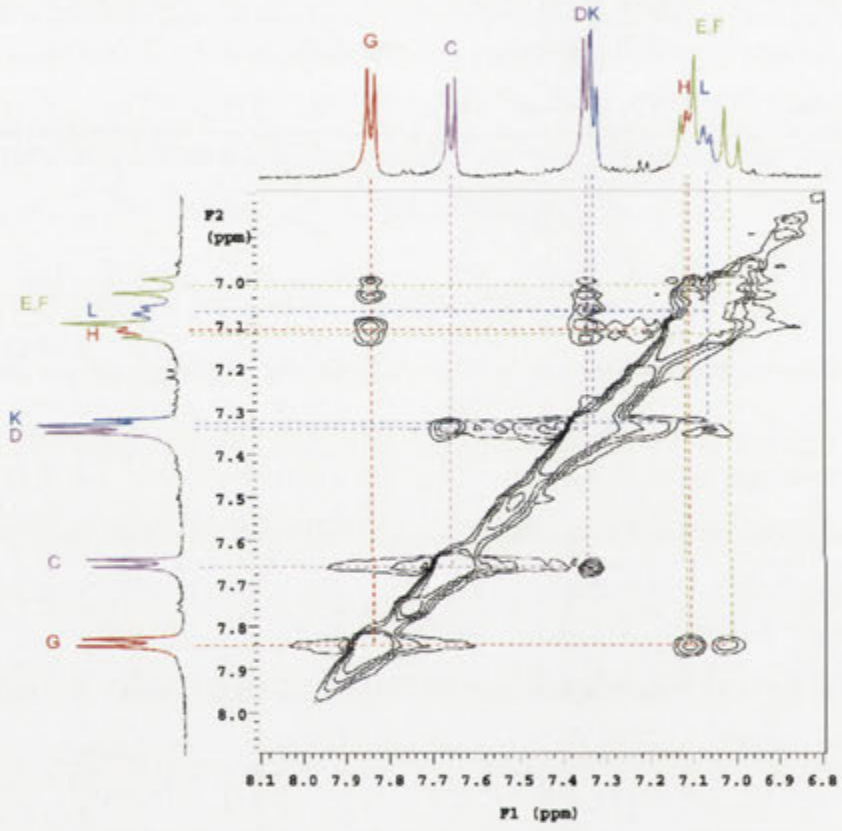

Figure 2.6. A section of the 500 MHz ROESY spectrum of the [2]-rotaxane **2.12** in d_4-methanol at 25 °C of the region where crosspeaks are observed between axle proton signals.

While this confirms the formation of a [2]-rotaxane, from the information gathered the exact orientation of the CD on the axle has not been deciphered. Before explaining how this was accomplished, the procedures used to determine the location of the CD on the axle of the second isomeric [2]-rotaxane **2.13** are described. This procedure was followed because if the CD had been positioned differently it may have

been possible that NOE interactions would indicate the orientation in that case and therefore also for the isomer **2.12**.

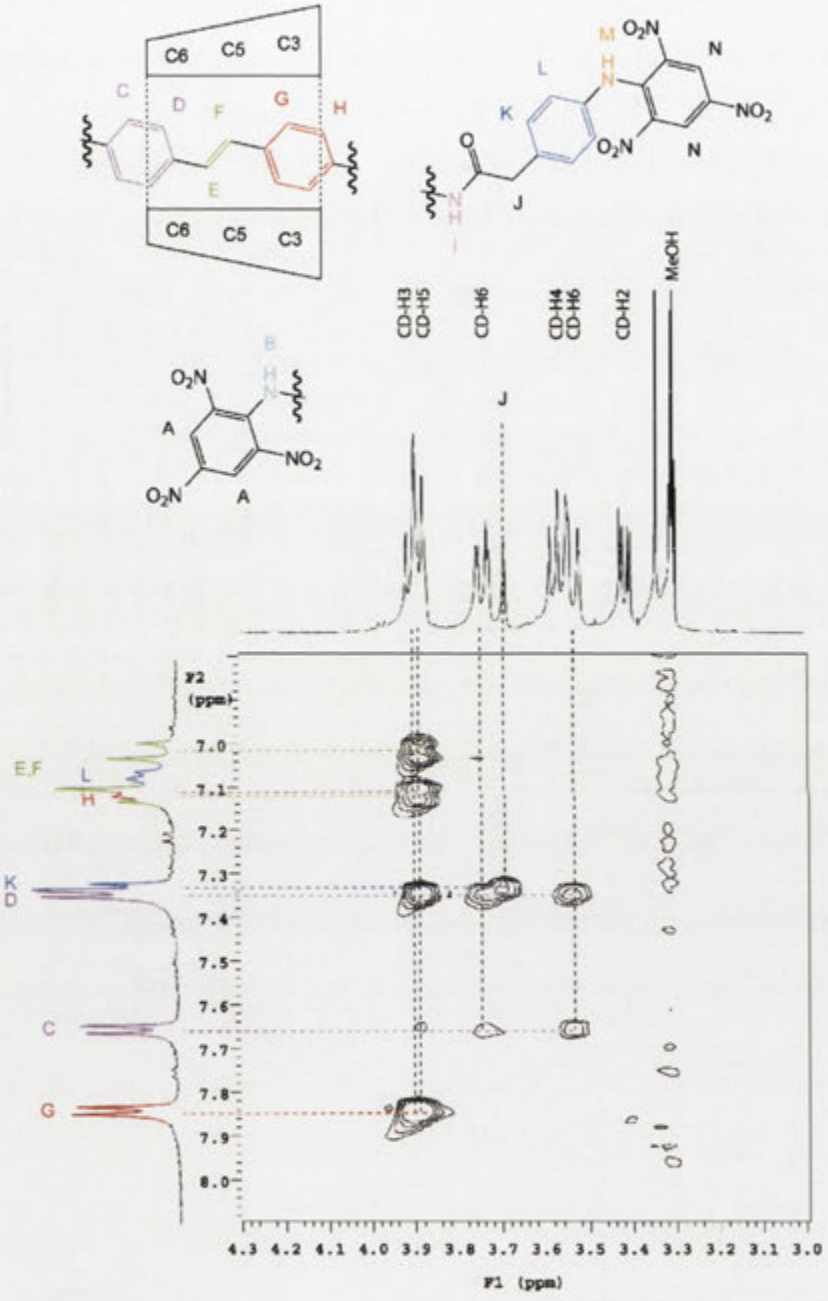

Figure 2.7. A section of the 500 MHz ROESY spectrum of the [2]-rotaxane **2.12** in d_4-methanol at 25 °C of the region where crosspeaks are observed between axle and cyclodextrin proton signals.

The first step again in the process to delineate the structure of the [2]-rotaxane **2.13** was to assign the CD region of the DQCOSY spectrum. From the contour plot,

shown in Figure 2.8, the signal of the CD-H1 protons is the furthest downfield and can be found at 4.91 ppm. The CD-H1 signal has one crosspeak with a signal at 3.43 ppm belonging to the CD-H2 protons. The CD-H2 signal shows a correlation with a signal at 3.85 ppm corresponding to the CD-H3 protons which interact with the CD-H4 protons for which the signal is at 3.57 ppm. The CD-H4 proton signal correlates with that of the CD-H5 protons at 3.88 ppm. The CD-H6^{A} and CD-H6^{B} proton signals show strong crosspeaks with each other and are found at 3.63 and 3.76 ppm.

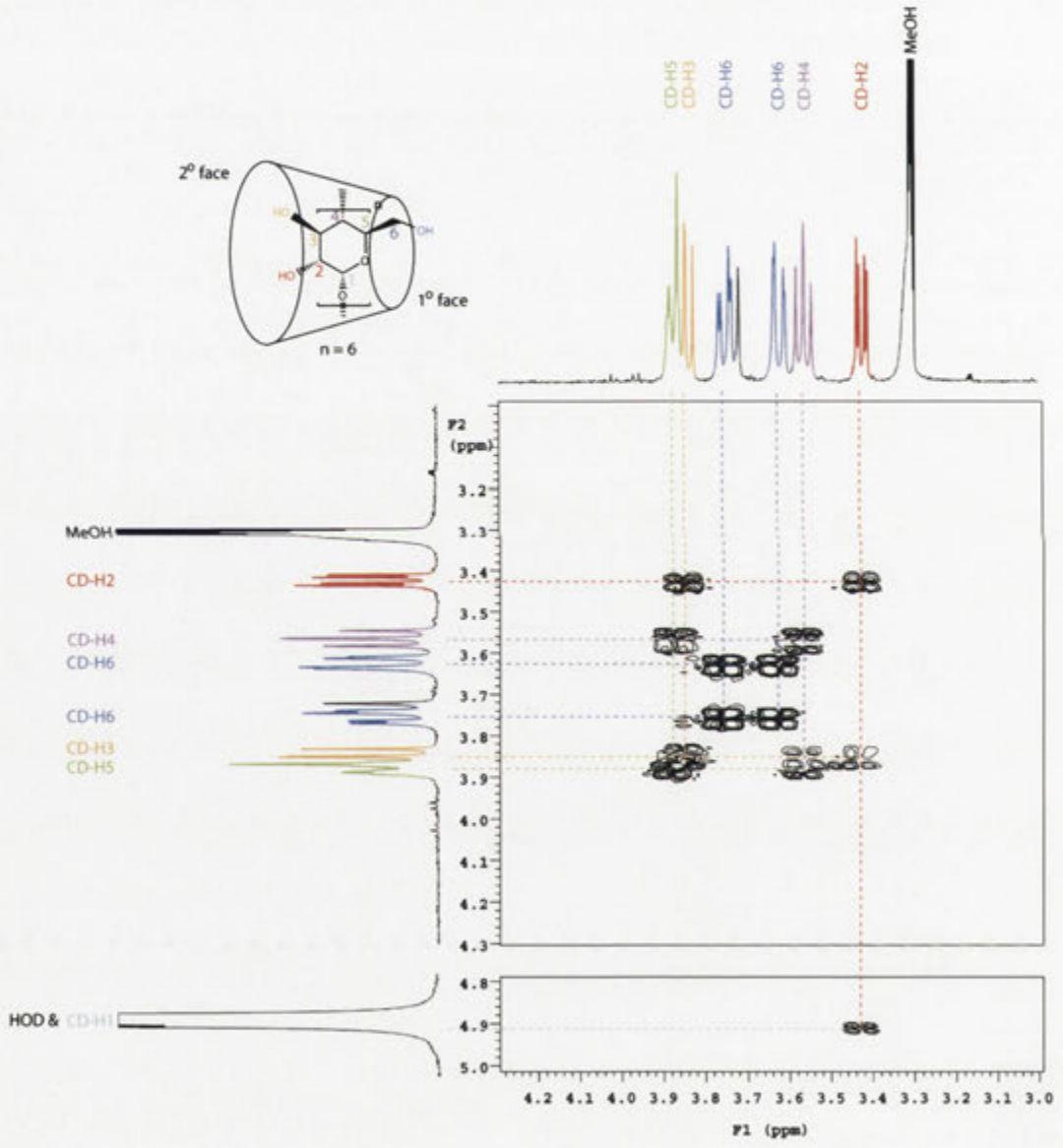

Figure 2.8. A section of the 500 MHz DQCOSY spectrum of the [2]-rotaxane **2.13** in d_4-methanol at 25 °C of the region where crosspeaks are observed between cyclodextrin proton signals.

The ^{1}H DQCOSY NMR spectrum of the aromatic region was used to determine which resonances of the axle were coupled and is shown in Figure 2.9. The signals of the olefinic protons F and E at 6.98 and 7.17 ppm show a strong DQCOSY correlation. The signals were determined to be due to olefinic protons due to their large coupling of 16 Hz, consistent with that of a *trans*-alkene.[76] The other six aromatic signals also reflect DQCOSY interactions. The signal due to protons C at 7.67 ppm shows an interaction with that of protons D at 7.90 ppm. The signal due to protons G at 7.31 ppm shows an interaction with the signal at 7.06 ppm corresponding to protons H. The signal of protons K at 7.38 ppm shows a crosspeak with the signal of the aromatic protons L at 7.11 ppm. This information allows the assignment of the resonances of the three *para*-substituted aromatic rings and the *trans*-olefinic bond as shown in Figure 2.9.

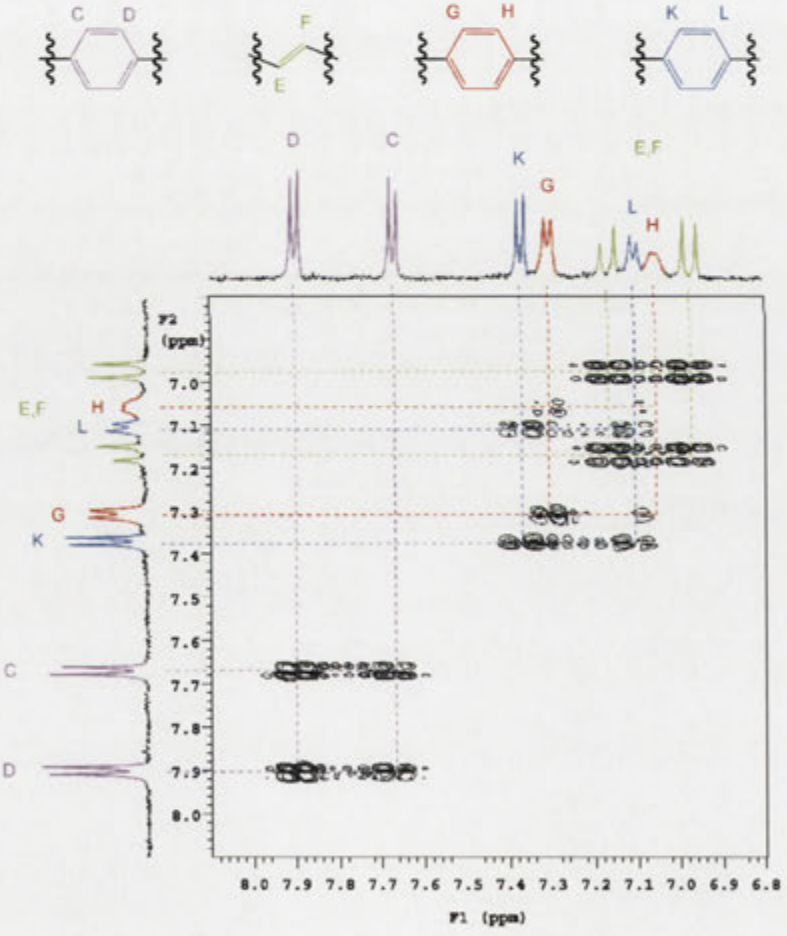

Figure 2.9. A section of the 500 MHz DQCOSY spectrum of the [2]-rotaxane **2.13** in d_4-methanol at 25 °C of the region where crosspeaks are observed between axle proton signals.

To assign the proton resonances of the stilbene subunit, the ^{1}H ROESY NMR spectrum of the same axle region was examined. From the contour plot, shown in Figure 2.10, it is evident that both the signals of the aromatic protons D and G show NOE crosspeaks with the signals of the olefinic protons E and F. As there is no apparent difference in the relative strengths of the interactions, it is not clear which olefinic proton is closer to which aromatic proton in terms of space. Again this exact assignment is not crucial in the following analysis of the position of the CD on the axle. Multiple NOE interactions between the signals of aromatic protons C and D, G and H, and K with L are also observable. The *para*-substituted aromatic of the phenyl second unit is comprised of the signals of the aromatic protons K and L as they are not a part of the stilbene unit.

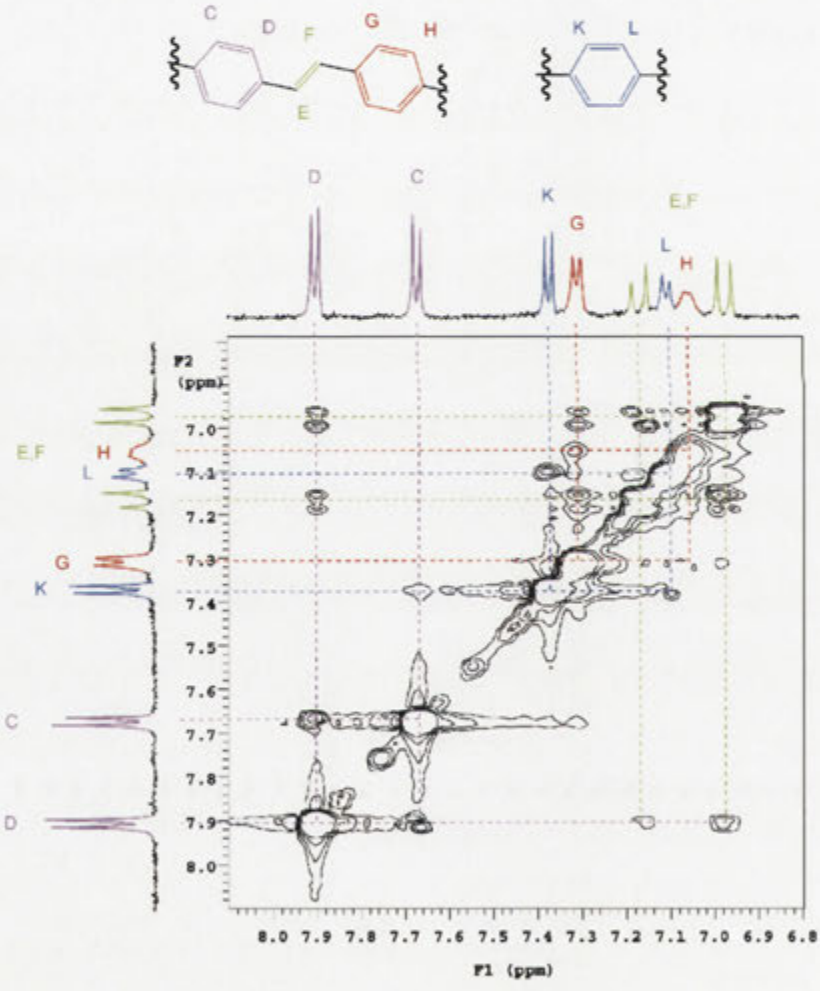

Figure 2.10. A section of the 500 MHz ROESY spectrum of the [2]-rotaxane **2.13** in d_4-methanol at 25 °C of the region where crosspeaks are observed between axle proton signals.

The contour plot of the ^{1}H ROESY spectrum of the [2]-rotaxane **2.13** that shows NOE interactions between the CD and axle can be seen in Figure 2.11. The y-axis contains the signals corresponding to the protons of the axle while on the x-axis the signals corresponding to the protons of the CD can be found. Again moving along the axle resonances, the position of the CD was established. The signal of protons C from the stilbene shows NOE interactions with the CD-H3 signal while the signal of protons D interacts with the CD-H3 and CD-H5 proton signals. This positions these aromatic stilbene protons at the secondary face of the CD. The signals of the olefinic protons E and F both show strong interactions with the signal of the CD-H5 protons positioning them centrally within the CD annulus. The signal of the stilbene protons G shows NOE crosspeaks with the signals of the CD-H5, CD-H6^A and CD-H6^B protons. Protons G are therefore situated at the primary face of the CD. The signal of the H protons shows no such interactions with any of the signals of the CD protons. This means that the H proton must be found outside the CD cavity far enough away to prevent any NOE interactions from being measured. The aromatic protons K and L also show no interaction with any of the CD protons placing them outside the CD cavity. One crosspeak does arise due to a NOE interaction between the signal of the alkyl protons J and the signal of the aromatic protons K. That means there are no interactions between the signals of the phenyl subunit and CD annulus. Therefore in its *trans* form, the CD is situated solely on the stilbene of the axle for the [2]-rotaxane **2.13**.

Again it is therefore confirmed that a [2]-rotaxane has been formed, but the exact orientation of the CD of each of the [2]-rotaxanes **2.12** and **2.13** was still ~~yet~~ to be determined. In each case the CD could be facing either way on the axle. Therefore a different means to decipher the orientation in each case had to be found.

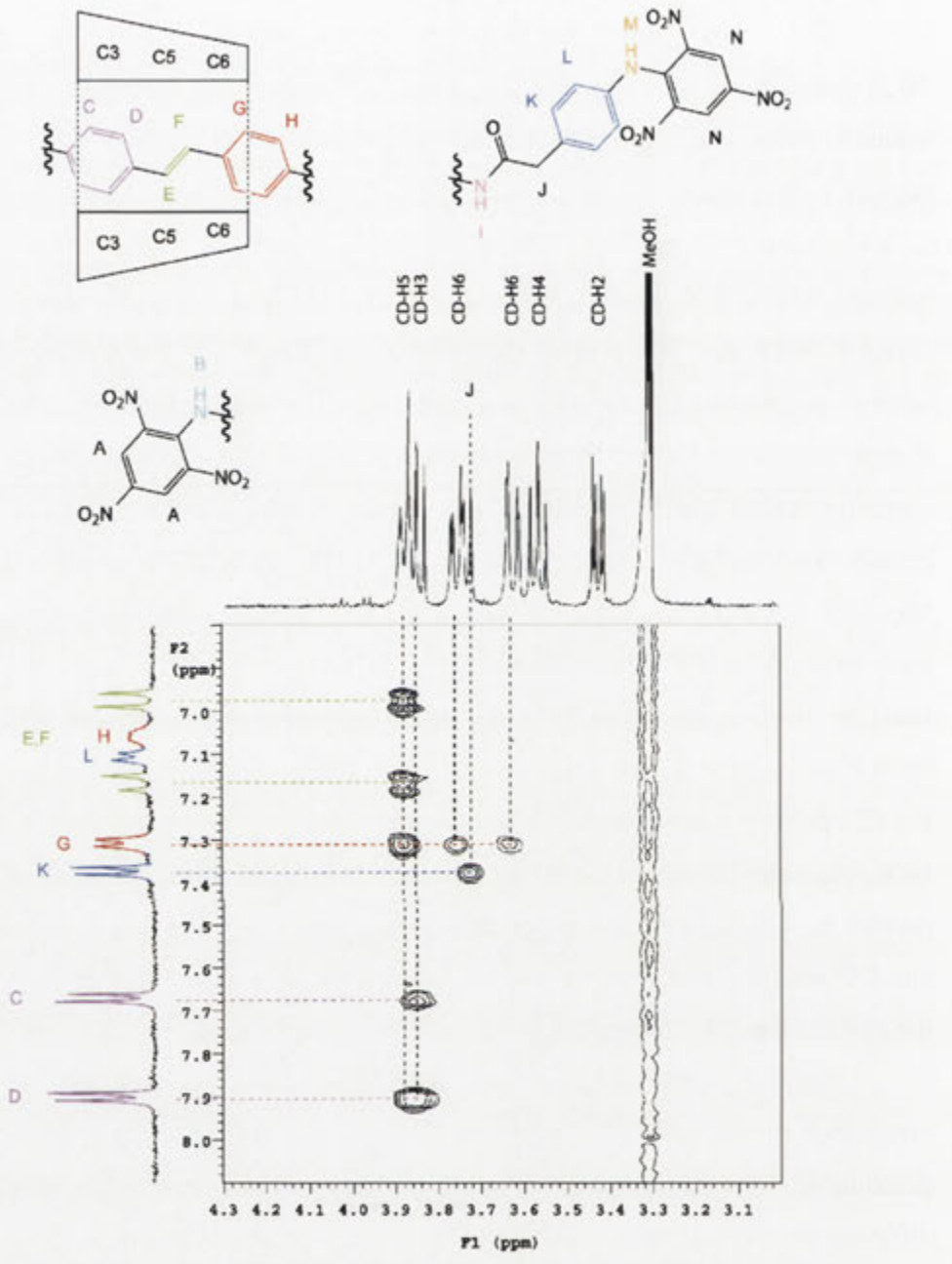

Figure 2.11. A section of the 500 MHz ROESY spectrum of the [2]-rotaxane **2.13** in d_4-methanol at 25 °C of the region where crosspeaks are observed between axle and cyclodextrin proton signals.

Many approaches were considered to determine the orientation of the CD for each of the [2]-rotaxanes **2.12** and **2.13** with some of them expected to be more problematic than others. One was to selectively modify the primary or secondary face of the CD with a group that would interact with the non-CD-bonded parts of the [2]-rotaxane. However,

because of the low yields often associated with CD modification, this method was deemed too difficult and a simpler idea was sought. A more straightforward solution would be to isomerise the [2]-rotaxane to its *cis*-isomer. If the CD then shifted onto the phenyl group, the direction of the CD might then be determined and hence the orientation of the parent *trans*-isomer would be known. This was attempted but the results were all but simple as is reported in the next chapter. The final strategy was the simplest of the three and proved to be the most effective. In the study by Isnin and Kaifer,[73] they were able to determine the orientation of their isomeric CD [2]-rotaxanes **2.16** and **2.17** by observing through space interactions between the signals of the amide protons of the axle and the alcohols of either the primary or secondary face of the CD. Because the previous conformational analysis of the isomeric [2]-rotaxanes **2.12** and **2.13** was carried out in d_4-methanol, their amine, amide and hydroxyl protons underwent deuterium exchange with the solvent. This removed their signals from the ^{1}H NMR spectrum. Therefore if a non-exchangeable solvent such as d_6-DMSO was used, it was anticipated that deuterium exchange would not occur enabling further NOE interactions in the ROESY spectrum to be seen that would identify the orientation of the CD in the [2]-rotaxane isomers **2.12** and **2.13**.

Looking firstly at the [2]-rotaxane **2.12** it can be seen that there are changes in the spectra resulting from the use of the non-exchangeable solvent d_6-DMSO. The DQCOSY spectrum of the CD region is shown in Figure 2.12. According to the review by Schneider *et al.*,[77] the CD-H1 proton signal in d_6-DMSO is found at 4.75 ppm. It has an interaction with the signal at 3.22 ppm due to the protons of CD-H2. This signal shows interactions with the signals of two sets of protons. The downfield signal at 5.44 ppm belongs to the CD-OH2 protons while the upfield signal is due to the CD-H3 protons located at 3.63 ppm. The signal of the CD-H3 protons show a further two interactions. Again the downfield signal is the result of the hydroxyl protons of CD-OH3 at 5.27 ppm while the upfield signal is from the CD-H4 protons at 3.45 ppm. The signal of the CD-H4 protons in turn shows a DQCOSY interaction with that of protons CD-H5 at 3.65 ppm. The characteristic strongly coupled CD-H6^A and CD-H6^B signals are found at 3.34 and 3.57 ppm. They both have an additional interaction with the downfield signal of the CD-OH6 protons at 4.34 ppm.

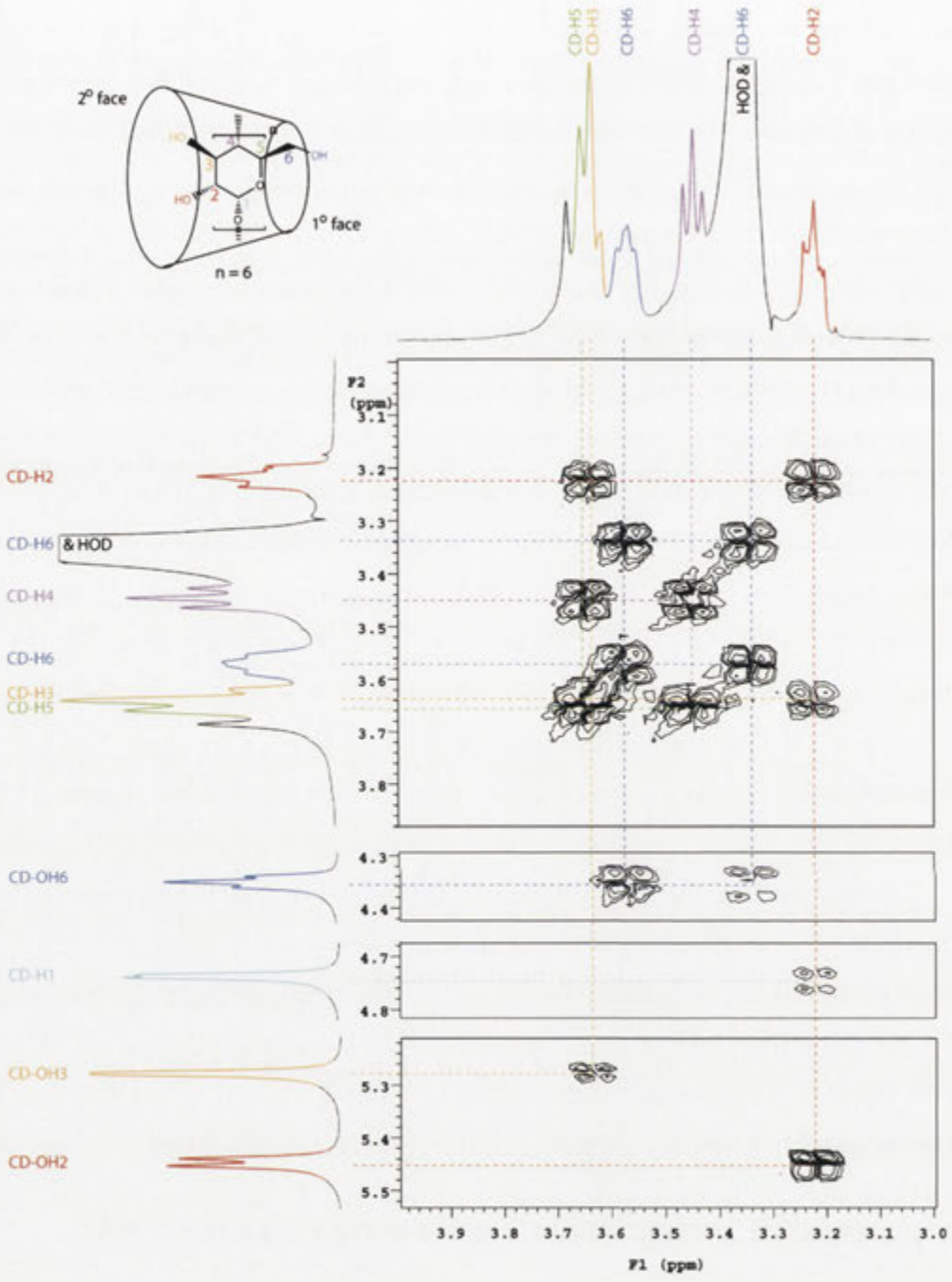

Figure 2.12. A section of the 500 MHz DQCOSY spectrum of the [2]-rotaxane **2.12** in d_6-DMSO at 25 °C of the region where crosspeaks are observed between cyclodextrin proton signals.

As in the previous assignments, the next step was to identify the aromatic signals of the axle protons. The DQCOSY and ROESY contour plots for the aromatic region of the spectrum of the [2]-rotaxane **2.12** are found in Figure 2.13 and Figure 2.14. From the

DQCOSY spectrum, no new crosspeaks arose due to the non-exchangeable solvent. The pairing of aromatic protons was undertaken as previously through the interactions of their signals. Interactions between the signals of the olefinic E and F protons are identifiable along with those of the aromatic G and H, and K and L protons. The multiplet over the region of 6.90-7.15 ppm has an integration of 7 H in comparison with the other sets of resonances. It can therefore be assumed that both the C and D signals are also found in the broad multiplet along with the L and F signals.

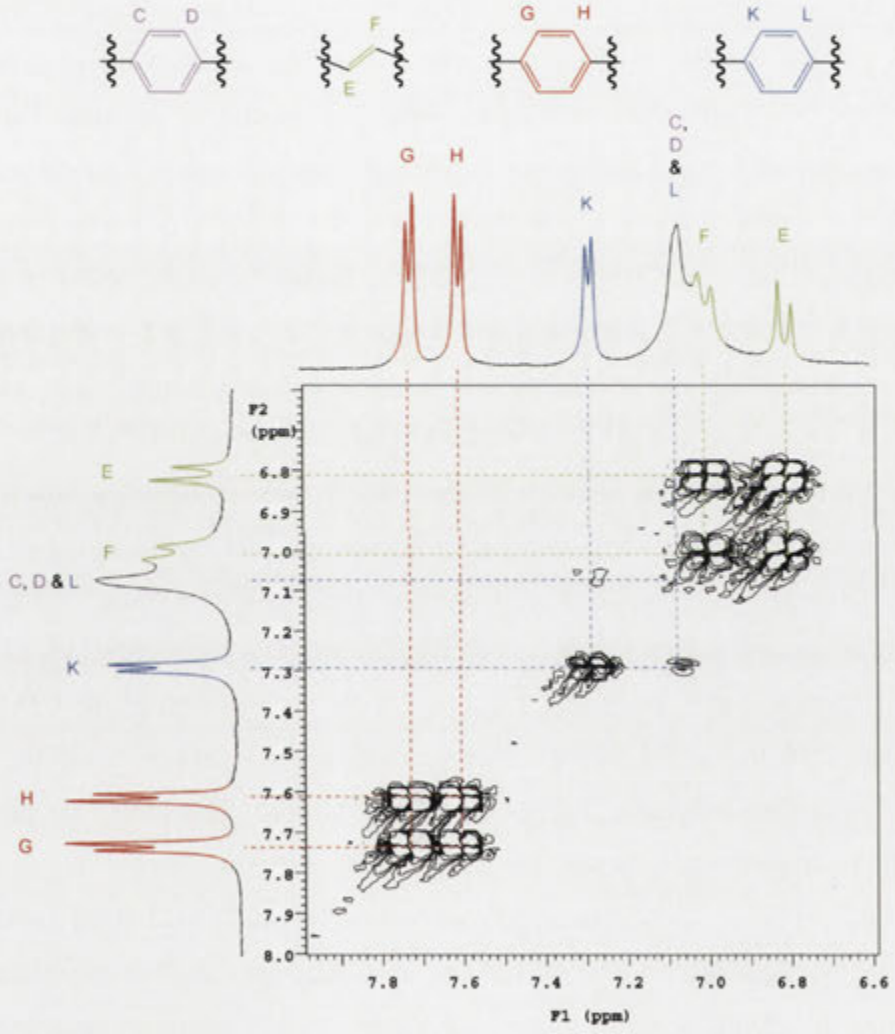

Figure 2.13. A section of the 500 MHz DQCOSY spectrum of the [2]-rotaxane **2.12** in d_6-DMSO at 25 °C of the region where crosspeaks are observed between axle protons.

From the ^{1}H ROESY NMR spectrum of the same axle region, shown in Figure 2.14, the emergence of a new peak led to the orientation of the stilbene unit in the axle

being determined. The new signal is found at 10.22 ppm and must be due to a nitrogen coupled proton from either of the secondary amines B or M or the amide proton I. This signal has NOE interactions with both the signals of the H and K aromatic protons and must therefore be the result of the amide proton I. Because the protons of the amines B and M are at the extremities of the axle, they could only interact with one coupled set of aromatic protons. In fact the secondary amine proton signals were not detected in the ^{1}H NMR spectrum. This is presumably because the corresponding protons rapidly exchange on the NMR time scale and cannot be observed. From the assignment of the H and K aromatic protons, the rest of the axle was assigned. The signal of the H protons shows both a DQCOSY and NOE interaction with that of the G protons. Further NOE interactions with the signals of the olefinic protons E and F established the relationships of the stilbene unit in the axle as shown in Figure 2.14. As the H aromatic protons belong to the stilbene, the K and hence the L aromatic protons must be found in the second binding unit. Unlike the previous conformational analyses, the arrangement of the stilbene in relation to the second binding unit was thus identified. This enabled the orientation of the CD in the [2]-rotaxane **2.12** to be determined, as follows.

To determine the CD orientation, the ROESY NOE interactions between the axle and CD signals were then investigated with the contour plot shown in Figure 2.15. The signals corresponding to the CD protons are found on the x-axis while the signals of the axle protons are on the y-axis. It was established from the assignment of the [2]-rotaxane **2.12** in d_4-methanol that the K and L protons were not included in the CD. Therefore from Figure 2.15, the signals of the stilbene protons C or D and not that of the L protons show an interaction with the signals of the CD-H6 protons. This places the primary face of the CD on the stilbene unit near the trinitrophenyl blocking group. The signals of the protons G and H both show interactions with those of the CD-H3 and CD-H5 protons. This places the secondary face of the CD on the stilbene unit near the central amide bond of the axle. The CD of the [2]-rotaxane **2.12** is therefore positioned on the stilbene unit of the axle as its protons only show interactions with those of the stilbene unit. It is orientated as shown by the structure in Figure 2.15 where the secondary face of the CD is directed towards the secondary binding unit.

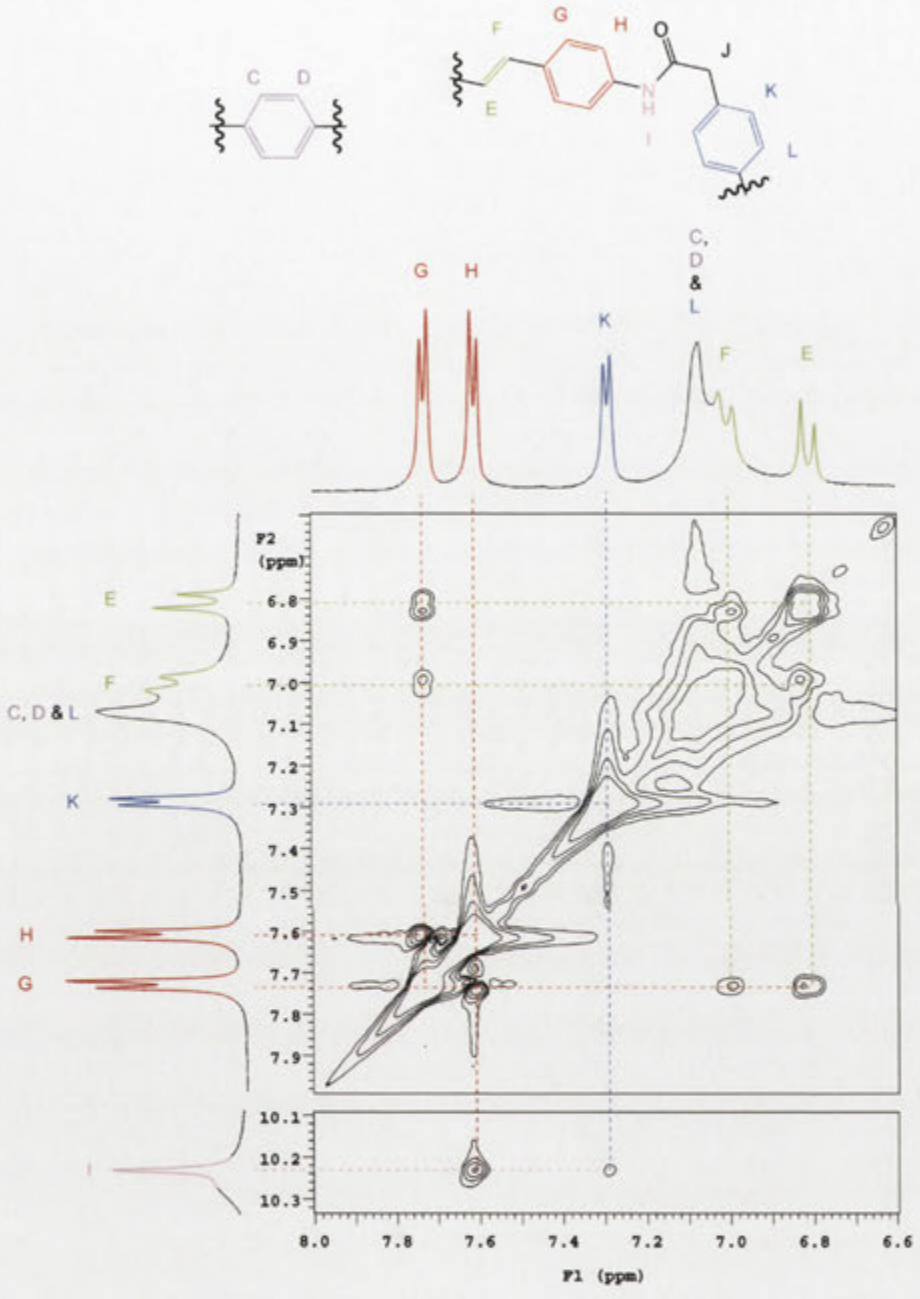

Figure 2.14. A section of the 500 MHz ROESY spectrum of the [2]-rotaxane **2.12** in d_6-DMSO at 25 °C of the region where crosspeaks are observed between axle proton signals.

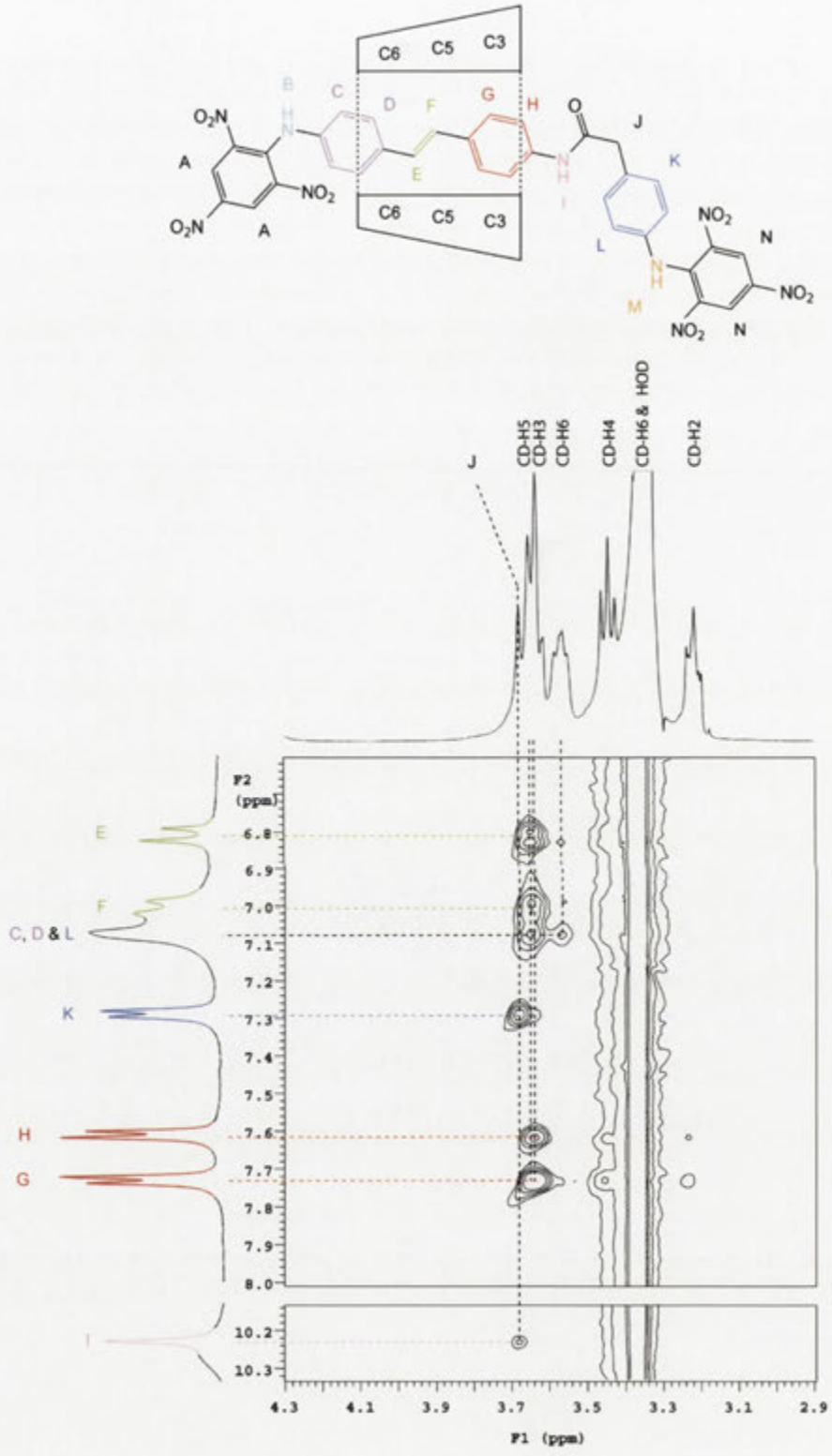

Figure 2.15. A section of the 500 MHz ROESY spectrum of the [2]-rotaxane **2.12** in d_6-DMSO at 25 °C of the region where crosspeaks are observed between axle and cyclodextrin proton signals.

With the orientation of the CD on the axle of the [2]-rotaxane isomer **2.12** deciphered, the [2]-rotaxane **2.13** was also subjected to the 2D NMR study in d_6-DMSO. This was to ascertain whether the CD faced the opposite direction to confirm the two [2]-rotaxanes **2.12** and **2.13** were orientational isomers. The assignment again started with the DQCOSY spectrum of the CD region which is found in Figure 2.16. As before, DQCOSY interactions originating through the downfield signal of the protons CD-H1 were used to completely assign each of the CD protons.

The axle was next assigned using the ROESY contour plot of the aromatic region shown in Figure 2.17. The key interactions that determined the axle assignments of the [2]-rotaxane **2.12** were also seen for the [2]-rotaxane **2.13**. The signal of the amide proton I is again shown, registering at 10.24 ppm. It shows NOE interactions with the signal of the stilbene protons H and the long range interaction with the signal of the K aromatic protons of the second binding unit. Further NOE interactions of the signals of the H stilbene and K aromatic protons enable all axle assignments to be determined as shown in Figure 2.17.

The ROESY 2D NMR contour plot that shows NOE interactions between the CD and axle proton signals is shown in Figure 2.18. The signals on the y-axis are attributed to the aromatic protons while those of the CD protons can be found on the x-axis. The orientation and location of the CD for the [2]-rotaxane **2.13** was determined through the interactions of the stilbene protons E, F and H. The signal of the protons H shows clear NOE interactions with the CD-H6^A and CD-H6^B signals while the signals of the E and F protons only show interactions with those of the CD-H3 or CD-H5 signals. As the signal of the H aromatic proton has previously shown a NOE interaction with the amide proton signal of I in Figure 2.17, the primary face of the CD is therefore situated near the amide bond centrally over the axle with the secondary face pointing towards the rest of the stilbene unit. This structure is shown and is confirmed by the remaining NOE interactions shown in the ROESY contour plot in Figure 2.18.

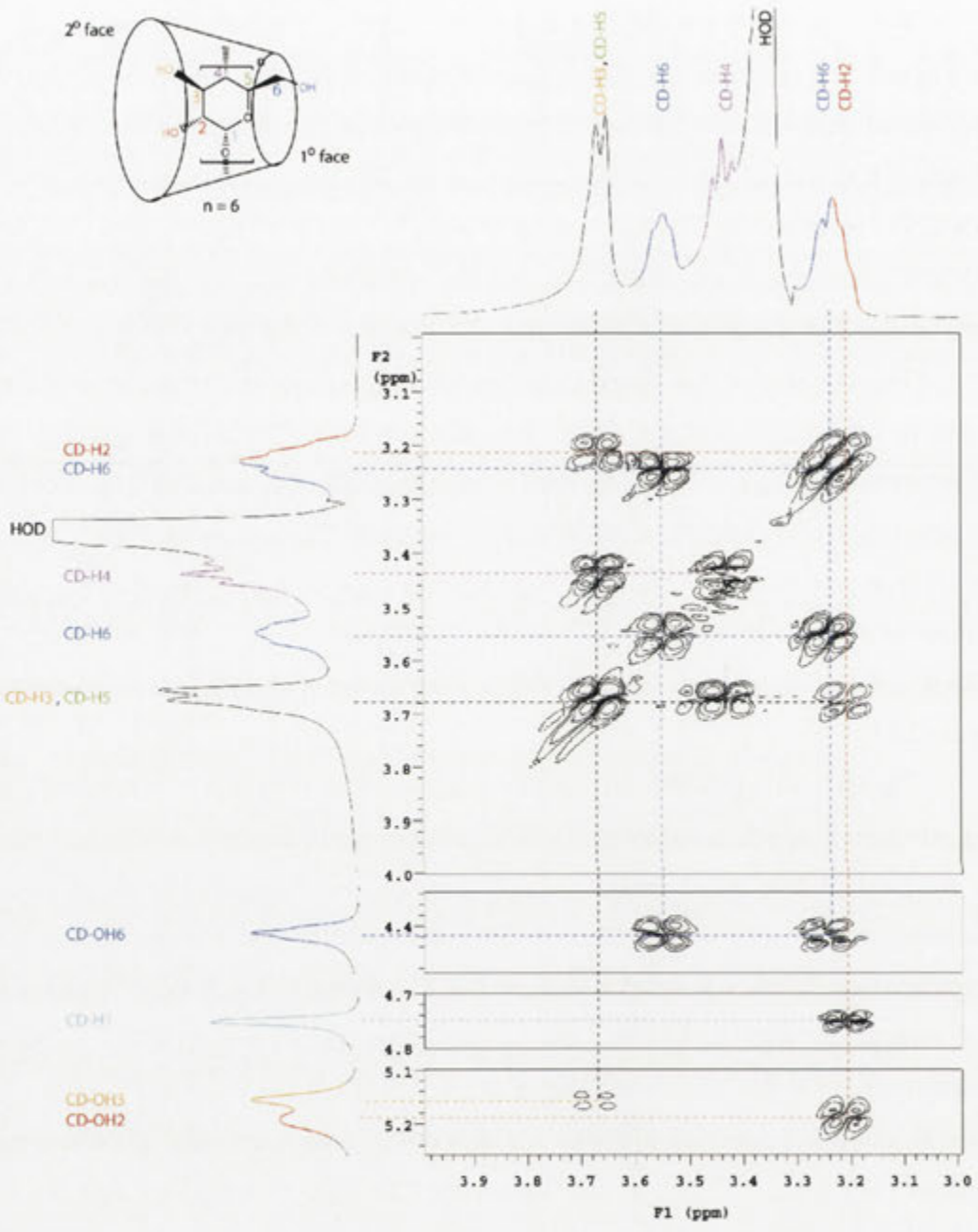

Figure 2.16. A section of the 500 MHz DQCOSY spectrum of the [2]-rotaxane **2.13** in d_6-DMSO at 25 °C of the region where crosspeaks are observed between cyclodextrin proton signals.

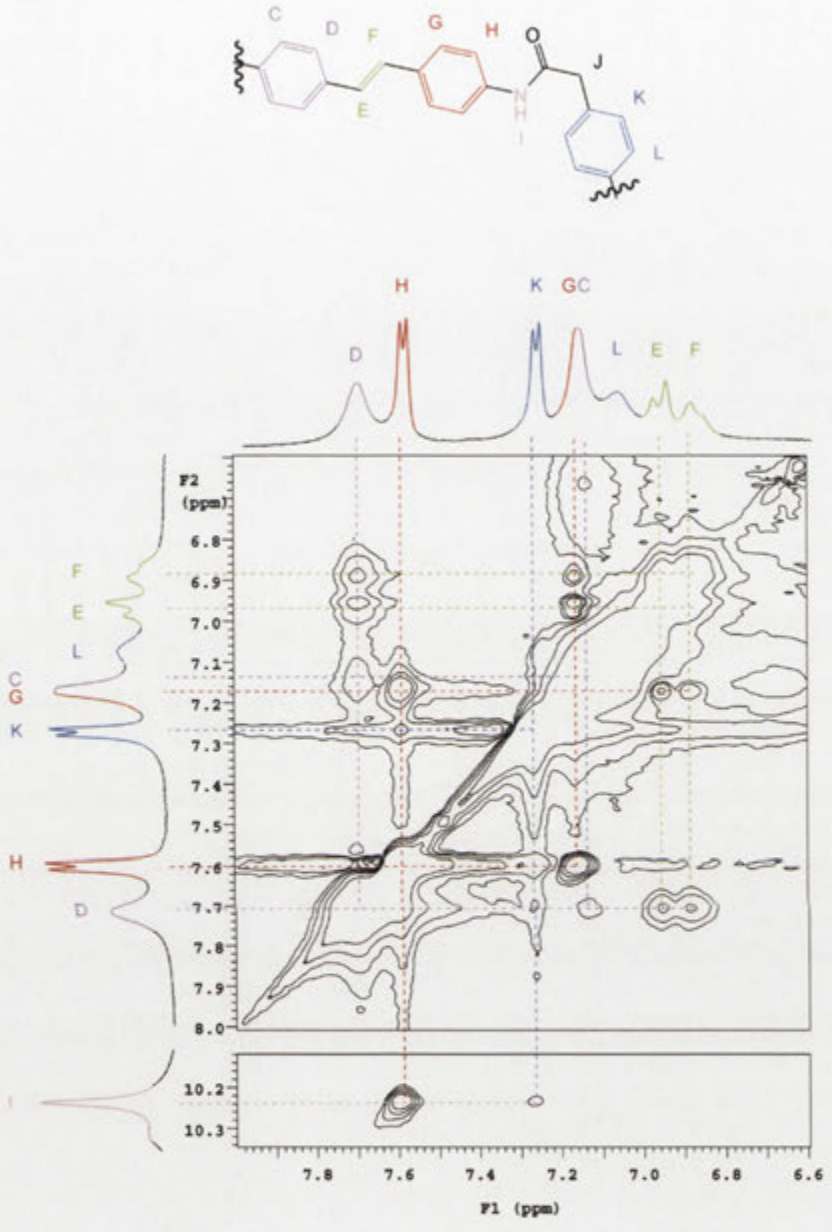

Figure 2.17. A section of the 500 MHz ROESY spectrum of the [2]-rotaxane **2.13** in d_6-DMSO at 25 °C of the region where crosspeaks are observed between axle proton signals.

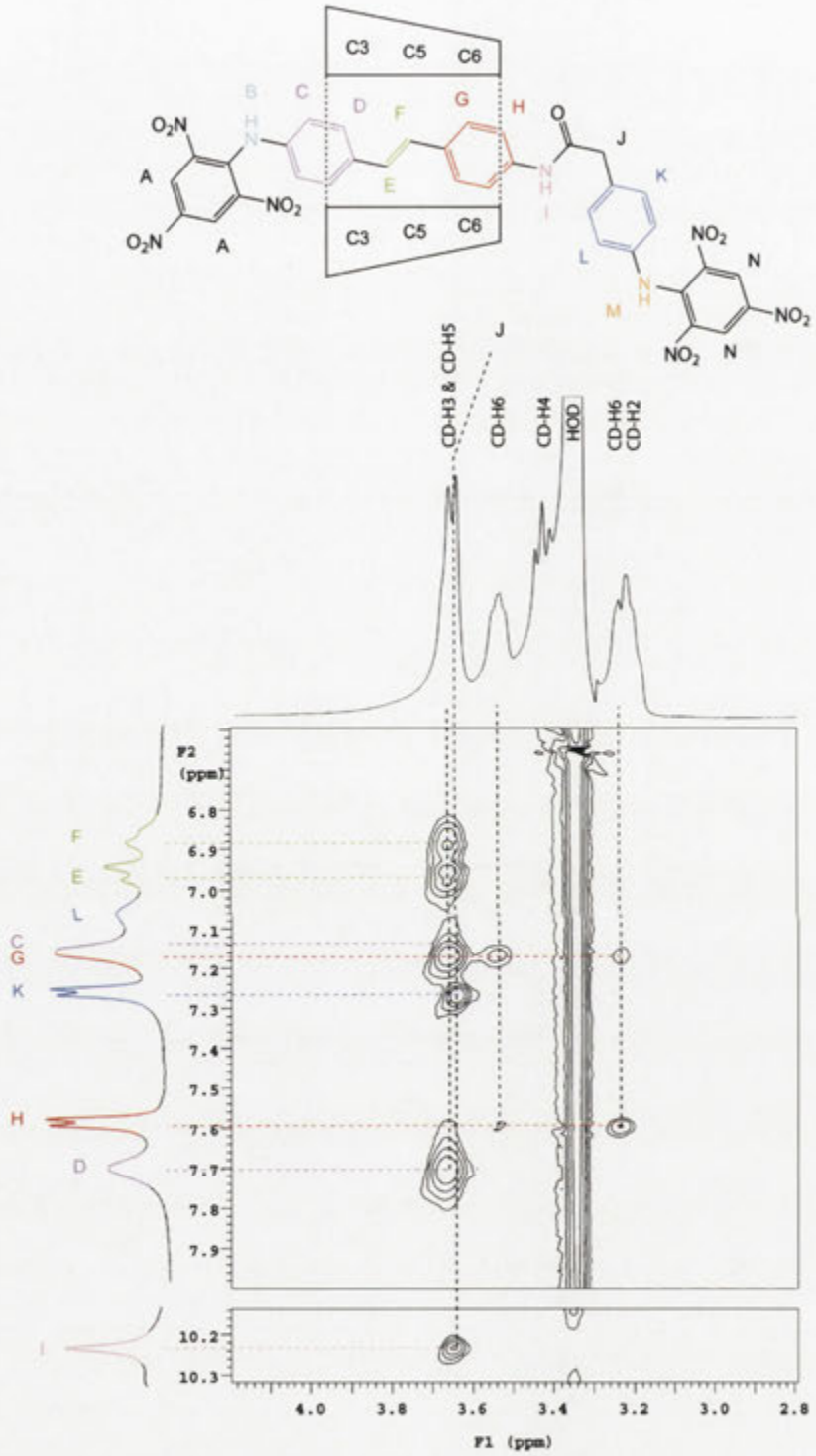

Figure 2.18. A section of the 500 MHz ROESY spectrum of the [2]-rotaxane **2.13** in d_6-DMSO at 25 °C of the region where crosspeaks are observed between axle and cyclodextrin proton signals.

In summary, the isolated two [2]-rotaxanes **2.12** and **2.13** are orientational isomers. In both cases the CD resides on the stilbene unit of the axle due to its stronger binding affinity in comparison to the phenyl based second binding unit. The structures of the isomeric [2]-rotaxanes after 2D NMR assignment are shown in Figure 2.19. The isomer **2.12** has the secondary face of the CD pointing towards the second binding unit while the isomer **2.13** has the primary face of the CD pointed towards the second binding unit. While the orientation was not able to be deciphered by NMR spectroscopy using d_4-methanol, the use of the solvent d_6-DMSO prevented exchange of the amide proton I allowing the full axle assignment and hence the conformational analysis to be completed.

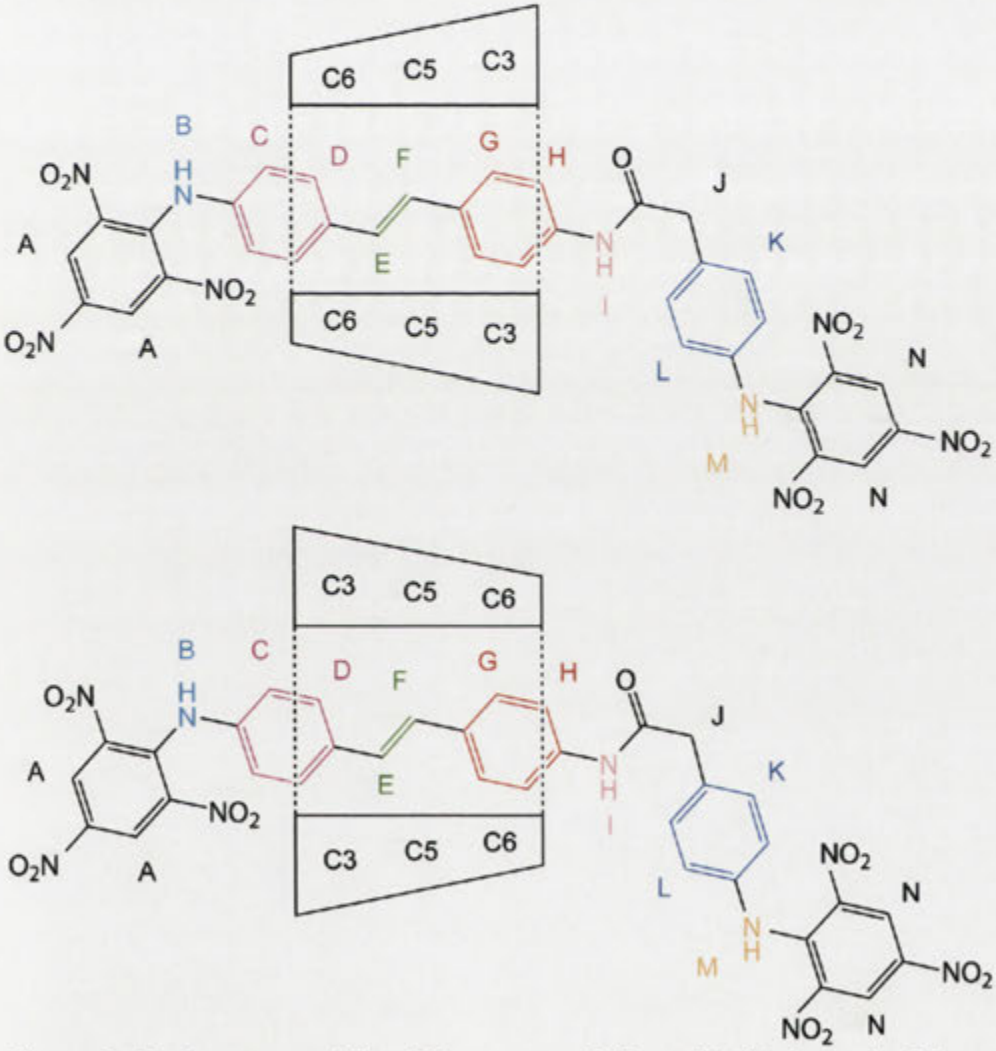

Figure 2.19. Structures of the [2]-rotaxanes **2.12** and **2.13** determined through ^{1}H 2D NMR assignment.

Chapter 3: Investigating the Potential of α-Cyclodextrin [2]-Rotaxanes as Molecular Shuttles

In the work described in the previous chapter the CD [2]-rotaxanes **2.12** and **2.13** were successfully synthesised using trinitrophenyl blocking groups. The conformations of these molecules were determined using 2D NMR spectroscopy and confirmed to be orientational isomers. With the conformational analysis completed, the photochemistry of the stilbene units was investigated to determine whether the isomers would act as molecular shuttles. This study was first carried out on the [2]-rotaxane **2.12** as shown in Scheme 3.1, but before the study could be undertaken, the wavelengths for irradiation had to be determined.

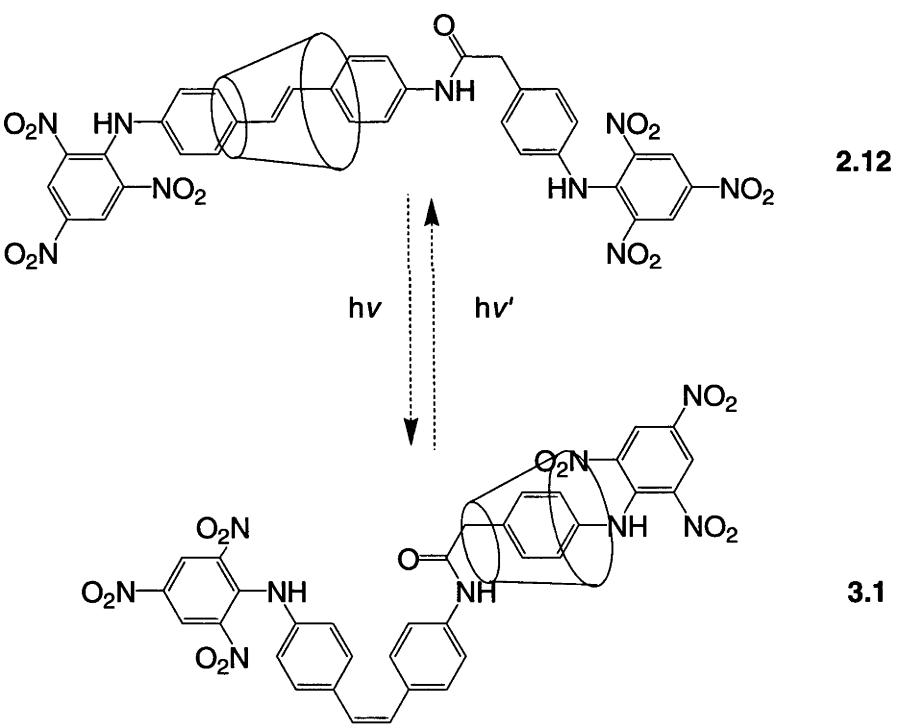

Scheme 3.1. Proposed behaviour of the [2]-rotaxane **2.12** as a molecular shuttle.

Isomerisation of a *trans*-stilbene proceeds by the selective excitation of the compound near its λ_{max} at a wavelength of light that is away from the λ_{max} of the *cis*-isomer. The reverse can be performed to reproduce the *trans*-isomer. In the isomerisation

of the *trans*-[2]-rotaxane **1.41** by Stainer *et al.*[67] as shown in Scheme 1.9 to produce the *cis*-isomer **1.42**, 340 nm light was used. This wavelength is near the λ_{max} of the *trans* [2]-rotaxane **1.41** where the *cis*-isomer **1.42** has very little absorbance. The reverse reaction used 265 nm light where the *cis*-isomer **1.42** had an increased absorbance while the absorbance of the *trans*-isomer **1.41** was diminished.

To determine the wavelengths required for the investigation into the isomerisation of the [2]-rotaxane **2.12**, its UV/visible spectrum was examined and interpreted. It is shown as the black line in Figure 3.1 for a 2.42×10^{-5} M solution in MQ H_2O. From the spectrum the λ_{max} at 338 nm is attributed to the *trans*-stilbene unit while the trinitrophenyl blocking group unit is responsible for the λ_{max} at 393 nm. For the isomerisation the three available sources of light were 254 nm, 300 nm and 350 nm fluorescent lamps. It was expected that the *cis*-isomer **3.1** would have a UV/visible spectrum similar to that of the [2]-rotaxane **1.42** where the maximum absorbance would be at around 265 nm. The 350 nm source was used as it was closest to the maximum absorbance of the *trans*-stilbene and was thought to be a wavelength where the expected *cis*-isomer **3.1** would not absorb so intensely. Because the [2]-rotaxane **2.12** has a diminished absorbance at about 280 nm in the UV/visible spectrum, the 254 nm source of light was used to attempt the reversal of the isomerisation to reform the *trans*-isomer **2.12**.

The attempted isomerisation was monitored using a combination of UV/visible spectroscopy and reverse phase analytical HPLC. A 3 cm^3 sample of the [2]-rotaxane **2.12** solution in MQ H_2O was irradiated with ten 350 nm lamps for a period of 24 hours in a sealed 10 mm i.d. quartz tube. At time intervals within this period the sample was analysed by UV/visible spectroscopy which spectra are seen as the red, orange, green and blue lines in Figure 3.1. The solution was then subjected to HPLC as shown in Figure 3.2. An attempt to reform the [2]-rotaxane **2.12** was undertaken by irradiation of the solution with ten 254 nm lamps for 15 minutes with an aliquot of the solution again subjected to HPLC.

Despite the long length of the irradiation with 350 nm light there was very little change in the UV/visible spectra shown in Figure 3.1. At the maximum absorbance of the *trans*-stilbene unit at 338 nm there was no change. From the HPLC traces shown in

Figure 3.2 it was determined that 52% of the starting material had been consumed after 24 hours irradiation. No significant new peaks arose as a consequence. After the irradiation with the 254 nm light the amount of the [2]-rotaxane **2.12** detected by HPLC decreased further to 41% of the original starting material as shown by the purple line in Figure 3.2.

It can therefore be concluded that the [2]-rotaxane **2.12**, upon irradiation near the λ_{max} of the *trans*-stilbene, did not form any of the *cis*-isomer **3.1**. After the irradiation, the λ_{max} at 338 nm, characteristic of the *trans*-stilbene unit, was largely unchanged. This means the *trans*-stilbene unit still existed. The decrease in the amount of the [2]-rotaxane **2.12** recorded by HPLC must therefore be due to the formation of other products containing the *trans*-stilbene unit. This is supported by the inability to reform the [2]-rotaxane **2.12**, as measured by HPLC, after irradiation with 254 nm light where the λ_{max} of the *cis*-isomer **3.1** was expected to be.

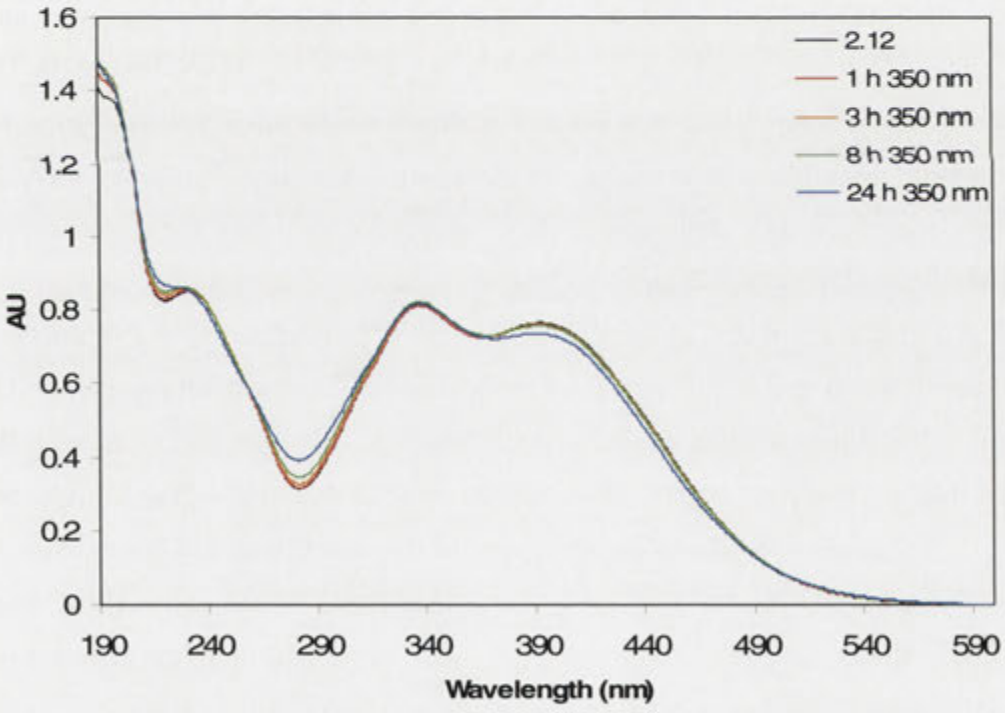

Figure 3.1. UV/visible spectra of a solution of the [2]-rotaxane **2.12** [2.42×10^{-5} M] in MQ H_2O and after exposure to 350 nm light.

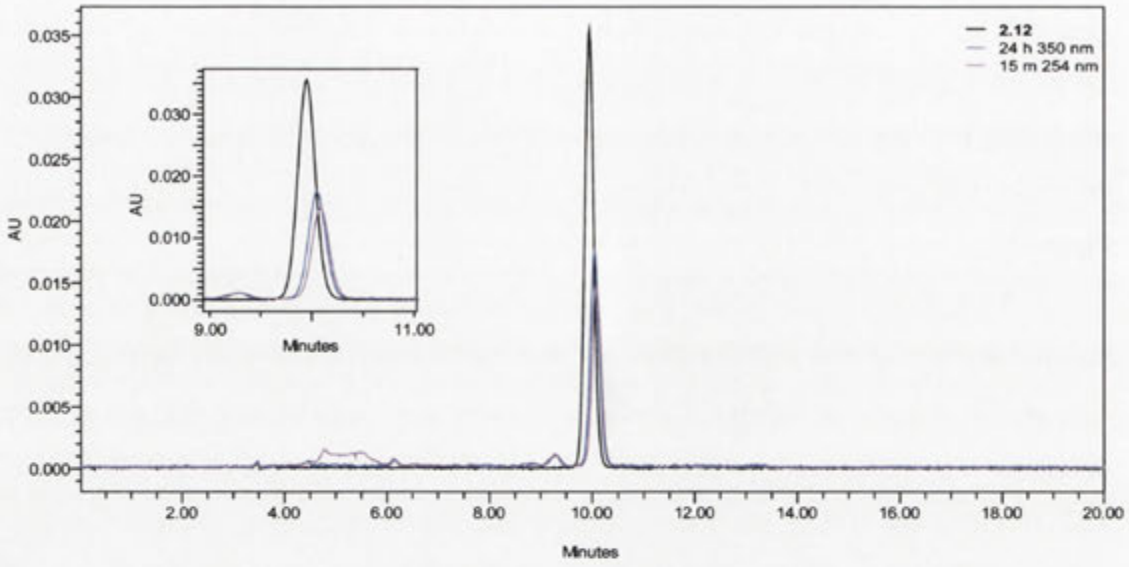

Figure 3.2. Reverse-phase HPLC chromatograms of the [2]-rotaxane **2.12** [2.42×10^{-5} M] in MQ H_2O before and after exposure to 350 and 254 nm light.

An attempt was also made to isomerise the [2]-rotaxane **2.13** to determine if the change in orientation of the CD had any affect on the isomerisation of the stilbene unit. For the photolytic study, the UV/visible spectrum of a 2.27×10^{-5} M solution of the [2]-rotaxane **2.13** in MQ H_2O was recorded and is shown as the black line in Figure 3.3. Because the spectrum appeared essentially the same as that of the [2]-rotaxane **2.12**, the same wavelengths of light and time lengths were used to study the isomerisation capabilities of the [2]-rotaxane **2.13**.

Upon irradiation of the [2]-rotaxane **2.13** over the 24 hour period at 350 nm, there was no significant change at the maximum absorbance of the *trans*-stilbene unit at 338 nm of the UV/visible spectrum as shown in Figure 3.3. From the HPLC trace of the irradiated material shown in Figure 3.4, it was determined that 60% of the [2]-rotaxane **2.13** was consumed in the reaction. The irradiation of the sample with 254 nm light for 15 minutes in an attempt to reform the [2]-rotaxane **2.13** is shown by the purple HPLC trace in Figure 3.4. The irradiation caused a further decrease in the amount of the [2]-rotaxane **2.13** to 35% of the original amount as determined through HPLC.

In similar results to the photolysis of the [2]-rotaxane **2.12**, the irradiation of the [2]-rotaxane **2.13** at 350 nm did not result in the formation of any *cis* material. This was indicated by the unchanged λ_{max} of the irradiated [2]-rotaxane **2.13** solution by

UV/visible spectroscopy. As was the case for the [2]-rotaxane **2.12**, the decrease in the amount of the [2]-rotaxane **2.13** as determined through HPLC indicated the formation of other unknown *trans*-stilbene containing products. This reaction was unable to be reversed by the irradiation of the solution with 254 nm light.

The stilbene units of each of the [2]-rotaxanes **2.12** and **2.13** were therefore unable to reversibly isomerise. The [2]-rotaxanes **2.12** and **2.13** were instead presumably converted to other *trans*-stilbene containing products. The desired formation of molecular shuttles powered by the isomerisation of a stilbene unit therefore failed in these cases. In the work of Stainer *et al.*,[67] the stilbene unit of the [2]-rotaxane **1.41** was able to be isomerised to form the *cis*-isomer **1.42** to shuttle the CD to a different part of the molecule. The main difference between the [2]-rotaxane **1.41** and the [2]-rotaxanes **2.12** and **2.13** is the type of blocking group. The trinitrophenyl blocking group used for the [2]-rotaxanes **2.12** and **2.13** therefore probably ~~interrupts~~ the *trans* to *cis* isomerisation pathway to form other *trans*-stilbene containing products.

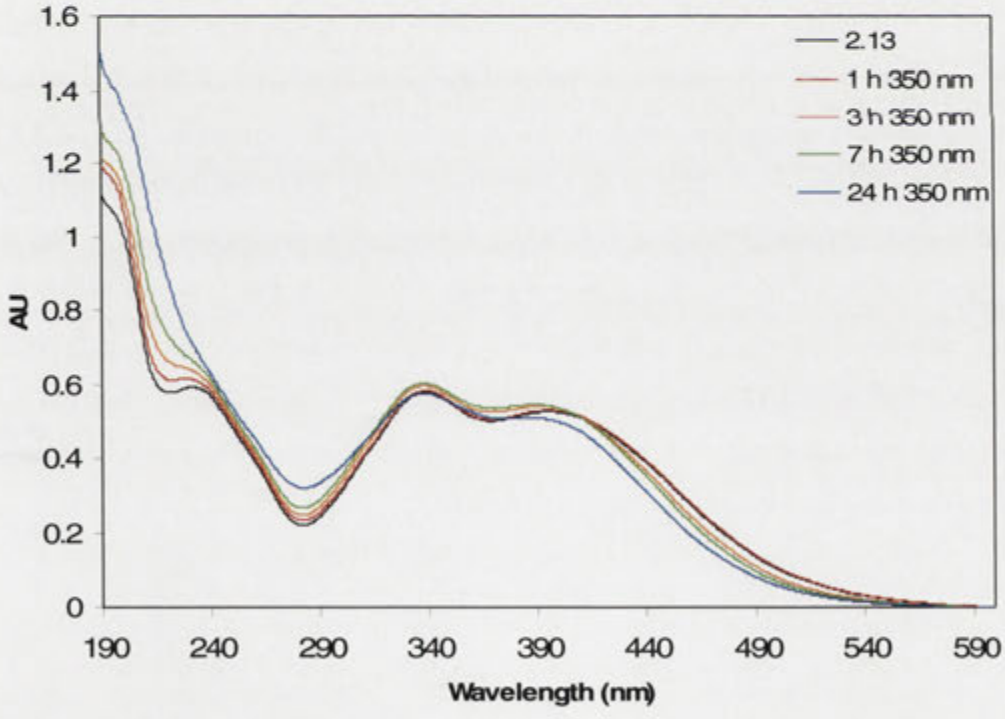

Figure 3.3. UV/visible spectra of a solution of the [2]-rotaxane **2.13** [2.27×10^{-5} M] in MQ H_2O and after exposure to 350 nm light.

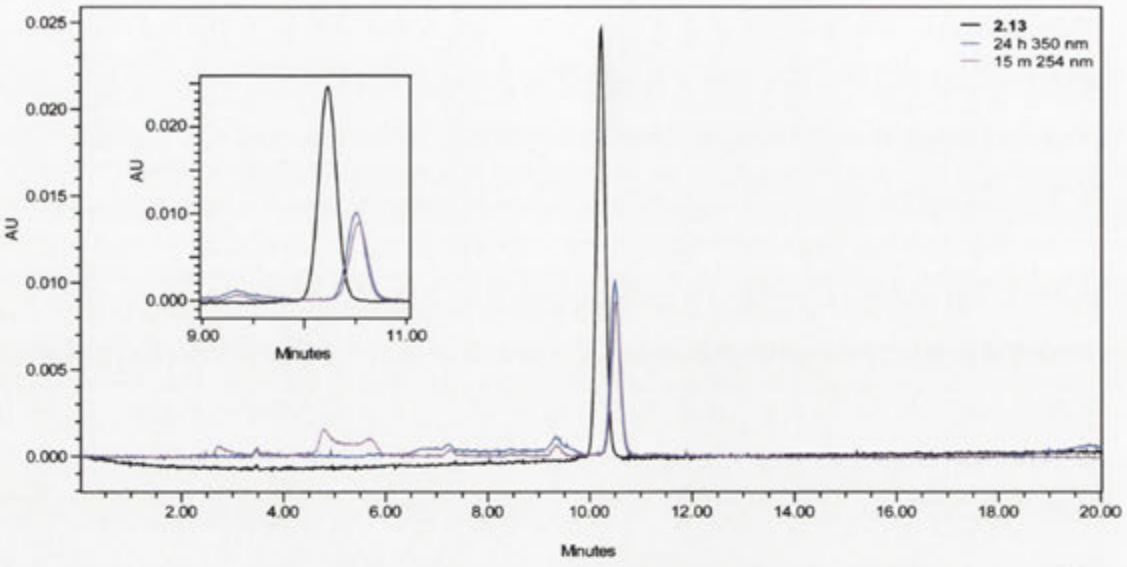

Figure 3.4. Reverse-phase HPLC chromatograms of the [2]-rotaxane **2.13** [2.27×10^{-5} M] in MQ H_2O before and after exposure to 350 and 254 nm light.

Alternative methods were therefore sought to utilise the [2]-rotaxanes **2.12** and **2.13** as potential molecular shuttles. One possibility that was considered was an acid-base control as used by Ashton *et al.*[78] and shown in Scheme 3.2. By adding either of the bases *i*-Pr_2NEt or Bu_3N, before subsequent addition of the acids CF_3CO_2H or TfOH, they were able to neutralise the secondary amine of the [2]-rotaxane **3.2** or protonate that of **3.3** to shift the dibenzo[24]crown-8 macrocycle to or from the 4,4'-bipyridinium binding group. In this case they altered the hydrogen bonding between the protonated amine and the ether oxygens to direct where the macrocycle was situated on the [2]-rotaxane. It was therefore considered what affect deprotonation of the secondary amines in each of the [2]-rotaxanes **2.12** and **2.13** would have on the location of the CD. The question was posed whether deprotonation of the amines would provide an attractive or repulsive ~~affect~~ effect with the CD causing it to move from the stilbene unit.

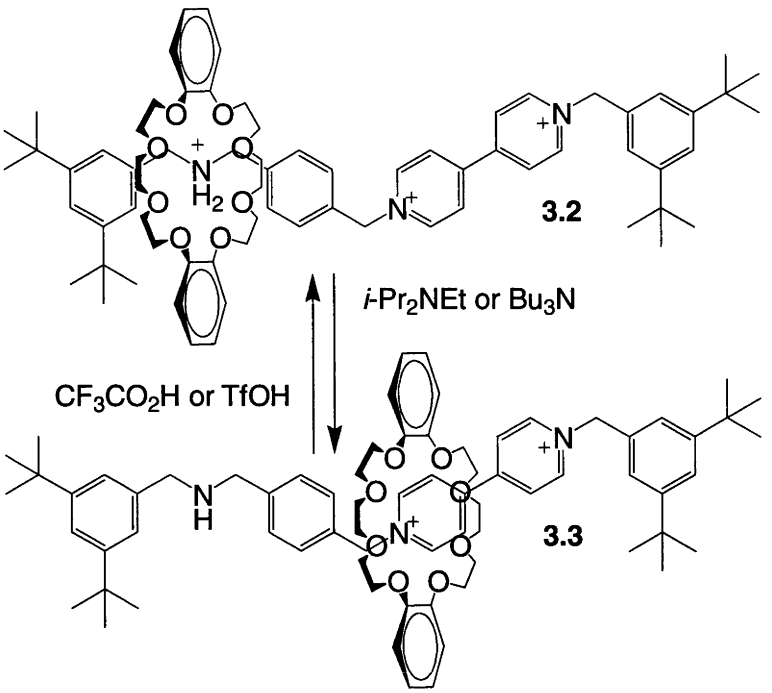

Scheme 3.2. An acid-base controlled molecular shuttle synthesised by Ashton *et al.*[78]

In the study by Easton *et al.*,[65] the secondary amines of the [2]-rotaxane **1.32** were determined to have pK_as of 9.3 and 9.6 through potentiometric titration. Their acidic nature is due to the electron withdrawing effects of the trinitrophenyl groups. With that system it was resolved that the deprotonation had no affect on the position of the CD. This was thought to be because the bulky trinitrophenyl groups at either end of the [2]-rotaxane **1.32** are close in space to the CD. The deprotonation of the secondary amines could have no affect as the CD would be prevented from moving due to the nearby blocking groups. As the [2]-rotaxanes **2.12** and **2.13** have a much greater distance between the blocking groups it was thought the deprotonation of the amines may enable attractive or repulsive forces to alter the CD location. The amines of the [2]-rotaxanes **2.12** and **2.13** were expected to have similar pK_as to those of the [2]-rotaxane **1.32** because they also have trinitrophenyl groups creating an electron withdrawing effect. Nevertheless a variable pH study was undertaken to examine this. The study was carried out on the isomer **2.12** by dissolving the compound in d_4-methanol to increase its solubility. As a consequence the measurements can only be considered as a rough guide to the actual pD as a true measurement requires an aqueous solution. The pD of the solution was then recorded with a micro combination pH electrode in an NMR tube

before a ^{1}H NMR experiment on the solution was performed. The pD was then adjusted with either NaOD or DCl solution and the ^{1}H NMR spectrum recorded again over the pD range of 3.6 to 11.4.

The ^{1}H NMR spectra of the aromatic region for the [2]-rotaxane **2.12** with changing pD are shown in Figure 3.5. Between a pD of 3.6 and 8.1 there is little change in the chemical shift of the signals of the aromatic protons. When the pD is elevated above 8.1 there are several upfield movements of the aromatic signals. The signals with the largest change in chemical shift are those belonging to the A and N protons with 0.47 ppm and 0.54 ppm upfield movements. The signals of the L and H protons also have large upfield movements of chemical shift. These movements have values of 0.40 and 0.39 ppm for the signals of the L and H protons respectively.

The upfield shift of the L and N signals is consistent with the loss of the amine proton M causing a shielding effect on the L and N protons through resonance. Loss of the amine proton B would also cause the upfield shift of the signal of the A protons, but it would also be expected to affect the signal of the protons C which are substantially unaffected. It may be that the CD twists the trinitrophenyl and amino groups out of coplanarity preventing the affect from the deprotonation registering on the aromatic protons C. The large shift of the signal of the protons H is also difficult to explain. The protons H are nearest to the amide proton I which would be expected to have a very large pK_a, based on the similar molecule phenylacetanilide, where the amide has a pK_a of 20.6.[79] The amide I should therefore not deprotonate even at the highest pD used for this study. The two inconsistencies are not due to an error in the assignment of the signals of the protons C and H, as a thorough re-examination established the assignments are correct.

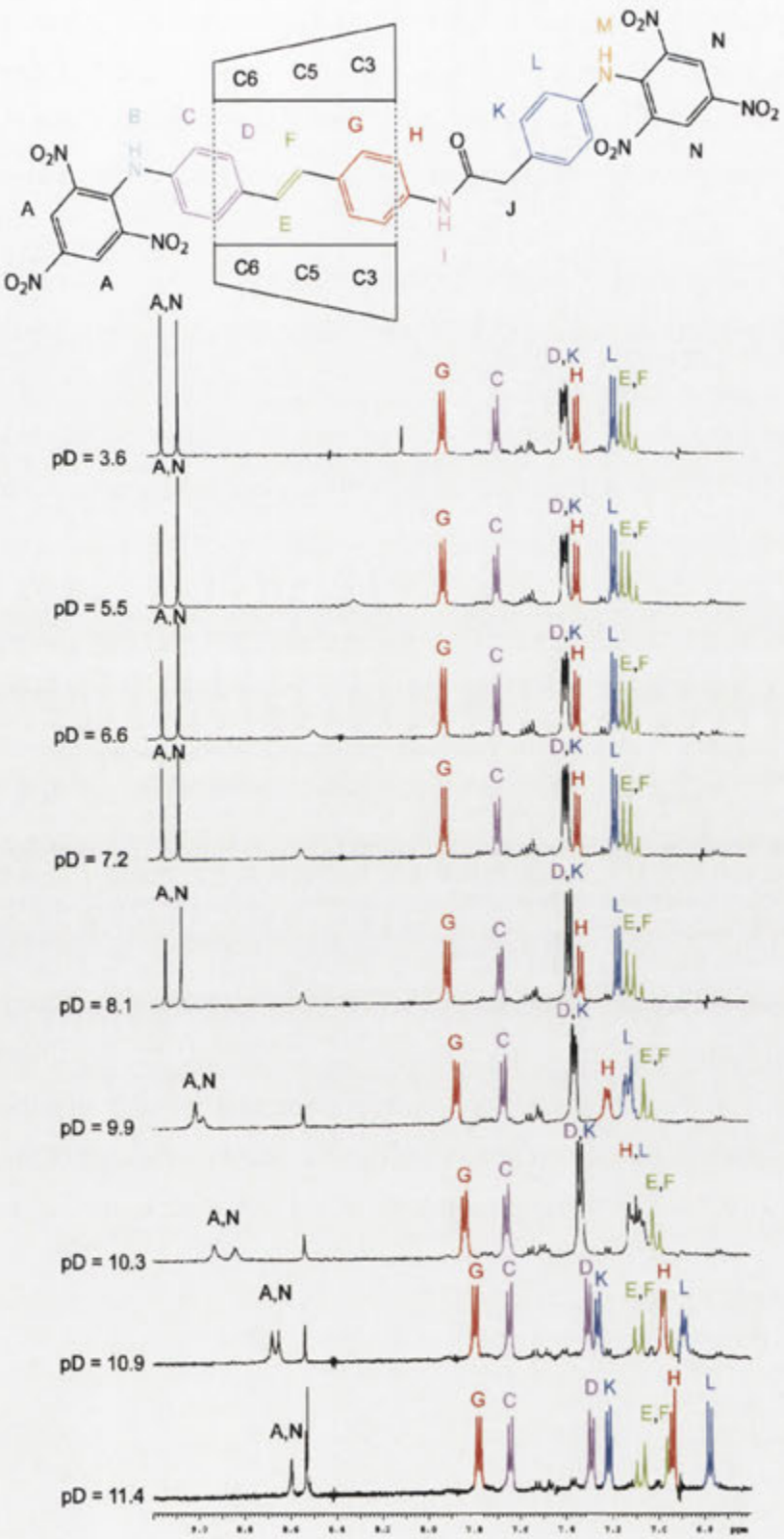

Figure 3.5. ^{1}H NMR spectra of the [2]-rotaxane **2.12** over the region of 6.6 ppm to 9.2 ppm in d_4-methanol with varying pD.

From the pD study of the [2]-rotaxane **2.12**, the secondary amines deprotonate at pD above 8.1. This conclusion is based on the similarity of the NMR signals in the pD range 3.6 to 8.1, before a large upfield shift of the signals of the A, L and N protons when the pD is raised above 8.1. To determine if the deprotonation of the secondary amines of the [2]-rotaxane **2.12** has any affect on the position of the CD, ROESY NMR spectroscopy was conducted on the [2]-rotaxane **2.12** at a pD of 7.8 and at 11.0. The pD of 7.8 was chosen as from the pD study the neutral species was expected to be present. The pD of 11.0 was chosen as from the pD study it was expected that the doubly deprotonated axle would be present. Also as the CD secondary alcohols have a pK_a of 12.33,[49] a pD lower than 12 was used to prevent their deprotonation complicating the study.

The 2D NMR spectra for the [2]-rotaxane **2.12** were first analysed at a pD of 7.8 to determine the conformation of the neutral species. The DQCOSY spectrum of the CD region is shown in Figure 3.6. The signals of the CD protons were assigned as in Chapter 2 from the DQCOSY interactions between the signals of the CD protons. The signals of the axle protons were then assigned using both the DQCOSY and ROESY 2D NMR contour plots of the region from 6.7 to 8.0 ppm found in Figures 3.7 and 3.8. The stilbene unit signals were assigned as described in Chapter 2. The ^{1}H ROESY contour plot shown in Figure 3.9 shows crosspeaks between the signals of the axle and CD annular protons which enables the location of the CD to be determined for the [2]-rotaxane **2.12** at a pD of 7.8. The plot gives clear evidence that the CD is situated on the stilbene unit of the axle with the signals of the C to H protons all showing interactions with those of the CD annular protons. The CD is therefore in the same location on the axle of the [2]-rotaxane **2.12** at a pD of 7.8 as it was when the pD was unadjusted in the work described in Chapter 2.

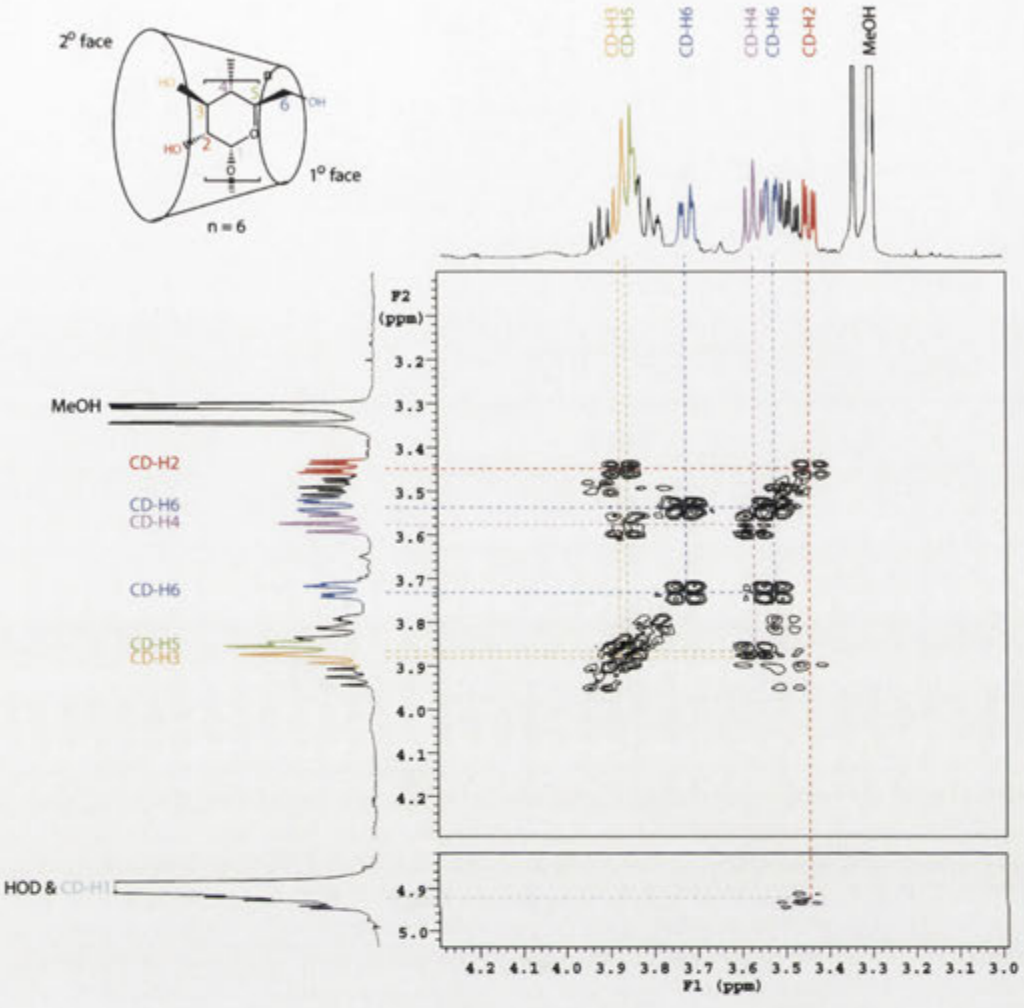

Figure 3.6. A section of the 500 MHz DQCOSY spectrum of the [2]-rotaxane **2.12** in pD 7.8 d_4-methanol at 25 °C of the region where crosspeaks are observed between the cyclodextrin proton signals.

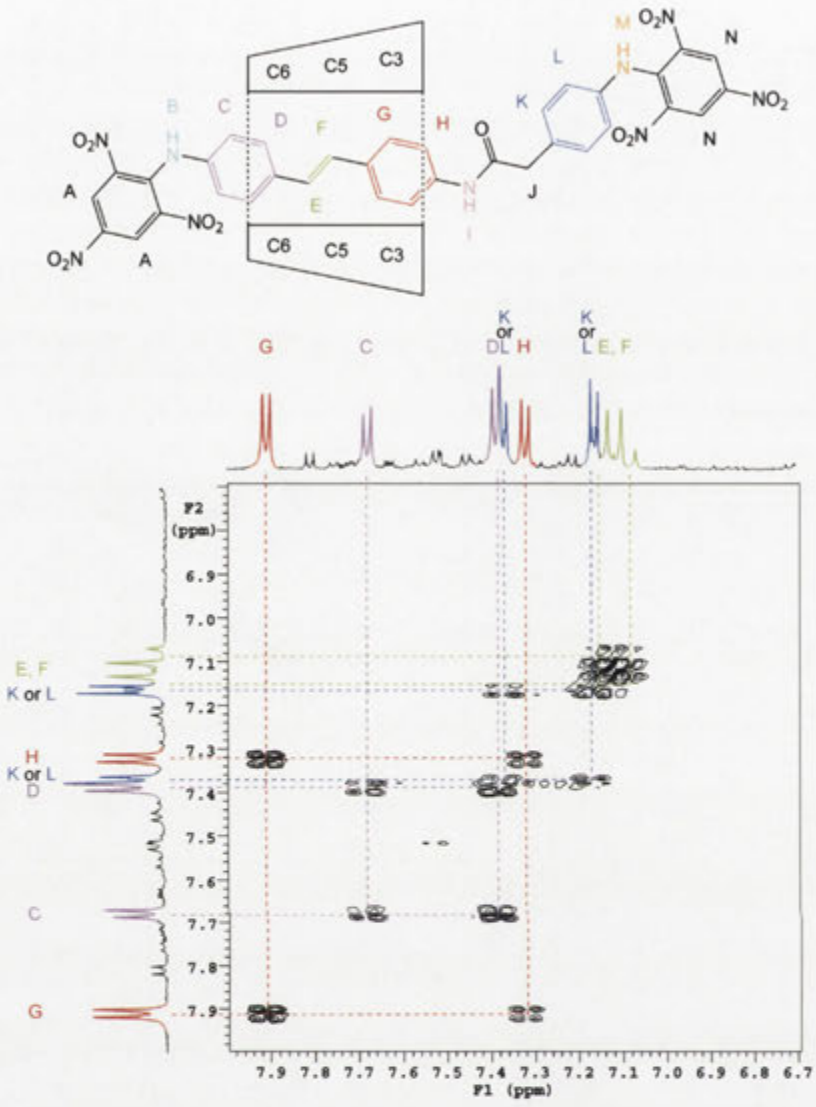

Figure 3.7. A section of the 500 MHz DQCOSY spectrum of the [2]-rotaxane **2.12** in pD 7.8 d_4-methanol at 25 °C of the region where crosspeaks are observed between axle proton signals.

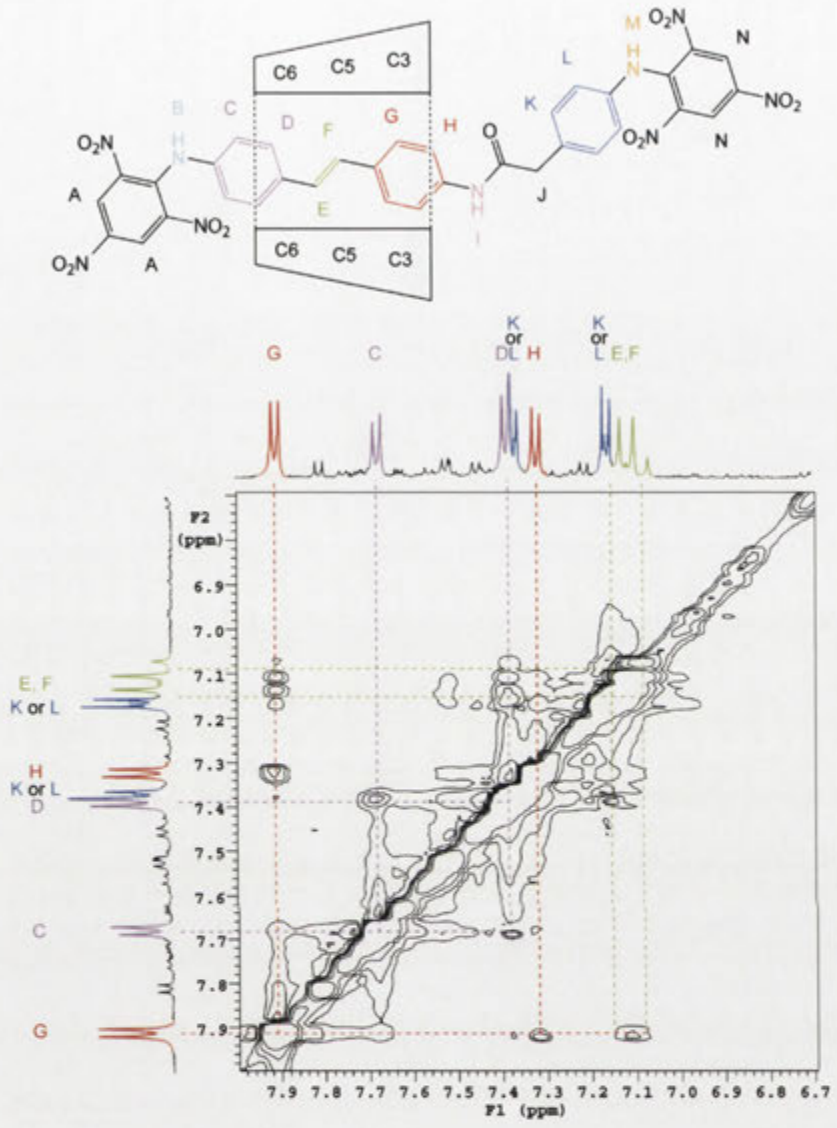

Figure 3.8. A section of the 500 MHz ROESY spectrum of the [2]-rotaxane **2.12** in pD 7.8 d_4-methanol at 25 °C of the region where crosspeaks are observed between the axle proton signals.

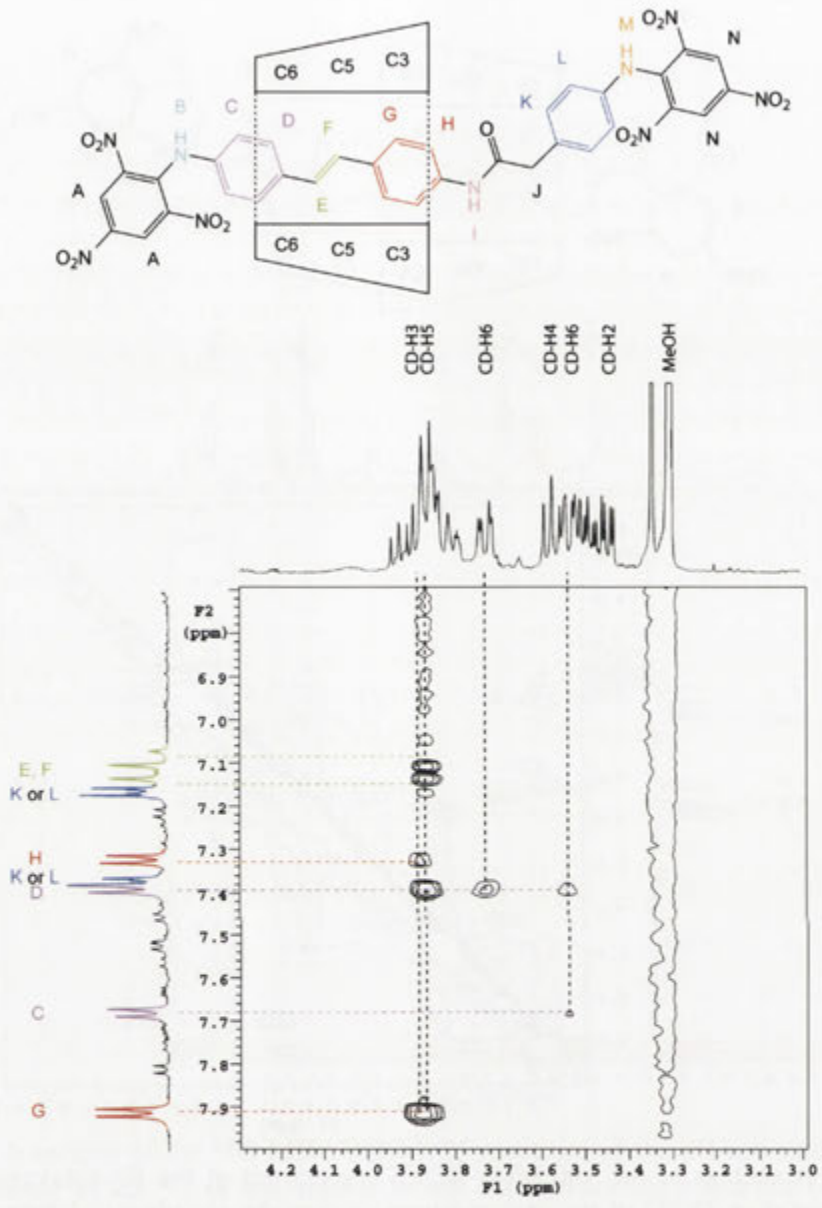

Figure 3.9. A section of the 500 MHz ROESY spectrum of the [2]-rotaxane **2.12** in pD 7.8 d_4-methanol at 25 °C of the region where crosspeaks are observed between axle and cyclodextrin proton signals.

The [2]-rotaxane **2.12** was next analysed at a pD of 11.0 to determine if the deprotonation of the secondary amines altered the position of the CD. The signals of the CD protons were firstly assigned using the DQCOSY spectrum of the CD region shown in Figure 3.10. The signals of the aromatic protons of the axle were again assigned using both DQCOSY and ROESY 2D NMR with their contour plots found in Figures 3.11 and 3.12. The ^{1}H ROESY contour plot found in Figure 3.13 shows crosspeaks between the

signals of the axle and CD annular protons of the [2]-rotaxane **2.12**. From the contour plot the signals of the D, E, F, G and H stilbene protons all show NOE interactions with those of the CD protons. From the NOE interactions the CD is positioned on the stilbene as shown in Figure 3.13. It follows that the deprotonation of the secondary amines by elevating the pD of the solution to 11.0 does not change the position of the CD from that determined for the neutral species at a pD of 7.8.

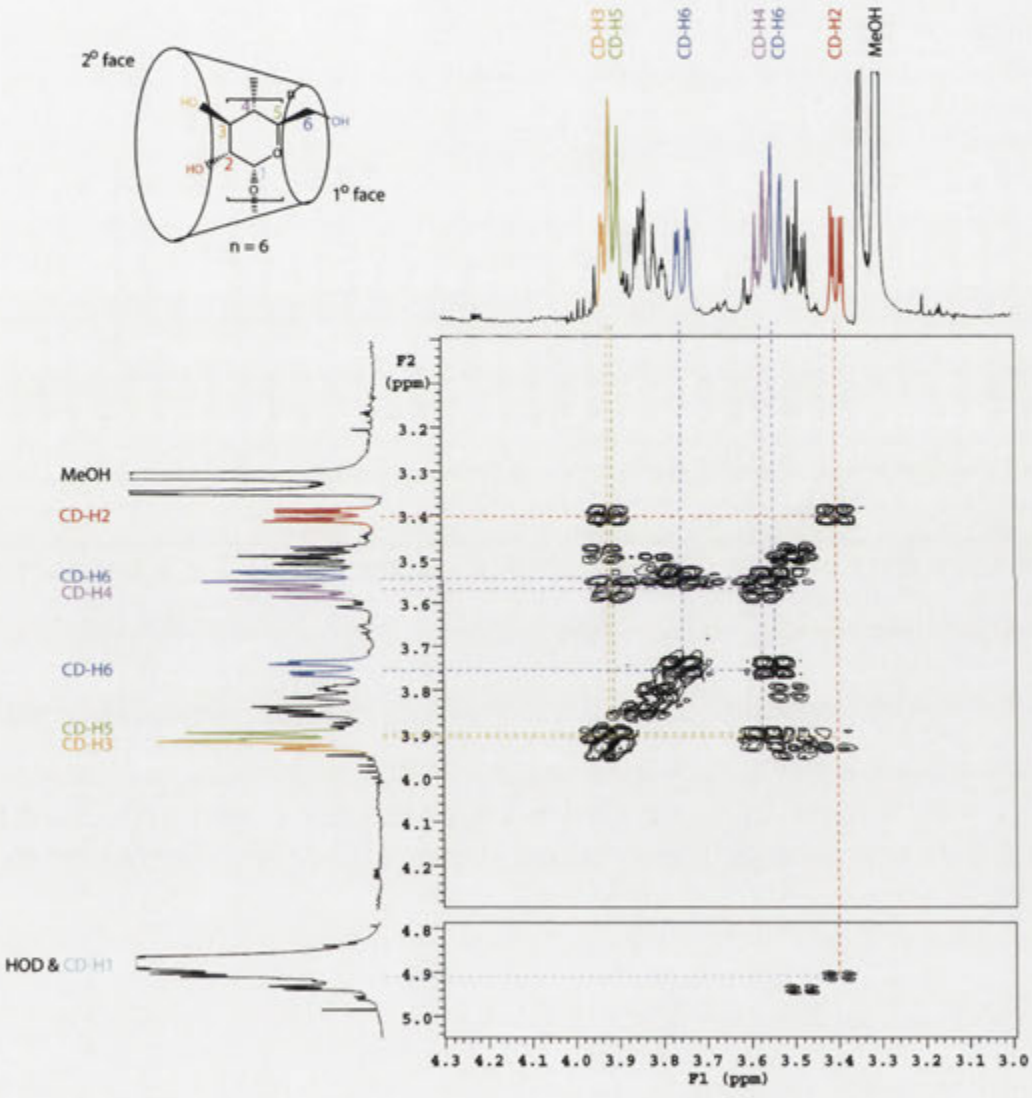

Figure 3.10. A section of the 500 MHz DQCOSY spectrum of the [2]-rotaxane **2.12** in pD 11.0 d_4-methanol at 25 °C of the region where crosspeaks are observed between the cyclodextrin proton signals.

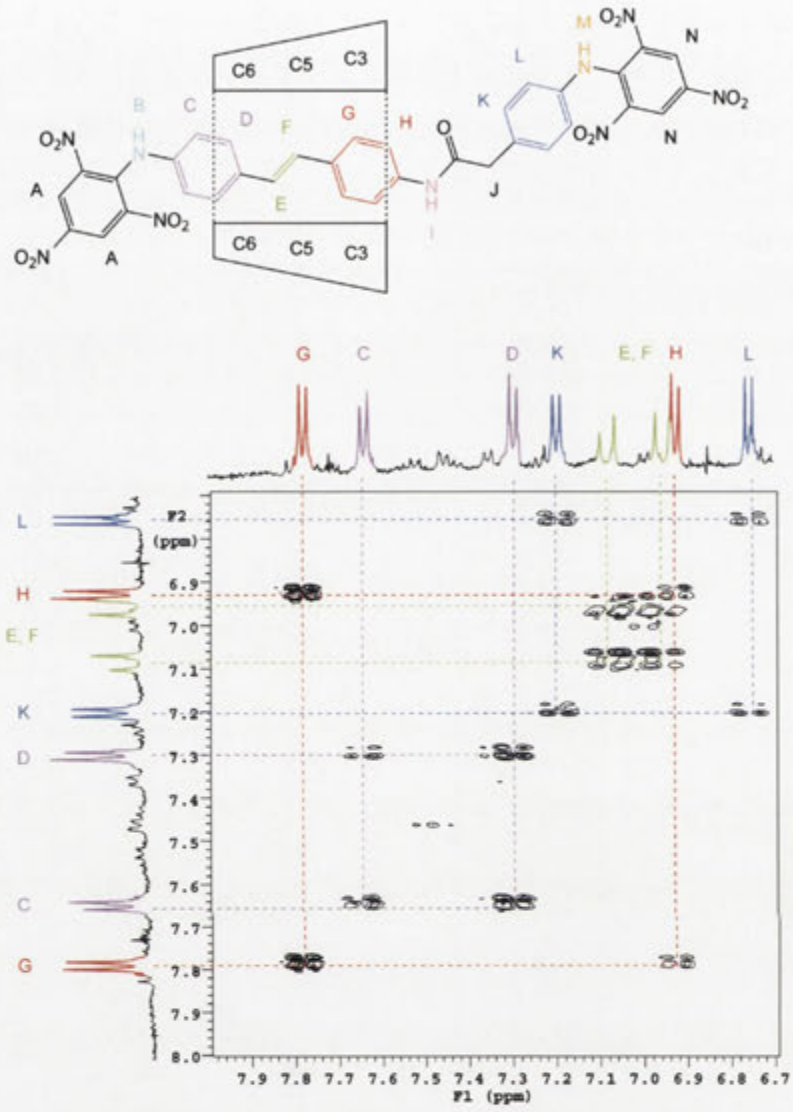

Figure 3.11. A section of the 500 MHz DQCOSY spectrum of the [2]-rotaxane **2.12** in pD 11.0 d_4-methanol at 25 °C of the region where crosspeaks are observed between axle proton signals.

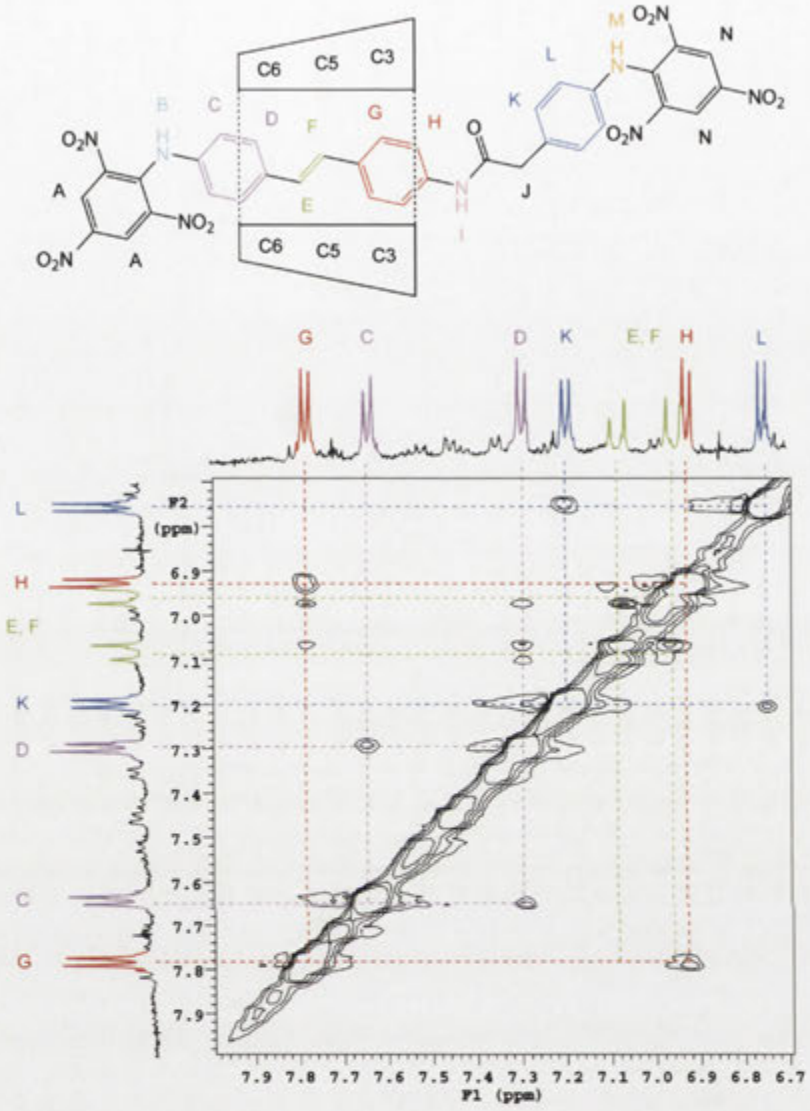

Figure 3.12. A section of the 500 MHz ROESY spectrum of the [2]-rotaxane **2.12** in pD 11.0 d_4-methanol at 25 °C of the region where crosspeaks are observed between the axle proton signals.

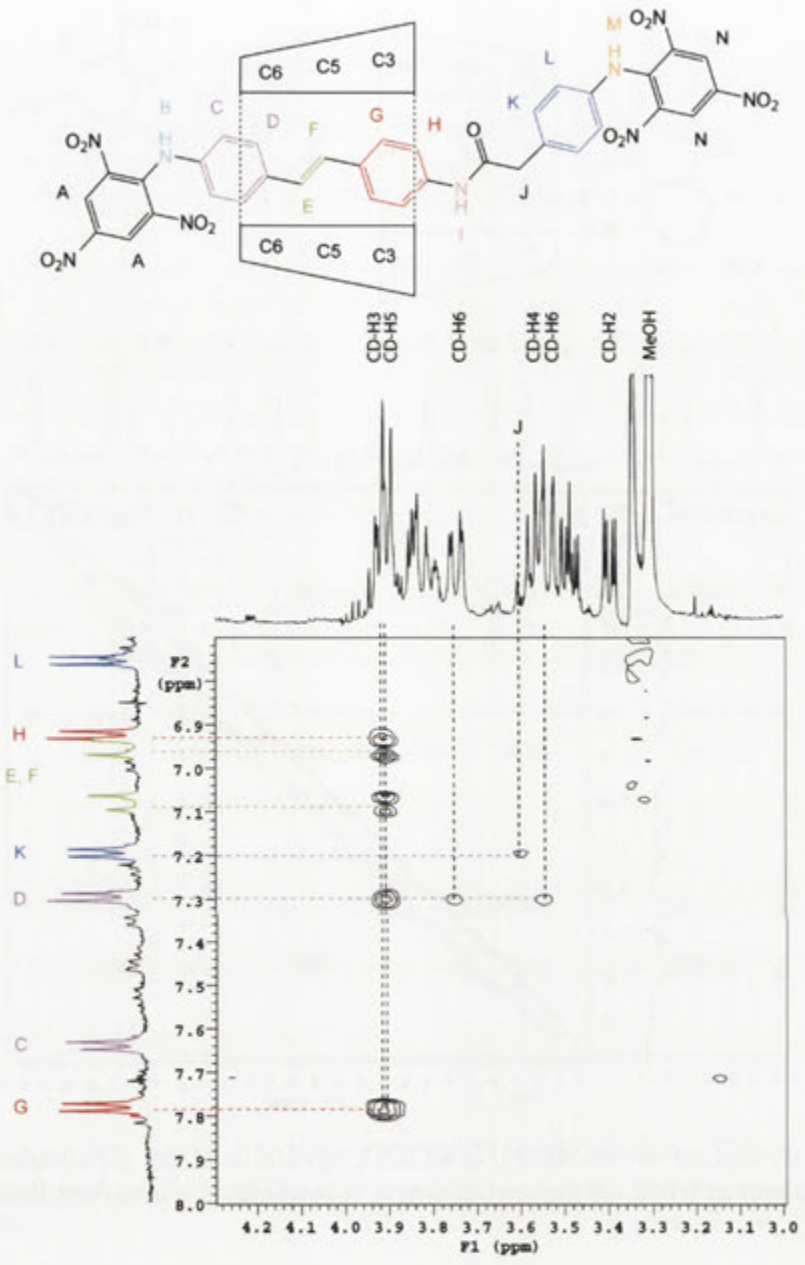

Figure 3.13. A section of the 500 MHz ROESY spectrum of the [2]-rotaxane **2.12** in pD 11.0 d_4-methanol at 25 °C of the region where crosspeaks are observed between axle and cyclodextrin proton signals.

Since the CD does not move as a result of adjusting the pD the [2]-rotaxane **2.12** is not an acid-base controlled molecular shuttle. A pD study on the [2]-rotaxane **2.13** was not conducted as it was anticipated that this [2]-rotaxane would show analogous

behaviour. Thus it was concluded that neither of the [2]-rotaxanes **2.12** nor **2.13** is suitable for use as either a photochemical or pH dependent molecular shuttle.

The difficulties with the photochemical isomerisation appear to stem from the use of the trinitrophenyl blocking groups. This conclusion is supported by the work of Cieslinski,[80] who reported the hermaphroditic [2]-rotaxane **3.4** as the basis of a molecular muscle, but found that upon irradiation it decomposed in preference to interconversion to and from the *cis,cis* form **3.5** (Scheme 3.3).

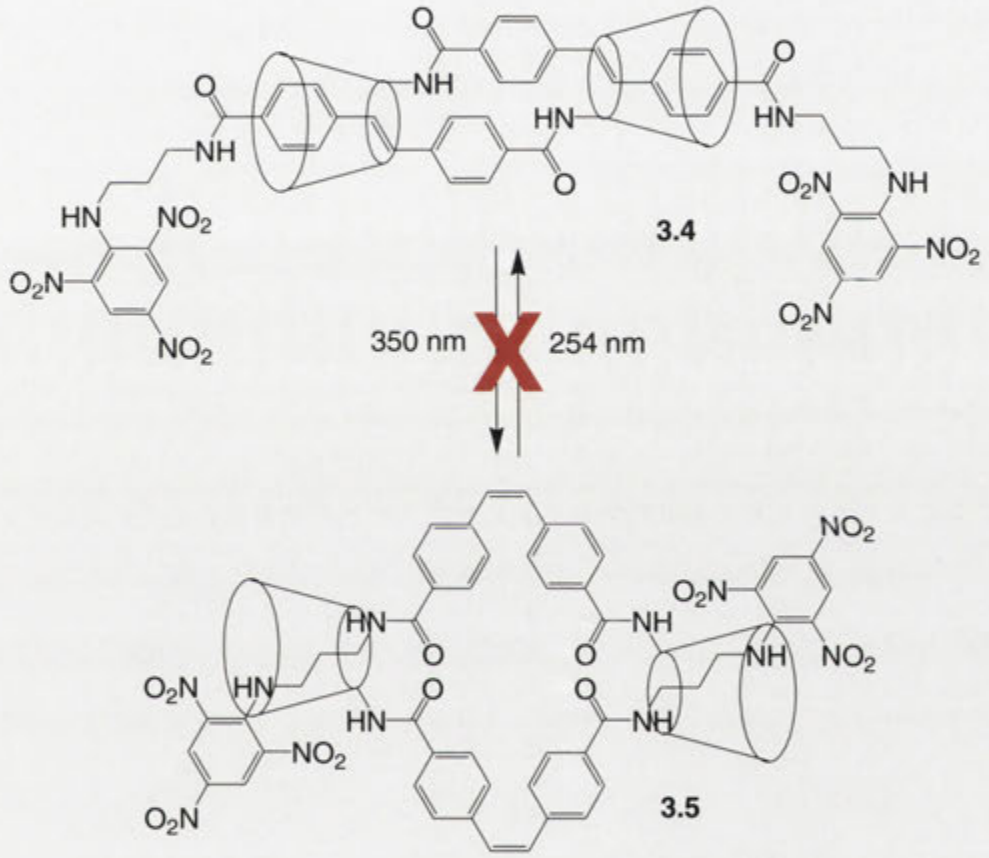

Scheme 3.3. Attempted isomerisation between the *trans,trans*-hermaphroditic [2]-rotaxane **3.4** and its *cis,cis* form **3.5**.

In light of these observations the use of the trinitrophenyl blocking group was abandoned. A related attempt to synthesise the hermaphroditic [2]-rotaxane **3.9**, as shown in Scheme 3.4, was also abandoned when difficulties were encountered with the synthesis. The succinic acid **3.6** had been made according to the procedure by Onagi,[57] which had been coupled to the amine **1.30** using DMT-MM to give the hermaphroditic CD **3.7**. Subsequent treatment with the blocking reagent **1.31** had resulted in the

formation of two products which were tentatively identified using MALDI mass spectrometry as the hermaphroditic CD **3.8** and the hermaphroditic [2]-rotaxane **3.9**. The dimer **3.9**, however, was only formed in a trace amount. The attempt to complete the synthesis and undertake photolysis studies was therefore stopped.

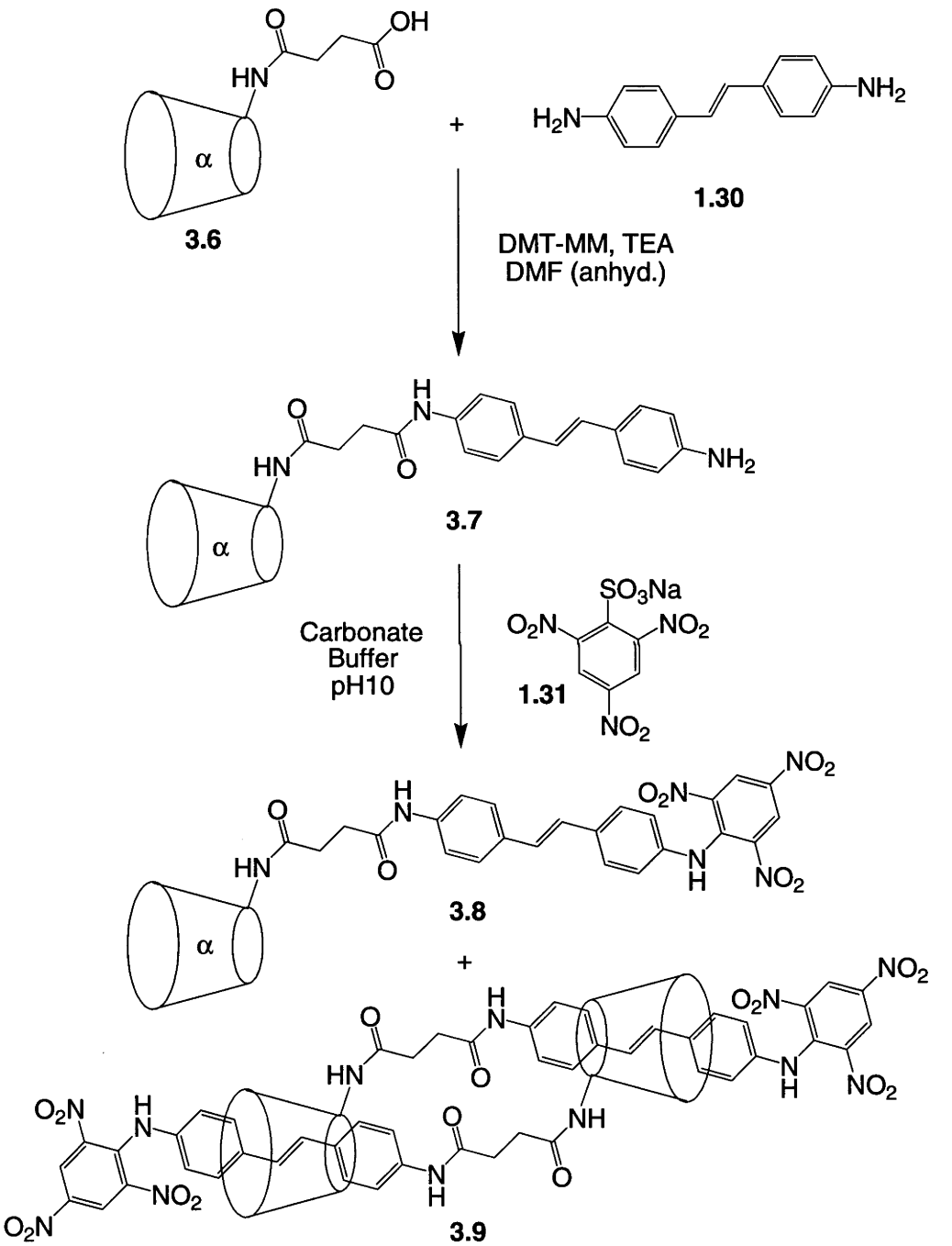

Scheme 3.4. Attempted synthesis of the hermaphroditic [2]-rotaxane **3.9**.

In summary trinitrophenyl blocked [2]-rotaxanes were found to be unsuitable as photochemical molecular devices. Alternative blocking groups were therefore sought to produce CD [2]-rotaxanes as molecular shuttles and muscles.

Chapter 4: 1,3-Dipolar Nitrile Oxide Cycloaddition in Attempted Synthesis of Hermaphroditic [2]-Rotaxanes

From the previous chapter, when the isomeric [2]-rotaxanes **2.12** and **2.13** were irradiated with light of various wavelengths, they did not undergo reversible isomerisation. It is thought that the trinitrophenyl groups interfere with the photochemistry of the stilbene unit. To overcome this problem, it was decided that alternative blocking groups would be investigated to attempt to synthesise a [2]-rotaxane with the ability to act as a molecular shuttle. One possibility that arose was the use of nitrile oxides in the capping of the [2]-rotaxanes.

When dipolarophiles in the form of alkenes or alkynes react with nitrile oxides they undergo [3+2] cycloadditions to form isoxazoles or 2-isoxazolines.[81,82] To construct a [2]-rotaxane using nitrile oxide cycloaddition chemistry a dipolarophile had to be attached to a CD binding group. Acryloyl chloride (**4.1**) was chosen to react with the diamine **1.30** to form a suitable substrate to undergo a cycloaddition reaction. After inclusion within αCD (**1.15**), the dipolarophile was expected to react with a nitrile oxide to form a [2]-rotaxane. The mesityl nitrile oxide **4.3** had previously been synthesised.[83,84] As a [2]-rotaxane had been synthesised using a 2,6-dimethylaniline blocking group,[80] the *ortho*-methyl groups of the mesityl group were expected to be sufficiently bulky to prevent dissociation of the CD from the cycloaddition product.

The diacrylamide **4.2** was synthesised by allowing the diamine **1.30** to react with the acid chloride **4.1** in DMF and TEA as shown in Scheme 4.1. The product was isolated in a yield of 71%. It was suspended in a solution of αCD (**1.15**) saturated MQ H_2O and the mixture was stirred for a period of 24 hours to allow an inclusion complex to form. The nitrile oxide **4.3** was then added and the mixture was stirred for three days. However, none of the desired [2]-rotaxane **4.4** was detected. Only the 2-isoxazoline **4.5** was isolated.

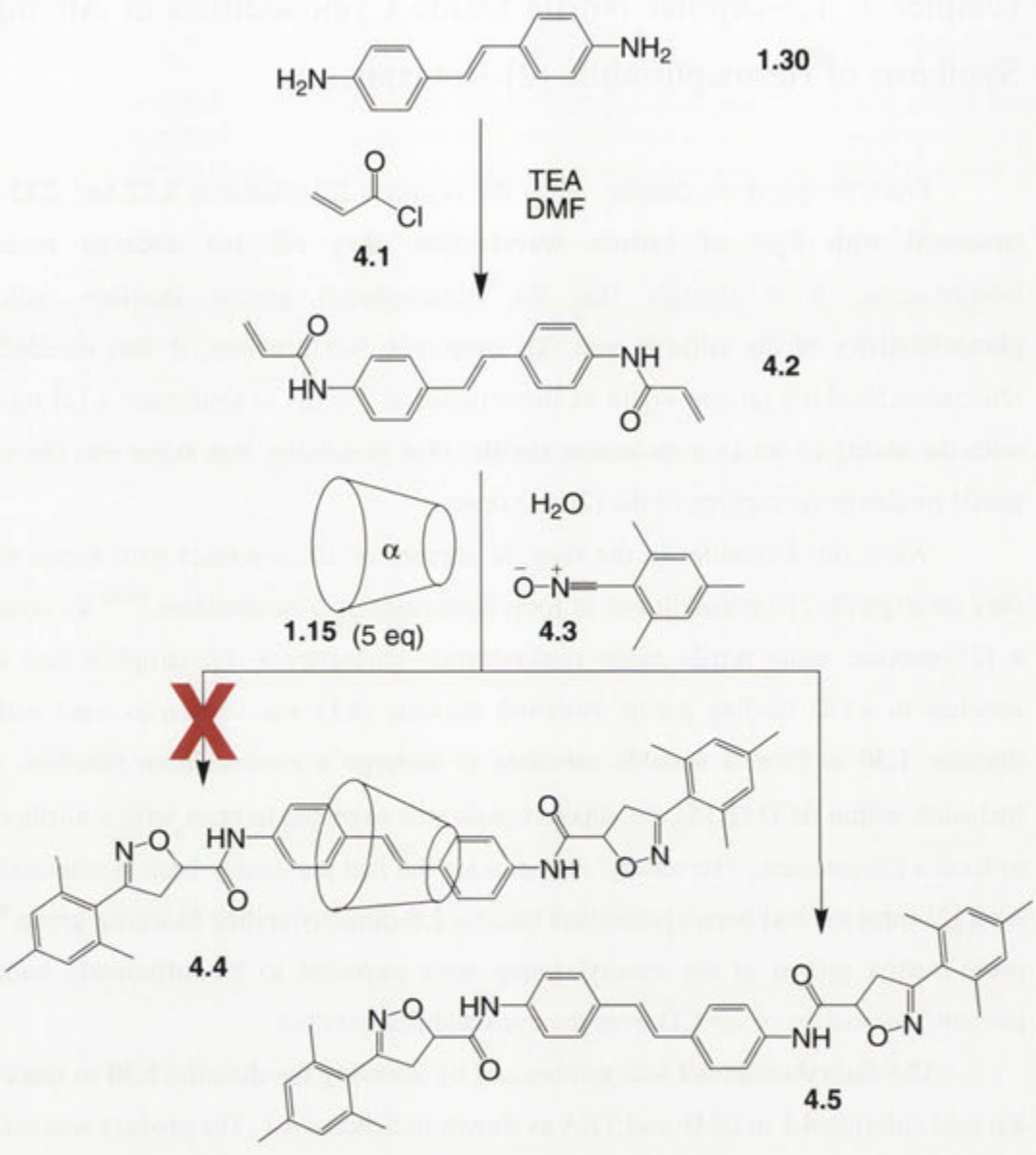

Scheme 4.1. Attempted synthesis of the [2]-rotaxane **4.4** using nitrile oxide cycloaddition chemistry.

To determine why the [2]-rotaxane **4.4** was not obtained, a ^{1}H NMR experiment was carried out on a 1:1 mixture of the diacrylamide **4.2** with αCD (**1.15**) in D_2O. There were no signals belonging to the acrylamide **4.2** or its inclusion complex with αCD (**1.15**) indicating that neither are present in solution to an appreciable extent. Various remedies were attempted to dissolve the acrylamide **4.2**. The use of sonication in water and mixed solvent systems, however, both failed to produce the desired [2]-rotaxane **4.4**.

Despite these setbacks, the plan to use nitrile oxide cycloadddition to synthesise [2]-rotaxanes was not abandoned completely. The direct attachment of the stilbene and acrylamide units to the CD was considered, whereby the acid chloride **4.1** would be allowed to react with the hermaphroditic CD **4.6** to form the acrylamide **4.7**. It was hoped that an hermaphroditic [2]-rotaxane would form when the activated alkene of the dimerically complexed hermaphroditic CD **4.7** underwent a cycloaddition reaction with the nitrile oxide **4.3**. This hermaphroditic [2]-rotaxane would have the ability to act as a molecular muscle with the 2-isoxazoline unit acting as a secondary binding unit upon isomerisation of the stilbene units. This method was thought to be sound as the solubility of the acrylamide unit in water was expected to be increased by the attachment to a hydrophilic CD. This theory is supported by the work of Meyer *et al.*,[85,86] who were able to synthesise 2-isoxazolines in water using an hermaphroditic CD acrylamide and phenyl based nitrile oxides. The likelihood of the acrylamide **4.7** forming a dimeric inclusion complex was supported by the work of Cieslinski *et al.*[80] The hermaphroditic CD **4.6** had been previously synthesised and shown to form an hermaphroditic [2]-rotaxane upon reaction with the trinitrophenyl blocking reagent **1.31**.

In the formation of the hermaphroditic CD **4.7**, the free amine **4.6** was firstly synthesised according to the method of Cieslinski *et al.*[80] The hermaphroditic CD **4.6** was then dissolved in MQ H_2O and allowed to react with the acid chloride **4.1** in the presence of TEA, to give the desired product **4.7** in 83% yield. To form an hermaphroditic [2]-rotaxane the dipolarophile **4.7** first had to form a dimeric inclusion complex. 2D ^{1}H NMR experiments on a sample of the hermaphroditic CD **4.7** in D_2O revealed that the dimeric inclusion complex **4.8** was formed as shown in Scheme 4.2.

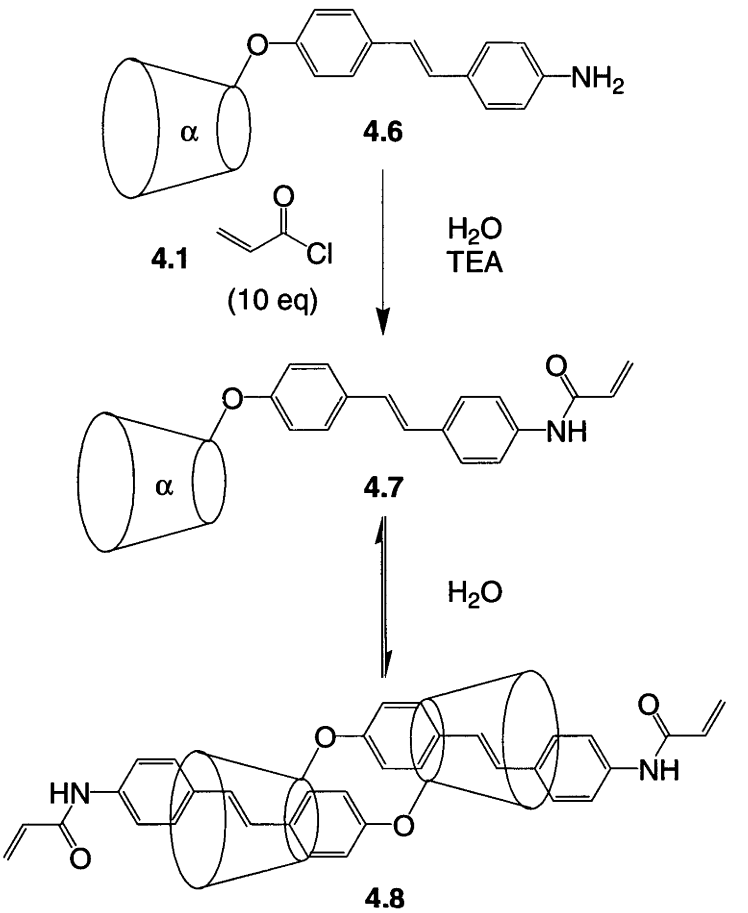

Scheme 4.2. Formation of the hermaphroditic cyclodextrin **4.7** and its dimeric inclusion complex **4.8**.

Formation of the inclusion complex **4.8** was established by firstly consulting the gHMQC NMR spectrum of the CD region of the contour plot shown in Figure 4.1. From the carbon resonances, the signal of the CD-C6-A carbon attached to the stilbene unit is distinguished from the signals belonging to the CD-C6-B to CD-C6-F carbons. The B to F carbon signals appear in the region 61.0 to 64.0 ppm, while the CD-C6-A signal appears downfield at 69.4 ppm. The stilbene is therefore connected to the CD with an ether linkage as an amine linkage, which might conceivably have resulted as an alternative product from reaction of the corresponding tosylate **1.19** with 4-amino-4'-hydroxystilbene, would be expected to shift the signal upfield to around 46.0 ppm. Crosspeaks are observable between the signal of the CD-C6-A carbon and the signals of the CD-H6-A protons. The identification of the signals of the CD-H6-A protons allows the signal of the aromatic stilbene protons closest to the CD to be assigned through

ROESY 2D NMR spectroscopy. The ROESY contour plot for the acrylamide **4.7** shown in Figure 4.3 shows NOE interactions between the signals of CD-H6-A and the stilbene protons A placing the A protons closest to the CD. This enables the signals of the stilbene unit to be fully assigned.

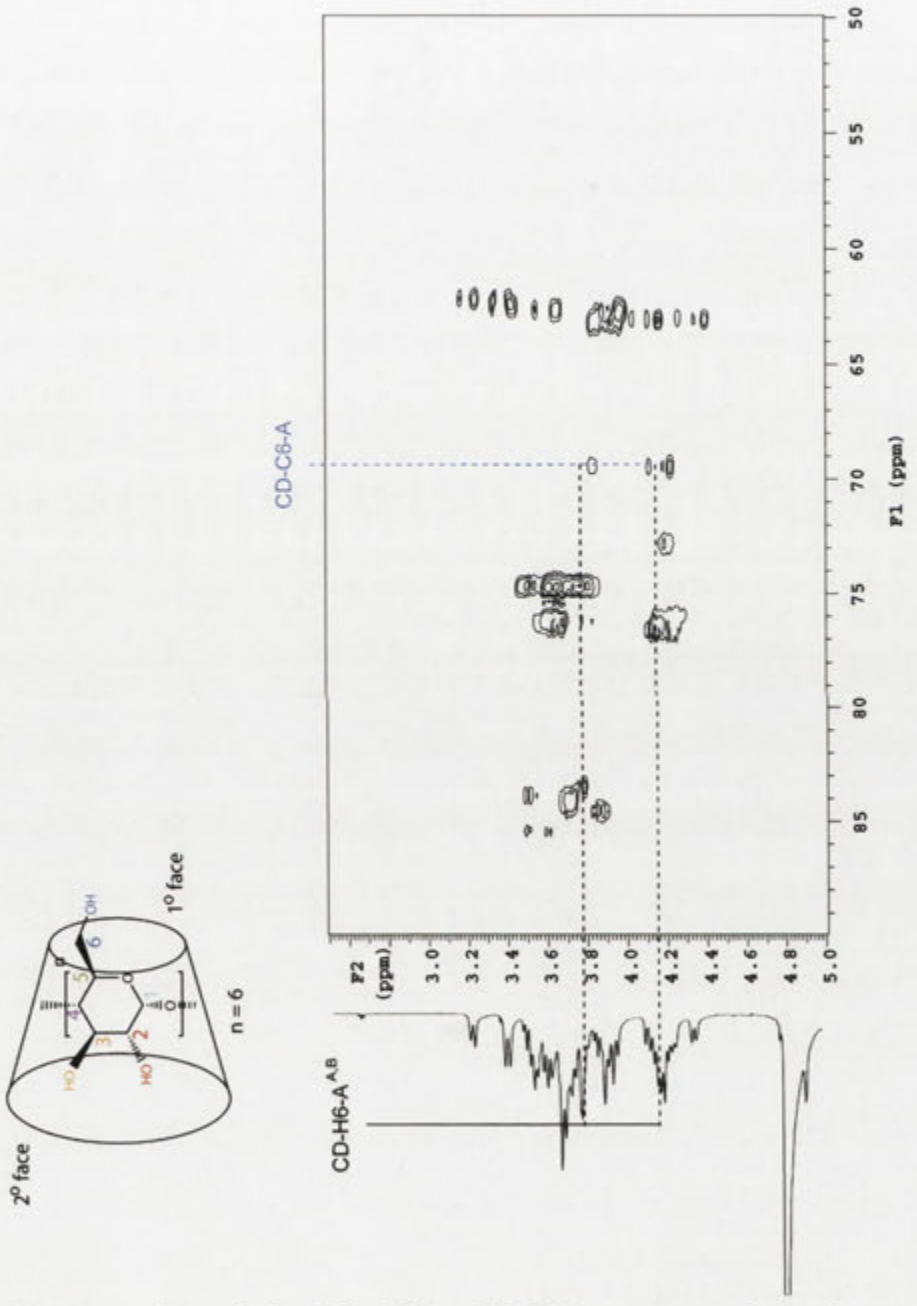

Figure 4.1. A section of the 500 MHz gHMQC spectrum of the hermaphroditic cyclodextrin **4.7** in D_2O at 25 °C of the region where crosspeaks are observed between cyclodextrin proton and carbon signals.

With the aromatic protons A signal assigned, the rest of the stilbene and acrylamide proton signals were distinguished using the ROESY contour plot shown in Figure 4.2, except that the E and F signals could not be distinguished as they both show interactions with the signals of the olefinic protons C and D.

The ROESY contour plot of the hermaphroditic CD **4.7** was used to establish the formation of a dimeric inclusion complex. The area that shows NOE interactions between the signals of the CD and those of the aromatic protons is shown in Figure 4.3. From the contour plot each of the signals of the stilbene protons A to F displays NOE interactions with signals that belong to the CD protons. An inclusion complex therefore forms between the CD and the stilbene unit. This inclusion complex exhibits symmetrical characteristics through the sharpness of the ^{1}H NMR signals. The complex can therefore be concluded to be dimeric as a non-dimeric binding mode would be non-symmetrical and result in a more complex spectrum. There are, however, no interactions between the signals of the vinyl protons and those of the CD. The vinyl group must therefore protrude from the secondary face of the CD. Therefore it was hoped that the protruding vinyl group would undergo a [3+2] cycloaddition reaction with the nitrile oxide **4.3** to form the hermaphroditic [2]-rotaxane **4.9**.

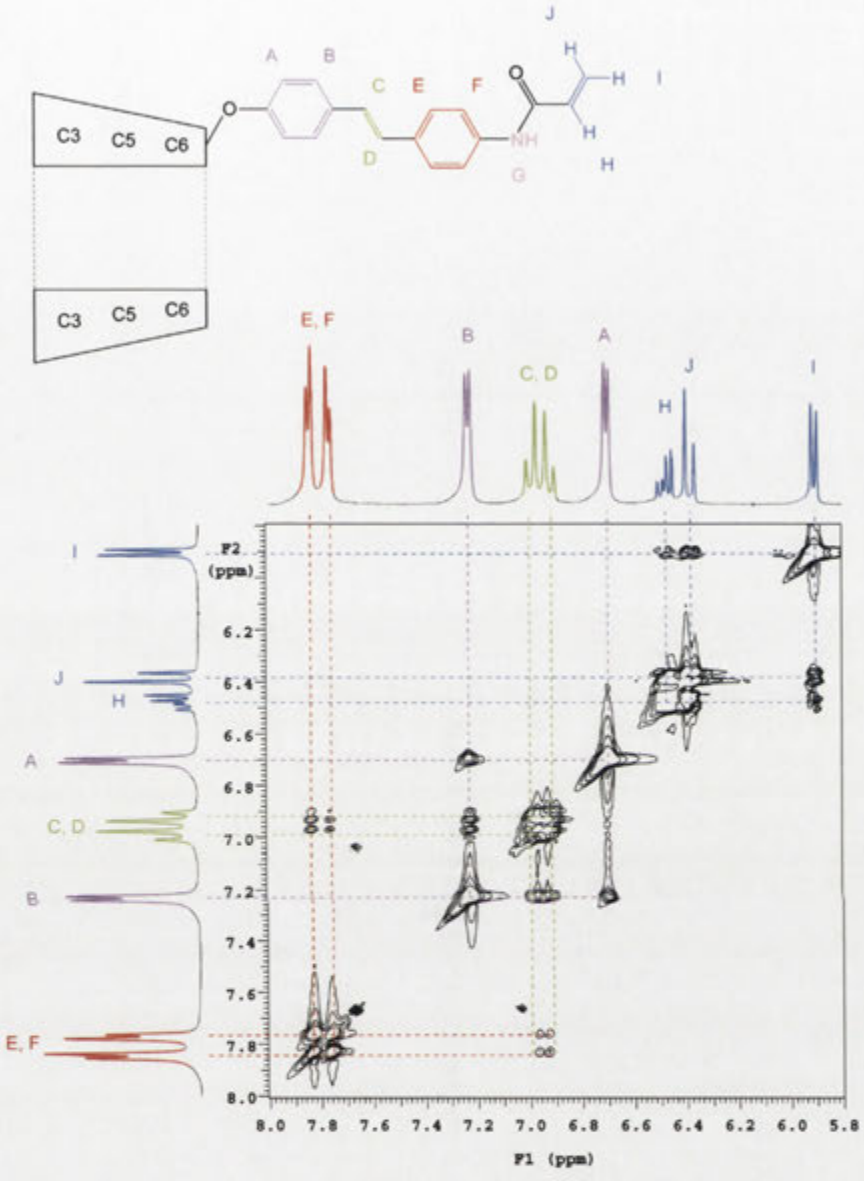

Figure 4.2. A section of the 500 MHz ROESY spectrum of the hermaphroditic cyclodextrin **4.7** in D_2O at 25 °C of the region where crosspeaks are observed between axle proton signals.

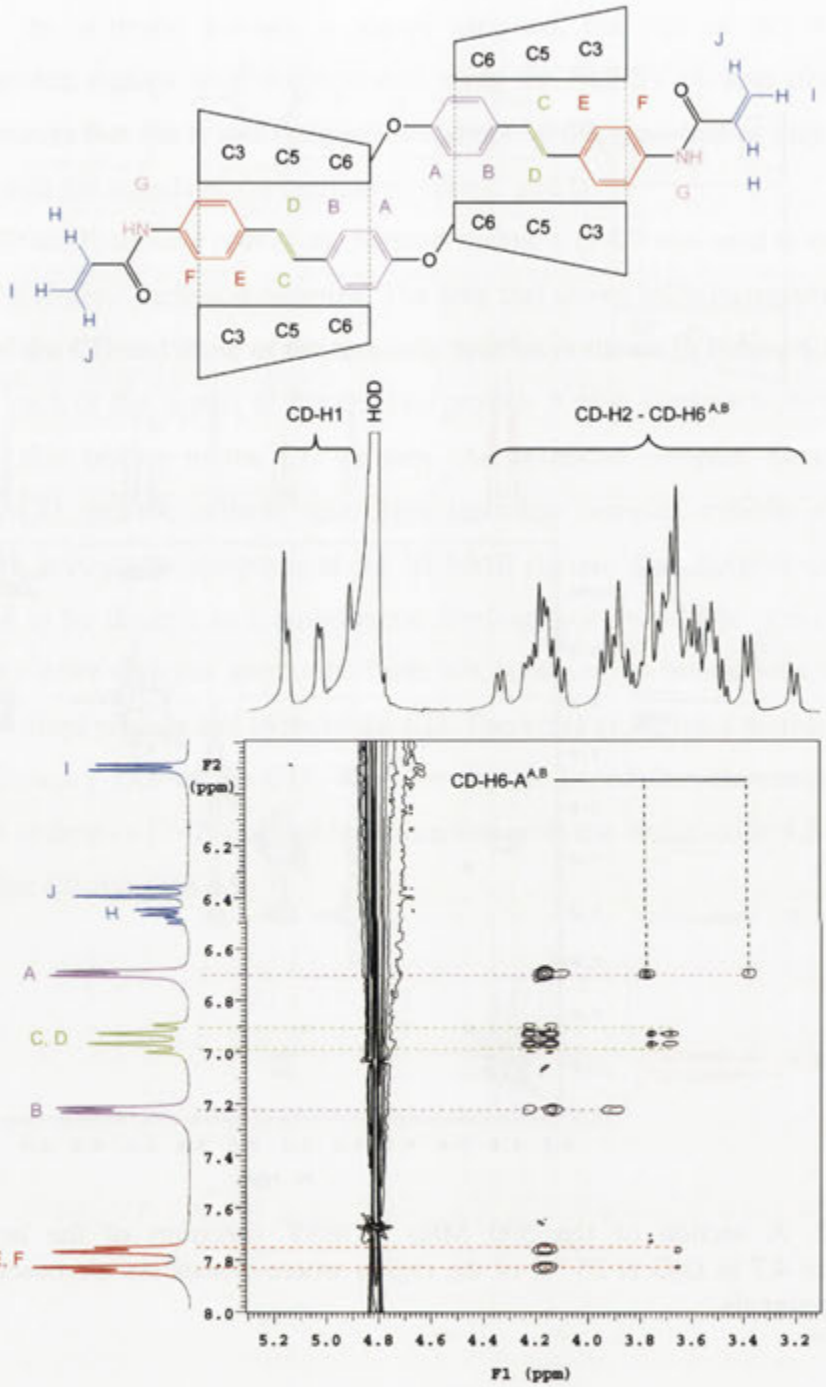

Figure 4.3. A section of the 500 MHz ROESY spectrum of the hermaphroditic cyclodextrin **4.7** in D_2O at 25 °C of the region where crosspeaks are observed between axle and cyclodextrin proton signals.

The formation of the hermaphroditic [2]-rotaxane **4.9**, however, was not successful (Scheme 4.3). The hermaphroditic CD **4.7** was stirred in MQ H_2O to form the

previously studied inclusion complex **4.8**. Into the mixture, 1.1 equivalents of the nitrile oxide **4.3** dissolved in minimal DMF were then added drop-wise. After seven days there appeared to be none of the nitrile oxide **4.3** left in solution so a further 0.9 equivalents of the nitrile oxide **4.3** dissolved in DMF was added. After ten days the reaction was deemed complete when none of the dipolarophile **4.7** was observable by TLC. Work up of the mixture including using reverse phase HPLC gave two compounds **4.10** and **4.11**. Each produced ESI mass spectra with ions of *m/z* 1230.4 and 1265.4. Neither of these corresponds to the mass expected for the hermaphroditic [2]-rotaxane **4.9**.

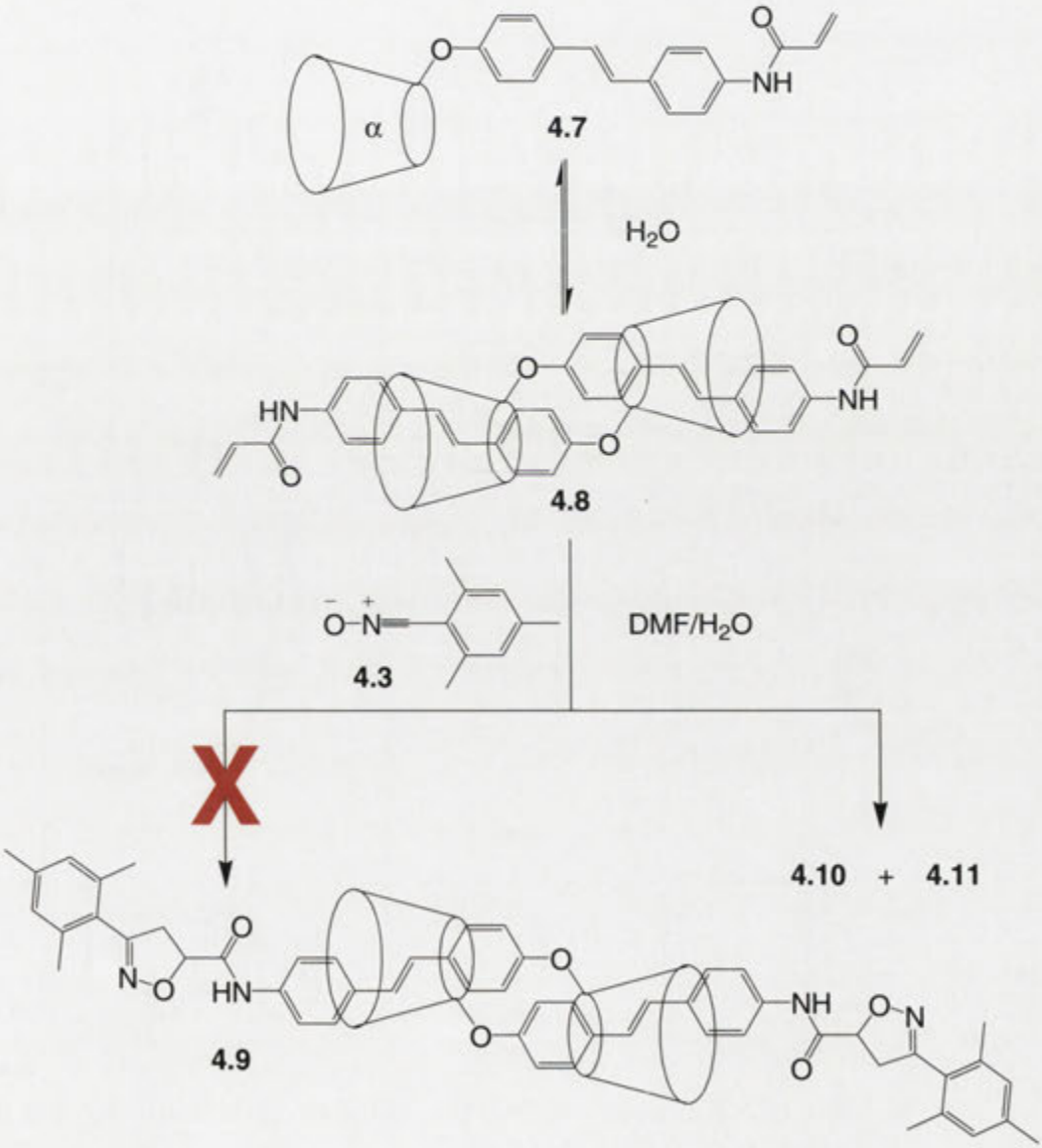

Scheme 4.3. Attempted synthesis of the hermaphroditic [2]-rotaxane **4.9** which instead resulted in the products **4.10** and **4.11**.

The ^{1}H NMR spectra of the products **4.10** and **4.11** in D_2O are shown in Figure 4.4. These do not show signals of vinyl protons. New signals arise in the region 2.5 to 3.5 ppm. One notable absence is any signal attributable to aromatic mesityl protons that would have been expected to appear in the vicinity of 7 ppm.

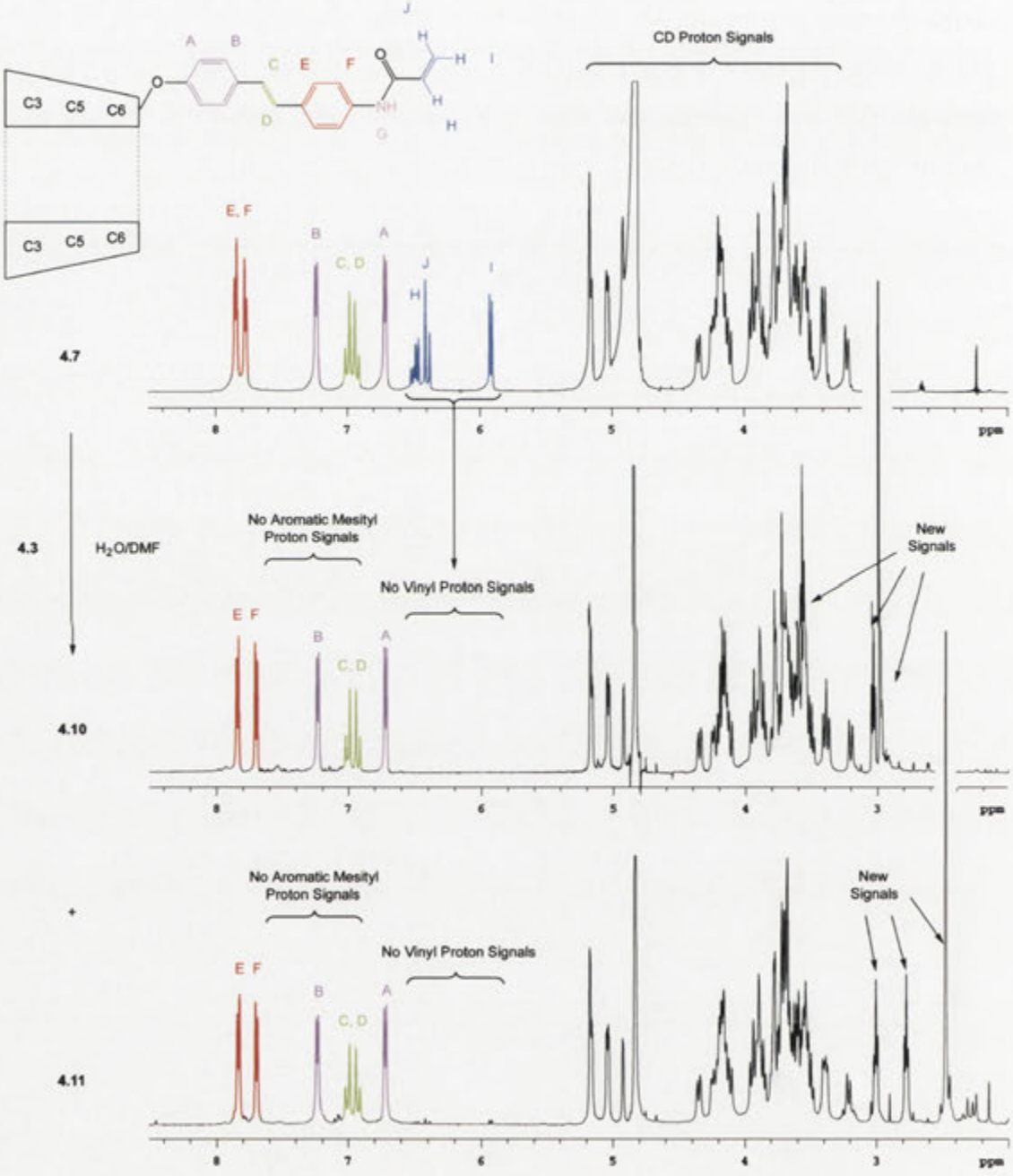

Figure 4.4. 500 MHz ^{1}H NMR spectra of the hermaphroditic cyclodextrin **4.7** and the cycloaddition products **4.10** and **4.11** in D_2O at 25 °C.

The absence of signals of vinyl protons and appearance of new signals upfield implies the hermaphroditic [2]-rotaxane **4.7** has undergone reaction. However, the absence of any signal of mesityl aromatic protons along with the mass spectral data indicates that neither of the products contains the mesityl group. The ion of *m/z* 1265.4 for each of the products **4.10** and **4.11** can be explained as the $M+H^+$ ion formed by the addition of CO_2 to the hermaphroditic CD **4.7**. The products **4.10** and **4.11** therefore may be regioisomers formed by cycloaddition followed by retro-cycloaddition or decomposition but the exact structures have not been determined. In any event it is clear that an hermaphroditic [2]-rotaxane was not formed.

Despite the exact structures not being able to be determined, through 2D NMR spectroscopy it was established that the products **4.10** and **4.11** are some form of hermaphroditic CD. Both the products contain stilbene units that form dimeric inclusion complexes in D_2O but not in d_4-methanol or d_6-DMSO.

In conclusion, the expected hermaphroditic [2]-rotaxane **4.9** was not formed by the [3+2] cycloaddition of the dipolarophile **4.7** with the nitrile oxide **4.3**. The ^1H NMR spectra of the products **4.10** or **4.11** did not contain signals of aromatic mesityl protons which, along with their respective mass spectral data and 2D NMR spectra pointed towards an undesired decomposition or retro-cyclisation to form regioisomeric hermaphroditic CD by-products. The attempted synthesis of an hermaphroditic [2]-rotaxane using 1,3-dipolar nitrile oxide cycloaddition chemistry was therefore abandoned. Alternative methods were explored to produce a [2]-rotaxane.

Chapter 5: A Photochemically Activated Hermaphroditic Cyclodextrin Switch for the Transport of Methyl Orange

From the work in Chapter 4 the attempted synthesis of the hermaphroditic [2]-rotaxane **4.9** proved unsuccessful using cycloaddition chemistry. The hermaphroditic [2]-rotaxane **4.9** would have had the potential to act as a molecular device in the form of a muscle. It has been previously shown that hermaphroditic CDs have other uses. In work by Coulston,[87] hermaphroditic CDs were used in the transport of methyl orange (**5.8**) along an HPLC column. In the work described in this chapter the possibility of an hermaphroditic CD based on the previously synthesised hermaphroditic CD **4.6** was explored for use as a similar molecular transport.

Previously, Coulston [87] used βCD (**1.16**) to produce the cinnamide **5.1(E)**. Upon irradiation with light of wavelength 300 nm, the *trans*-olefinic bond isomerised to give the *cis*-cinnamide **5.1(Z)** as shown in Scheme 5.1. This reaction was reversed by irradiation with 254 nm light, a deuterium arc lamp (190 nm – 600 nm), or addition of iodine with a sunlight lamp. Using the Hummel and Dryer method[88] described below, as exploited by Croft *et al.*,[89] each of the isomers **5.1(E)** and **5.1(Z)**, along with natural βCD (**1.16**), was tested for their association constant (K_a) with the dye **5.8** using HPLC. Because in the HPLC study, the dye **5.8** is bound to the CD and carried through the column faster than normally would be the case, the association constant can be viewed as a molecular transport coefficient (K). Different values of the transport coefficient then depict different hosts' abilities to transport the dye **5.8** through the HPLC column. From the study by Coulston,[87] the *trans*-isomer **5.1(E)** was revealed to have a transport coefficient of 2385 ± 169 dm^3 mol^{-1}, the *cis*-isomer **5.1(Z)** had a value of 618 ± 46 dm^3 mol^{-1} and βCD (**1.16**) a value of 3790 ± 228 dm^3 mol^{-1}. While the *trans*-isomer **5.1(E)** had a lower transport coefficient than the natural βCD (**1.16**), the value for the *cis*-isomer **5.1(Z)** was much lower, which was suggested to be due to self inclusion of the cinnamoyl group. The isomerisation between the *trans*-isomer **5.1(E)** and the *cis*-isomer **5.1(Z)** acted as a molecular switch for the transport of the dye **5.8**.

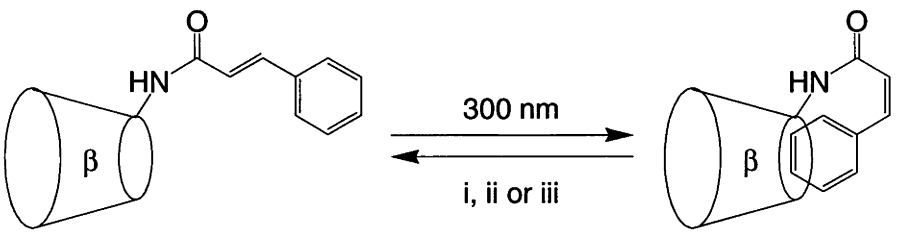

5.1(E)

i) 254 nm
ii) 190 - 600 nm
iii) I_2 + Sunlight

5.1(Z)

Scheme 5.1. Reversible isomerisation of the *trans*-cinnamide **5.1(E)** and the *cis*-isomer **5.1(Z)** reported by Coulston.[87]

In the present work stilbene-substituted CDs were investigated for the transport of the dye **5.8**. Cieslinski,[80] had prepared the stilbene based hermaphroditic CDs **5.2(E)** and **5.2(Z)** and shown their interconversion upon photolysis as illustrated in Scheme 5.2. The *trans*-isomer **5.2(E)** formed the dimeric inclusion complex **5.3** while the *cis*-isomer **5.2(Z)** did not form an inclusion complex leaving the CD annulus free to potentially complex a guest. Systems of this type were thought to be good candidates for new molecular transport devices. It was expected that the *cis*-isomers would have transport coefficients for the dye **5.8** similar to that of αCD (**1.15**) while the *trans*-isomers would have significantly lower coefficients due to the dimeric inclusion.

The specific system chosen was based on the hermaphroditic CD **4.6** described in Chapter 4. The hermaphroditic CD **4.6** was acylated to avoid ionisation of the amino group which might have affected guest binding. The reaction scheme is found in Scheme 5.3. The acetamide **5.5(E)** was isolated in a yield of 53% and its ESI mass spectrum showed an $M+H^+$ ion at *m/z* 1208.0.

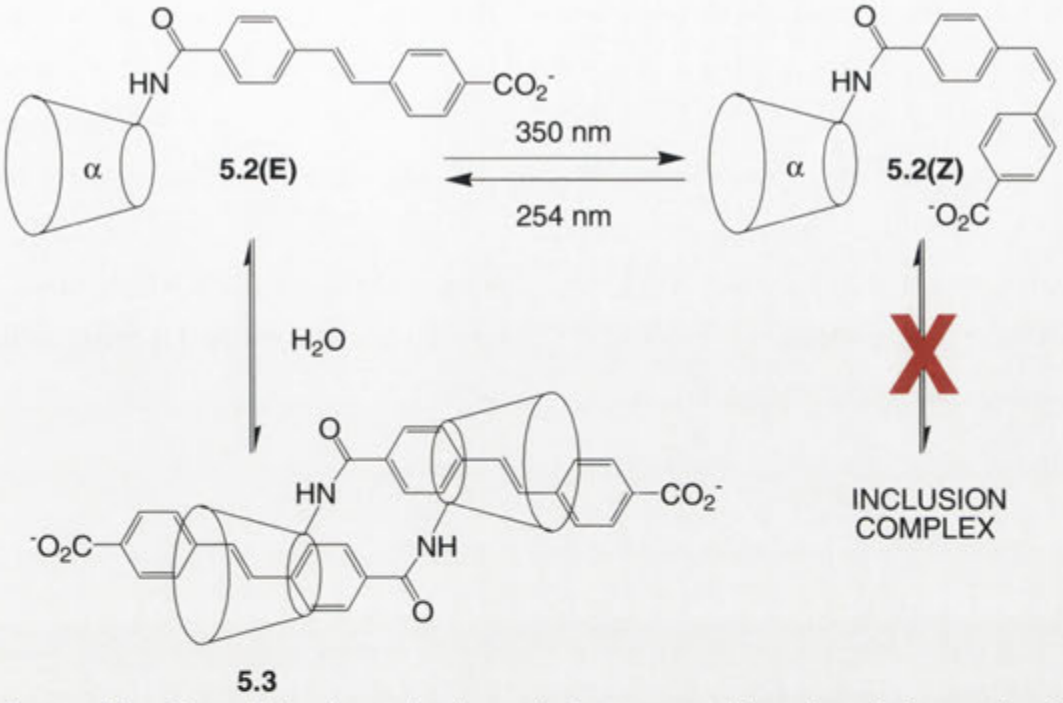

Scheme 5.2. Reversible isomerisation of the *trans*-stilbene-based hermaphroditic cyclodextrin **5.2(E)** and the *cis*-isomer **5.2(Z)** where the *trans*-isomer **5.2(E)** forms the dimeric inclusion complex **5.3** while the *cis*-isomer **5.2(Z)** does not form a complex.

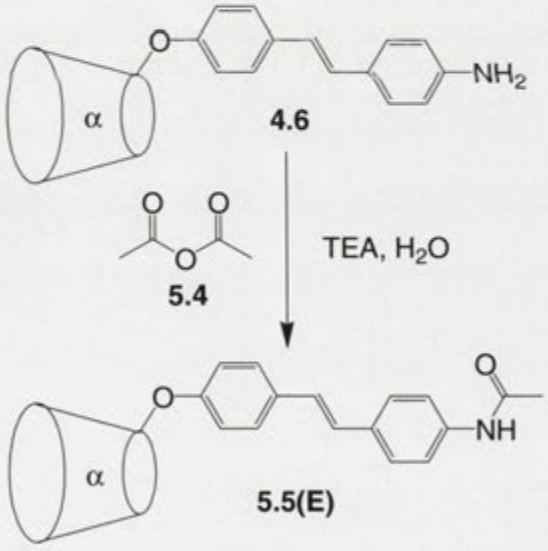

Scheme 5.3. Formation of the acetamide **5.5(E)**.

2D NMR spectroscopy showed that the acetamide **5.5(E)** formed a dimeric inclusion complex in D_2O. The assignment of the signals of the stilbene unit only required the ROESY contour plot shown in Figure 5.1. From the ROESY contour plot in Figure 5.2, crosspeaks between each of the signals of the stilbene protons with those of

the CD protons established the formation of an inclusion complex. The inclusion complex is assumed to be a symmetrical dimer for a variety of reasons. The stilbene cannot be self-included as its long rigid structure would prevent this. Any non-symmetrical complex would result in a more complicated ^{1}H NMR spectrum, and the dimer is likely to be the most favoured symmetrical complex in entropy terms. Finally, the hermaphroditic CD **4.6**, upon which the synthesis of the acetamide **5.5(E)** is based, has been previously shown by Cieslinski[80] to form an hermaphroditic [2]-rotaxane upon reaction with the trinitrophenyl blocking reagent **1.31**.

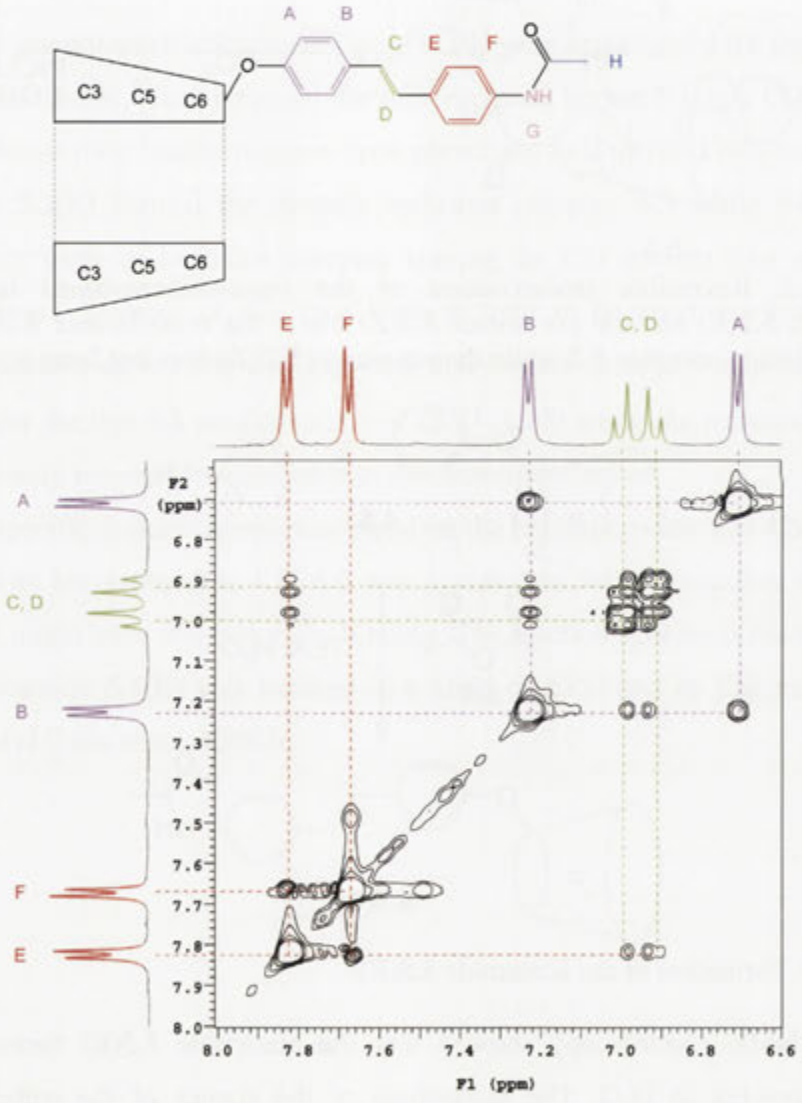

Figure 5.1. A section of the 500 MHz ROESY spectrum of the acetamide **5.5(E)** in D_2O at 25 °C of the region where crosspeaks are observed between stilbene proton signals.

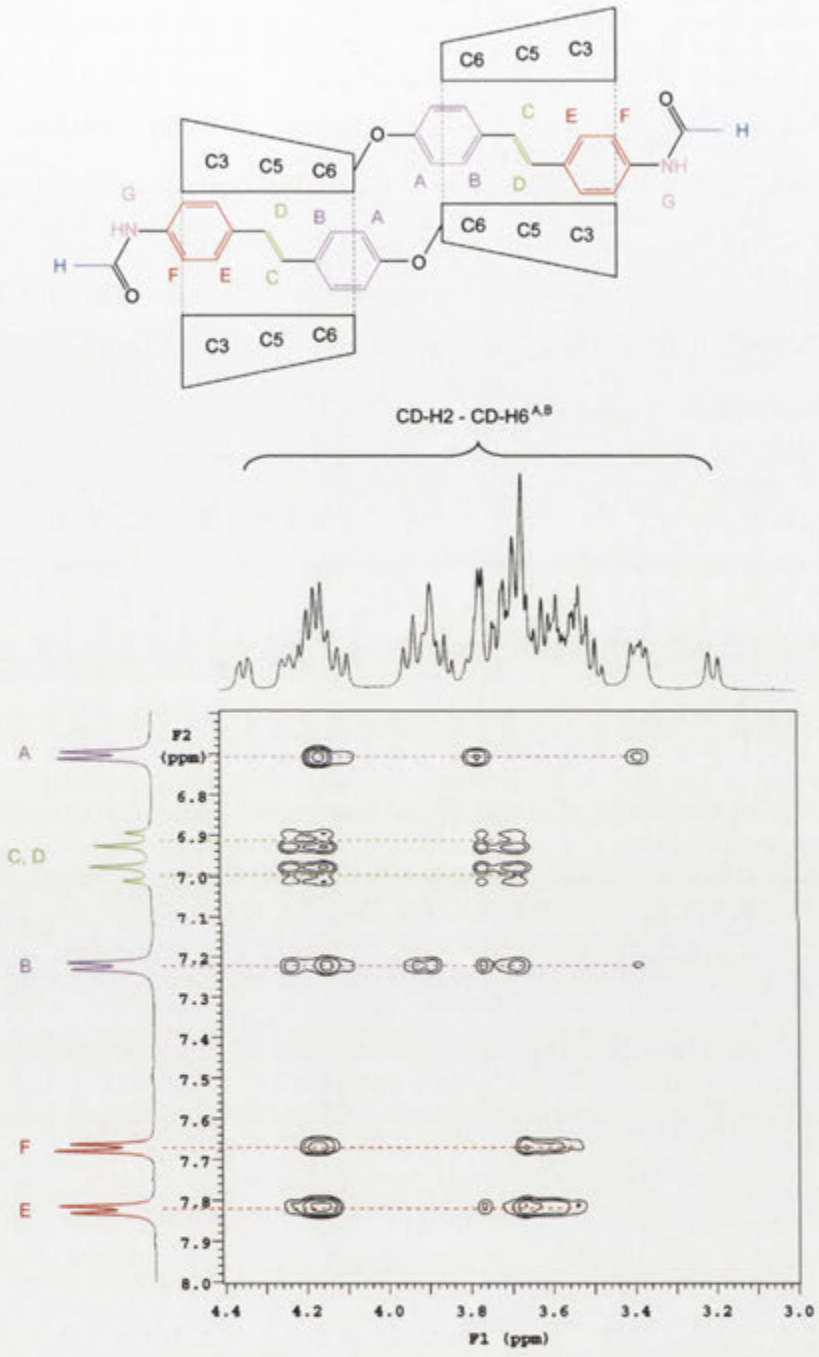

Figure 5.2. A section of the 500 MHz ROESY spectrum of the acetamide **5.5(E)** in D_2O at 25 °C of the region where crosspeaks are observed between stilbene and cyclodextrin proton signals.

The acetamide **5.5(Z)** was then formed by the photoisomerisation of the acetamide **5.5(E)** using light of wavelength 350 nm as shown in Scheme 5.4. The irradiation wavelength was determined from the UV/visible spectrum of the *trans*-isomer

5.5(E) as illustrated in Figure 5.5. As noted previously, photoexcitation of a *trans*-stilbene at a wavelength at or near its maximum absorbance results in the formation of the *cis*-isomer. A 350 nm light source was used as it was the closest available wavelength to the λ_{max} of the *trans*-isomer **5.5(E)** at 338 nm. At 350 nm absorption of light by the *cis*-isomer **5.5(Z)** and its isomerisation was expected to be limited. Initially irradiation of a 3.55×10^{-2} M solution of the acetamide **5.5(E)** gave the *cis*-isomer **5.5(Z)** which was isolated in a yield of 19%. The HI-RES ESI mass spectrum of another product showed a peak that corresponds to the $M+Na^+$ ion of *m/z* 2438.8257 of the dimer **5.6**. It is assumed that a [2+2] photocyclisation of the olefinic bonds of two separate stilbene units forms a mixture of isomers of the dimer **5.6**. It was thought that the formation of the dimer **5.6** was due to the concentrated solution allowing two molecules to come into contact. The irradiation of the acetamide **5.5(E)** with 350 nm light was therefore repeated at a lower concentration of 2.51×10^{-5} M. Under these conditions the *cis*-isomer **5.5(Z)** was then isolated in a yield of 40%.

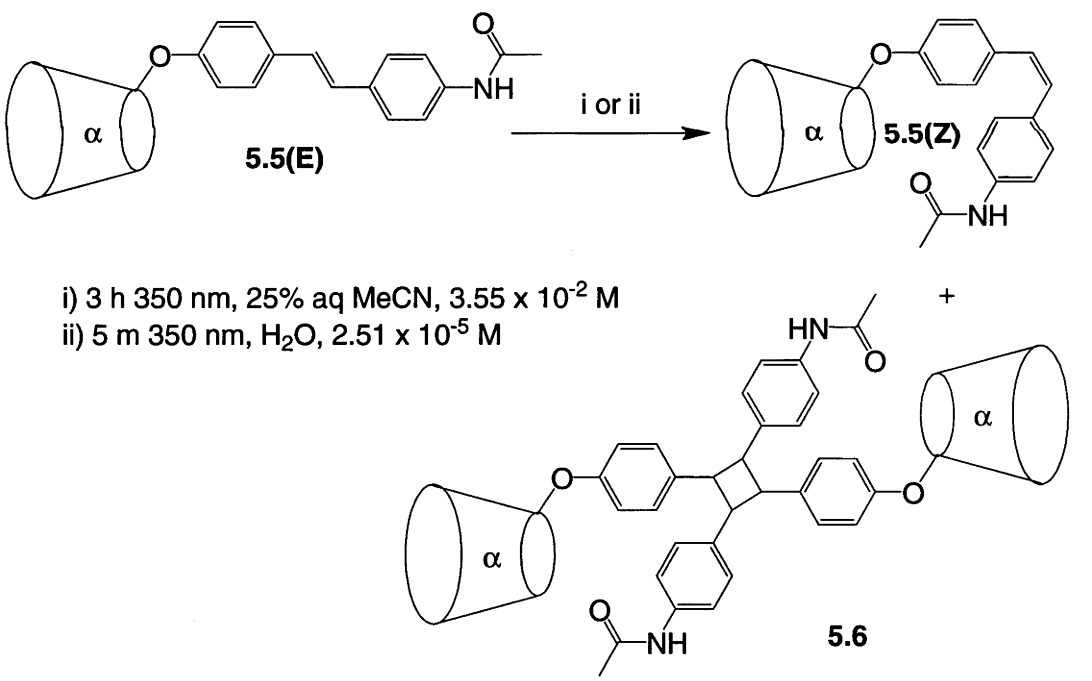

Scheme 5.4. Isomerisation of the acetamide **5.5(E)** with 350 nm light to form the *cis*-isomer **5.5(Z)** and the dimeric by-product **5.6**.

The complexation characteristics of the acetamide **5.5(Z)** were then determined using 2D NMR spectroscopy. The 2D NMR ROESY contour plot in Figure 5.3 was

firstly used to assign the signals of the stilbene unit. From the ROESY contour plot in Figure 5.4, crosspeaks between the signals of the CD and stilbene protons were used to determine if the acetamide **5.5(Z)** formed an inclusion complex. The only crosspeaks visible were between the signal of the stilbene protons A and the signals of the CD protons. The ROESY interactions arise due to the vicinity of the CD-H6 protons to the stilbene unit as a result of their ether connection. The *cis*-isomer **5.5(Z)** therefore does not form a CD inclusion complex.

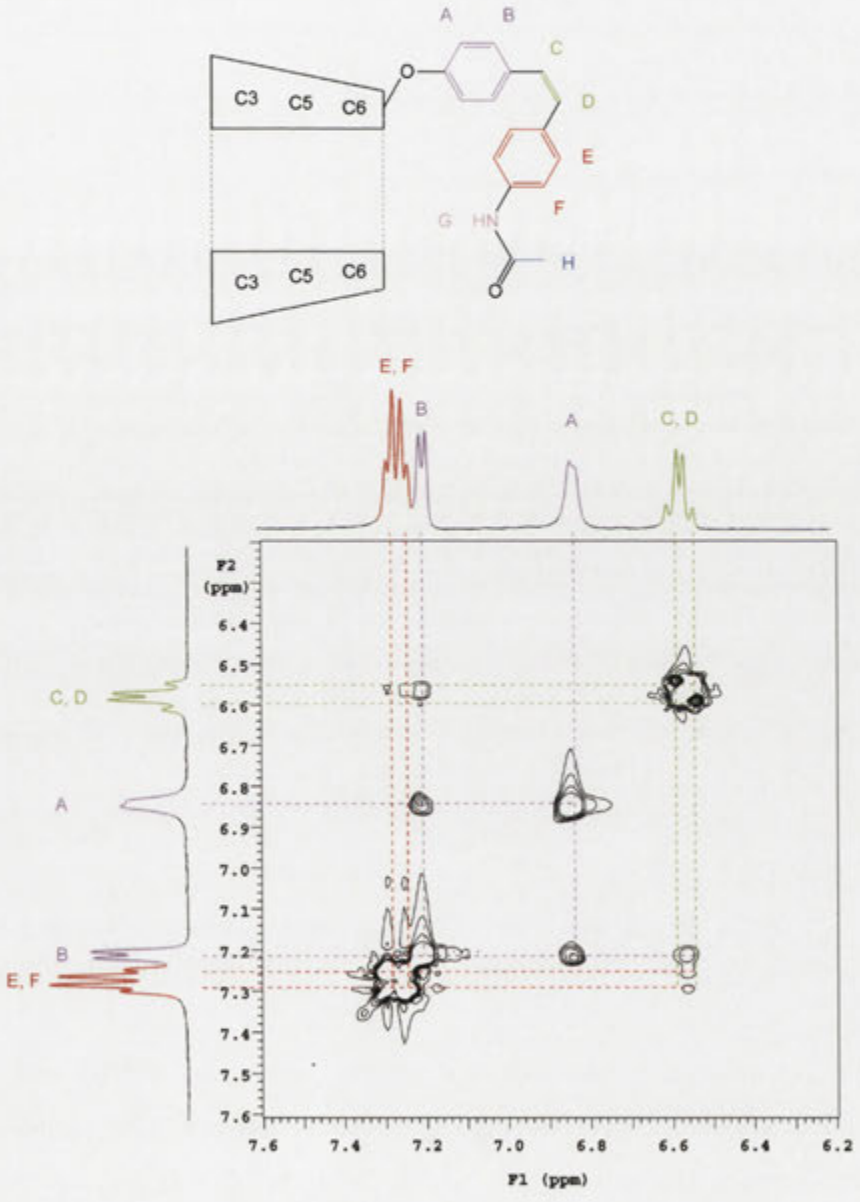

Figure 5.3. A section of the 500 MHz ROESY spectrum of the acetamide **5.5(Z)** in D_2O at 25 °C of the region where crosspeaks are observed between stilbene proton signals.

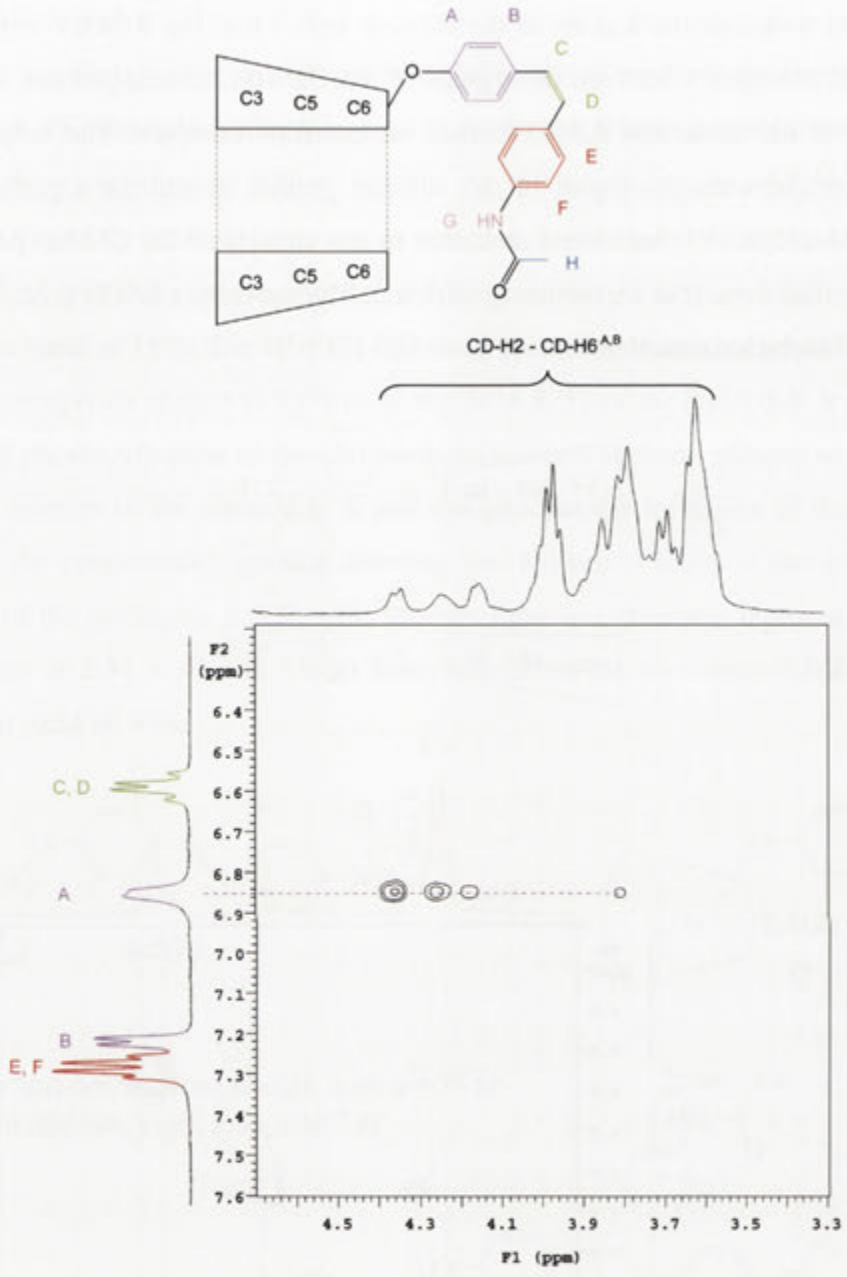

Figure 5.4. A section of the 500 MHz ROESY spectrum of the acetamide **5.5(Z)** in D_2O at 25 °C of the region where crosspeaks are observed between stilbene and cyclodextrin proton signals.

The complexation characteristics of the acetamides **5.5(E)** and **5.5(Z)** are summarised in Scheme 5.5. The *trans*-isomer **5.5(E)** forms a dimeric inclusion complex. The conformation of the stilbene unit of the *cis*-isomer **5.5(Z)** prevents any inclusion complex from forming. Before the isomerisation between the acetamide **5.5(E)** and the

cis-isomer **5.5(Z)** could be labelled a switch and each of the isomers tested for their ability to act as a molecular transport, the reversibility of the interconversion between the isomers had to be measured.

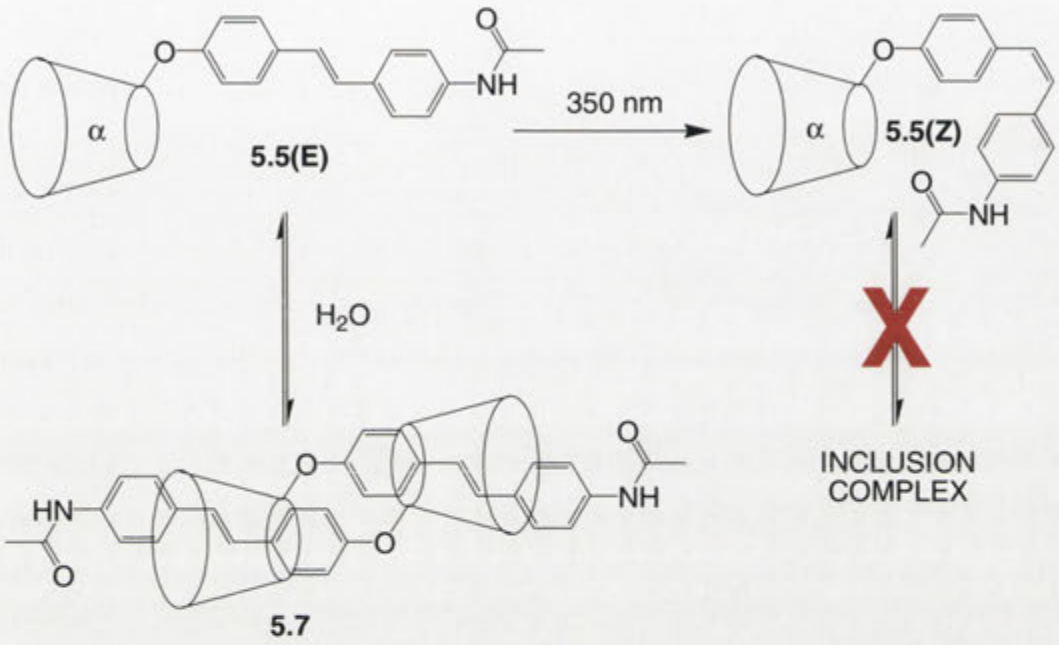

Scheme 5.5. Isomerisation of the *trans*-stilbene-based hermaphroditic cyclodextrin **5.5(E)**, which forms the dimeric inclusion complex **5.7**, to the *cis*-isomer **5.5(Z)** which does not form a complex.

The reversibility of the interconversion between the acetamides **5.5(E)** and **5.5(Z)** was measured using reverse-phase HPLC and UV/visible spectroscopy. Firstly the irradiation wavelengths were determined for each of the isomers. The *trans*-isomer **5.5(E)** was irradiated at wavelength 350 nm to produce the *cis*-isomer **5.5(Z)** as discussed above. To determine the irradiation wavelength to use with the *cis*-isomer **5.5(Z)**, its UV/visible spectrum was examined and is shown as the black line in Figure 5.7. The spectrum shows a λ_{max} at 298 nm. The wavelengths of light available closest to this λ_{max} were 254 nm and 350 nm. The light of wavelength 254 nm was used to irradiate the *cis*-isomer **5.5(Z)**. At 254 nm, the absorption of light by the *trans*-isomer **5.5(E)** and its isomerisation was expected to be less than that for the *cis*-isomer **5.5(Z)**.

The UV/visible spectra and HPLC traces of a 2.48×10^{-5} mol dm^{-3} solution of the acetamide **5.5(E)** before and after irradiation with light of wavelengths 350 nm and 254

nm are found in Figures 5.5 and 5.6 respectively. From its HPLC trace, the peak corresponding to the acetamide **5.5(E)** has a retention time of 17.7 minutes. The *cis*-isomer **5.5(Z)** was made up to a concentration of 1.65×10^{-5} mol dm^{-3} in MQ H_2O and its UV/visible spectra and HPLC traces before and after irradiation with light of wavelengths 254 nm and 350 nm were recorded and are shown in Figures 5.7 and 5.8 respectively. From its HPLC trace, the peak corresponding to the acetamide **5.5(Z)** has a retention time of 20.5 minutes.

From the study it was apparent that the irradiation of the acetamide **5.5(E)** with light of wavelength 350 nm produced the *cis*-isomer **5.5(Z)**. In the UV/visible spectra, the absorbance at 338 nm corresponding to the *trans*-isomer **5.5(E)** decreases after the irradiation. The irradiated solution has a maximum absorbance at 298 nm corresponding to the *cis*-isomer **5.5(Z)**. The irradiation of the *cis*-isomer **5.5(Z)** with light of wavelength 254 nm produced the *trans*-isomer **5.5(E)**. From the UV/visible spectra, upon irradiation, the absorbance at 338 nm increased corresponding to the formation of the *trans*-isomer **5.5(E)**. Thus it was established that the interconversion between the acetamides **5.5(E)** and **5.5(Z)** is reversible. The basis of a photochemical switch mechanism had therefore been established. The next step was to investigate whether the change in the conformation of the stilbene unit between the acetamide **5.5(E)** and the *cis*-isomer **5.5(Z)** was able to fulfil the purpose of a machine to do work on a guest for the transport of the dye **5.8** through a HPLC column.

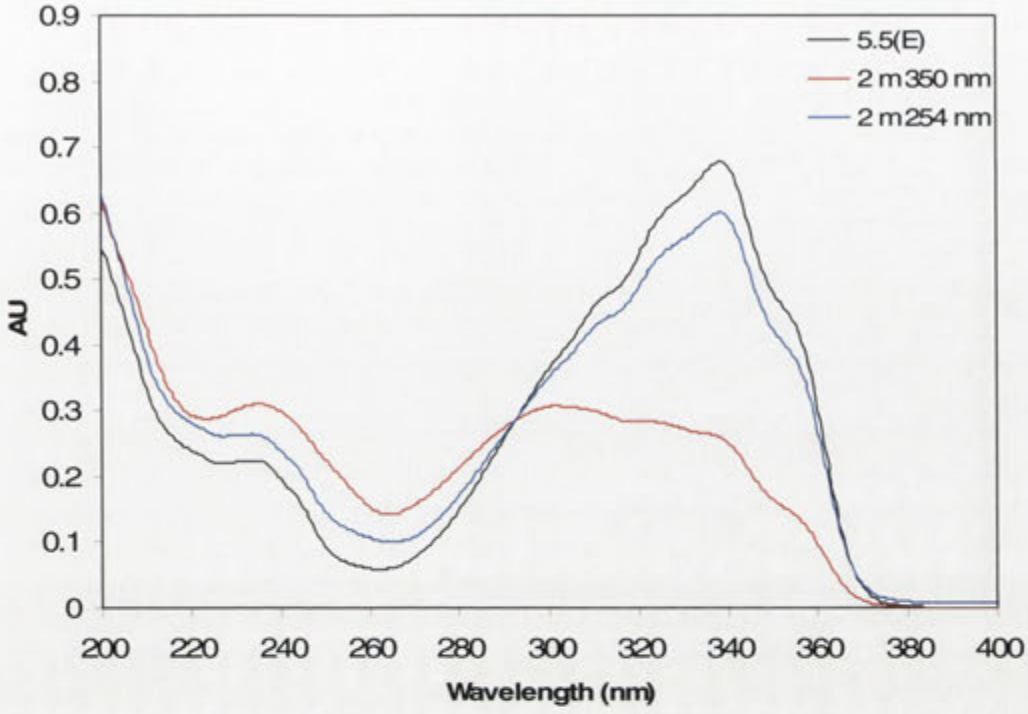

Figure 5.5. UV/visible spectra of the acetamide **5.5(E)** [2.48×10^{-5} M] in MQ H_2O and after subsequent exposure to 350 and 254 nm light after periods of time as indicated in the graph.

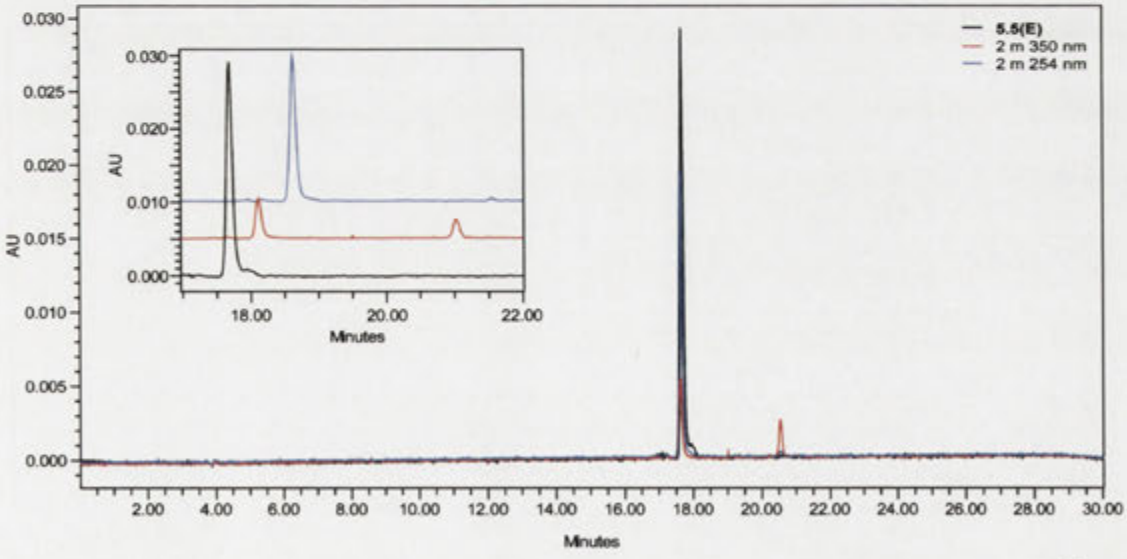

Figure 5.6. Reverse-phase HPLC chromatograms of the acetamide **5.5(E)** [2.48×10^{-5} M] in MQ H_2O and after subsequent exposure to 350 and 254 nm light after periods of time as indicated in the graph. The spectra in the insert are offset horizontally by 0.5 minutes and vertically by 0.005 AU for clarity.

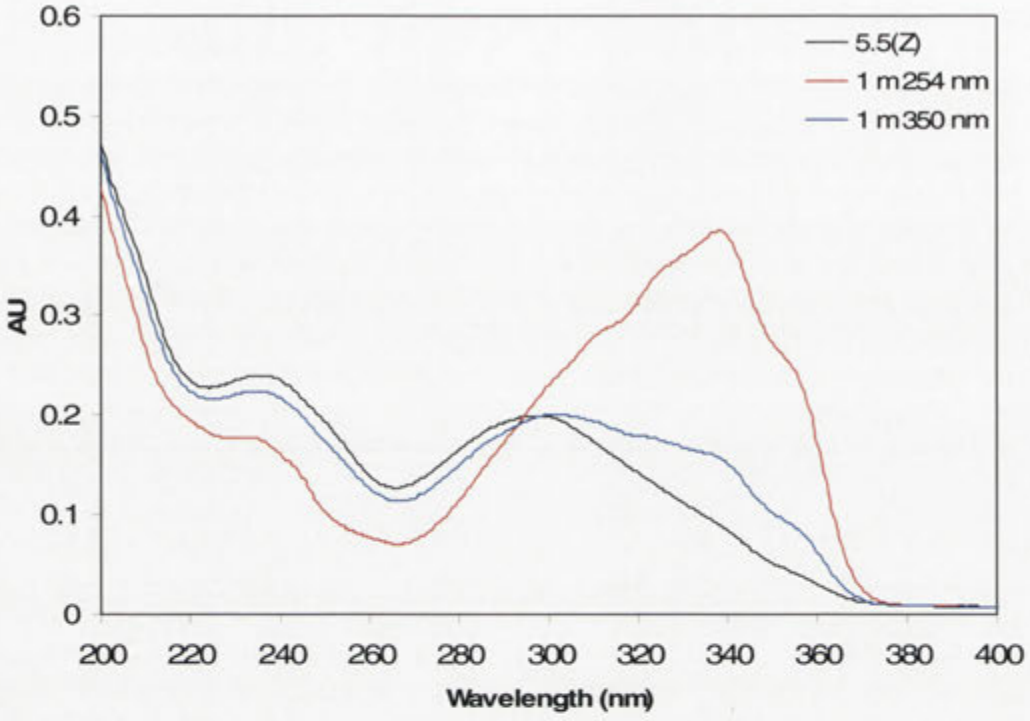

Figure 5.7. UV/visible spectra of the acetamide **5.5(Z)** [1.65×10^{-5} M] in MQ H_2O and after subsequent exposure to 254 and 350 nm light after periods of time as indicated in the graph.

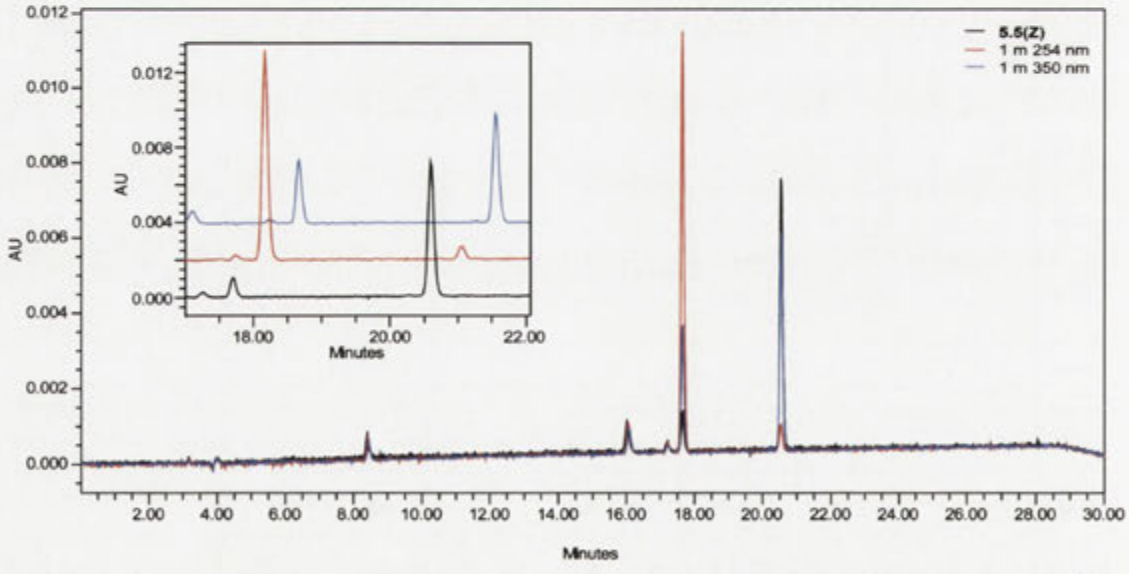

Figure 5.8. Reverse-phase HPLC chromatograms of the acetamide **5.5(Z)** [1.65×10^{-5} M] in MQ H_2O and after subsequent exposure to 254 and 350 nm light after periods of time as indicated in the graph. The spectra in the insert are offset horizontally by 0.5 minutes and vertically by 0.002 AU for clarity.

To test their ability to act as molecular transports, the transport coefficients of each of the acetamides **5.5(E)** and **5.5(Z)** along with αCD (**1.15**) for the dye **5.8** were calculated. The transport coefficients were obtained using the Hummel and Dryer method,[88] as adapted by Croft *et al.*[89] In the method, a solution of the dye **5.8** of a known concentration is pumped through an HPLC column. A solution of one of the CDs **1.15**, **5.5(E)** or **5.5(Z)** is then injected through the same HPLC column. As seen in the HPLC trace in Figure 5.9, binding of the dye **5.8** with the CDs **1.15**, **5.5(E)** or **5.5(Z)** results in a positive peak. The CDs **1.15**, **5.5(E)** and **5.5(Z)** have shorter retention times than the dye **5.8** under the conditions of the HPLC run and cause the bound dye **5.8** to be carried at a faster rate through the HPLC column than the unbound dye **5.8**. When the CD bound dye **5.8** passes off the HPLC column there is an increased local amount of the UV active dye **5.8** and a positive peak in the HPLC trace. Due to the binding of the dye **5.8** to the CD a void of the dye **5.8** is left on the column which results in a negative peak later in the HPLC trace. The molar amount of the dye **5.8** transported by the CD is then determined by comparing with a blank injection of borate buffer. Plotting the molar ratio ($\bar{r}$) of guest bound to host injected against $\bar{r}$/[guest] in a Scatchard plot[90] enabled the transport coefficient (*K*) for each of the CDs **1.15**, **5.5(E)** and **5.5(Z)** for the dye **5.8** to be determined.

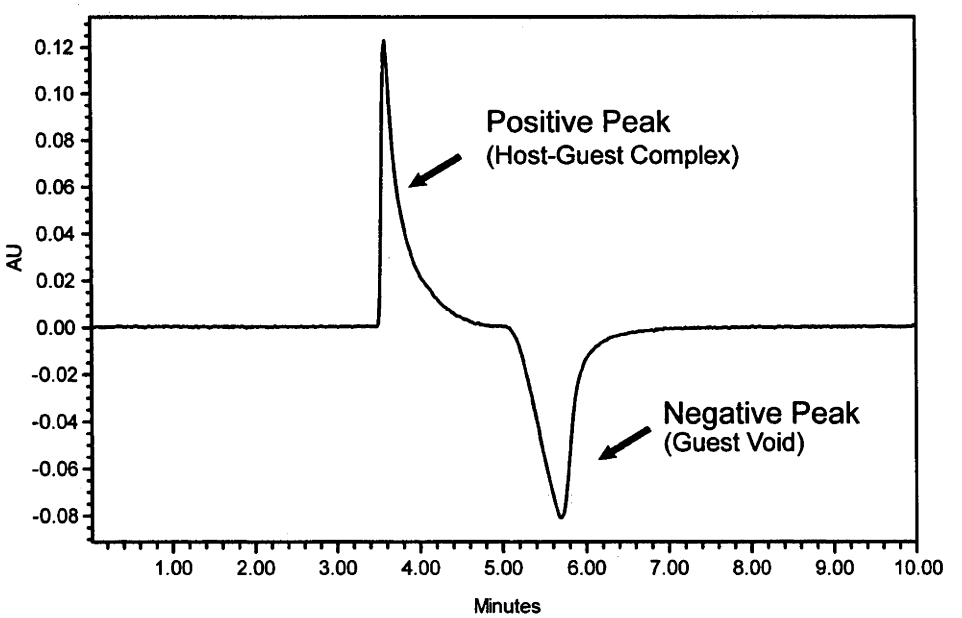

Figure 5.9. Example of a reverse-phase HPLC chromatogram at 450 nm of a cyclodextrin in a solution of the dye **5.8**.

The Scatchard plots for αCD (**1.15**) and the acetamides **5.5(E)** and **5.5(Z)** are represented in a combined graph in Figure 5.10. The transport coefficients of each of the CDs **1.15**, **5.5(E)** and **5.5(Z)** for the dye **5.8** are extrapolated from the y-intercepts of the plots and are summarised in Table 5.1. In the Scatchard plots, there are variations of the points at lower concentrations of the dye **5.8** (closest to the y-axis) from the lines of best fit. These errors are due to fluctuations created by the limited sensitivity for the detection of the dye **5.8** at low concentrations by the diode array detector of the HPLC. The transport coefficient of αCD (**1.15**) for the dye **5.8**, however, was calculated as 7900 dm^3 mol^{-1} which is comparable to literature values ranging from 6200 to 11700 dm^3 mol^{-1} determined using other methods.[91-95] Before the study was undertaken it was anticipated that due to the dimeric complex observed in the 2D NMR study of the acetamide **5.5(E)**, its ability to bind the dye **5.8** would be diminished in comparison to αCD (**1.15**). The transport coefficient of the acetamide **5.5(E)** was calculated at 2800 dm^3 mol^{-1} which is almost three times lower than that of unmodified αCD (**1.15**). As the acetamide **5.5(Z)** was shown to not form a self-inclusion complex, it was expected that the ability to bind the dye **5.8** would be larger in comparison to the *trans*-isomer **5.5(E)**. Due to the substitution of the CD, however, the transport coefficient of the *cis*-isomer **5.5(Z)** was expected to be comparable but lower than the unhindered αCD (**1.15**). The result obtained was very surprising with the transport coefficient of the acetamide **5.5(Z)** for the dye **5.8** calculated to be 30300 dm^3 mol^{-1} which is approximately four times greater than for αCD (**1.15**). The conformations of the stilbene units of the acetamides **5.5(E)** and **5.5(Z)** therefore have a large bearing on the ability to transport of the dye **5.8** along the HPLC column. Further investigation was needed to explain why the binding of the acetamide **5.5(Z)** for the dye **5.8** was so strong.

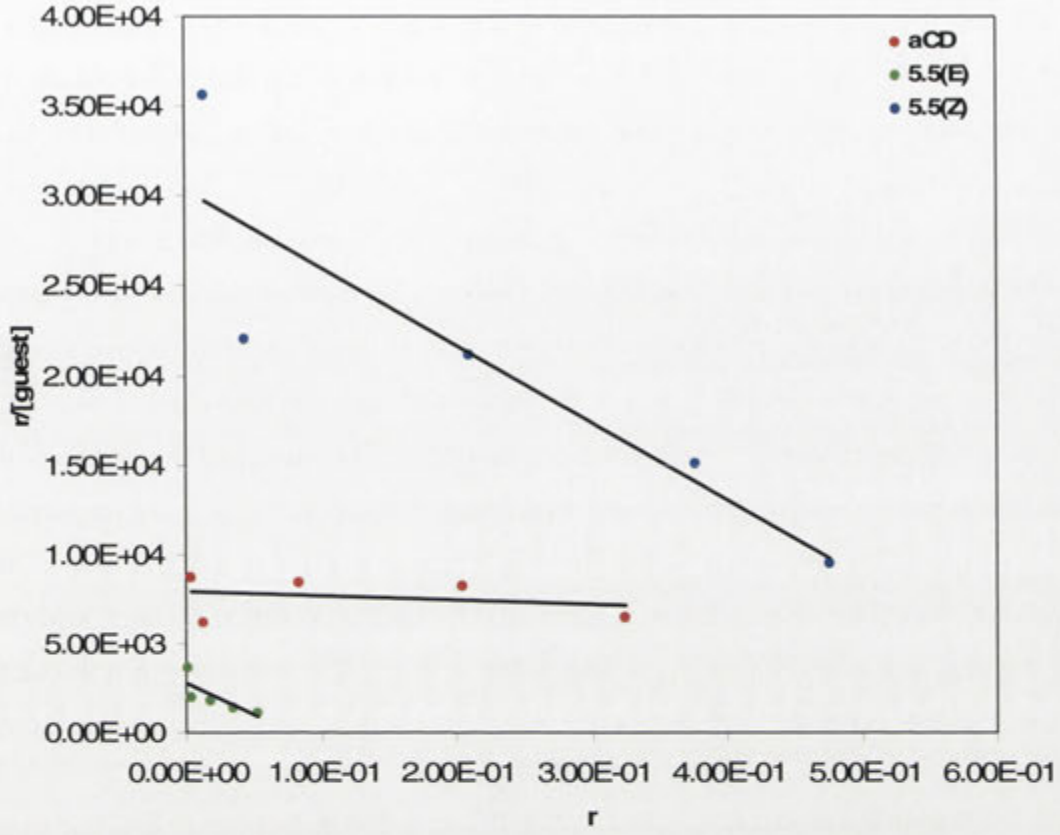

Figure 5.10. Scatchard plots for the dye **5.8** with αCD (**1.15**) and the acetamides **5.5(E)** and **5.5(Z)**.

Cyclodextrin	Transport Coefficient (*K*) ($dm^3\ mol^{-1}$)
αCD (**1.15**)	7900
5.5(E)	2800
5.5(Z)	30300

Table 5.1. Transport coefficients of the dye **5.8** by αCD (**1.15**), the acetamides **5.5(E)** and **5.5(Z)** from the Scatchard plots in Figure 5.10.

To investigate the increased binding of the dye **5.8** by the acetamide **5.5(Z)**, ROESY 2D NMR spectroscopy was conducted on an equimolar solution of the acetamide **5.5(Z)** and the dye **5.8** to identify any possible reasons for the unusual result. The ROESY contour plot of the aromatic region is shown in Figure 5.11. From the ten signals resulting from both the stilbene (A-F) and azobenene (AZO) proton signals, only those of

the *cis*-stilbene were assigned. The signals of the stilbene unit were assigned through interactions with the signals of the olefinic protons C and D which arise as one singlet at 6.33 ppm. The remaining signals are a result of the protons of the azobenzene of the dye **5.8**. From the ROESY contour plot in Figure 5.11 there are no identifiable NOE interactions between the signals of the stilbene and azobenzene protons that would signify a reason for the increased binding of the dye **5.8** for the acetamide **5.5(Z)**.

The ROESY contour plot in Figure 5.12 shows interactions between the signals of the CD protons and those of the aromatic protons. It was determined above that the stilbene of the acetamide **5.5(Z)** is not included. With no stilbene inclusion within the CD, the crosspeaks observed between the signals of the CD protons and the signals of the azobenzene protons of the dye **5.8** were anticipated. Interestingly, there are interactions observable between the signals of the *N*-methyl protons of the dye **5.8** and each of the signals of the *cis*-stilbene protons. The proximity of the *N*-methyl protons with the stilbene unit may arise as a result of a secondary binding interaction between the units. Presumably the secondary interactions create a cooperative binding effect to stabilise the inclusion complex and increase the transport coefficient.

The ROESY 2D NMR spectrum of the acetamide **5.5(E)** in D_2O with an added equivalent of the dye **5.8** was then studied. It had previously been determined from the HPLC transport assay that the dye **5.8** was limited in including within the CD due to the acetamide **5.5(E)** favouring a much stronger dimeric inclusion complex. From the ROESY contour plot shown in Figure 5.13, only NOE crosspeaks between the signals of the stilbene protons and those of the CD protons arise, confirming that the dye **5.8** does not displace the stilbene from the CD. The dimeric inclusion complex of the acetamide **5.5(E)** is therefore much stronger than its binding for the dye **5.8**. This strong dimeric inclusion complex would result in a reduced transport coefficient for the dye **5.8** by the acetamide **5.5(E)**.

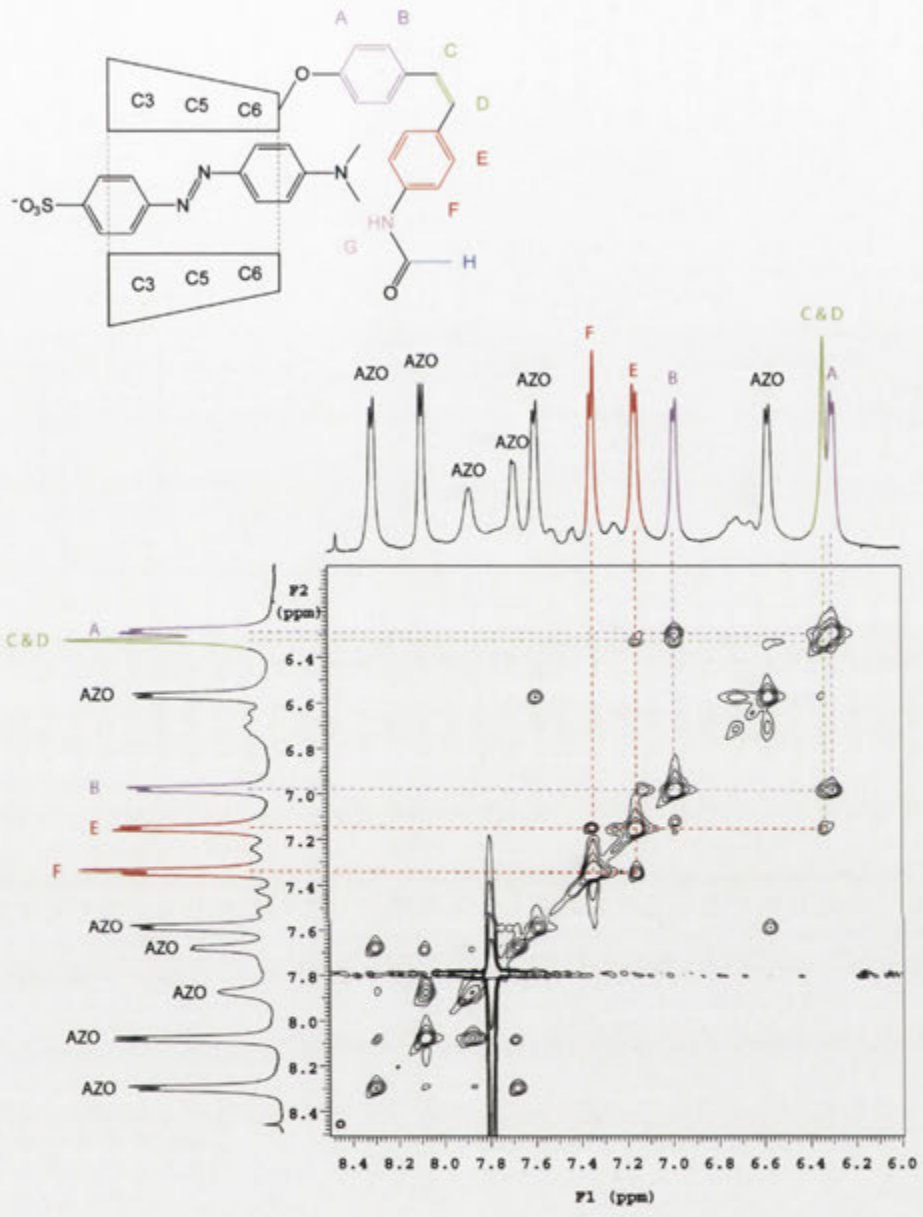

Figure 5.11. A section of the 500 MHz ROESY spectrum of the acetamide **5.5(Z)** with the dye **5.8** in D_2O at 25 °C of the region where crosspeaks are observed between aromatic proton signals.

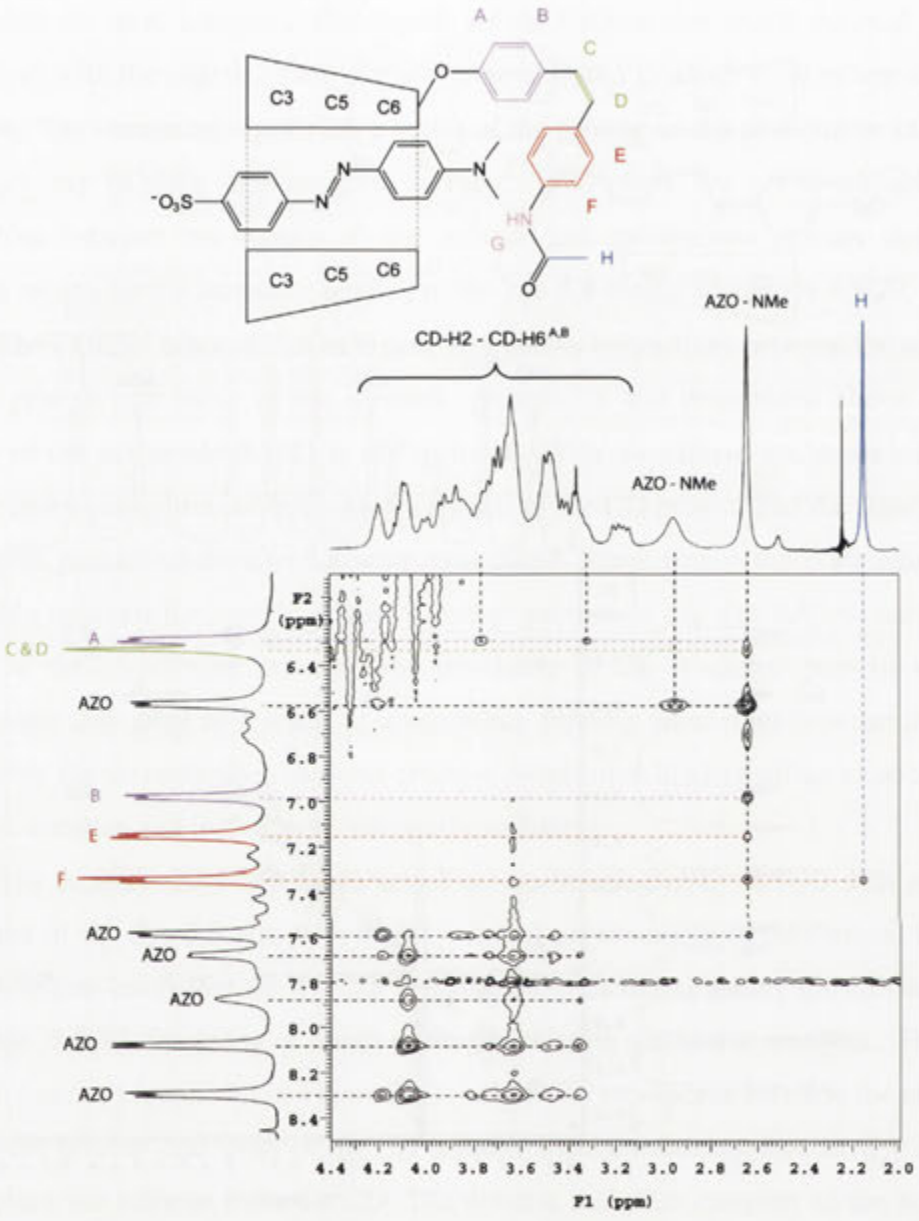

Figure 5.12. A section of the 500 MHz ROESY spectrum of the acetamide **5.5(Z)** with the dye **5.8** in D_2O at 25 °C of the region where crosspeaks are observed between aromatic proton signals and cyclodextrin or *N*-methyl proton signals.

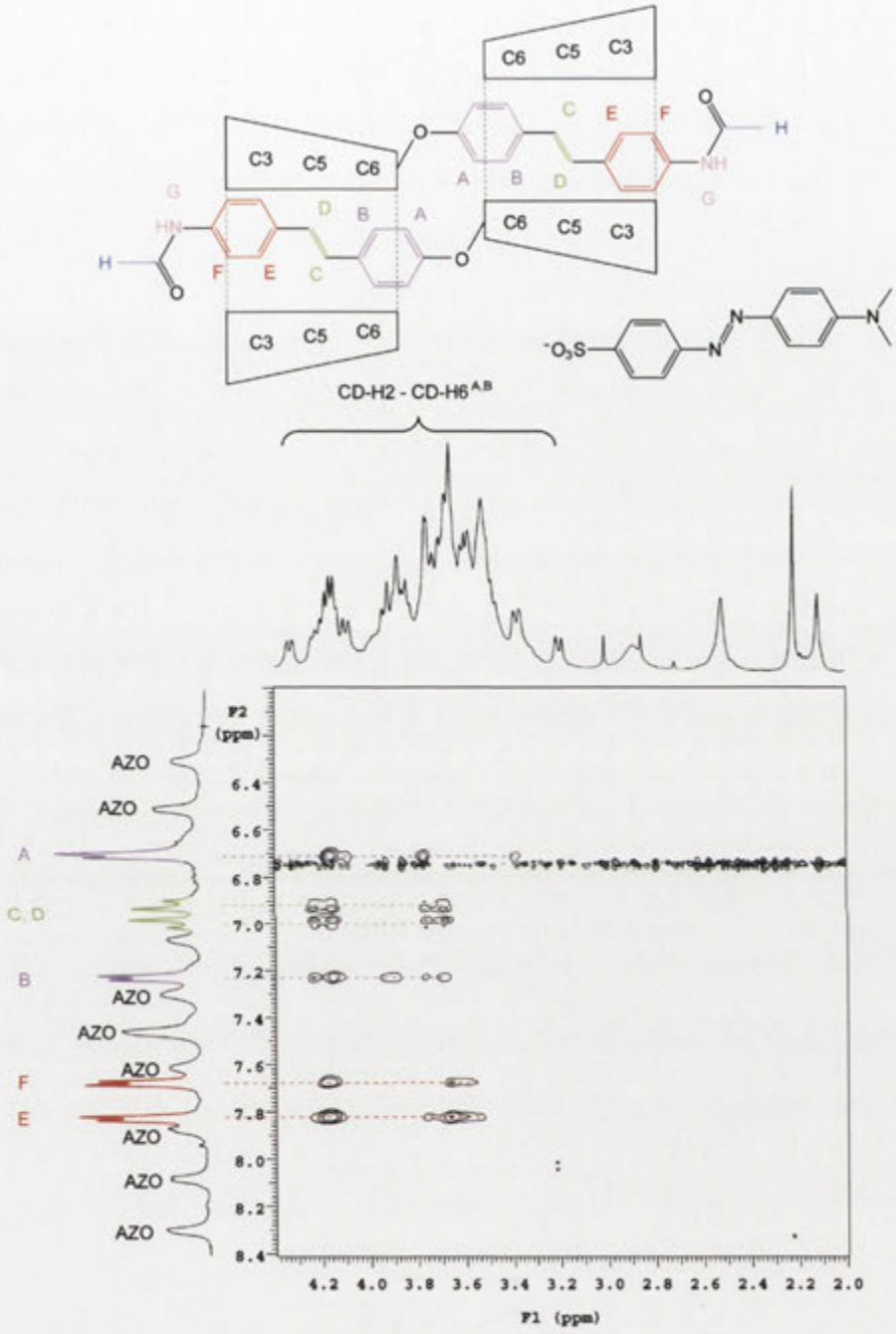

Figure 5.13. A section of the 500 MHz ROESY spectrum of the acetamide **5.5(E)** with the dye **5.8** in D_2O at 25 °C of the region where crosspeaks are observed between aromatic proton signals and cyclodextrin or *N*-methyl proton signals.

The conditions, however, for each of the NMR experiments differ from the HPLC study in terms of the concentrations at which they are able to be undertaken. An increased concentration is required for NMR spectroscopy that may result in exaggerated binding

effects. Inclusion complex formation is concentration dependent which would increase the likelihood of the acetamide **5.5(E)** forming a dimeric inclusion complex in the NMR spectroscopy study than at the lower concentration of the HPLC study. Nevertheless, the NMR study can be used as a strong guide to the behaviour of the acetamide **5.5(E)** as a dimeric inclusion complex is likely to have formed in the HPLC study to reduce its transport coefficient with the dye **5.8**.

An hermaphroditic CD molecular switch has therefore been constructed which can be powered through photochemical energy. The binding characteristics for the acetamides **5.5(E)** and **5.5(Z)** for the dye **5.8** are summarised in Scheme 5.6. Light of wavelength 350 nm has been shown using UV/visible spectroscopy, NMR spectroscopy and HPLC to convert the acetamide **5.5(E)** to the *cis*-isomer **5.5(Z)**. This reaction is reversible through irradiation with light of wavelength 254 nm. The acetamide **5.5(E)** forms the dimeric inclusion complex **5.7** to hinder the transport of the dye **5.8** while the *cis*-isomer **5.5(Z)** allows the dye **5.8** to include facilitating its transport. The ROESY 2D NMR spectrum of the acetamide **5.5(Z)** with the dye **5.8** also shows NOE interactions between the signals of the *N*-methyl protons of the dye **5.8** and those of the *cis*-stilbene unit that may be the result of a secondary interaction that increases the transport coefficient of the *cis*-isomer **5.5(Z)** for the dye **5.8**.

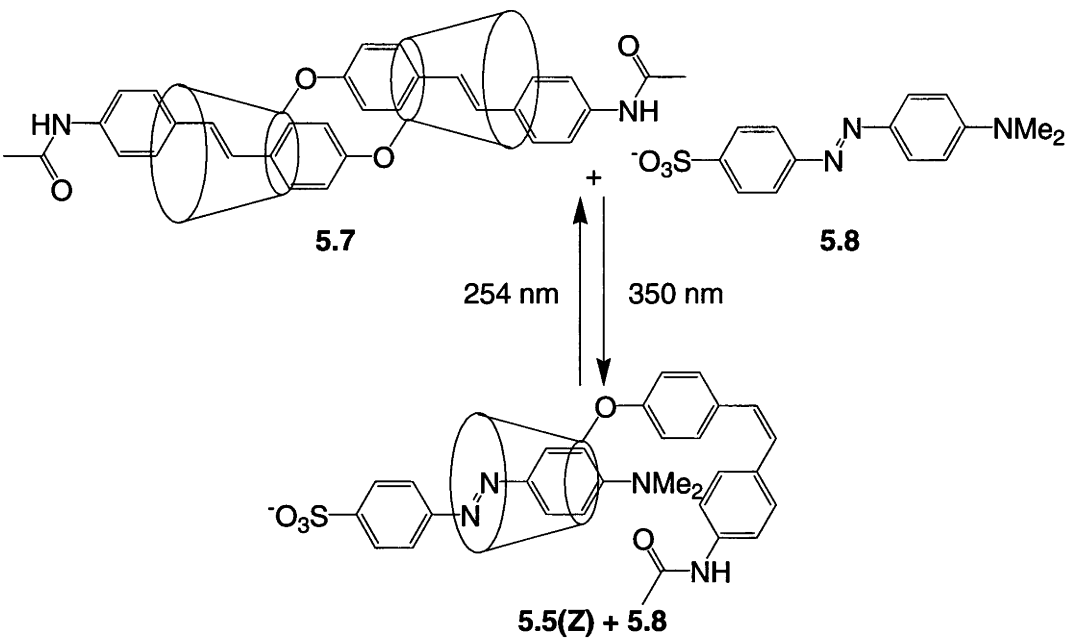

Scheme 5.6. Operation of a photochemically switchable device for the transport of methyl orange (**5.8**).

Chapter 6: Synthesis of α-Cyclodextrin [2]-Rotaxanes Using Methoxytriazine Blocking Groups

In the work described in Chapter 2 it was shown that [2]-rotaxanes with ditopic axles containing stilbenes are able to be made using trinitrophenyl blocking groups. These molecules are unable to photochemically interconvert been their *trans*- and *cis*-isomers to act as molecular shuttles due to interference of the trinitrophenyl blocking groups. In an attempt to find alternative blocking groups to construct a [2]-rotaxane molecular shuttle, nitrile oxide cycloaddition chemistry was used but proved unsuccessful. A different approach was therefore sought using a triazine as a blocking reagent to form [2]-rotaxanes.

In the related synthesis conducted by Kunitake *et al.*,[96] shown in Scheme 6.1, 2,4,6-trichloro-1,3,5-triazine (**6.1**) was substituted with the naphthalene **6.2** to produce the triazine **6.3**. Upon addition to a solution of the HCl salt of the stilbene **1.30** and βCD (**1.16**), followed by the addition of aniline (**6.4**), the triazinyl [2]-rotaxane **6.5** was formed. Due to the success of this strategy, tests were undertaken to see if this could be applied in the synthesis of [2]-rotaxanes and hermaphroditic [2]-rotaxanes that would act as molecular shuttles and muscles. Small modifications were made to adapt the synthesis to install some preferred features. The CD was changed from βCD (**1.16**) to αCD (**1.15**) as αCD (**1.15**) has a much larger affinity for stilbenes.[68] The methoxy-substituted triazines **6.6** and **6.9** were commercially available and used in the reactions.

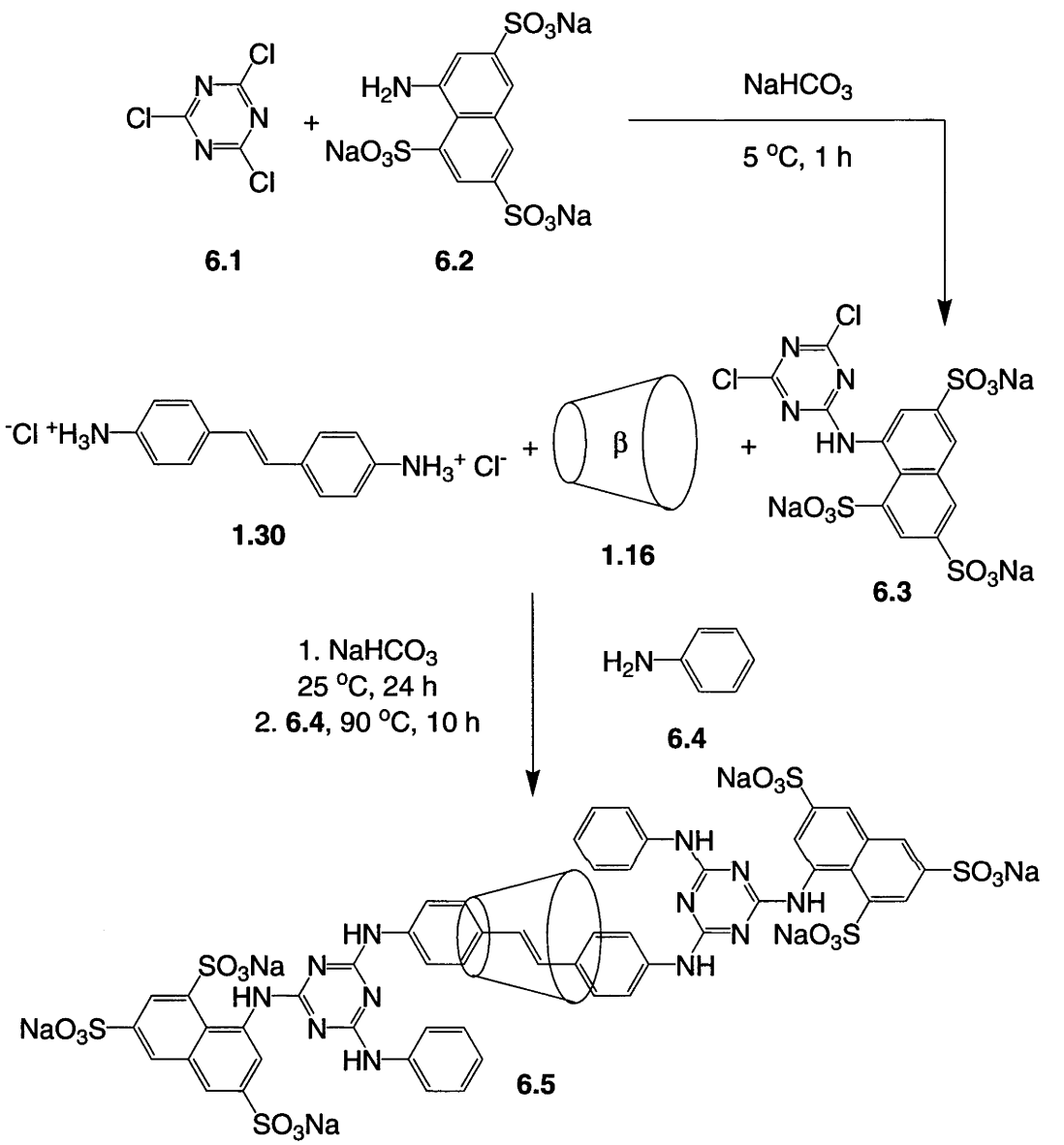

Scheme 6.1. Formation of the triazine capped [2]-rotaxane **6.5** as reported by Kunitake *et al.*[96]

The methoxytriazine **6.6** was used first as shown in Scheme 6.2. To a stirred suspension of the stilbene **1.30** and αCD (**1.15**) in MQ H_2O, the triazine **6.6** was added. The triazinyl [2]-rotaxane **6.7** was isolated from the reaction mixture in a yield of 20% and its HI-RES ESI mass spectrum showed an $M+Na^+$ ion of *m/z* 1491.3960.

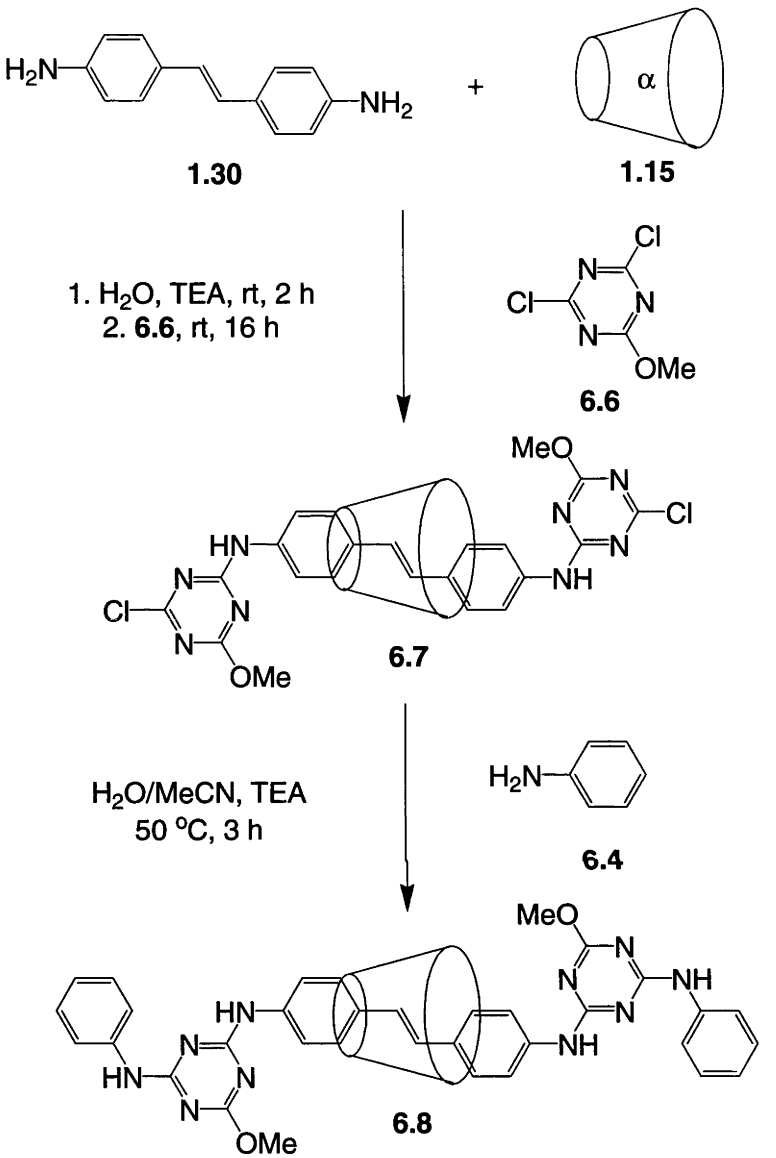

Scheme 6.2. Formation of the [2]-rotaxane **6.8**.

With the [2]-rotaxane **6.7** in hand, 2D NMR spectroscopy was used to determine the position of the CD on the axle. The CD proton signals were firstly assigned from the DQCOSY contour plot found in Figure 6.1. The signals of the stilbene unit of the [2]-rotaxane **6.7** were then assigned using both the DQCOSY and ROESY 2D NMR spectra shown in Figures 6.2 and 6.3.

Crosspeaks between the signals of the CD and stilbene protons were then sought in the ROESY contour plot shown in Figure 6.4. As the study was conducted in d_6-

DMSO which does not favour CD inclusion complexes, any crosspeaks between the signals would indicate the formation of a [2]-rotaxane. In the plot, NOE interactions are visible between each of the signals of the stilbene protons with the signals of the CD protons. The signal of the aromatic protons C shows interactions with those of the CD-H6 protons indicating the aromatic protons reside at the primary face of the CD. The signals of the protons G and H show interactions with those of the CD-H3 and CD-H5 protons indicating the protons G and H reside at the secondary face of the CD. The structure of the [2]-rotaxane **6.7** can therefore be drawn as shown in Figure 6.4.

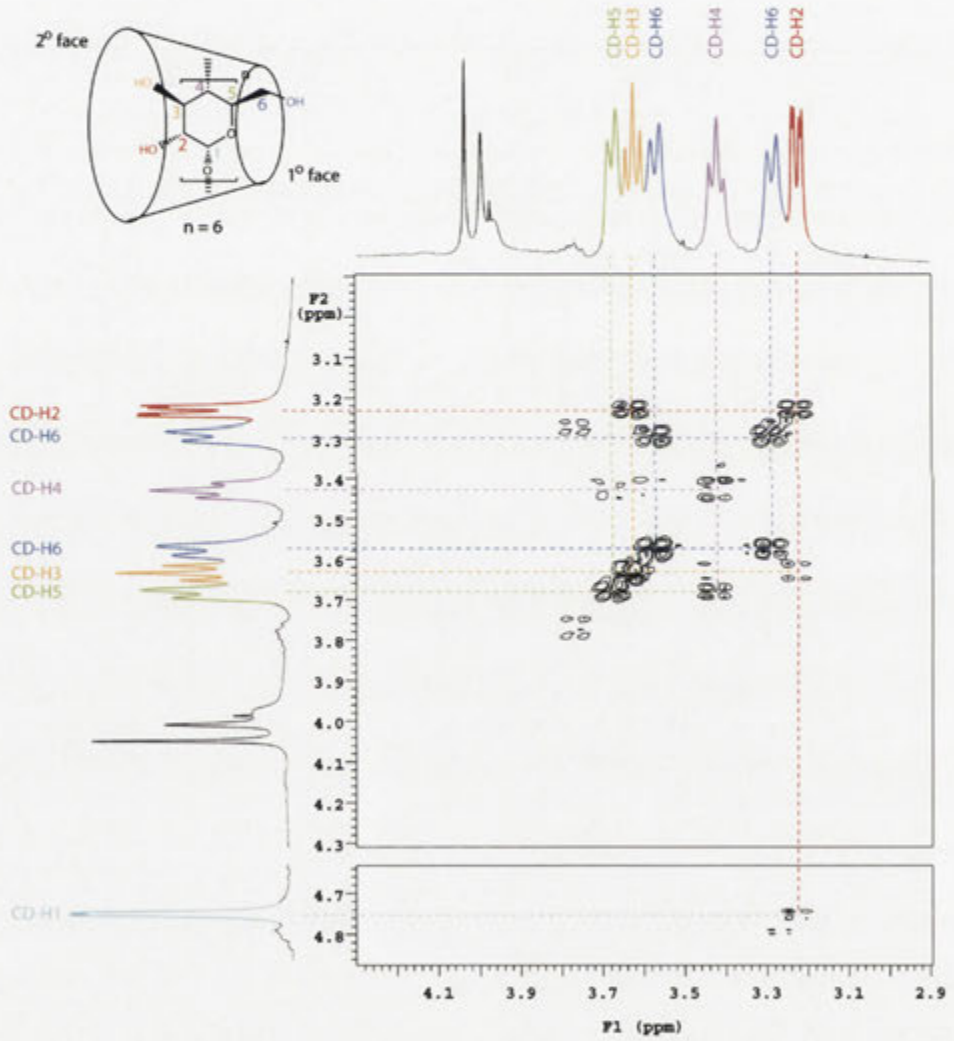

Figure 6.1. A section of the 500 MHz DQCOSY spectrum of the [2]-rotaxane **6.7** in d_6-DMSO at 25 °C of the region where crosspeaks are observed between cyclodextrin proton signals.

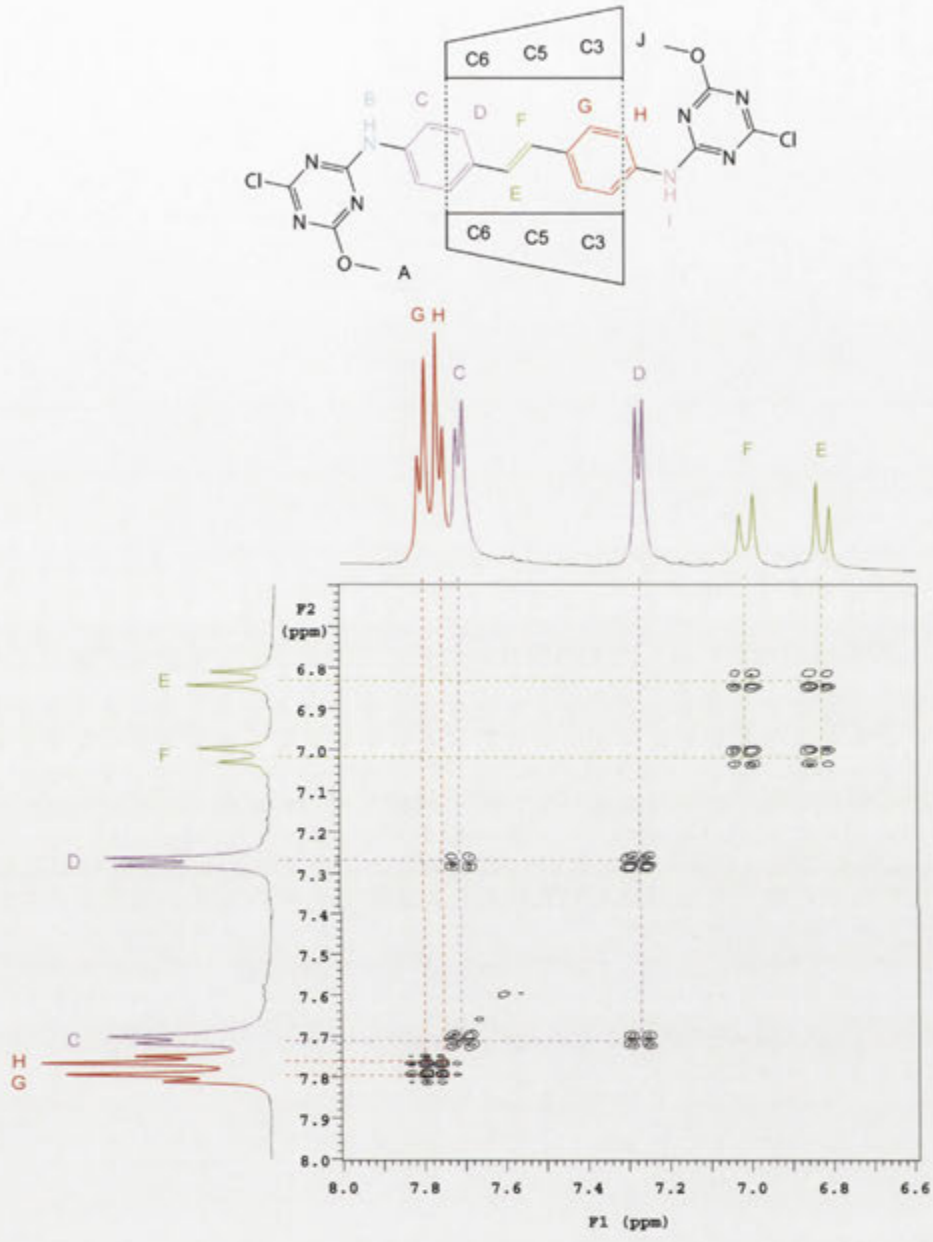

Figure 6.2. A section of the 500 MHz DQCOSY spectrum of the [2]-rotaxane **6.7** in d_6-DMSO at 25 °C of the region where crosspeaks are observed between stilbene proton signals.

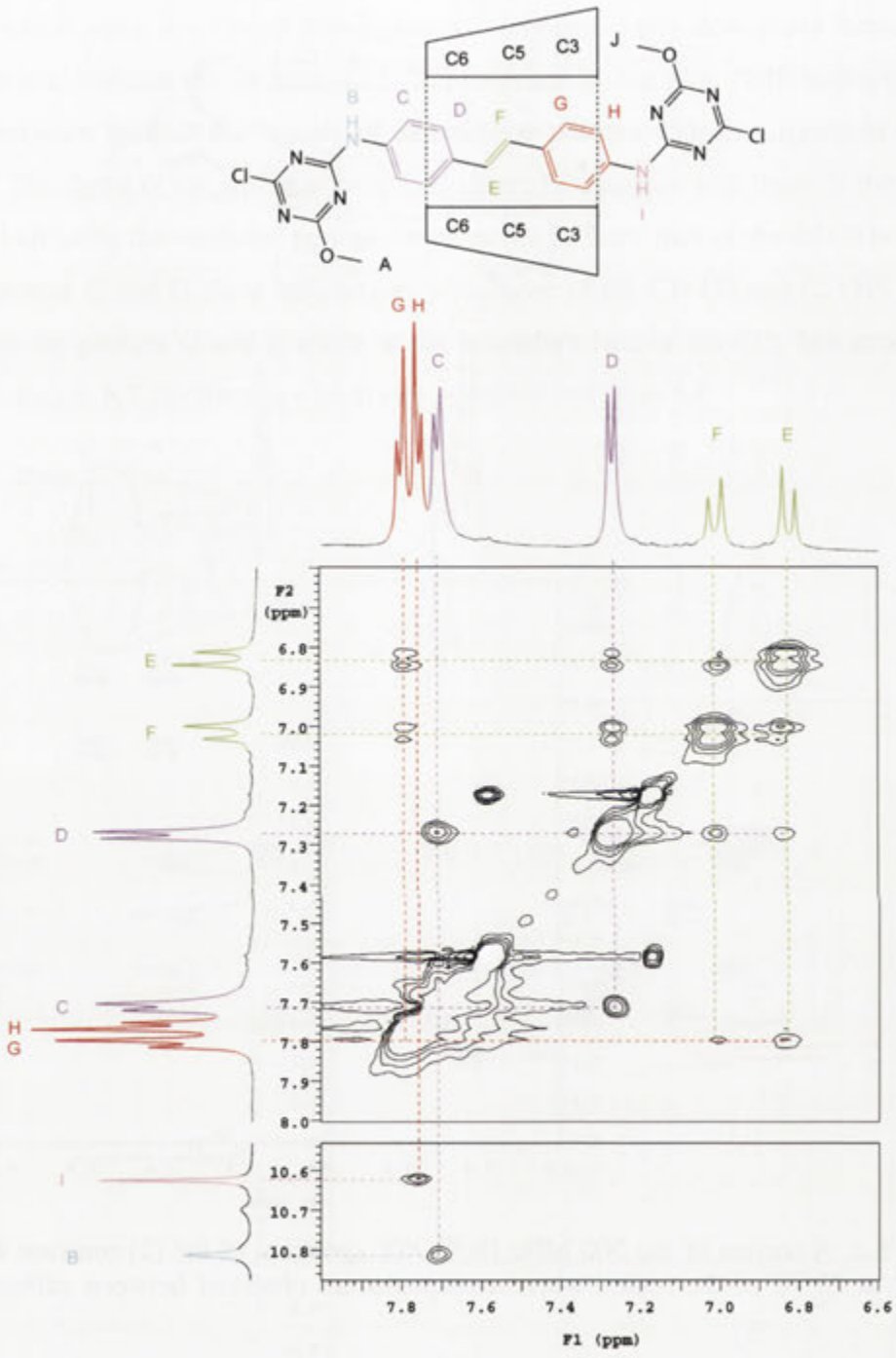

Figure 6.3. A section of the 500 MHz ROESY spectrum of the [2]-rotaxane **6.7** in d_6-DMSO at 25 °C of the region where crosspeaks are observed between stilbene proton signals.

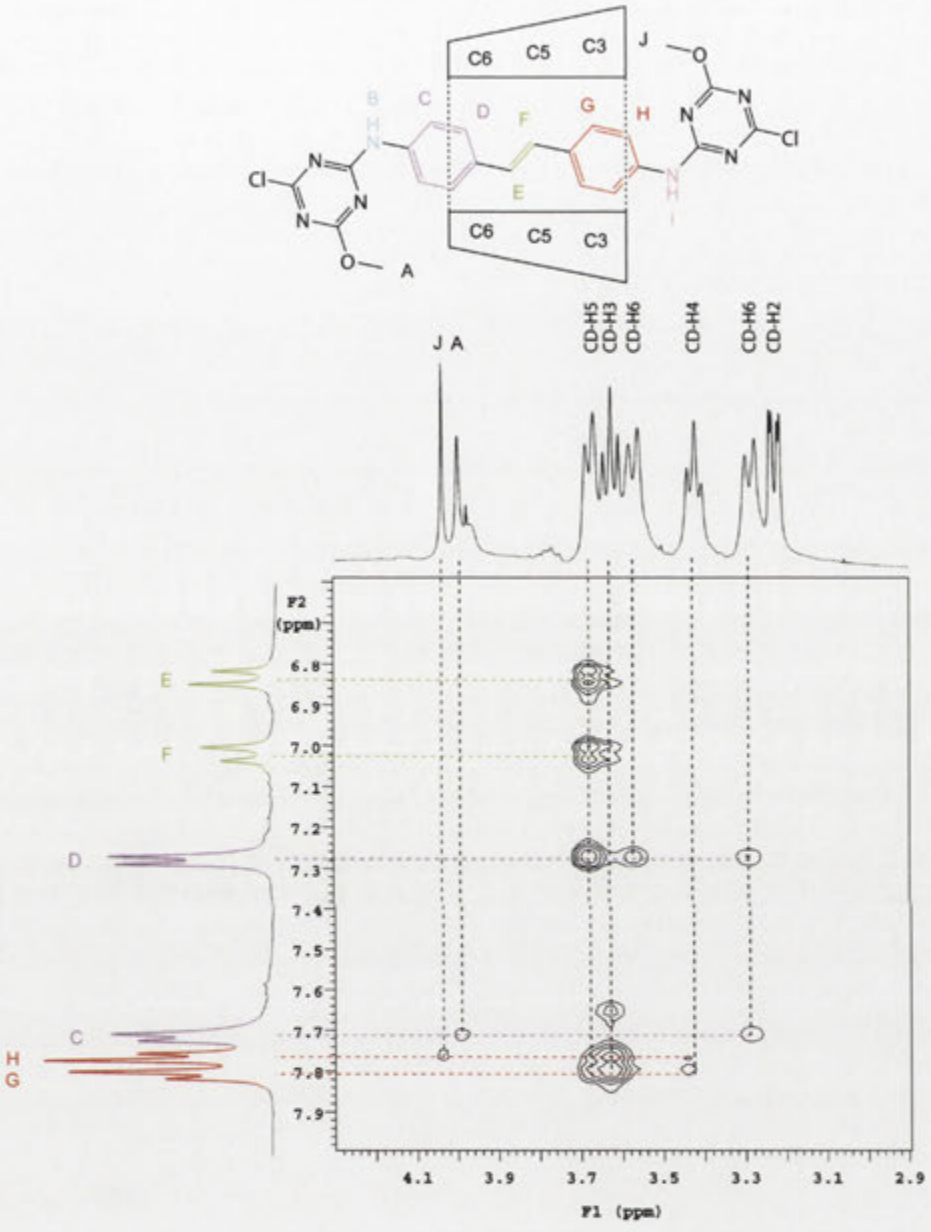

Figure 6.4. A section of the 500 MHz ROESY spectrum of the [2]-rotaxane **6.7** in d_6-DMSO at 25 °C of the region where crosspeaks are observed between stilbene and cyclodextrin proton signals.

While the triazinyl [2]-rotaxane **6.7** was formed it appeared it was not entirely stable. This was evident by the formation of a decomposition product as noted by extra signals appearing in the ^{1}H NMR spectrum. Over the course of several days the signals resulting from the protons of the [2]-rotaxane **6.7** disappeared. Assuming this was due to the reactivity of the chlorotriazine moiety a final substitution was therefore performed on

the [2]-rotaxane **6.7** with aniline (**6.4**) to form the aniline substituted [2]-rotaxane **6.8** as detailed in Scheme 6.2. The [2]-rotaxane **6.8** was isolated in a yield of 33% and its HI-RES ESI mass spectrum showed an $M+H^+$ ion of *m/z* 1583.3780.

2D NMR spectroscopy was then conducted on the [2]-rotaxane **6.8** to assign its signals. Using the DQCOSY contour plot shown in Figure 6.5, the signals of the CD protons were assigned as depicted.

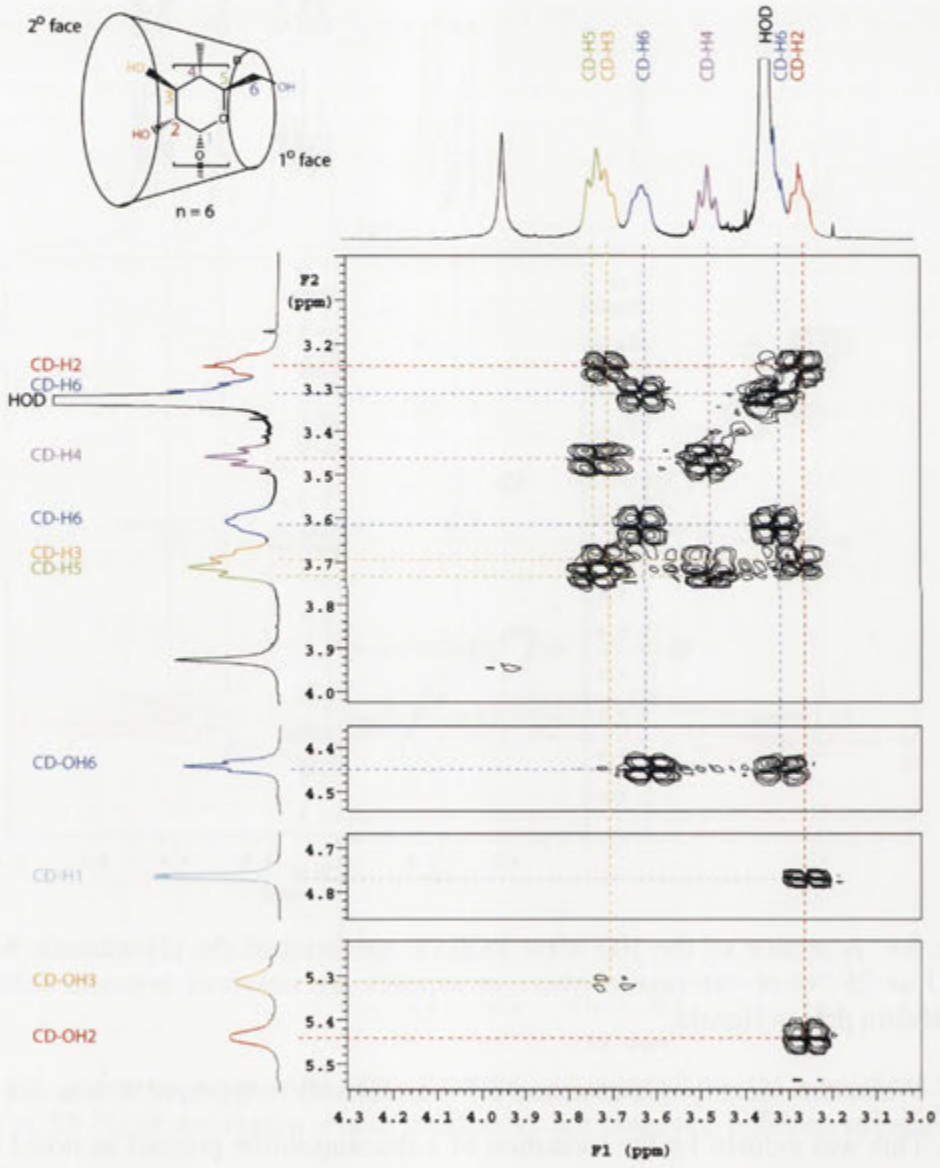

Figure 6.5. A section of the 500 MHz DQCOSY spectrum of the [2]-rotaxane **6.8** in d_6-DMSO at 25 °C of the region where crosspeaks are observed between cyclodextrin proton signals.

The axle proton signals were then assigned from a combination of both the DQCOSY and ROESY contour plots shown in Figures 6.6 and 6.7. The signals of the aniline protons A, B, C, P, Q and R at either end of the [2]-rotaxane **6.8** were able to be assigned through their integration and DQCOSY interactions. The remaining signals of the stilbene protons were assigned through their DQCOSY and ROESY interactions.

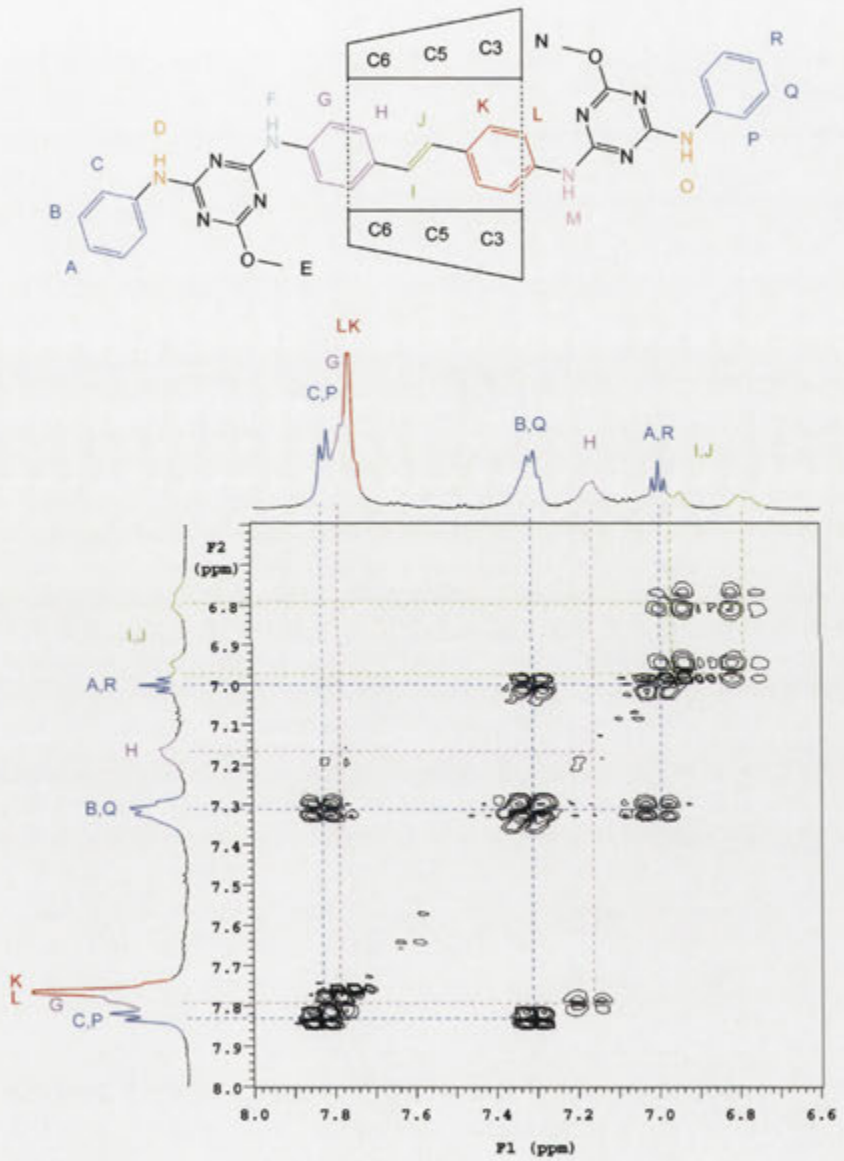

Figure 6.6. A section of the 500 MHz DQCOSY spectrum of the [2]-rotaxane **6.8** in d_6-DMSO at 25 °C of the region where crosspeaks are observed between axle proton signals.

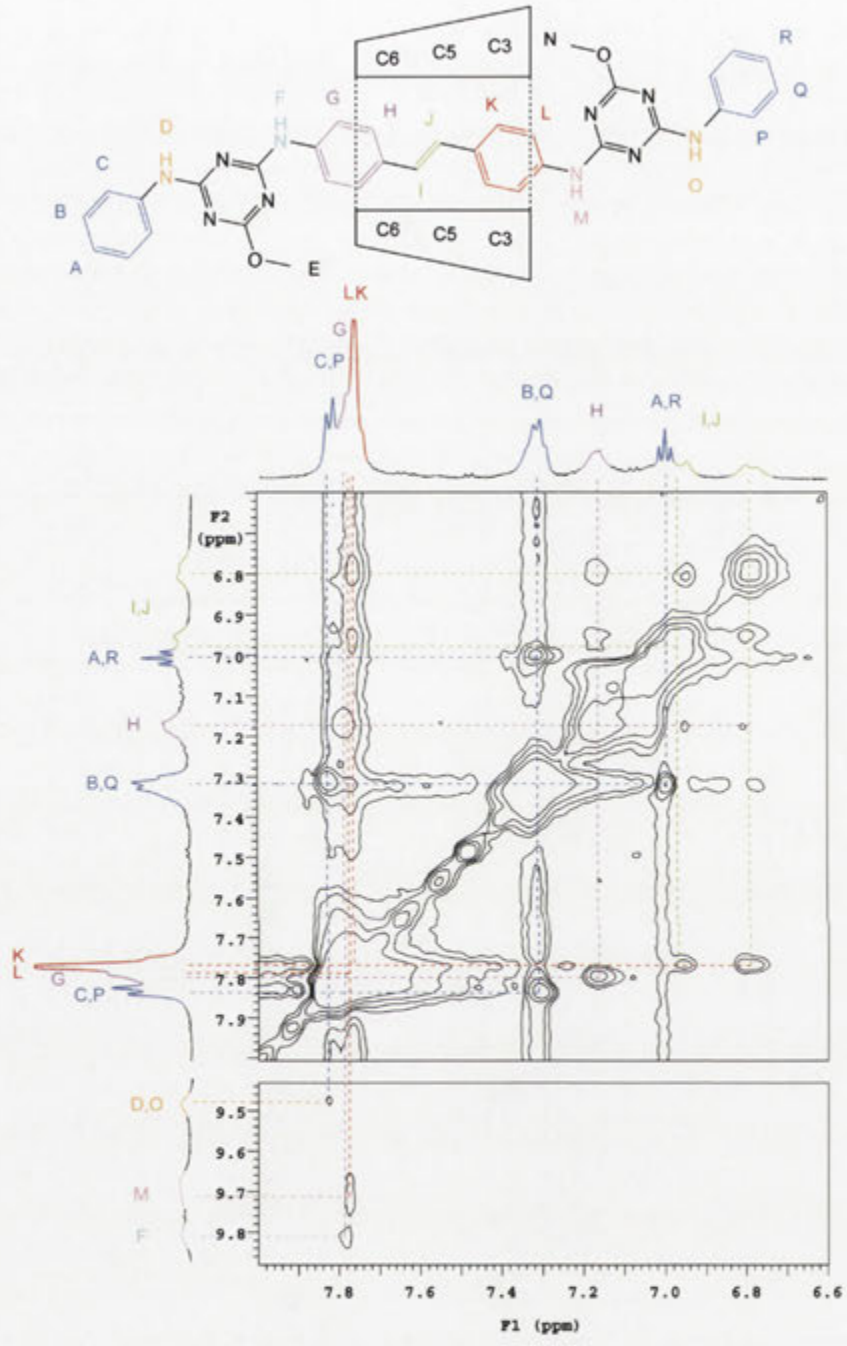

Figure 6.7. A section of the 500 MHz ROESY spectrum of the [2]-rotaxane **6.8** in d_6-DMSO at 25 °C of the region where crosspeaks are observed between axle proton signals.

The ROESY contour plot in Figure 6.8 shows crosspeaks between the signals of the CD protons and those of the stilbene protons. The signals of the aniline protons show no interaction with the CD. Their three relatively sharp signals are due to their chemical

equivalence in not being associated with the CD. The signal of the aromatic protons H shows an interaction with the signal of the CD-H6 protons while the signals of the olefinic protons I and J do not. This places the CD on the axle as shown in Figure 6.8. From the plot there is therefore no change in the CD binding as a result of the final substitution of the triazine ring with the amine **6.4**.

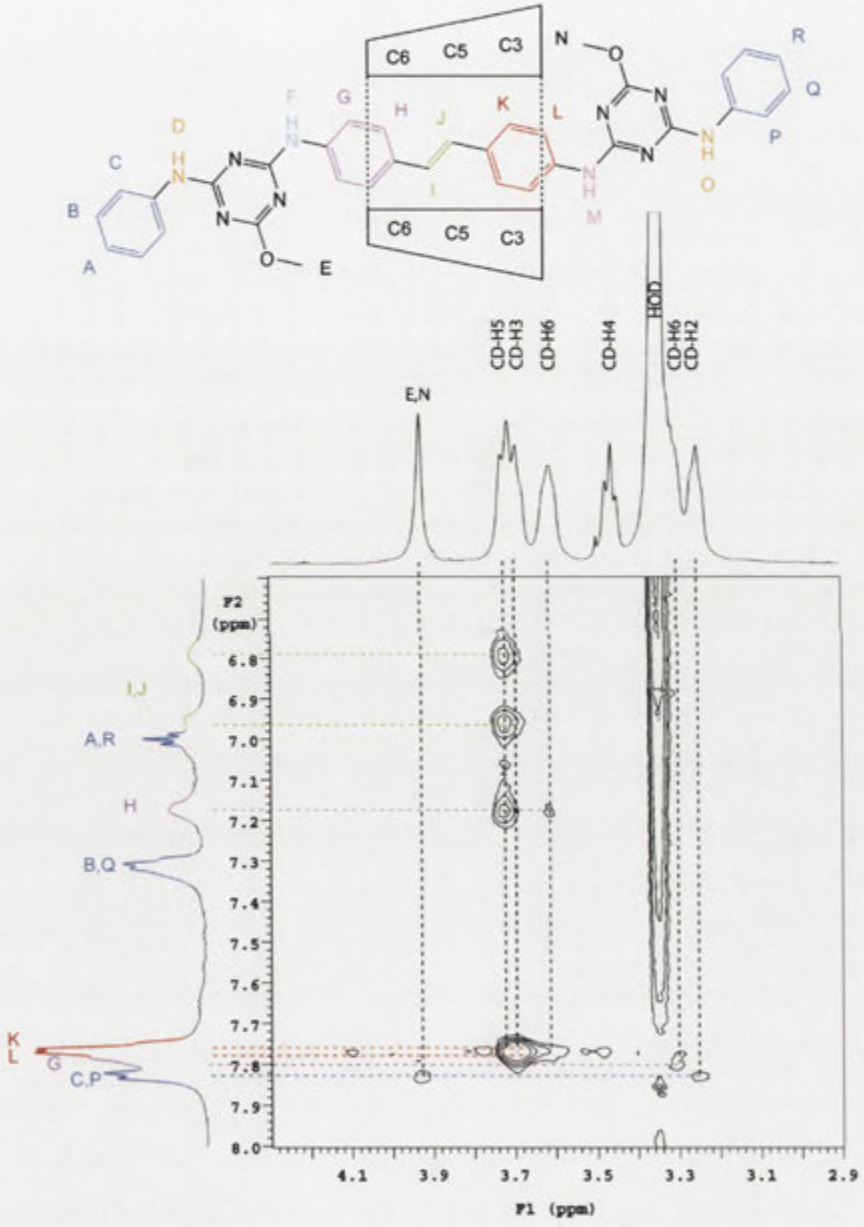

Figure 6.8. A section of the 600 MHz DQCOSY spectrum of the [2]-rotaxane **6.8** in d_6-DMSO at 25 °C of the region where crosspeaks are observed between axle and cyclodextrin proton signals.

An alternative one step procedure was investigated to form a triazinyl [2]-rotaxane, in which the dimethoxytriazine **6.9** was used as the blocking reagent. The reaction scheme is illustrated in Scheme 6.3. The [2]-rotaxane **6.10** was isolated in 4.8% yield and its HI-RES ESI mass spectrum showed an $M+Na^+$ ion of *m/z* 1461.5141.

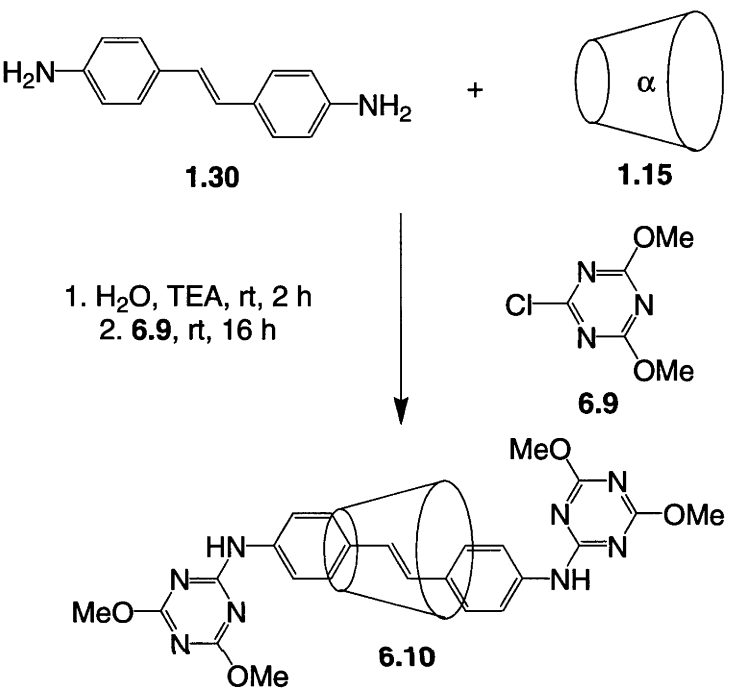

Scheme 6.3. Formation of the dimethoxytriazinyl [2]-rotaxane **6.10**.

The ^1H NMR assignment using 2D NMR spectroscopy on the [2]-rotaxane **6.10** was carried out by firstly assigning the signals of the CD protons from the DQCOSY contour plot shown in Figure 6.9.

Next examining the aromatic region of the ROESY contour plot in Figure 6.10, the signals of the stilbene protons were assigned. In previous assignments the DQCOSY spectrum was also consulted but in this case it was not required.

From the ROESY NMR contour plot shown in Figure 6.11, the position of the CD on the stilbene unit of the [2]-rotaxane **6.10** was assigned. The signals of the olefinic protons E and F show strong interactions with the signals of the CD-H5 protons and weak interactions with the signals of the CD-H3 protons. This places the olefinic protons centrally within the CD annulus. The signal of the aromatic protons D shows interactions with the signals of the CD-H5, CD-$H6^A$ and CD-$H6^B$ protons. This places this part of the

stilbene at the primary face of the CD. Therefore the structure of the [2]-rotaxane **6.10** can be drawn as shown in Figure 6.11.

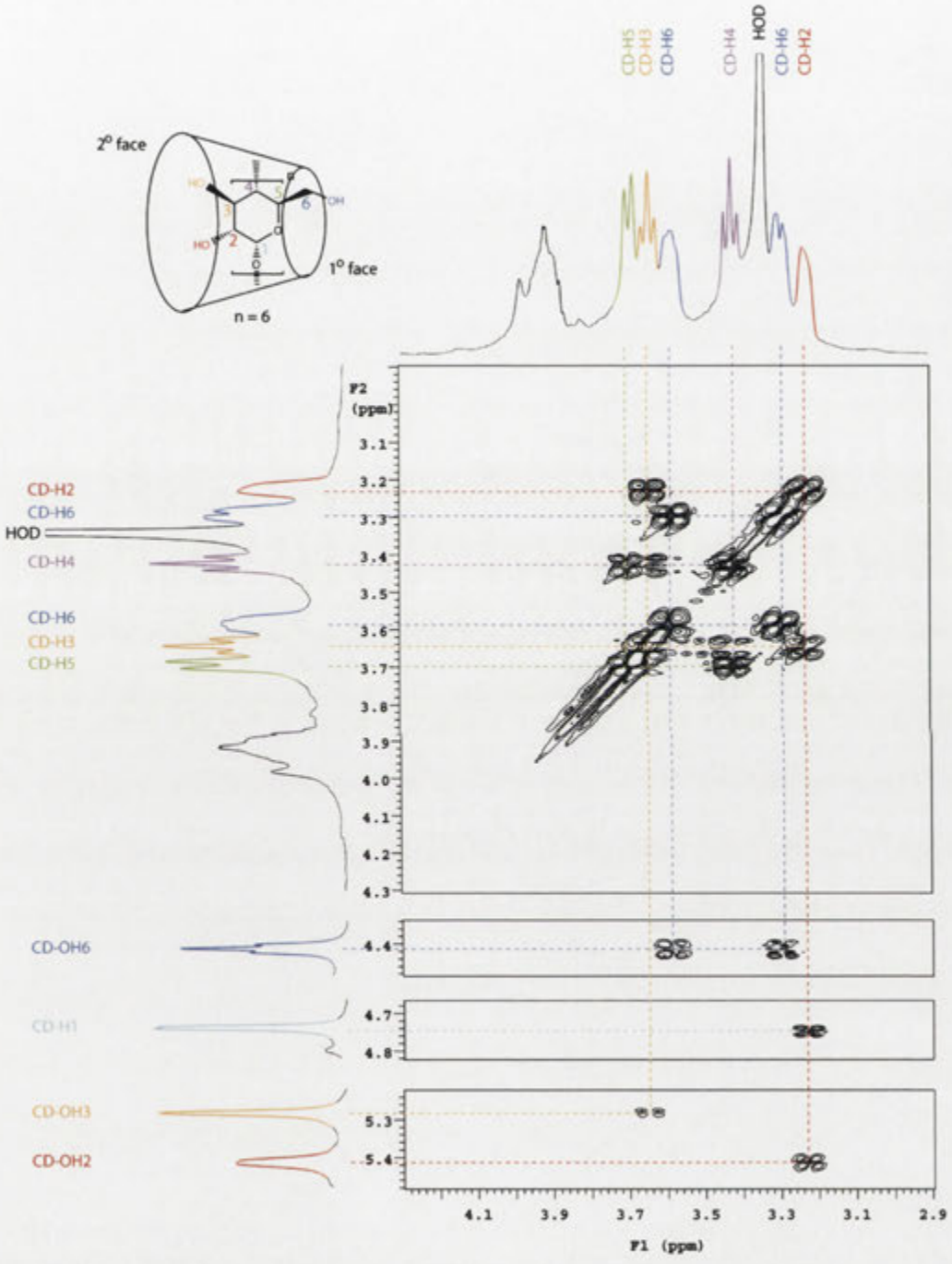

Figure 6.9. A section of the 500 MHz DQCOSY spectrum of the [2]-rotaxane **6.10** in d_6-DMSO at 25 °C of the region where crosspeaks are observed between cyclodextrin proton signals.

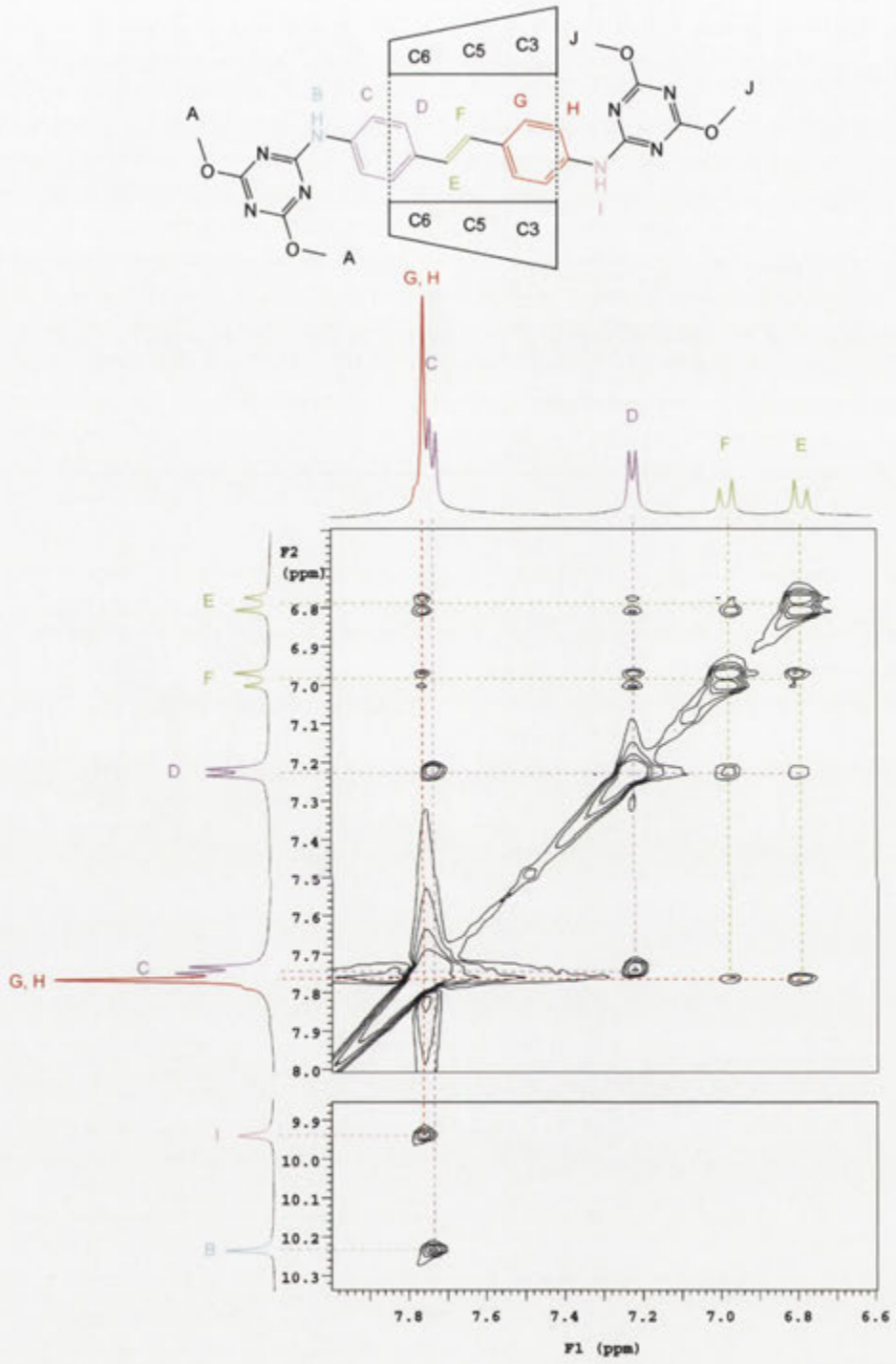

Figure 6.10. A section of the 500 MHz ROESY spectrum of the [2]-rotaxane **6.10** in d_6-DMSO at 25 °C of the region where crosspeaks are observed between stilbene proton signals.

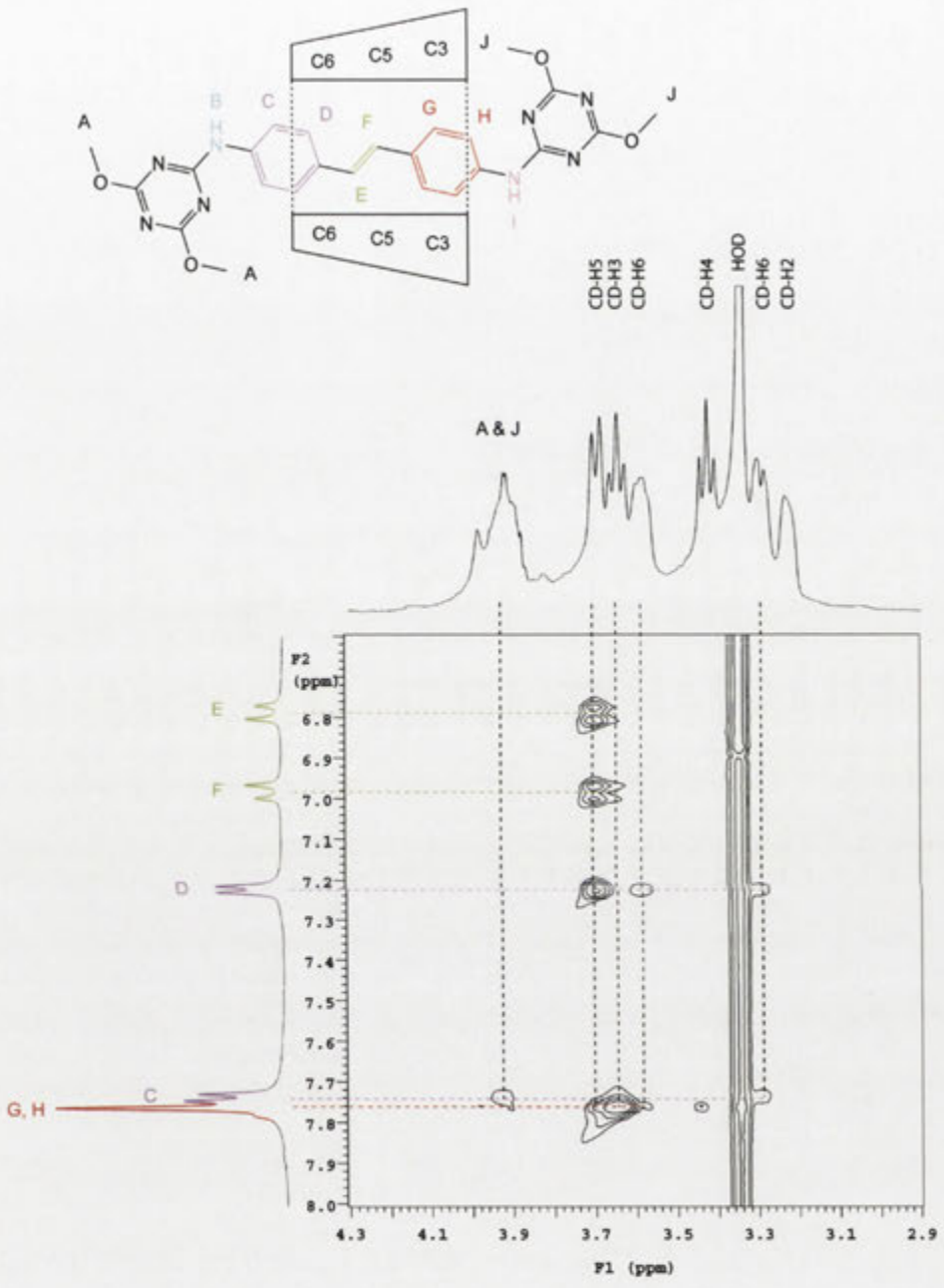

Figure 6.11. A section of the 500 MHz ROESY spectrum of the [2]-rotaxane **6.10** in d_6-DMSO at 25 °C of the region where crosspeaks are observed between stilbene and cyclodextrin proton signals.

In summary, the synthesis of the [2]-rotaxanes **6.7**, **6.8** and **6.10** provides a means to produce a [2]-rotaxane with an alternative blocking group to the trinitrophenyl systems. The structures as a result of their 2D NMR assignment are shown in Figure 6.12.

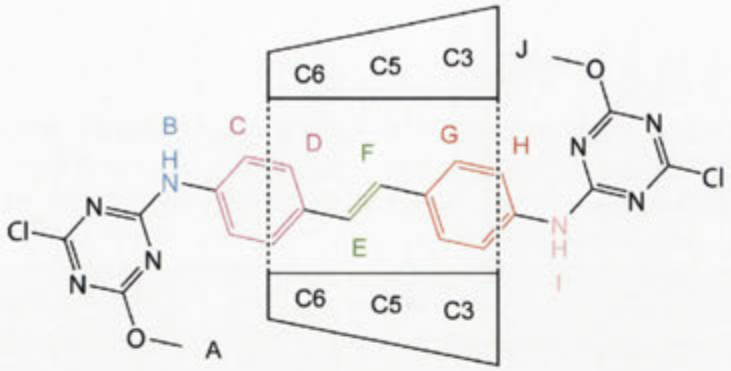

6.7

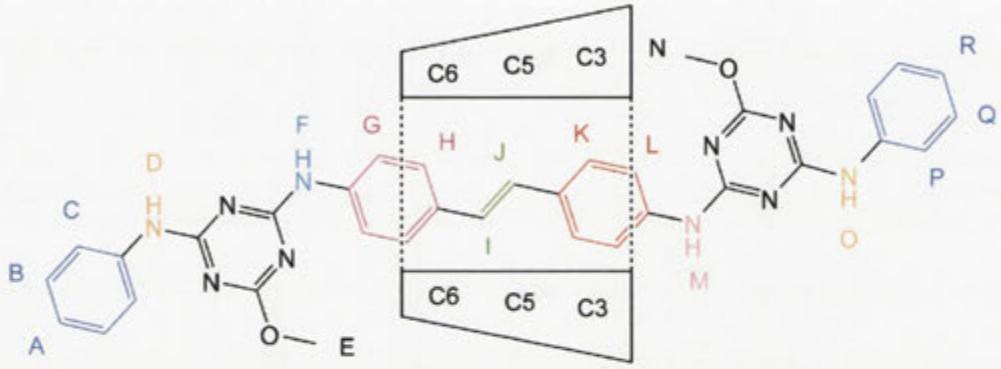

6.8

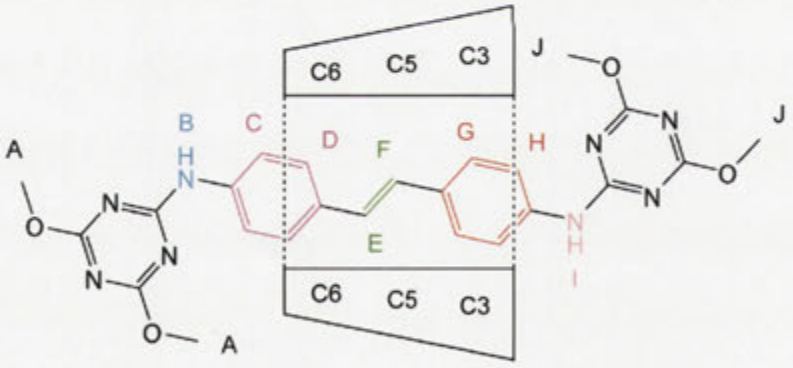

6.10

Figure 6.12. Structures of the [2]-rotaxanes **6.7**, **6.8** and **6.10** determined through 2D ^{1}H NMR spectral assignment.

Chapter 7: Isomeric Dimethoxytriazine Blocked [2]-Rotaxanes that Act as Molecular Shuttles

The synthesis of the new triazine blocked [2]-rotaxanes **6.7**, **6.8** and **6.10** provides alternatives to the use of the trinitrophenyl blocking reagent **1.31** used previously. Triazine blocking groups were therefore used in the synthesis of potential molecular shuttles and muscles. From the previous chapter it was observed that the stability of the dichloro-[2]-rotaxane **6.7** came into question. A further substitution with the amine **6.4** was required to form the [2]-rotaxane **6.8** to prevent any decomposition. The synthesis of the [2]-rotaxane **6.10** was completed in one step with no such complications. Despite the lower yield for the reaction using the triazine blocking reagent **6.9** to form the [2]-rotaxane **6.10**, as the product of the reaction was more stable the triazine **6.9** was used in the syntheses detailed in this chapter.

An axle suitable for the synthesis of a simple shuttle system was therefore required. The ditopic diamine **2.11**, whose synthesis was described in Chapter 2, was deemed ideal to produce a [2]-rotaxane with the potential to act as a simple molecular shuttle. The synthetic scheme for the formation of the [2]-rotaxanes **7.1** and **7.2** is shown in Scheme 7.1. The diamine **2.11** was stirred in MQ H_2O with αCD (**1.15**) before the triazine blocking reagent **6.9** was added. The [2]-rotaxanes **7.1** and **7.2** were determined to be formed in a ratio of 69:31, using HPLC, and were isolated in yields of 3.4% and 1.3% respectively. The formation of the [2]-rotaxanes **7.1** and **7.2** was confirmed by ESI mass spectroscopy where they each produced $M+H^+$ ions of *m/z* 1594.5 in their mass spectra.

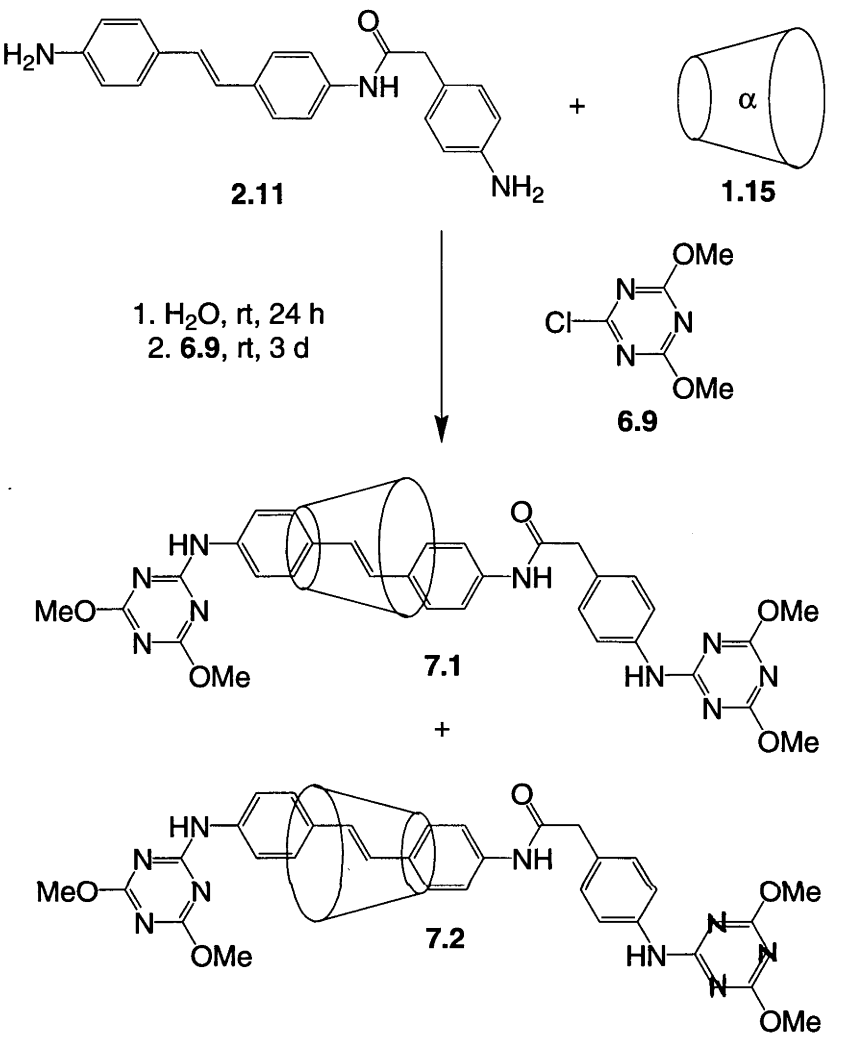

Scheme 7.1. Formation of the [2]-rotaxanes **7.1** and **7.2**.

The isomeric [2]-rotaxanes **2.12** and **2.13** differ in the orientation of the CD on the axle. The orientation of the CD was determined using ROESY 2D NMR spectroscopy where NOE interactions between the signals of the CD annular protons and the signals of the axle protons arise as crosspeaks in the contour plot. 2D NMR spectroscopy was conducted on each of the [2]-rotaxanes **7.1** and **7.2** to confirm that they were also orientational isomers.

Firstly, in the assignment of the signals of the [2]-rotaxane **7.1**, those of the CD protons were assigned as in the previous chapters. The DQCOSY spectrum was used with the contour plot of the CD region shown in Figure 7.1. The initial assignment of the signal of the CD-H1 protons located at 4.75 ppm was made according to the literature

review by Schneider *et al.*[77] DQCOSY interactions between the signals of neighbouring protons of the CD enable the signals to be assigned as shown in Figure 7.1.

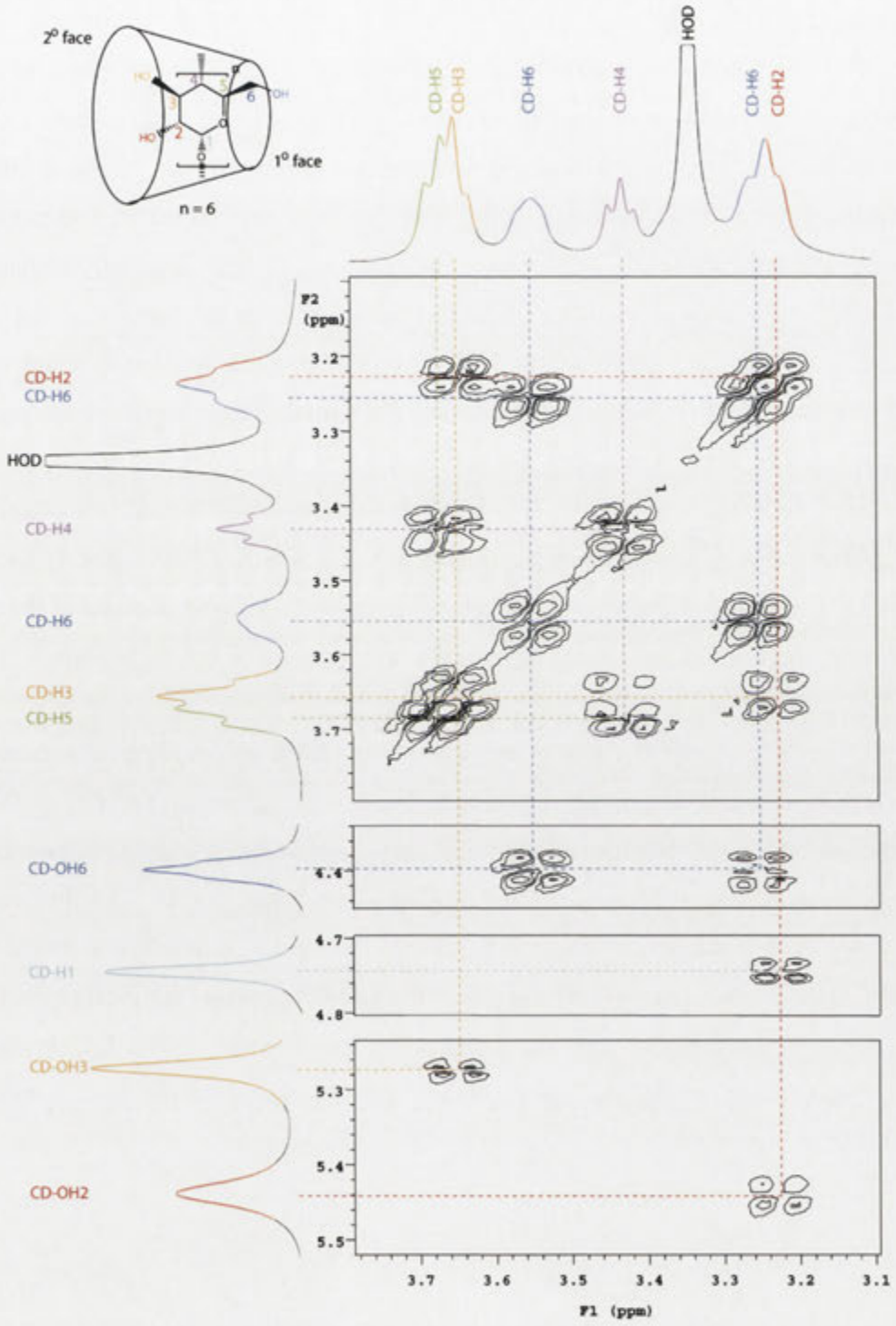

Figure 7.1. A section of the 500 MHz DQCOSY spectrum of the [2]-rotaxane **7.1** in d_6-DMSO at 25 °C of the region where crosspeaks are observed between cyclodextrin proton signals.

Using both DQCOSY and ROESY NMR spectroscopy, the signals of the axle of the [2]-rotaxane **7.1** were then assigned. A section of the DQCOSY contour plot of the [2]-rotaxane **7.1** is shown in Figure 7.2. The signals of the E and F protons show DQCOSY interactions with each other. These signals are therefore the result of a *trans*-olefin as they each have a coupling of 16 Hz. The rest of the signals show DQCOSY interactions and they can be assigned as illustrated in Figure 7.2. At this point in the assignment it can only be determined that there are three *para*-substituted aromatic rings. Through the ROESY contour plot shown in Figure 7.3, the axle was fully assigned. The signal of the protons D exhibits an NOE interaction with the signals of the olefinic protons E and F. The signals of the olefinic protons also show an interaction with the multiplet caused by the signals of the C and G protons. As the signal of the protons C already interacts with that of the protons D which is close to the olefin, the protons G must be close in space to the olefinic bond. With the signals of the stilbene assigned, the rest of the axle was deciphered by assigning the interactions of the signal of the amide proton I. The signal of the proton I shows an interaction with both of those of the protons H and K. The overall assignment of the axle can therefore be drawn as shown in Figure 7.3.

The ROESY contour plot of the [2]-rotaxane **7.1** found in Figure 7.4 shows NOE interactions between the signals of the CD and stilbene protons. The CD is therefore positioned on the stilbene unit of the axle. The signal of the protons D shows an NOE interaction with both the signals of the protons CD-H5 and CD-H6. The protons D are therefore found at the primary face of the CD. As the signals of the olefinic protons E and F only have interactions with the signal of the CD-H5 protons, the olefinic bond must reside closer towards the secondary face than the D proton. The CD is therefore orientated in such a way that its secondary face is closest to the phenyl moiety as illustrated in Figure 7.4.

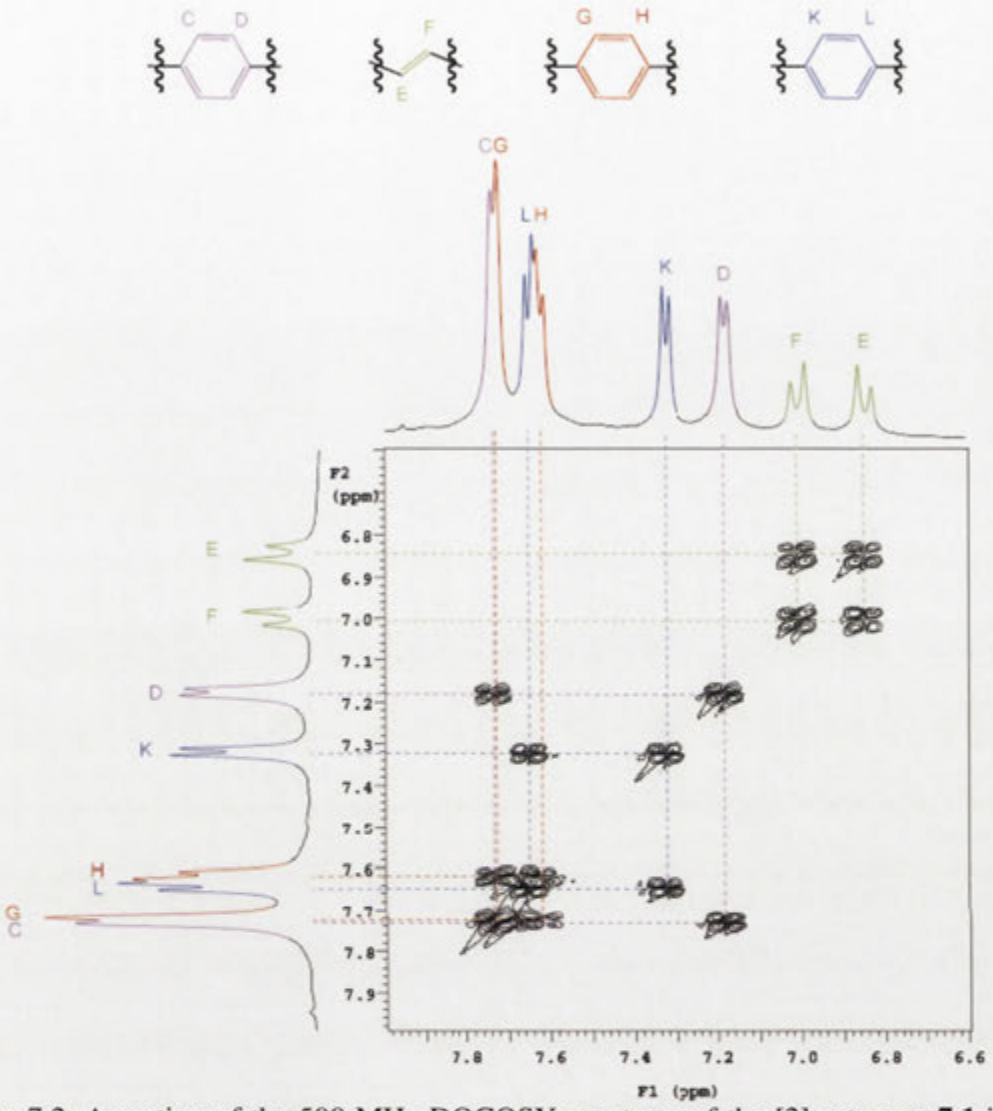

Figure 7.2. A section of the 500 MHz DQCOSY spectrum of the [2]-rotaxane **7.1** in d_6-DMSO at 25 °C of the region where crosspeaks are observed between axle proton signals.

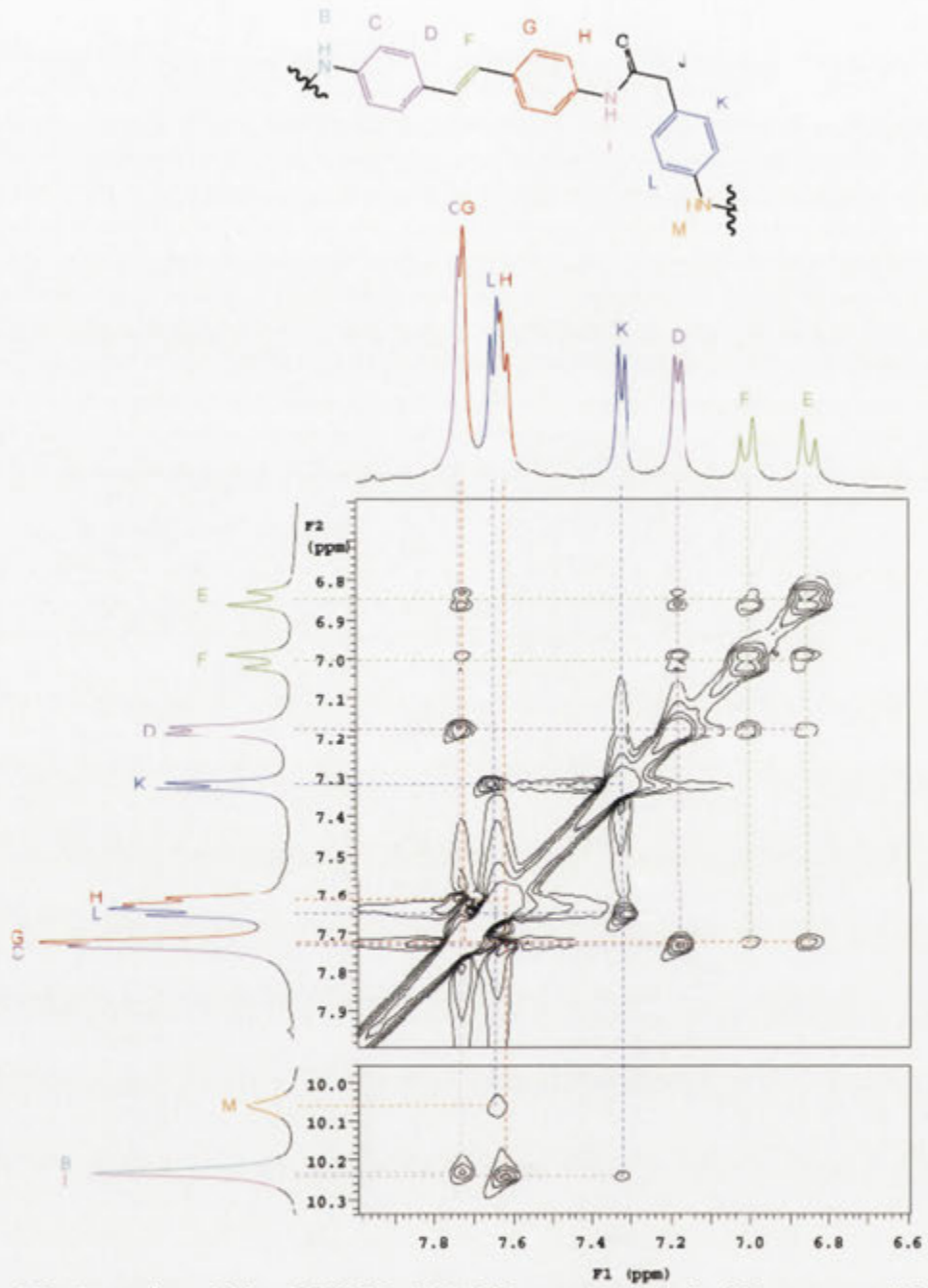

Figure 7.3. A section of the 500 MHz ROESY spectrum of the [2]-rotaxane **7.1** in d_6-DMSO at 25 °C of the region where crosspeaks are observed between axle proton signals.

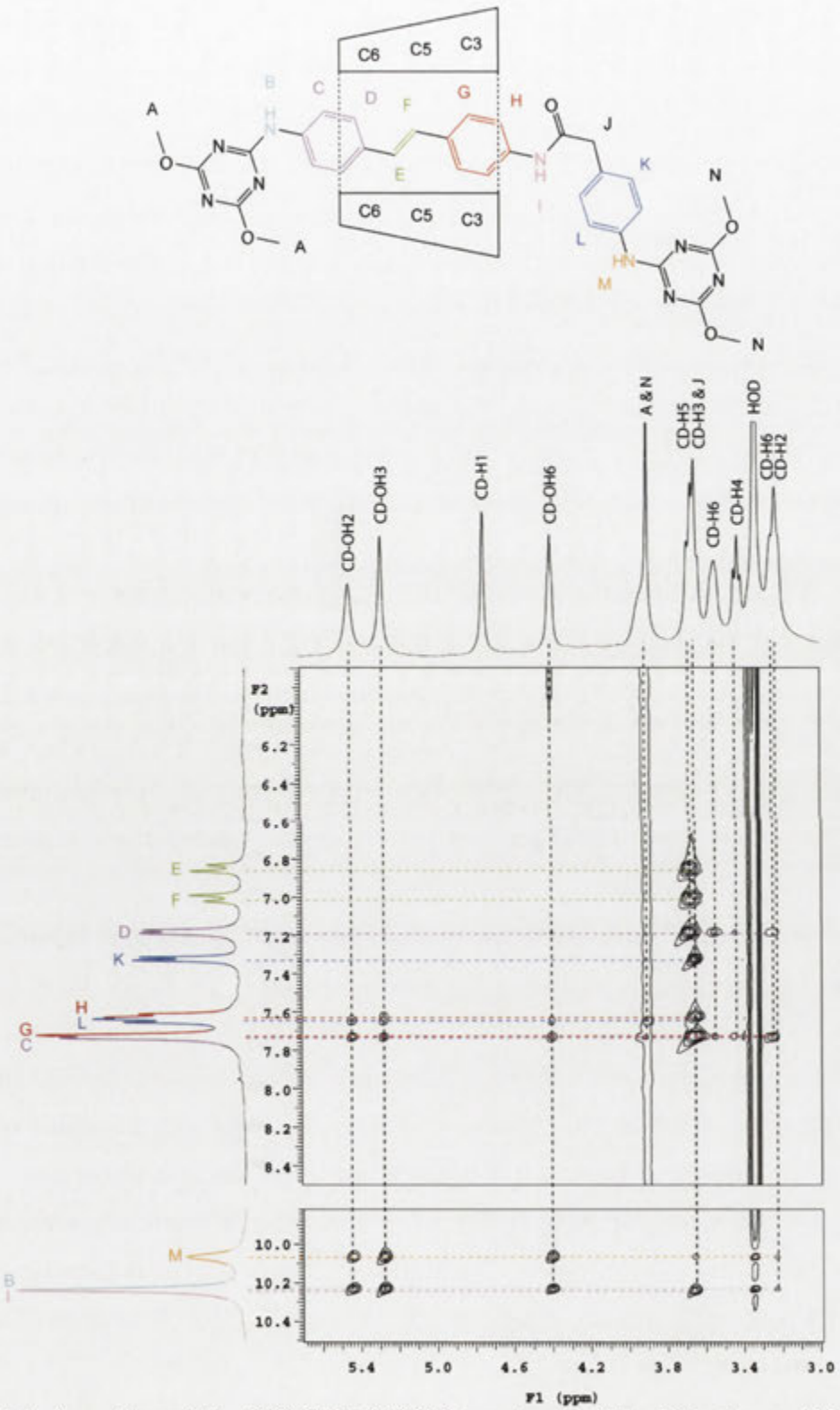

Figure 7.4. A section of the 500 MHz ROESY spectrum of the [2]-rotaxane **7.1** in d_6-DMSO at 25 °C of the region where crosspeaks are observed between axle and cyclodextrin proton signals.

2D NMR spectroscopy was then conducted on the [2]-rotaxane **7.2** to confirm whether the orientation of the CD on the axle was the opposite to that of the [2]-rotaxane **7.1**. This would re-affirm that the [2]-rotaxanes **7.1** and **7.2** were orientational isomers. The assignment again started with the DQCOSY spectrum of the CD region shown in Figure 7.5. As before, DQCOSY interactions originating through the signal of the CD-H1 protons at 4.74 ppm were used to completely assign each of the signals of the CD protons.

For the assignment of the axle signals of the [2]-rotaxane **7.2**, only ROESY 2D NMR spectroscopy was required. The aromatic region of the ROESY contour plot is shown in Figure 7.6. The signals E and F are the result of *trans*-olefinic protons as they have a coupling of 16 Hz. NOE interactions between the signals of the olefinic protons E and F and the signals of the aromatic protons enabled the signals of the stilbene to be assigned as shown in Figure 7.6. From the contour plot in Figure 7.6, it is impossible to tell which of the stilbene protons are closest to the aromatic protons K. Neither of the signals of the protons B or I show any interactions with the aromatic protons K. The full assignment of the axle protons, however, was able to be completed using the ROESY contour plot in Figure 7.7. The signal of the alkyl protons J shows interactions with the signal of the nitrogen coupled proton I and the signal of the aromatic protons K. This results in the axle assignment as shown in Figure 7.7.

The ROESY NMR contour plot of the [2]-rotaxane **7.2** shown in Figure 7.7 shows interactions between the signals of the stilbene protons C to H and those of the CD protons. The CD is therefore situated on the stilbene unit of the axle of the [2]-rotaxane **7.2**. The signal of the protons H shows interactions with the signal of the CD-H6 protons while the signal of the aromatic protons G shows interactions with the signals of the CD-H5 and CD-H6 annular protons. The primary face of the CD is therefore near the centre of the axle. The signals of the C, D, E and F protons all show interactions with the signals of the CD-H3 and CD-H5 protons. The secondary face of the CD is therefore closest to the triazine blocking group. Therefore the structure of the [2]-rotaxane **7.2** can be represented as shown in Figure 7.7.

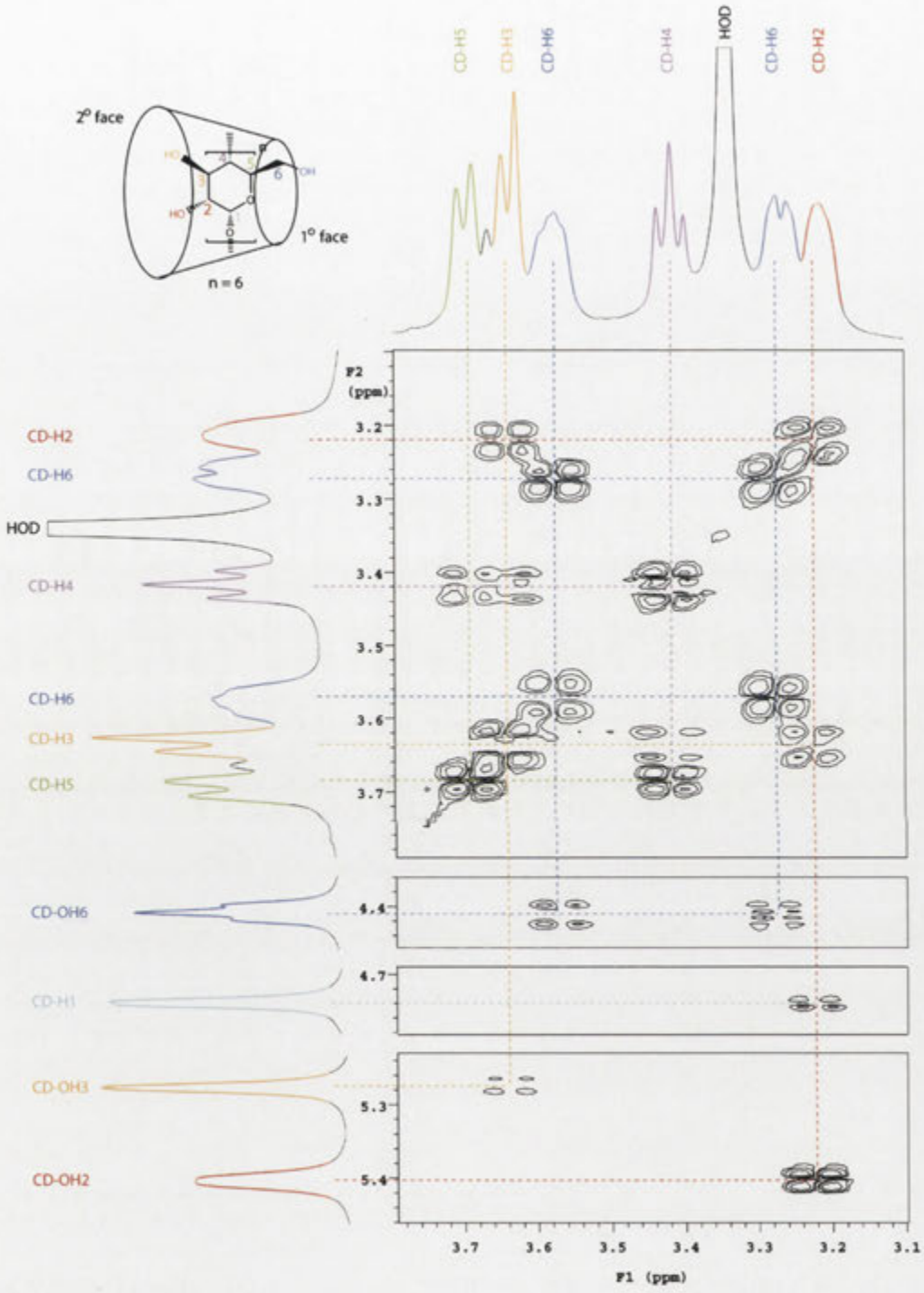

Figure 7.5. A section of the 500 MHz DQCOSY spectrum of the [2]-rotaxane **7.2** in d_6-DMSO at 25 °C of the region where crosspeaks are observed between cyclodextrin proton signals.

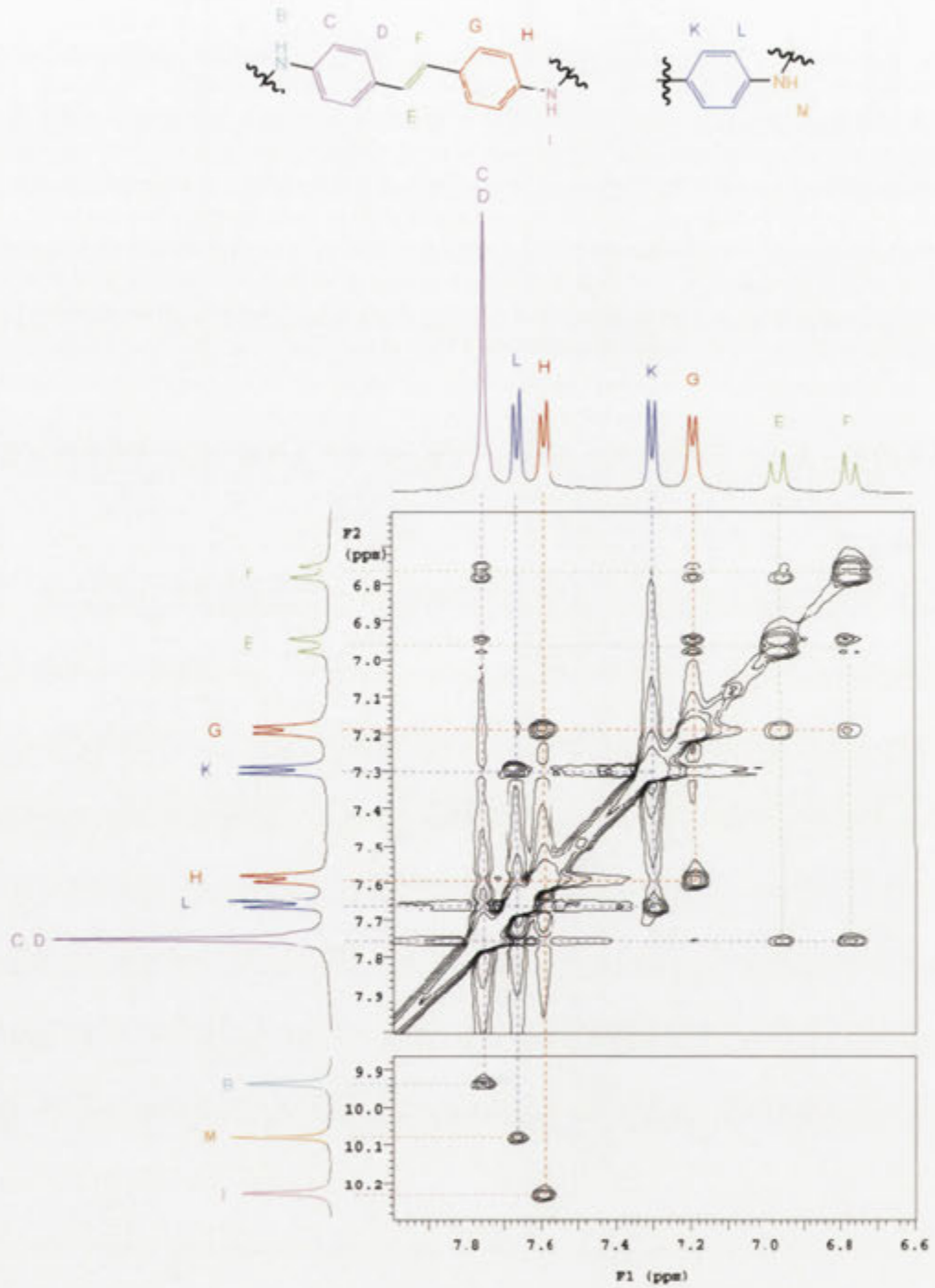

Figure 7.6. A section of the 500 MHz ROESY spectrum of the [2]-rotaxane **7.2** in d_6-DMSO at 25 °C of the region where crosspeaks are observed between axle proton signals.

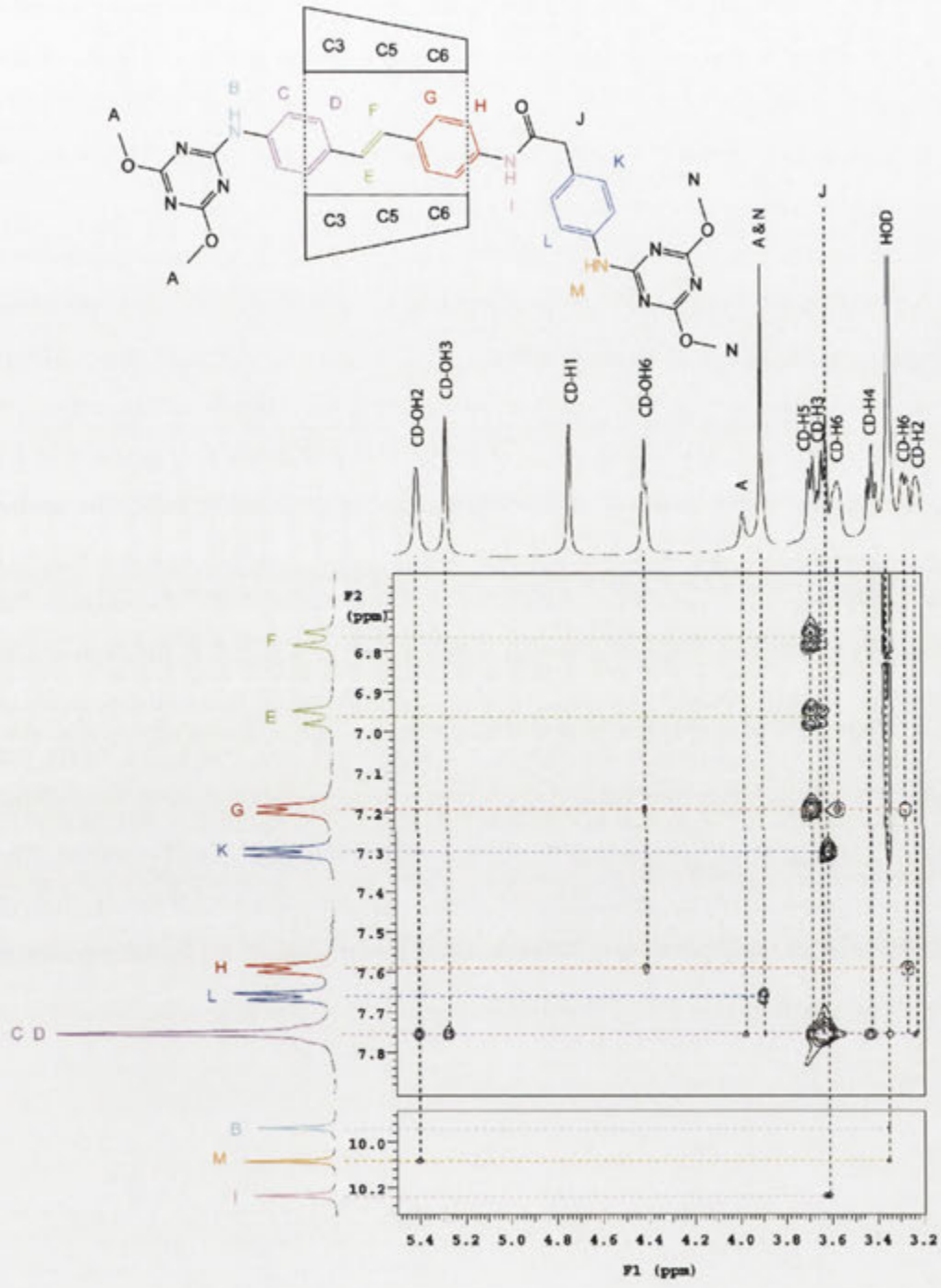

Figure 7.7. A section of the 500 MHz ROESY spectrum of the [2]-rotaxane **7.2** in d_6-DMSO at 25 °C of the region where crosspeaks are observed between axle and cyclodextrin proton signals.

The [2]-rotaxanes **7.1** and **7.2** are therefore orientational isomers of each other and were formed in a ratio of 69:31. From the 2D NMR assignment of each of the [2]-rotaxanes **7.1** and **7.2**, the CD resides on the stilbene unit of the axle. The isomer **7.1** has the secondary face of the CD facing the phenyl unit while the isomer **7.2** has the primary face of the CD pointed towards the phenyl unit.

A second variety of [2]-rotaxane was also sought to provide a comparison in both the synthesis and the eventual photoisomerisation studies. The type of second CD binding group was changed to a short alkyl chain. An alkyl chain was thought to be sufficient to allow the CD to move from the stilbene unit when it was isomerised from the favoured *trans* conformation to the less favoured *cis* form. The BOC protected amino acid **7.3** was commercially available and was ideal to be coupled to the stilbene **1.30**. The amine **1.30** and the protected amino acid **7.3** were dissolved in DMF with the amide coupling agent BOP under anhydrous conditions with TEA as the activating base. The product **7.4** was isolated in 70% yield. The diamine **7.5** was formed in 80% yield by deprotecting the carbamate **7.4** using TFA. The diamine **7.5** was then stirred in a solution of excess of αCD (**1.15**) in $NaHCO_3$ before the triazine **6.9** was added. From the HPLC of the reaction filtrate, two peaks were observed in a ratio of 22:78. The ESI mass spectra of the two separated products both contained $M+H^+$ ions corresponding to a [2]-rotaxane. The [2]-rotaxane **7.6** was isolated in a yield of 0.4% and gave a HI-RES $M+H^+$ ion of *m/z* 1532.5528 while the [2]-rotaxane **7.7** was isolated in a yield of 1.7% and gave an $M+H^+$ ion of *m/z* 1532.6.

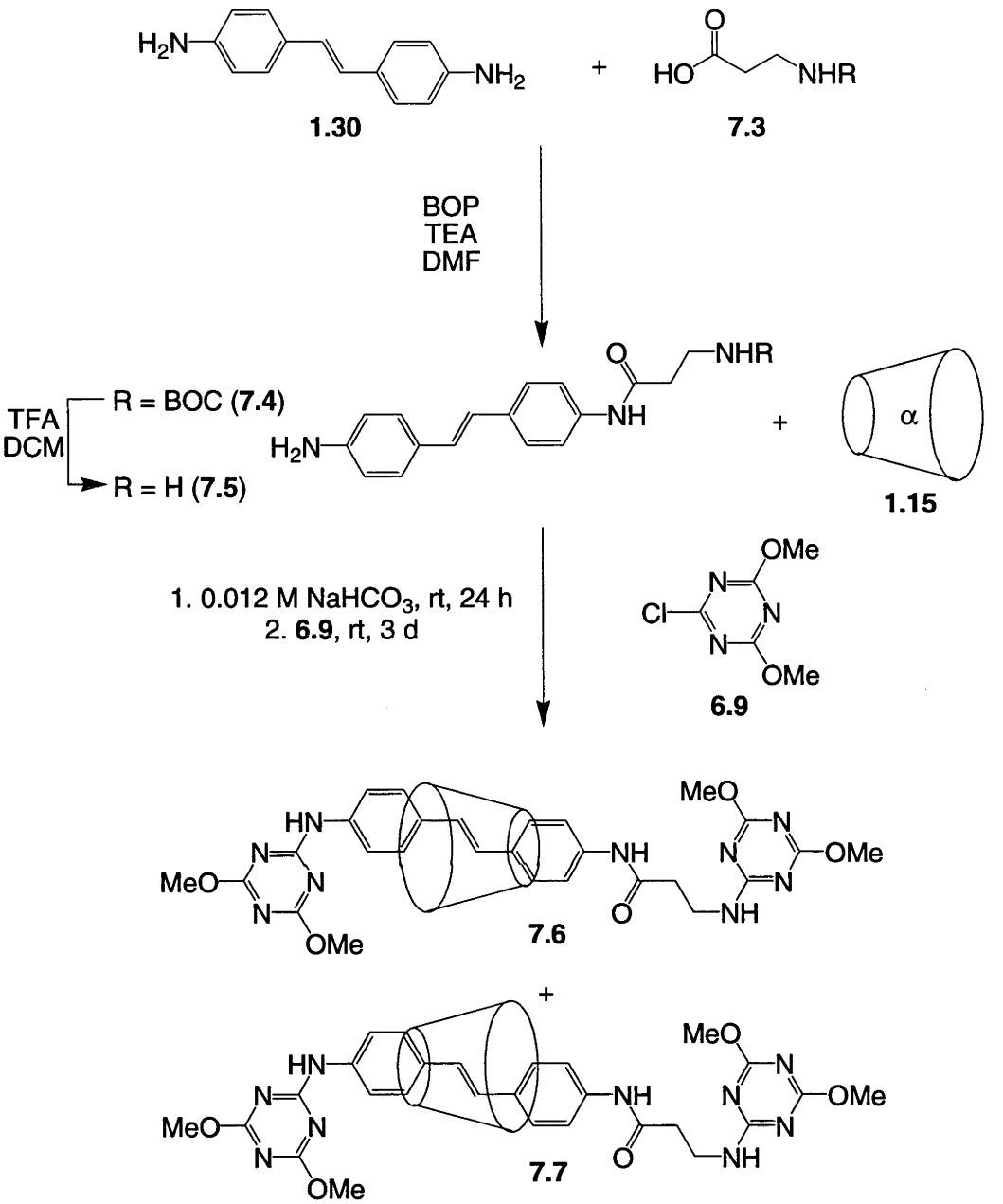

Scheme 7.2. Formation of the [2]-rotaxanes **7.6** and **7.7**.

2D NMR spectroscopy was undertaken on each of the [2]-rotaxanes **7.6** and **7.7** to determine where the CD resides on the axle and the orientation of the CD in each case. In Figure 7.8, the DQCOSY NMR contour plot was able to be used to assign the signals of the CD protons of the [2]-rotaxane **7.6**. From the assignment of the signal of the CD-H1 proton from the literature at 4.74 ppm,[77] DQCOSY interactions between the respective signals enabled the other assignments as shown in Figure 7.8. In the same plot the signals

of the alkyl protons J and K could also be assigned. The triplet signal of the alkyl protons J at 2.64 ppm shows an interaction with the signal of the protons K that is hidden by the CD region of the spectrum. The signal of the alkyl protons K shows an interaction with the triplet of the proton L at 7.96 ppm which must be the secondary amino group of the β-alanine second binding unit. Therefore the amine proton L must be furthest proton away from the stilbene as shown in Figure 7.10.

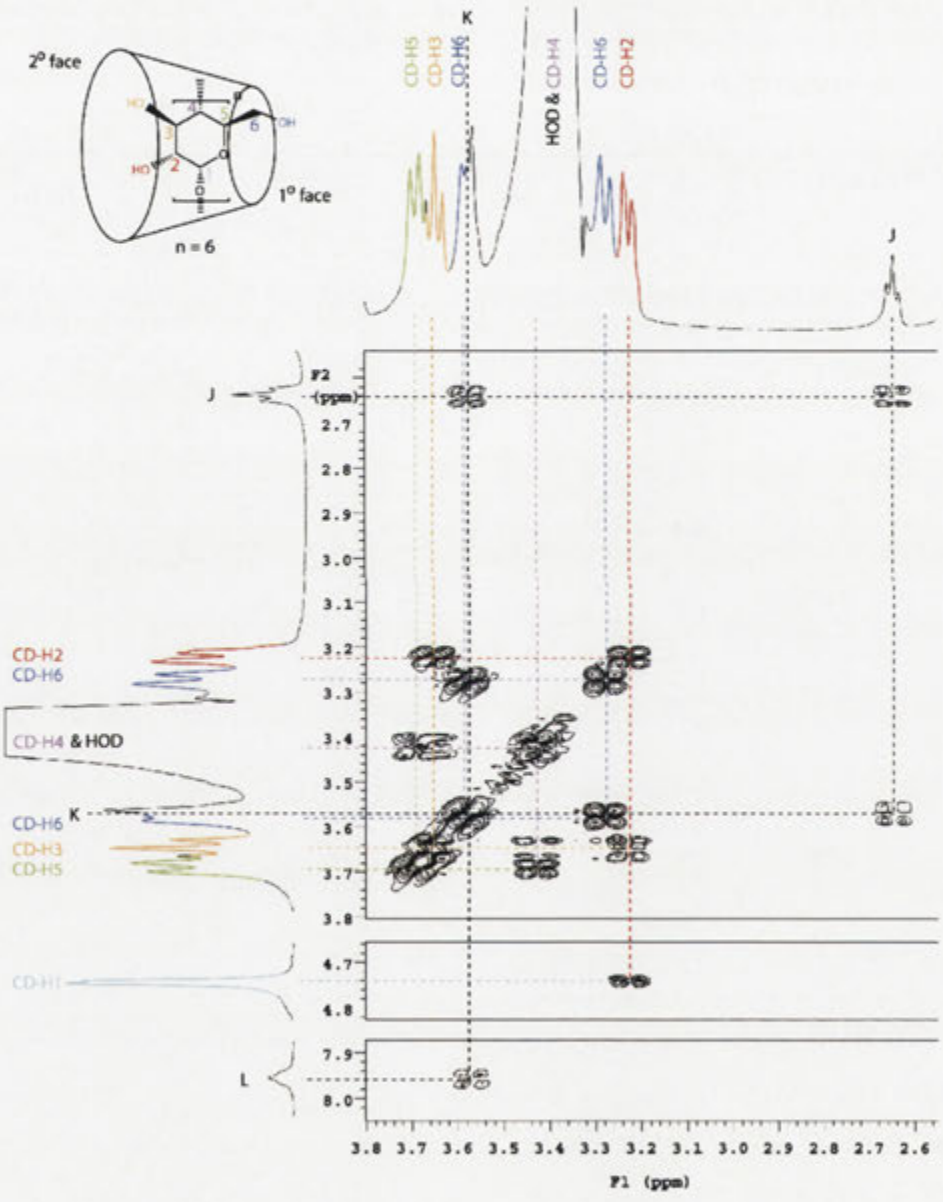

Figure 7.8. A section of the 500 MHz DQCOSY spectrum of the [2]-rotaxane **7.6** in d_6-DMSO at 25 °C of the region where crosspeaks are observed between cyclodextrin proton signals and between alkyl proton signals.

The remainder of the axle of the [2]-rotaxane **7.6** was assigned from the ROESY 2D NMR spectrum. The contour plot of the aromatic region of the ROESY spectrum is shown in Figure 7.9. The signals of the olefinic protons E and F were assigned from their larger coupling of 16 Hz. From their NOE interactions, the signals of the protons C, D, G and H were assigned as part of the stilbene unit as shown in Figure 7.9. It was not possible, however, from this contour plot to determine if the C or H protons were closest to the protons J. From the ROESY contour plot in Figure 7.9, it is obvious that the signal of the proton I shows an NOE interaction with the signal of the stilbene protons H. In the ROESY contour plot in Figure 7.10 the signal of the proton I also shows a small interaction with the signal of the alkyl protons J. The signal I is therefore the result of an amide proton. The stilbene protons H are therefore closer to the alkyl protons J than the stilbene protons C. The axle structure of the [2]-rotaxane **7.6** can therefore be represented as shown in Figure 7.10.

The ROESY contour plot shown in Figure 7.10 shows NOE interactions between the signals of the stilbene protons and those of the CD. The CD therefore is situated on the stilbene unit of the [2]-rotaxane **7.6**. The orientation of the CD with respect to the axle can also be determined. The contour plot shows interactions between the signals of the stilbene protons G and H with both of the signals of the protons CD-H6^{A} and CD-H6^{B}. This places the primary face of the CD at the centre of the axle. The overlapping signals of the aromatic protons C and D show NOE interactions with the signals of the protons CD-H3 and CD-H5. Therefore the secondary face of the CD must be further away from the centre of the axle. The structure of the [2]-rotaxane **7.6** as a result of the 2D NMR assignment can be represented as shown in Figure 7.10.

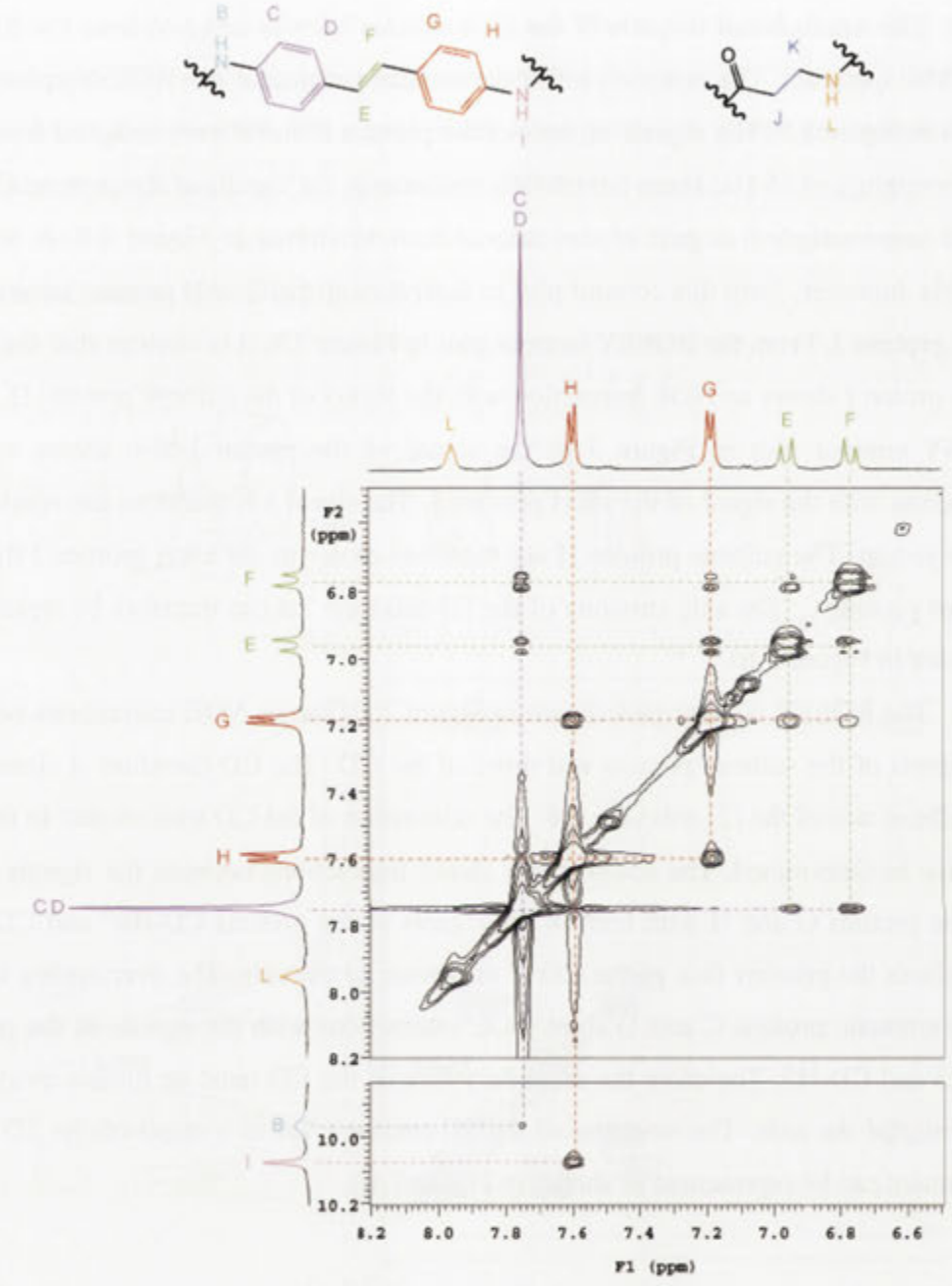

Figure 7.9. A section of the 500 MHz ROESY spectrum of the [2]-rotaxane **7.6** in d_6-DMSO at 25 °C of the region where crosspeaks are observed between axle proton signals.

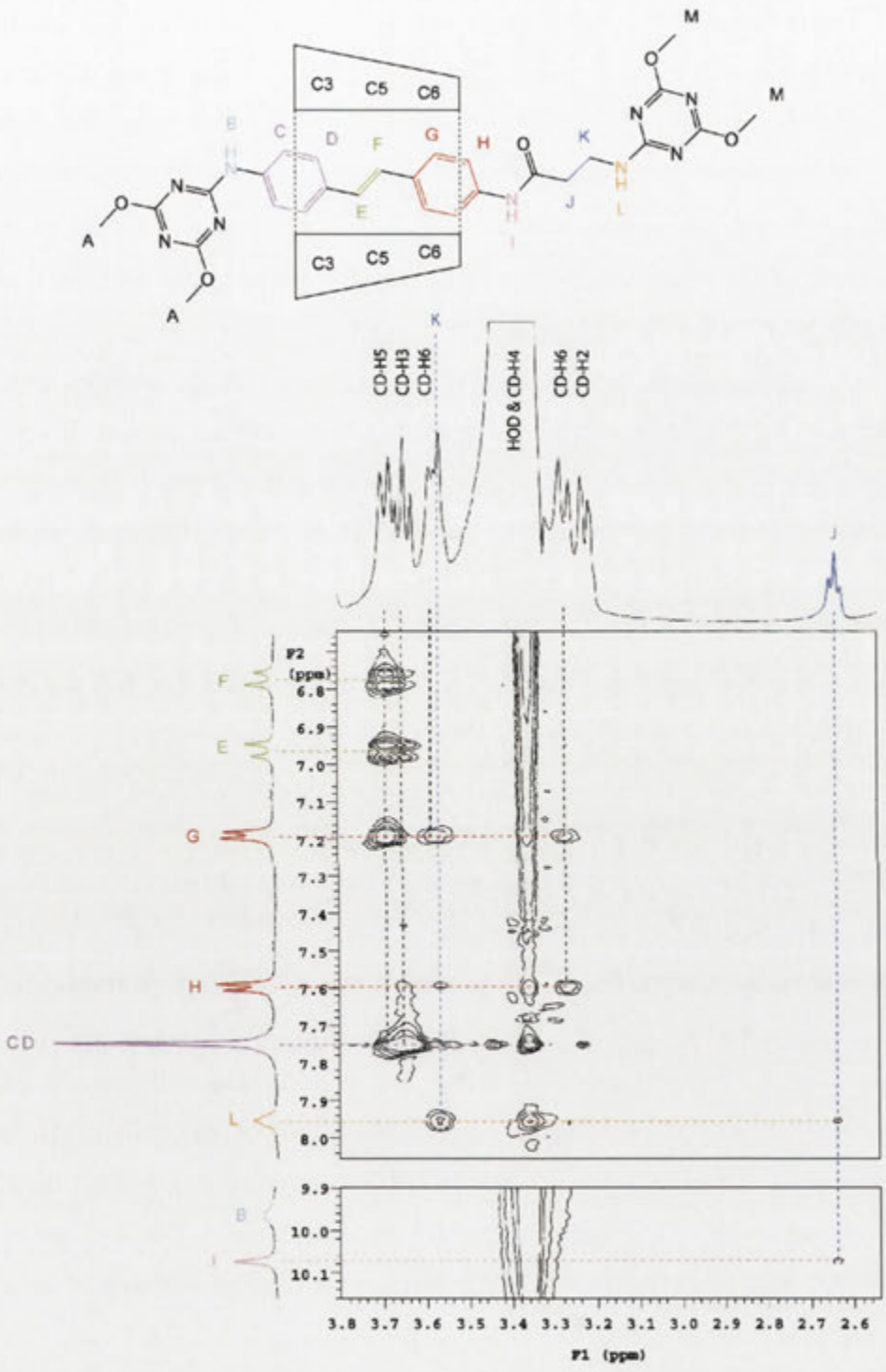

Figure 7.10. A section of the 500 MHz ROESY spectrum of the [2]-rotaxane **7.6** in d_6-DMSO at 25 °C of the region where crosspeaks are observed between axle and cyclodextrin proton signals.

The [2]-rotaxane **7.7** was also studied by 2D NMR spectroscopy to confirm if the products **7.6** and **7.7** were isomeric. The DQCOSY spectrum of the [2]-rotaxane **7.6** enables the CD signals to be assigned as shown in Figure 7.11. Also, the signal of the alkyl protons K which is embedded within the CD region of the ^{1}H NMR spectrum shows an interaction with the signal of the alkyl protons J which in turn shows an interaction with the signal of the amino proton L. This enables the assignment of the β-alanine as shown in Figure 7.12.

The signals of the stilbene protons were assigned from the aromatic region of the ROESY contour plot in Figure 7.12. The signals of the olefinic protons E and F of the stilbene unit were assigned by their large coupling of 16 Hz. The stilbene assignment was completed as shown in the figure from the NOE interactions between the signals of the olefinic protons E and F and those of the aromatic protons. Again the complete assignment of the axle could not be completed from the contour plot in Figure 7.12. The signal of the aromatic protons H shows an interaction with the signal of the proton I. In Figure 7.13, the signal of the proton I shows a small interaction with the signals of the alkyl protons J. The signal I is therefore a result of an amide proton and the axle assignment can be represented as shown in Figure 7.13.

The ROESY contour plot in Figure 7.13 shows NOE interactions between the signals of the stilbene protons and those of the CD. The CD therefore is situated on the stilbene unit of the [2]-rotaxane **7.7**. The orientation of the CD with respect to the axle can also be determined. The signal of the aromatic protons D shows interactions with the signals of protons CD-H5 and CD-H6. The primary face of the CD must reside on the stilbene unit closest to the triazine group. The signal of the protons H shows an interaction with the signal of the protons CD-H3. The secondary face of the CD must therefore reside over the stilbene unit near the centre of the axle. The structure of the [2]-rotaxane **7.7** as a result of the 2D NMR assignment may be represented as shown in Figure 7.13.

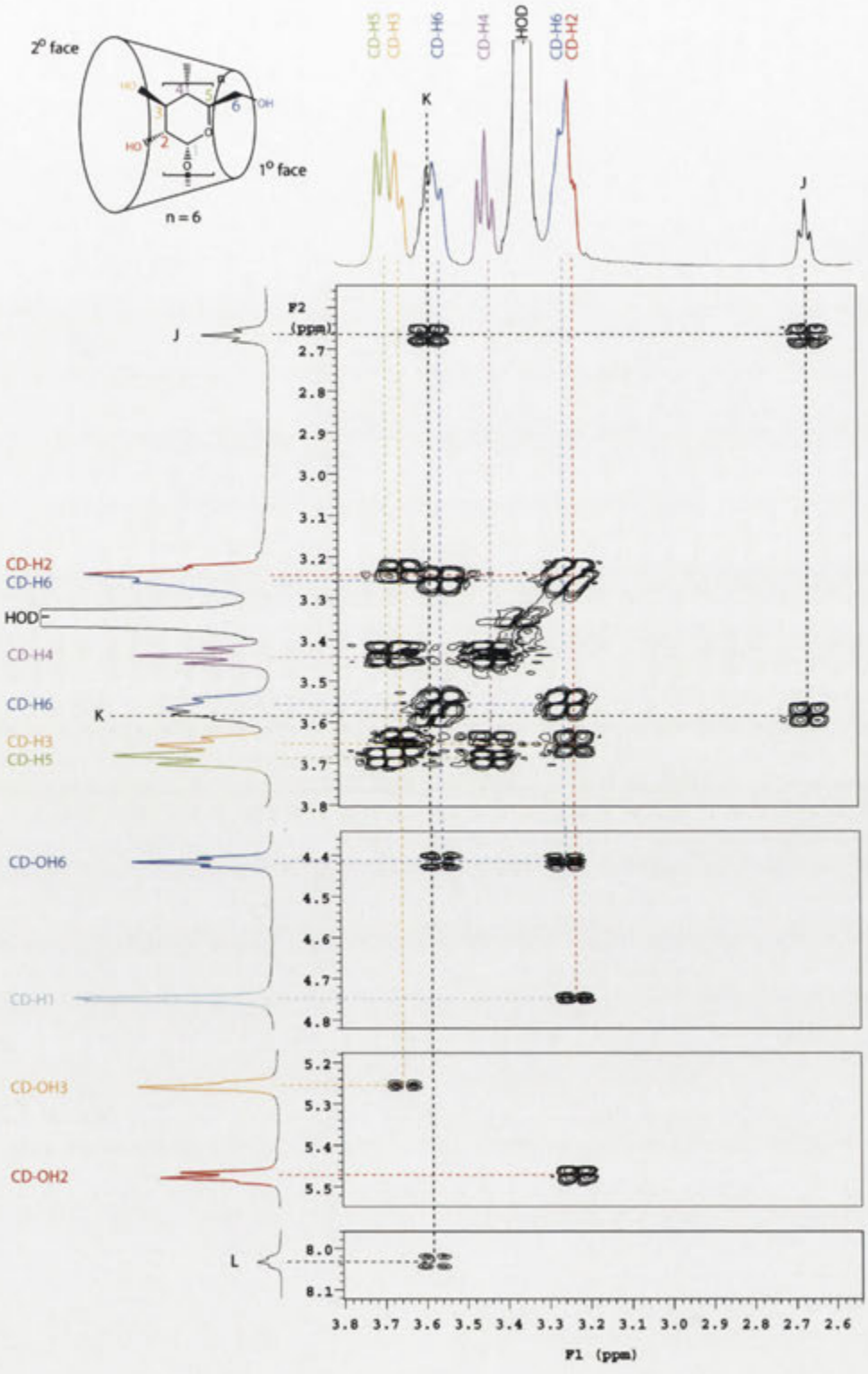

Figure 7.11. A section of the 500 MHz DQCOSY spectrum of the [2]-rotaxane **7.7** in d_6-DMSO at 25 °C of the region where crosspeaks are observed between cyclodextrin proton signals and between alkyl proton signals.

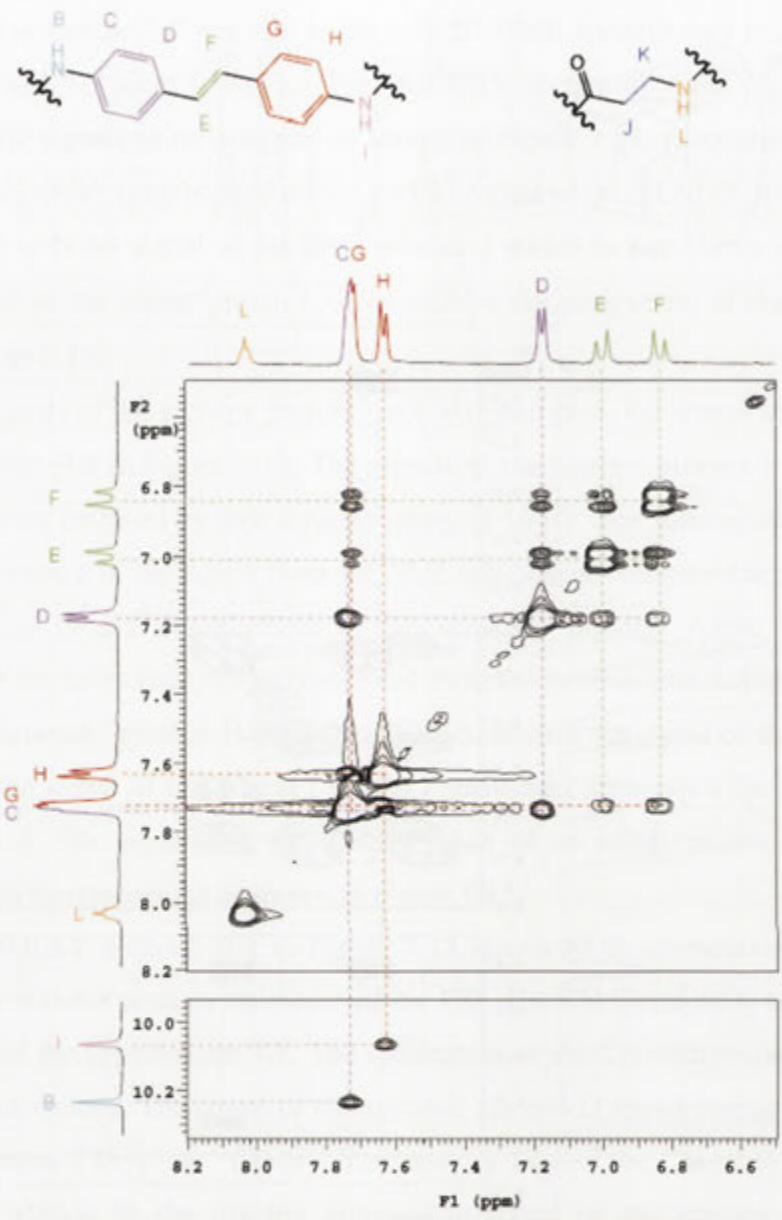

Figure 7.12. A section of the 500 MHz ROESY spectrum of the [2]-rotaxane **7.7** in d_6-DMSO at 25 °C of the region where crosspeaks are observed between axle proton signals.

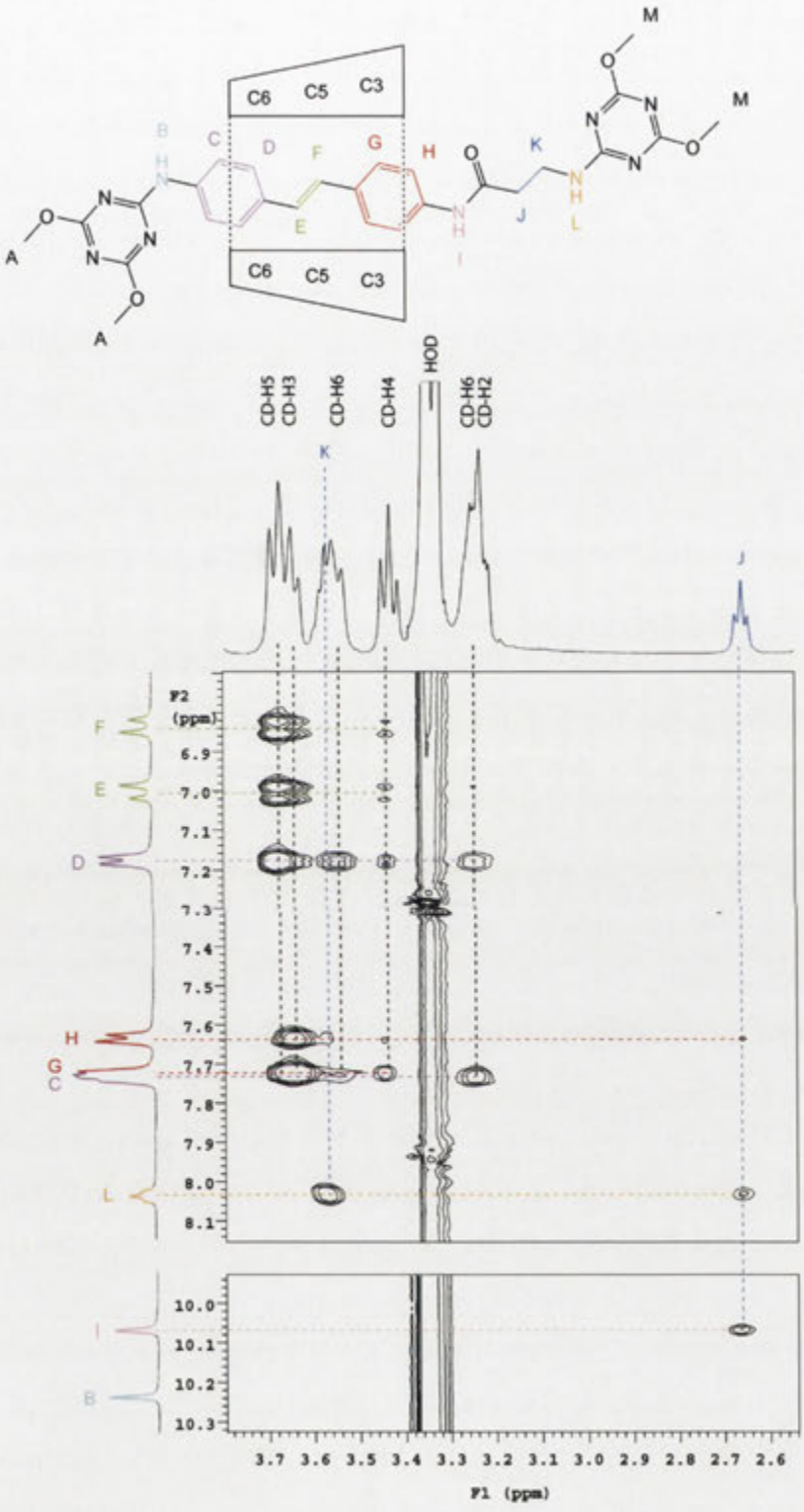

Figure 7.13. A section of the 500 MHz ROESY spectrum of the [2]-rotaxane **7.7** in d_6-DMSO at 25 °C of the region where crosspeaks are observed between axle and cyclodextrin proton signals.

With the [2]-rotaxanes **7.1**, **7.2**, **7.6** and **7.7** in hand, UV/visible spectroscopy and reverse phase HPLC was used to measure the ability of each of them to photoisomerise to and from their *cis*-counterparts. A change in conformation of the stilbene was envisioned to be enough of a stimulus to cause the CD to move to the second CD binding unit. Firstly the irradiation wavelengths were determined for each of the [2]-rotaxanes **7.1**, **7.2**, **7.6** and **7.7** in attempts to form the *cis*-isomers. Two irradiation wavelengths were chosen at 350 nm and 370 nm as the λ_{max} of each of the [2]-rotaxanes **7.1**, **7.2**, **7.6** and **7.7** was determined to be in the range of 345 nm to 350 nm as shown below. At 350 nm or 370 nm, absorption of light by the corresponding *cis*-isomers and their isomerisations were expected to be limited. The maximum absorbance of the new products formed as a result of the irradiation of each of the [2]-rotaxanes **7.1**, **7.2**, **7.6** and **7.7** was in the region of 265 nm. The wavelengths of light available closest to this maximum absorbance were 254 nm and 300 nm. The wavelength used for the reverse isomerisation was 254 nm as at this wavelength the absorption of light by the [2]-rotaxanes **7.1**, **7.2**, **7.6** and **7.7** and their isomerisation was expected to be less than that for the new products.

The isomerisation towards the *cis*-isomer and then back to the *trans*-isomer was designated to be one cycle. For a molecular machine to be utilised it would have to perform the same task a multitude of times. For this reason the isomerisation cycle was conducted three times to establish a trend for the reversibility of the shuttles. The reversibility of the isomerisations is depicted in graphs of the percentage amount of the [2]-rotaxanes **7.1**, **7.2**, **7.6** or **7.7** determined by HPLC.

The UV/visible spectra of a 1.51×10^{-5} M solution of the [2]-rotaxane **7.1** before and after irradiation with light of wavelengths 350 nm or 370 nm and 254 nm are found in Figures 7.14 and 7.15 respectively. The graph of the percentage amount of the [2]-rotaxane **7.1** before and after irradiation is shown in Figure 7.16.

Upon irradiation of the sample with light of wavelength 370 nm or 350 nm, there is a decrease in absorbance at 350 nm and a slight increase in absorbance at about 265 nm. Irradiation with 254 nm light causes a decrease at 265 nm and an increase at 345 nm. In each case the maximum absorbance does not reach its original level after the 254 nm irradiation. The degree of change is much greater for the irradiation with 370 nm light than for 350 nm light. From the HPLC study, the percentage amount of the [2]-rotaxane

7.1 decreased by 9% upon irradiation with 350 nm light. The percentage amount of the [2]-rotaxane **7.1** decreased by 28% upon irradiation with 370 nm light. In each case irradiation with 254 nm light increased the amount of the [2]-rotaxane **7.1** to within 98% of the original amount. The loss of material is presumably due to decomposition of the [2]-rotaxane **7.1** upon photolysis.

The irradiation with 350 nm or 370 nm light before irradiation with light of wavelength 254 nm therefore reversibly isomerised the [2]-rotaxane **7.1**. There was an increase in the absorbance at 265 nm of the solution irradiated with 350 nm or 370 nm light. From the HPLC traces a new peak emerged corresponding to a product that had a maximum absorbance at 265 nm, characteristic of the *cis*-isomer of the [2]-rotaxane **7.1**.

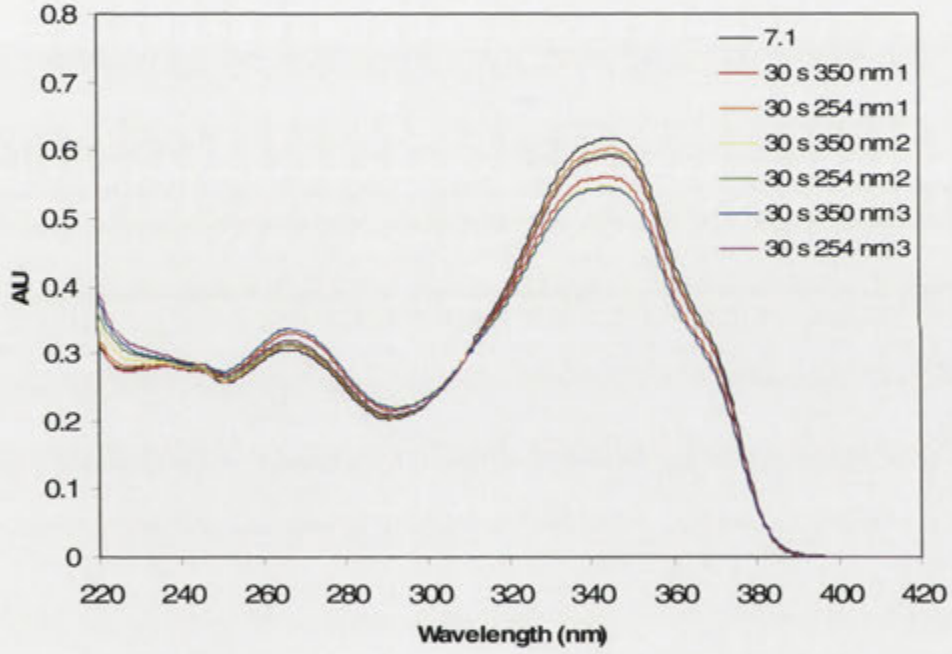

Figure 7.14. UV/visible spectra of the [2]-rotaxane **7.1** [1.51 × 10^{-5} M] in MQ H_2O and after subsequent exposure to 350 and 254 nm light after periods of time as indicated in the graph.

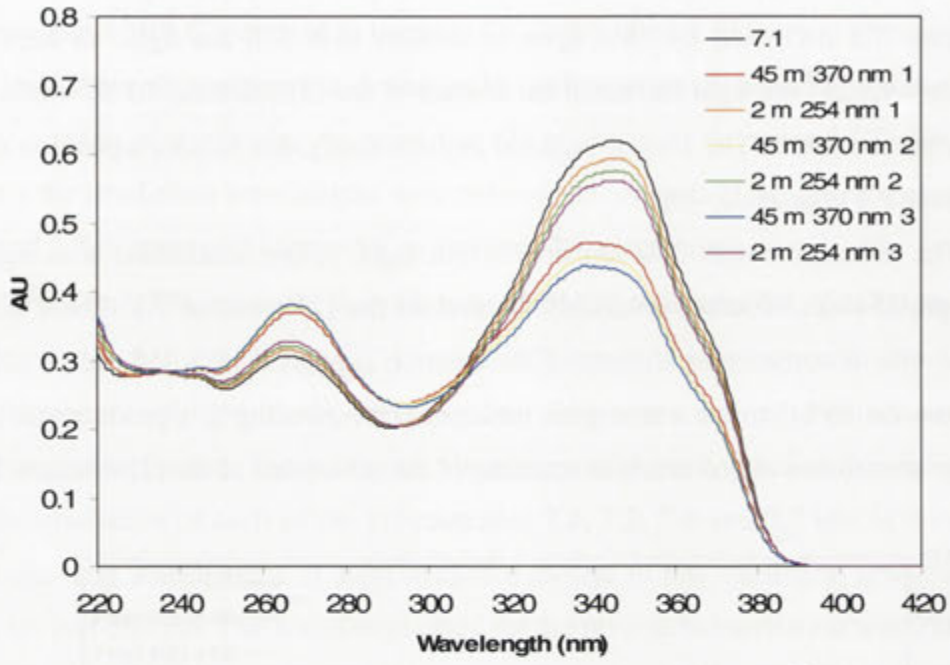

Figure 7.15. UV/visible spectra of the [2]-rotaxane **7.1** [1.51×10^{-5} M] in MQ H_2O and after subsequent exposure to 370 and 254 nm light after periods of time as indicated in the graph.

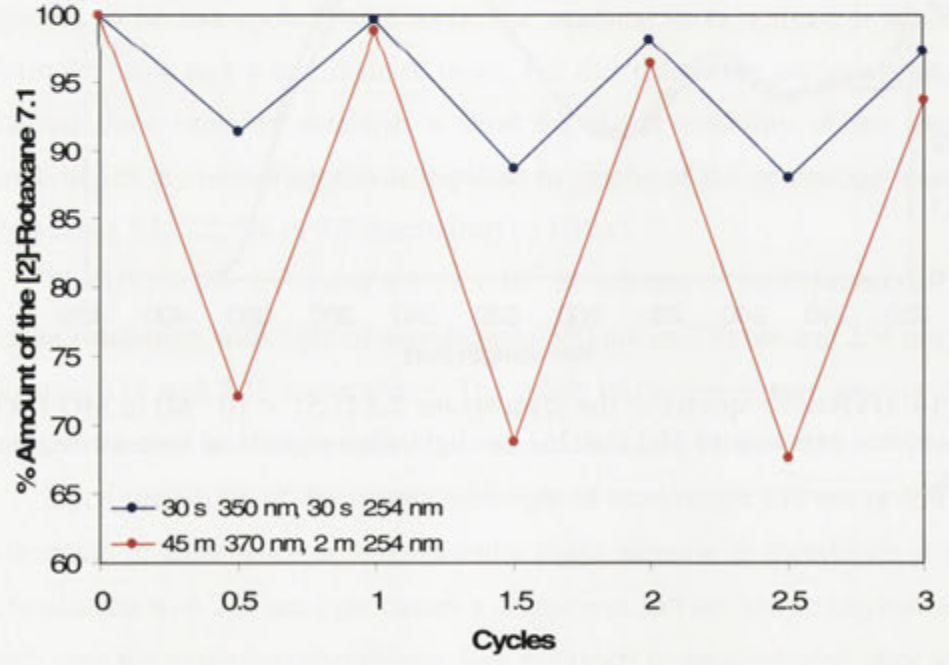

Figure 7.16. Percentage amount of the [2]-rotaxane **7.1** from the reverse-phase HPLC chromatograms monitored at a wavelength of 347 nm. One cycle as indicated on the graph denotes irradiation with 350 nm or 370 nm light before irradiation with 254 nm light.

For the photoisomerisation study on the [2]-rotaxane **7.2**, a 1.88×10^{-5} M solution was made up in MQ H_2O and subjected to the same irradiation conditions as used with the [2]-rotaxane **7.1**. The UV/visible spectra recorded after the 350 nm or 370 nm irradiations followed by the 254 nm irradiations are shown in Figures 7.17 and 7.18 respectively. The graph of the percentage amount of the [2]-rotaxane **7.2** before and after irradiation is shown in Figure 7.19.

The irradiation of the [2]-rotaxane **7.2** with 350 nm or 370 nm light caused a decrease in the maximum absorbance at 347 nm in the UV/visible spectra. There was also an increase at 265 nm corresponding to the formation of the *cis*-isomer. The reverse isomerisation with the 254 nm light caused the absorbance at 347 nm to increase and the absorbance at 265 nm to decrease. The irradiation with 370 nm light caused the greatest change in the absorbance just as was the case for the [2]-rotaxane **7.1**. From the HPLC data, irradiation at 350 nm consumed 35% of the starting material. Using light of the higher wavelength of 370 nm produced an even better conversion. From the HPLC study in Figure 7.19 it was apparent that the amount of the [2]-rotaxane **7.2** converted to its *cis*-isomer after irradiation with 370 nm light was 57%. After one cycle employing the 350 nm irradiation the reversibility was 94% while for the 370 nm irradiation the reversibility was 98%.

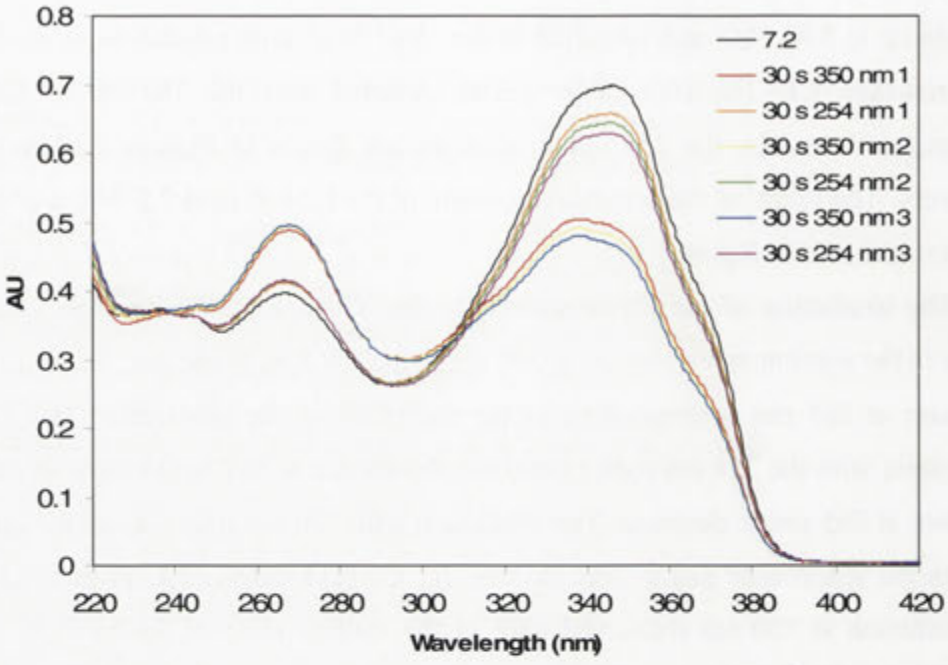

Figure 7.17. UV/visible spectra of the [2]-rotaxane **7.2** [1.88×10^{-5} M] in MQ H_2O and after subsequent exposure to 350 and 254 nm light after periods of time as indicated in the graph.

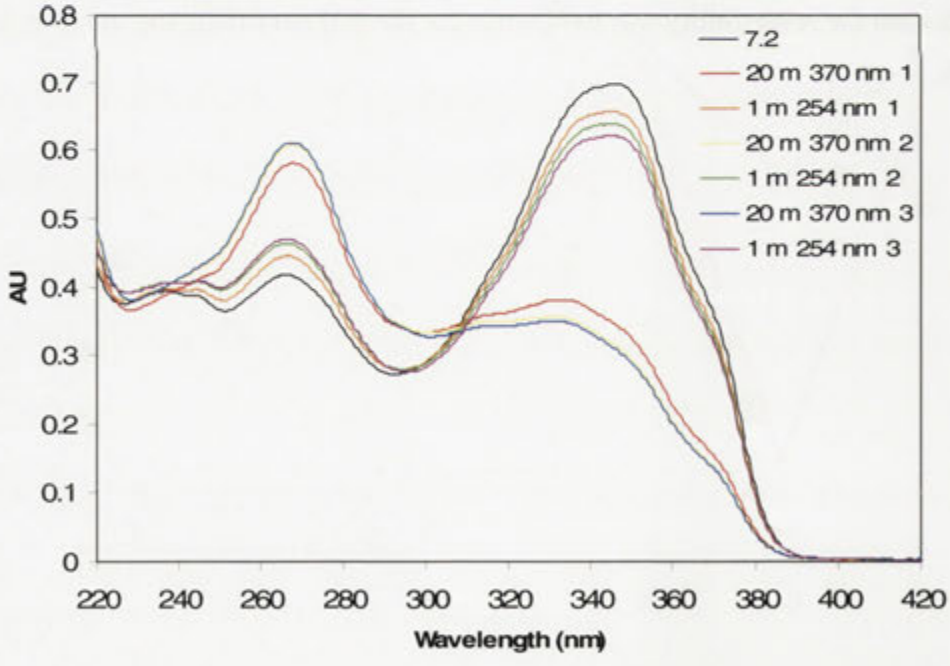

Figure 7.18. UV/visible spectra of the [2]-rotaxane **7.2** [1.88×10^{-5} M] in MQ H_2O and after subsequent exposure to 370 and 254 nm light after periods of time as indicated in the graph.

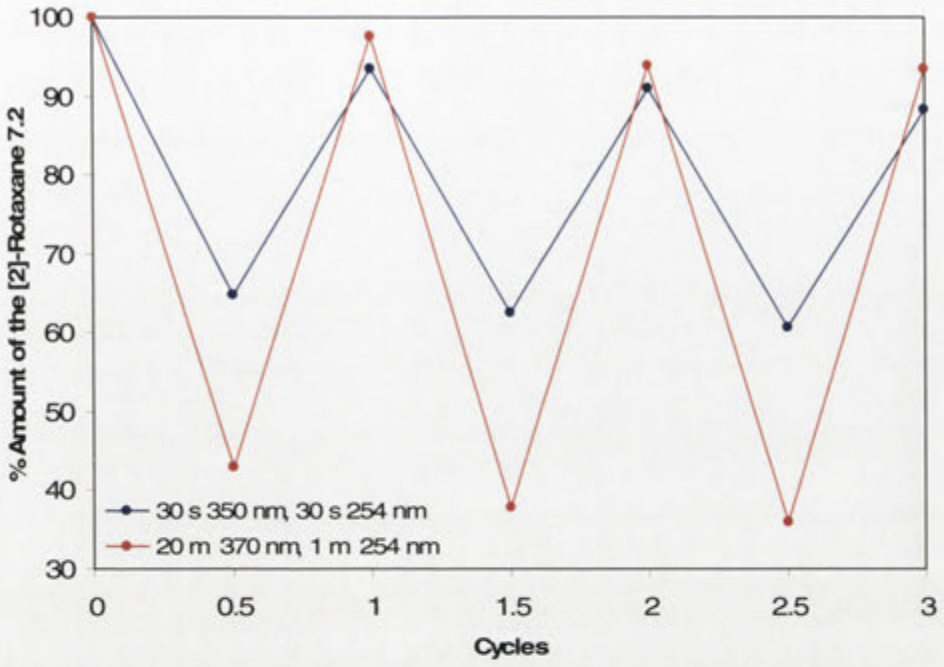

Figure 7.19. Percentage amount of the [2]-rotaxane **7.2** from the reverse-phase HPLC chromatograms monitored at a wavelength of 347 nm. One cycle as indicated on the graph denotes irradiation with 350 nm or 370 nm light before irradiation with 254 nm light.

For the [2]-rotaxanes **7.6** and **7.7**, the same methods for the isomerisation and monitoring were used. The UV/visible spectra of a 2.22×10^{-5} M solution of the [2]-rotaxane **7.6** before and after irradiation with light of wavelength 350 nm or 370 nm followed by light of wavelength 254 nm are shown in Figures 7.20 and 7.21 respectively. The UV/visible spectra of a 1.96×10^{-5} M solution of the [2]-rotaxane **7.7** before and after irradiation with light of wavelength 350 nm or 370 nm followed by light of wavelength 254 nm are shown in Figures 7.23 and 7.24 respectively. The graphs of the percentage amounts of the [2]-rotaxanes **7.6** and **7.7** before and after irradiation are shown in Figures 7.22 and 7.25 respectively.

From the UV/visible spectra of the isomerisation of the [2]-rotaxanes **7.6** and **7.7** it is apparent that there is a decrease in the maximum absorbance at 348 nm along with an increase in the absorbance at 265 nm upon irradiation with the 350 nm and 370 nm light. The changes are reversed with irradiation of light of wavelength 254 nm. The reversibility for each of the irradiations is very high, in the region of 97-99%. Irradiation

of the isomeric [2]-rotaxanes **7.6** and **7.7** with 350 nm light enabled 24% and 10% of the starting materials to be converted to their corresponding *cis*-isomers respectively. The amount of the *cis*-isomers formed was increased substantially to 44% and 30% upon irradiation with 370 nm light. The increased formation of the *cis*-isomers was reflected in increased amounts of the peaks corresponding to the *cis*-isomers from the HPLC traces post irradiation.

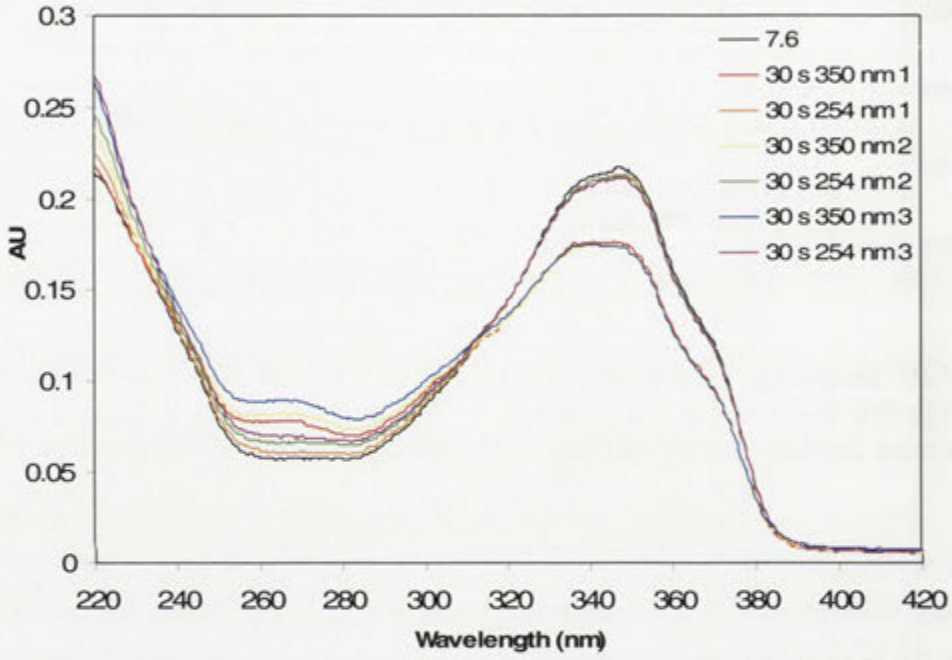

Figure 7.20. UV/visible spectra of the [2]-rotaxane **7.6** [2.22×10^{-5} M] in MQ H_2O and after subsequent exposure to 350 and 254 nm light after periods of time as indicated in the graph.

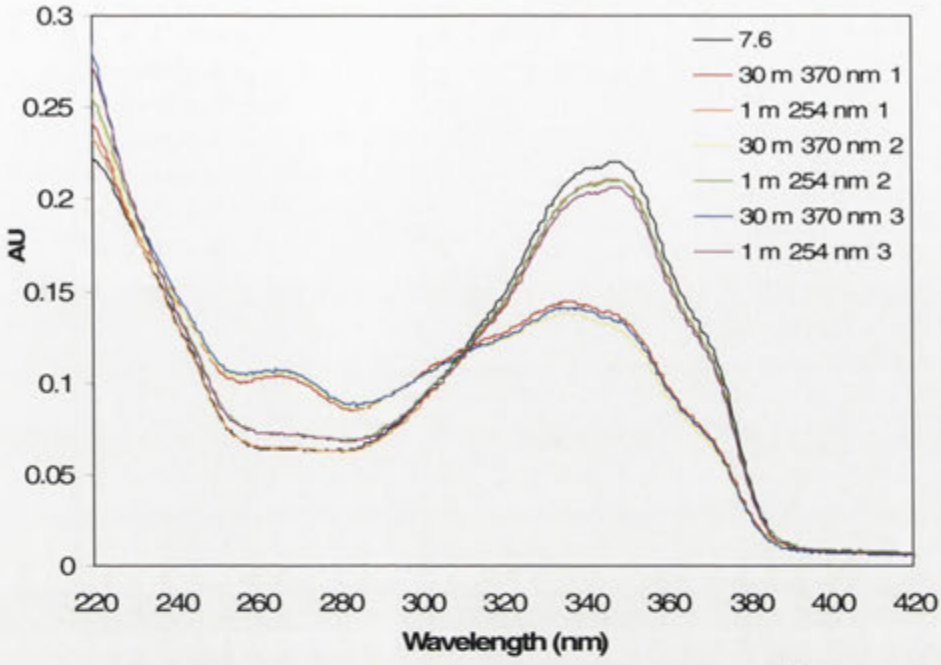

Figure 7.21. UV/visible spectra of the [2]-rotaxane **7.6** [2.22×10^{-5} M] in MQ H_2O and after subsequent exposure to 370 and 254 nm light after periods of time as indicated in the graph.

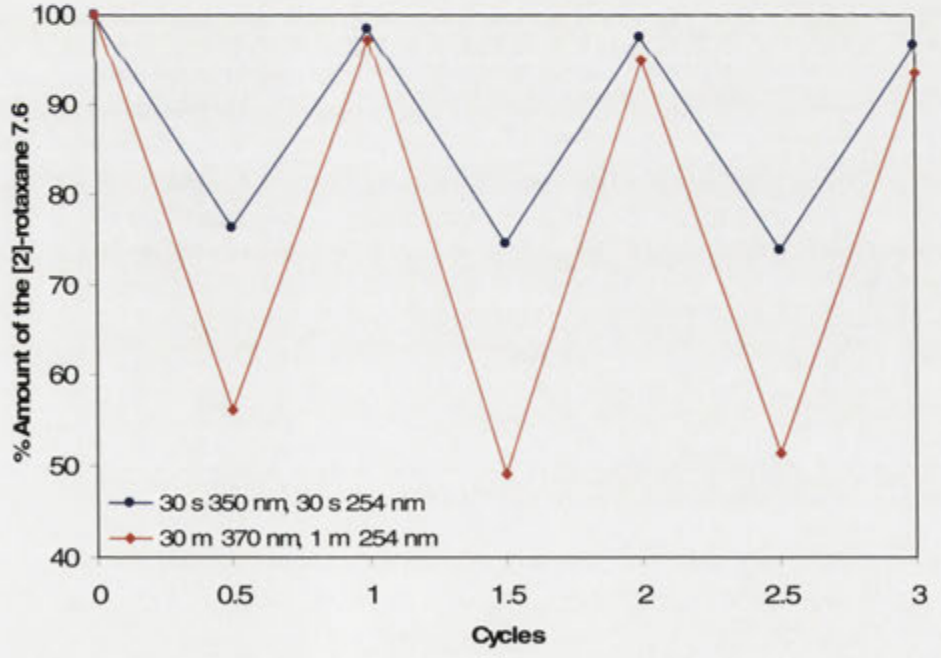

Figure 7.22. Percentage amount of the [2]-rotaxane **7.6** from the reverse-phase HPLC chromatograms monitored at a wavelength of 347 nm. One cycle as indicated on the graph denotes irradiation with 350 nm or 370 nm light before irradiation with 254 nm light.

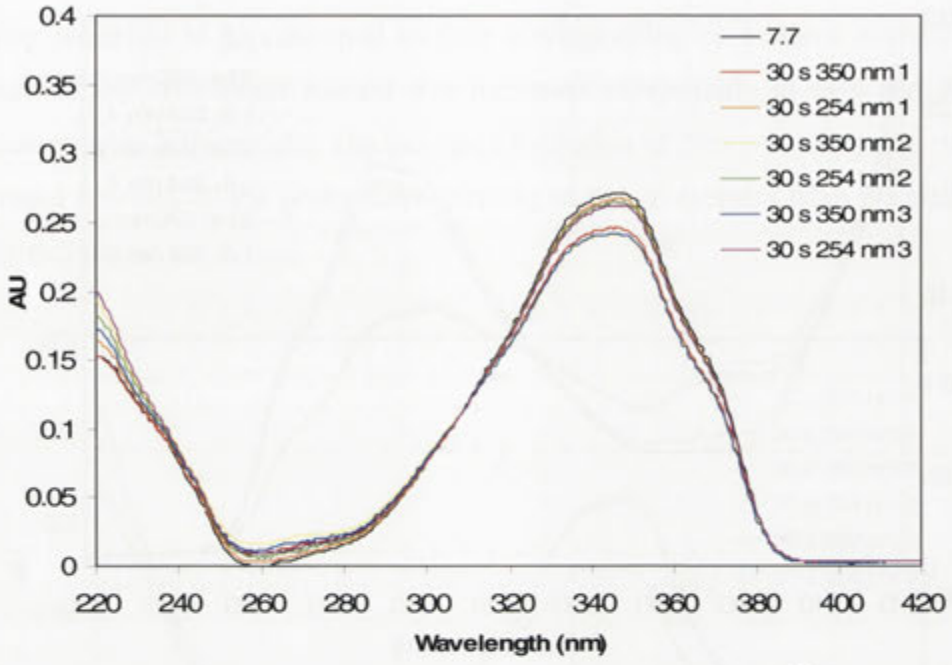

Figure 7.23. UV/visible spectra of the [2]-rotaxane **7.7** [1.96×10^{-5} M] in MQ H_2O and after subsequent exposure to 350 and 254 nm light after periods of time as indicated in the graph.

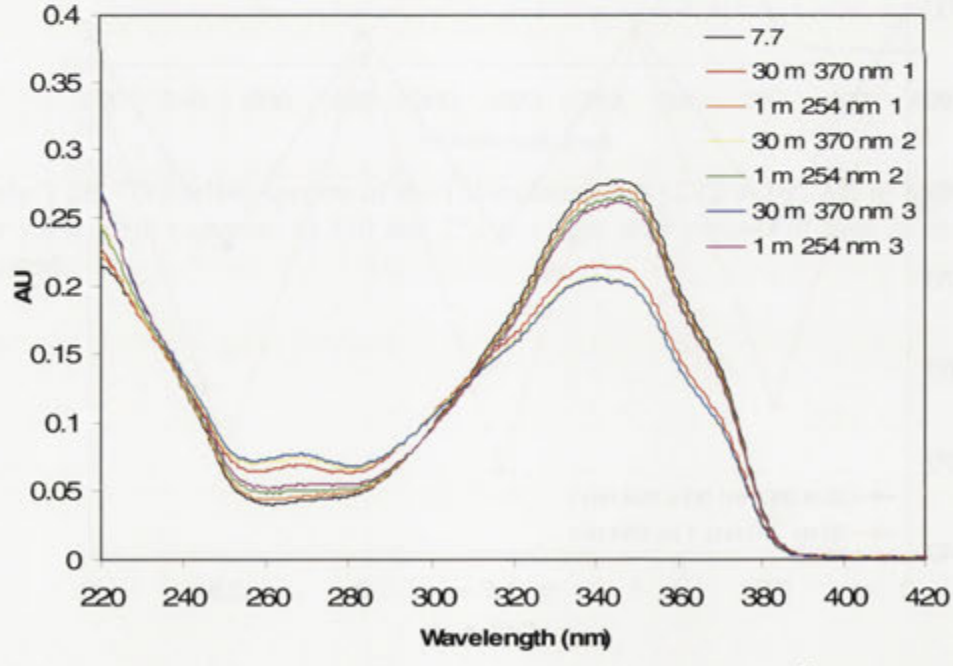

Figure 7.24. UV/visible spectra of the [2]-rotaxane **7.7** [1.96×10^{-5} M] in MQ H_2O and after subsequent exposure to 370 and 254 nm light after periods of time as indicated in the graph.

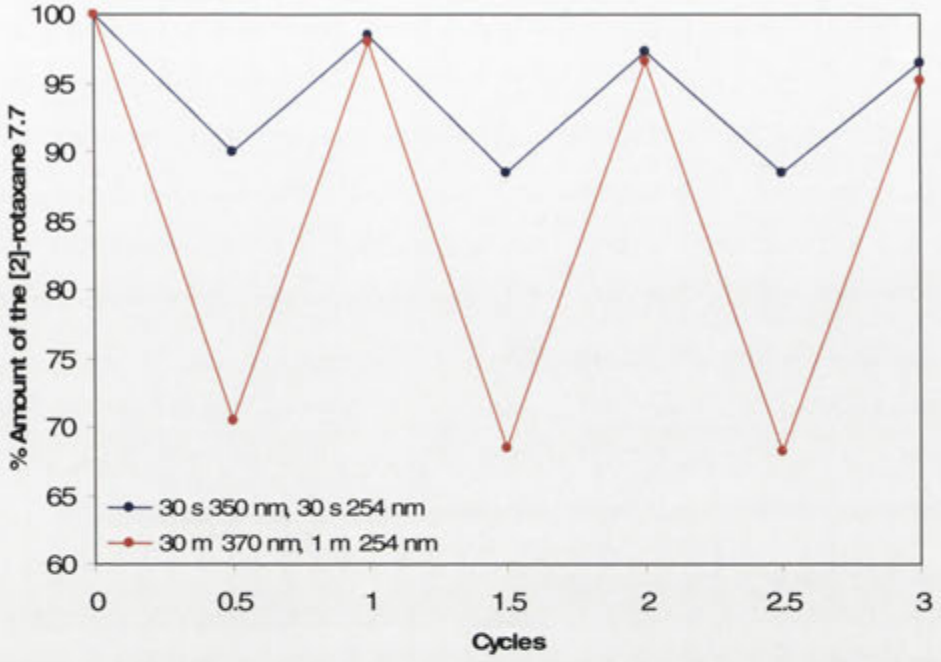

Figure 7.25. Percentage amount of the [2]-rotaxane **7.7** from the reverse-phase HPLC chromatograms monitored at a wavelength of 347 nm. One cycle as indicated on the graph denotes irradiation with 350 nm or 370 nm light before irradiation with 254 nm light.

In each case 370 nm light isomerises a greater percentage of the [2]-rotaxanes **7.1**, **7.2**, **7.6** and **7.7** than does 350 nm light. It appears that one orientational isomer of each pair also isomerises more effectively. Of the isomeric [2]-rotaxanes **7.1** and **7.2**, the latter is more effectively transformed. At 370 nm, 57% of the [2]-rotaxane **7.2** isomerises, while only 28% of the [2]-rotaxane **7.1** isomerises. As shown in Figure 7.7, the CD in the [2]-rotaxane **7.2** is situated on the stilbene unit with its primary face pointing towards the second CD binding unit. As the only difference between the [2]-rotaxanes **7.1** and **7.2** is the CD orientation, the structure described must be more favourable for the isomerisation and presumably the CDs movement along the axle. In the isomerisation of the [2]-rotaxanes **7.6** and **7.7** at 370 nm, 44% of the [2]-rotaxane **7.6** is converted to its *cis*-isomer in comparison to 30% for the [2]-rotaxane **7.7**. As it is shown in Figure 7.10, the structure of the [2]-rotaxane **7.6** has the CD situated on the stilbene with its primary face pointed towards the second CD binding unit, as is the case with the analogue **7.2**.

To confirm that the [2]-rotaxanes **7.1**, **7.2**, **7.6** and **7.7** isomerise to their corresponding *cis*-isomers, as indicated by the changes in their UV/visible spectra and HPLC traces after irradiation with UV light, and to determine the conformations of those *cis*-isomers, 2D NMR spectroscopy was undertaken. Samples of the *cis*-isomers **7.1(Z)** and **7.2(Z)** were isolated by preparative HPLC from irradiated solutions of the [2]-rotaxanes **7.1** and **7.2**, respectively. The samples each contain starting material that reforms during the analysis. The yields of the *cis*-isomers of the [2]-rotaxanes **7.6** and **7.7** were too low for their isolation and analysis to be practical.

The DQCOSY NMR contour plot of the CD region of the [2]-rotaxane **7.1(Z)** is shown in Figure 7.26. From the signal of the CD-H1 protons at 4.76 ppm, DQCOSY interactions were able to be used to assign the remaining signals as shown.

The signals of the axle of the [2]-rotaxane **7.1(Z)** were able to be assigned from the ROESY 2D NMR contour plots in Figures 7.27 and 7.28. From the contour plot in Figure 7.27 the signals of the olefinic protons E and F are identifiable by their interaction with the signals of the aromatic protons D and G. The olefinic bond is *cis* as the signals of the olefinic protons E and F show a coupling constant of 12.5 Hz. The signals of the protons D and G show interactions with the C and H proton signals to complete the assignment of the stilbene signals. There is also an observable interaction between the signals of the protons K and L. The complete assignment of the axle, however, could not be determined from the contour plot in Figure 7.27. The assignment was able to be completed using the contour plot in Figure 7.28. The signals of the aromatic protons C and L both show NOE interactions with the signals of the methoxy protons A and N. This enables the signals of the axle of the [2]-rotaxane **7.1(Z)** to be assigned as shown in Figure 7.29.

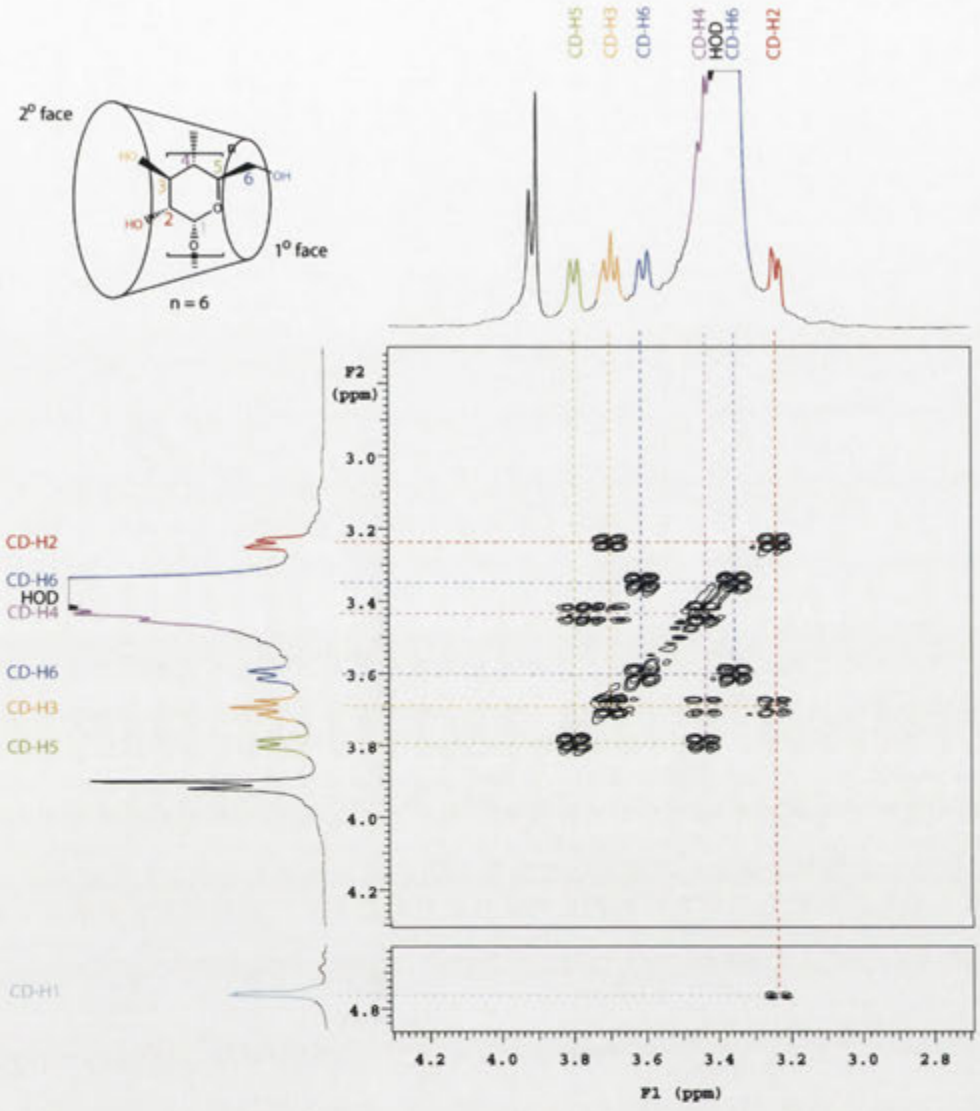

Figure 7.26. A section of the 500 MHz DQCOSY spectrum of the [2]-rotaxane **7.1(Z)** in d_6-DMSO at 25 °C of the region where crosspeaks are observed between cyclodextrin proton signals.

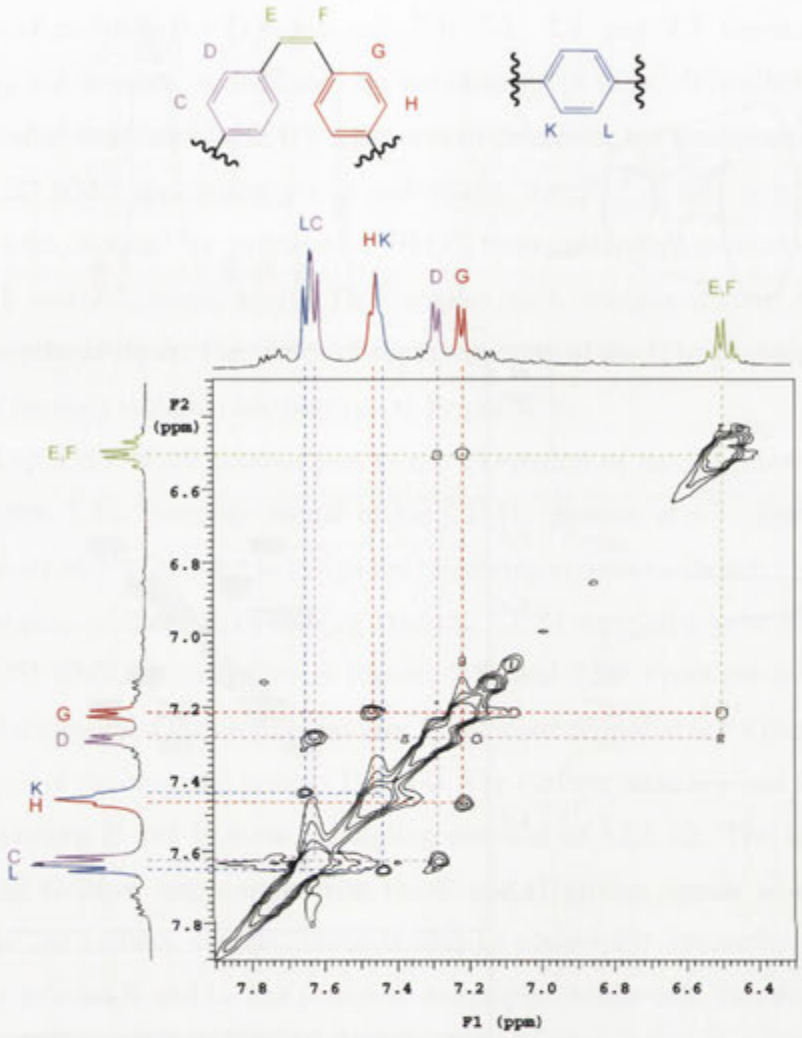

Figure 7.27. A section of the 500 MHz ROESY spectrum of the [2]-rotaxane **7.1(Z)** in d_6-DMSO at 25 °C of the region where crosspeaks are observed between axle proton signals.

In the assignment of the CD location on the axle of the [2]-rotaxane **7.1(Z)**, it appeared from the ROESY contour plot in Figure 7.28 that there are two different conformations. These structures are illustrated in Figure 7.29. From the contour plot in Figure 7.28 the signals of the protons K show NOE interactions with both the signals of the protons CD-H3 and CD-H5 while the signal of the stilbene protons H shows a slight interaction with one of the signals of the CD-H6 protons. These interactions place the CD as shown in the upper structure of Figure 7.29 where it is situated over the secondary CD binding unit. The NOE interaction that points to the formation of a second conformation is that of the strong NOE crosspeak between the signal of the stilbene protons D and that

of the CD-H3 protons. There is also a possible interaction between the signal of the aromatic protons C and the signals of the CD-H3 and CD-H5 protons. These interactions place the CD as shown in the lower structure in Figure 7.29. It is clear though that the CD is distant from the olefinic bond as there are no observable interactions between the E and F proton signals and the CD annular proton signals. The isomerisation of the stilbene unit of the [2]-rotaxane **7.1** to its *cis*-isomer **7.1(Z)** has caused the CD to move to two separate parts of the axle. From the HPLC separation, only one *cis*-product was identified and separated. It is likely that the two states are in equilibrium with each other. The exchange between the two states must be fast on the NMR timescale and therefore results in only one set of ^{1}H NMR signals.

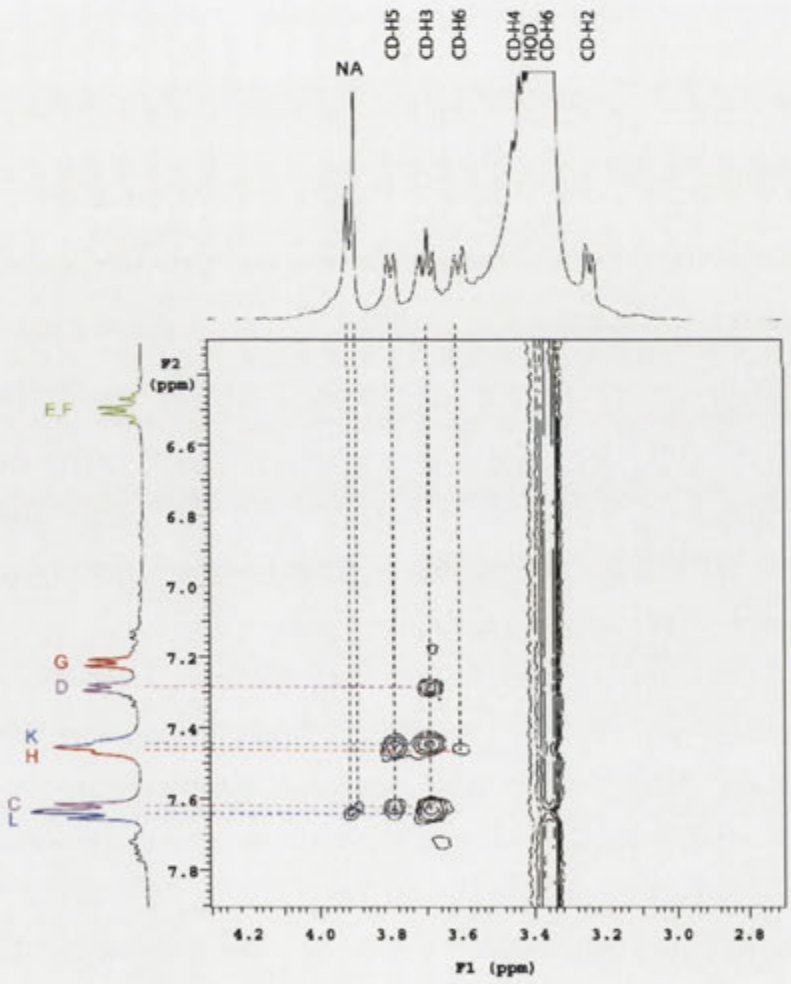

Figure 7.28. A section of the 500 MHz ROESY spectrum of the [2]-rotaxane **7.1(Z)** in d_6-DMSO at 25 °C of the region where crosspeaks are observed between axle and cyclodextrin proton signals.

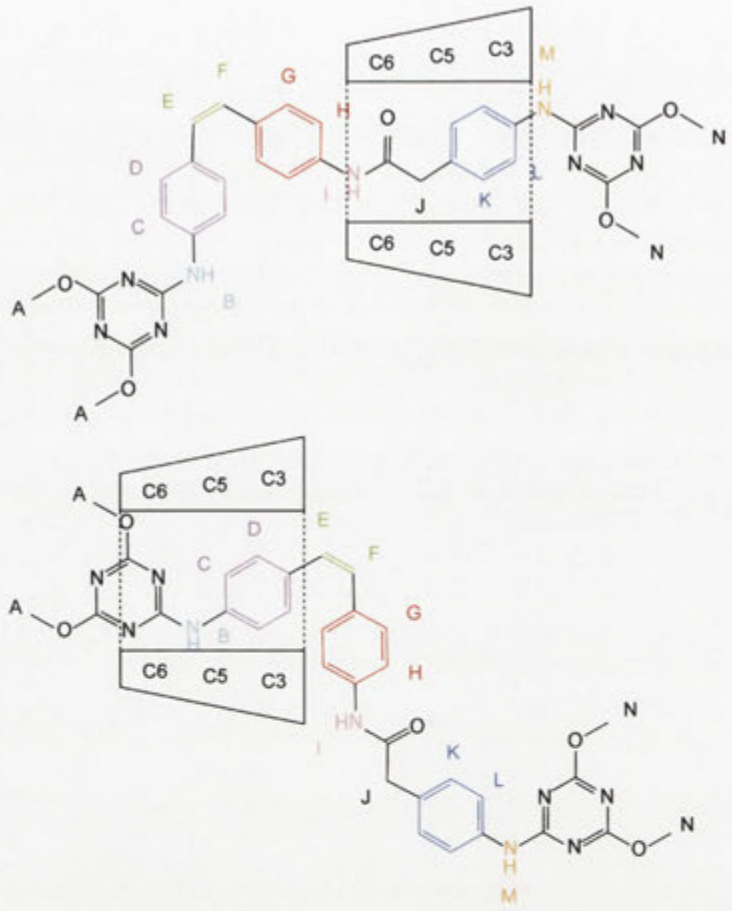

Figure 7.29. Assigned structures of the [2]-rotaxane **7.1(Z)** based on 2D NMR spectra.

In the assignment of conformation of the [2]-rotaxane **7.2(Z)** the DQCOSY NMR contour plot of the CD region, shown in Figure 7.30, was used to decipher the CD signals. From the characteristic downfield CD-H1 signal at 4.74 ppm, DQCOSY interactions were used to assign the remaining signals.

The signals of the axle of the [2]-rotaxane **7.2(Z)** were assigned using the ROESY 2D contour plots shown in Figures 7.31 and 7.32. NOE interactions are apparent between the signals of the olefinic protons E and F and those of the aromatic protons D and G. The signals of the protons D and G show interactions with the C and H proton signals to allow complete assignment of the stilbene signals. The signals of the phenyl protons K and L were also able to be determined from this spectrum. The assignment of the axle signals was completed using the contour plot shown in Figure 7.32. The stilbene protons C were determined to be near the triazine blocking group due to the NOE interaction of the latter's signals with the signal of the methoxy protons A. The aromatic protons K were

determined to be closer than protons L to the stilbene unit due to their NOE interaction with the signal of the alkyl protons J. The axle assignment can therefore be represented as shown in Figure 7.32.

Unlike the previous assignment of the CD position in the [2]-rotaxane **7.1(Z)**, the investigation into the CD positioning of the [2]-rotaxane **7.2(Z)** was much simpler with the CD only residing in one position on the axle. The ROESY contour plot used to determine this positioning is shown in Figure 7.32. From the contour plot it is clear that the CD does not reside over the olefinic bond as there is no NOE interaction between the signals of the olefinic protons E and F with the signals of the CD protons. The signal of the phenyl protons K shows an interaction with the signal of the protons CD-H3 while it is likely the signal of the protons L shows an interaction with both the signals of the protons CD-H5 and CD-H3. The interactions between these signals places the CD as shown in Figure 7.32 and this assignment is supported by the absence of any NOE interactions of the signals between the axle protons and that of the protons CD-H6 which resides near the triazine ring. The isomerisation of the stilbene unit of the [2]-rotaxane **7.2** to the *cis*-isomer **7.2(Z)** has therefore caused the CD to move to the second CD binding unit of the axle. It is possible that the CD of the [2]-rotaxane **7.2(Z)** also dynamically shuttles across the stilbene unit just as was the case for the [2]-rotaxane **7.1(Z)**. However, the structure shown in Figure 7.32 must be relatively more stable increasing its population to leave it as the only one observable through NOE interactions.

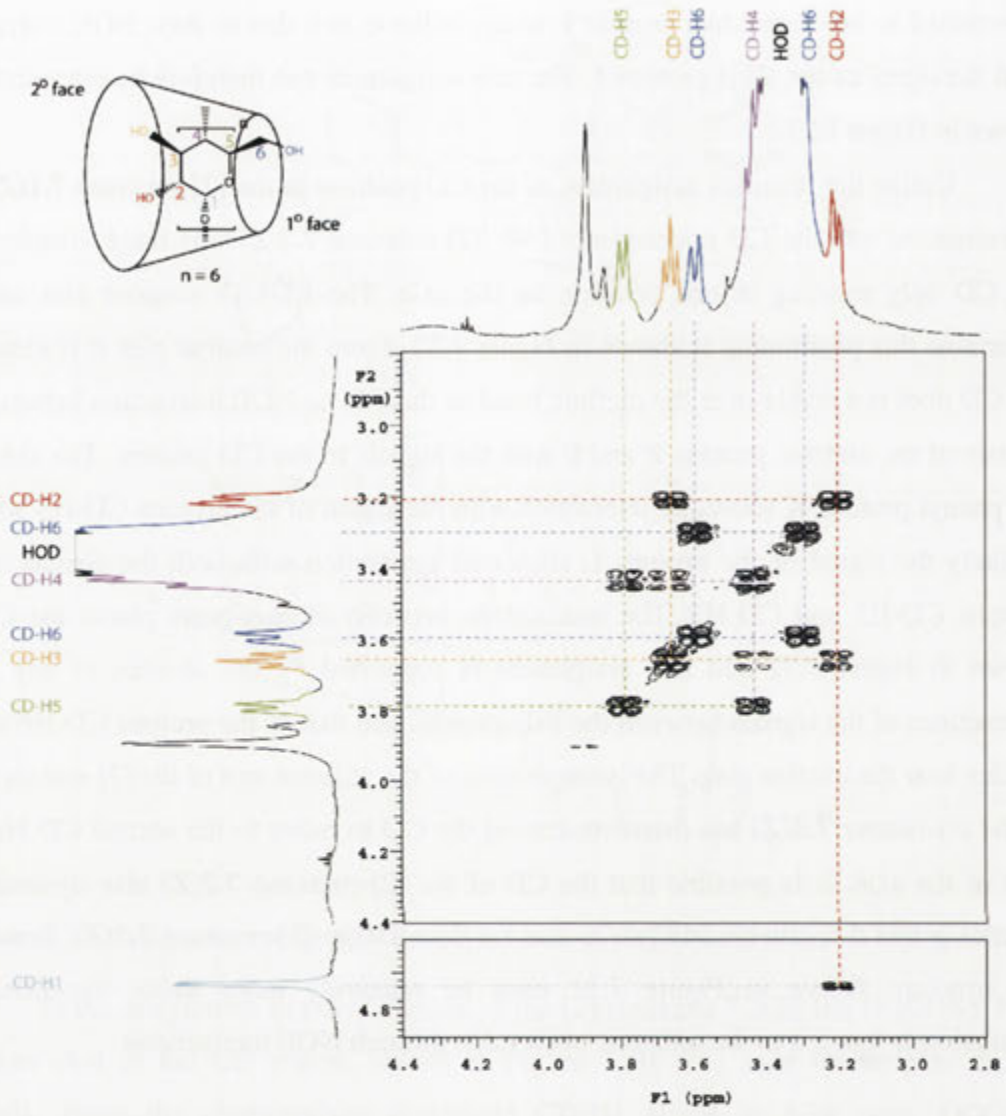

Figure 7.30. A section of the 500 MHz DQCOSY spectrum of the [2]-rotaxane **7.2(Z)** in d_6-DMSO at 25 °C of the region where crosspeaks are observed between cyclodextrin proton signals.

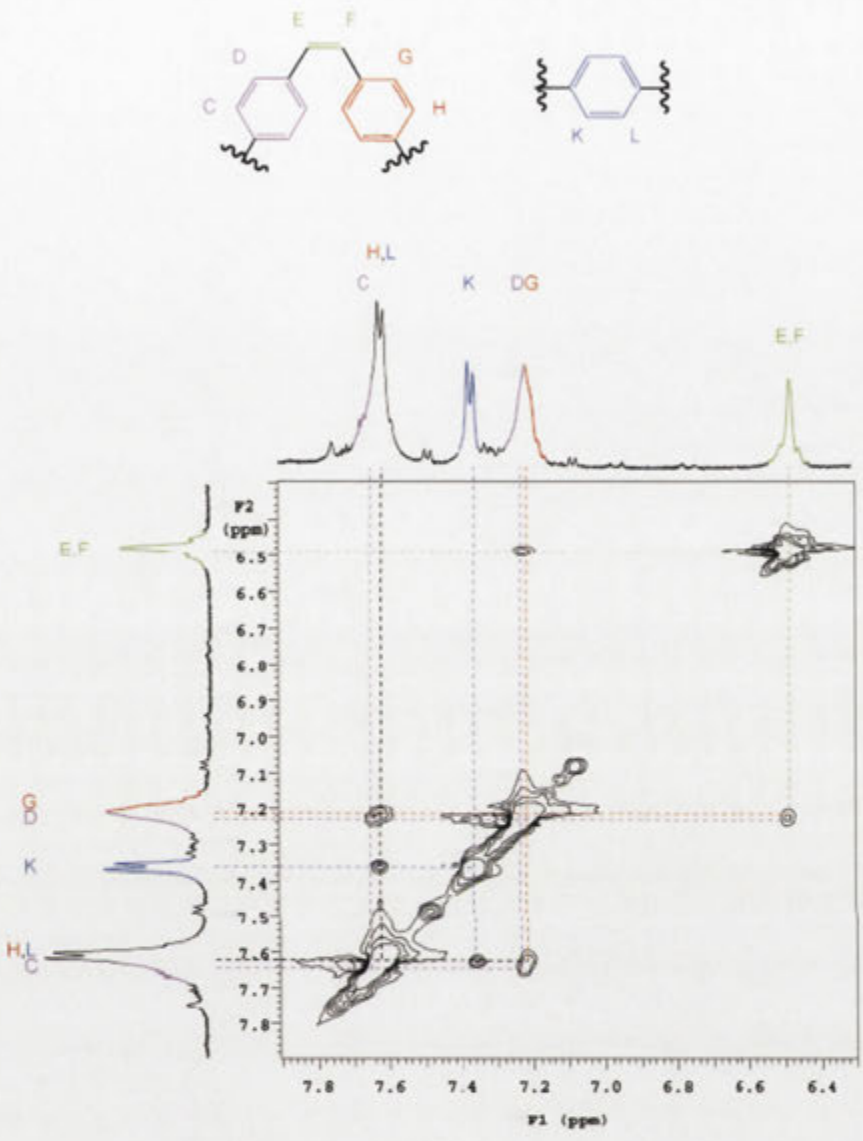

Figure 7.31. A section of the 500 MHz ROESY spectrum of the [2]-rotaxane **7.2(Z)** in d_6-DMSO at 25 °C of the region where crosspeaks are observed between axle proton signals.

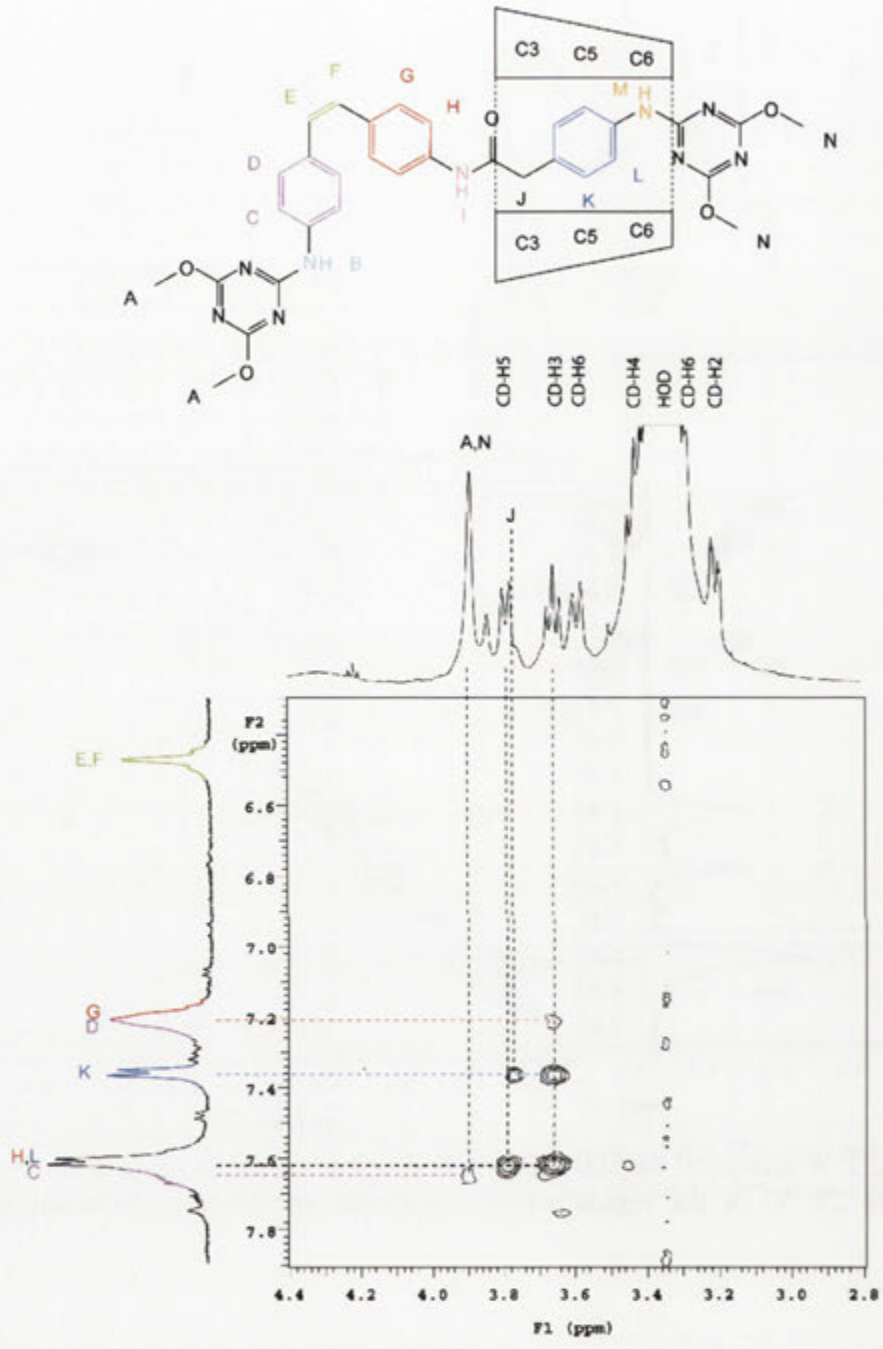

Figure 7.32. A section of the 500 MHz ROESY spectrum of the [2]-rotaxane **7.2(Z)** in d_6-DMSO at 25 °C of the region where crosspeaks are observed between axle and cyclodextrin proton signals.

In summary, the [2]-rotaxanes **7.1**, **7.2**, **7.6** and **7.7** were synthesised and their conformations determined by 2D NMR spectroscopy. Each of the isomers was established to isomerise to its corresponding *cis*-isomer, using HPLC and UV/visible

spectroscopy. The use of the higher wavelength of light of 370 nm proved to be far more effective than the 350 nm light source in each of the [2]-rotaxane isomerisations. This is thought to be due to smaller amounts of the *cis*-isomer undergoing the reverse reaction. When comparing the pairs of the isomeric [2]-rotaxanes **7.1** and **7.2**, and **7.6** and **7.7**, it appears that the isomers **7.2** and **7.6** with the primary face of the CD facing towards the second CD binding unit isomerise more effectively than the isomers **7.1** and **7.7** having the CD facing the opposite direction. The reason for this bias may be explained by the structures determined by 2D NMR spectroscopy for the *cis*-isomers **7.1(Z)** and **7.2(Z)**. In each case isomerisation of the stilbene unit causes the CD to shift to another part of the axle. The isomerisation of the [2]-rotaxane **7.1**, which is less favoured, causes the CD to be in a dynamic equilibrium between two different positions on the axle. Neither of these is apparently particularly favoured. The isomerisation of the [2]-rotaxane **7.2**, which is more favoured, produces only one conformation as determined by 2D NMR spectroscopy. Presumably this is more stable. In the case of the [2]-rotaxane **7.1**, the isomerisation is likely to be disfavoured ~~favoured~~ due to the steric hindrance of the dimethoxytriazine blocking group near the more restricted primary face of the CD.

Chapter 8: A Dimethoxytriazine Blocked Hermaphroditic [2]-Rotaxane that Acts as a Molecular Muscle

As the [2]-rotaxanes **7.1**, **7.2**, **7.6** and **7.7** were observed to have the ability to undergo reversible photochemical isomerisation, a further objective was to use the dimethoxytriazine blocking reagent **6.9** in the formation of an hermaphroditic [2]-rotaxane as shown in Scheme 8.1. Upon irradiation it was hoped the *trans,trans*-hermaphroditic [2]-rotaxane **8.1** would form the *cis,cis*-isomer **8.2**. The isomerisation to the *cis,cis*-isomer **8.2** would reduce the length of the molecule in what can be seen as a molecular muscle. The hermaphroditic [2]-rotaxane **3.4** had been previously synthesised by Cieslinski[80] using the trinitrophenyl blocking reagent **1.31**. The hermaphroditic [2]-rotaxane **3.4** proved ineffective for the reversible isomerisation of the stilbene units presumably due to the interference of the trinitrophenyl group. It was thought that the use

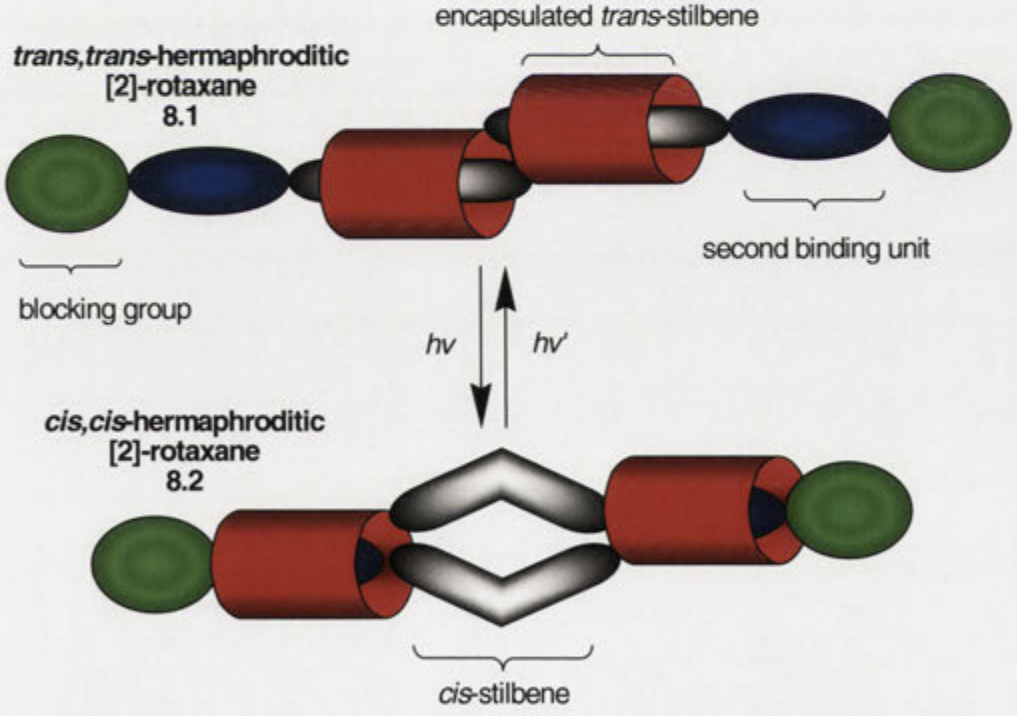

Scheme 8.1. Expected photochemical isomerisation of the stilbene unit of the *trans,trans*-hermaphroditic [2]-rotaxane **8.1** to produce a *cis,cis*-hermaphroditic [2]-rotaxane **8.2** that would cause the cyclodextin to shuttle to the second cyclodextrin binding unit

of the alternative blocking reagent **6.9** would allow an hermaphroditic [2]-rotaxane to be prepared and allow this to isomerise and act as a molecular muscle.

The synthesis of the hermaphroditic [2]-rotaxane **8.5(E,E)** is summarised in Scheme 8.2. The amine **8.3** is a known compound after its synthesis by Cieslinski[80] and was stirred in MQ H_2O presumably to form the dimeric included species **8.4**. The hermaphroditic [2]-rotaxane **8.5(E,E)** was formed after the addition of the blocking reagent **6.9** with its formation monitored by TLC. The hermaphroditic [2]-rotaxane **8.5(E,E)** was isolated using HPLC in 12% yield as a colourless powder and its ESI mass spectrum showed an $M+H^+$ ion of *m/z* 2836.3.

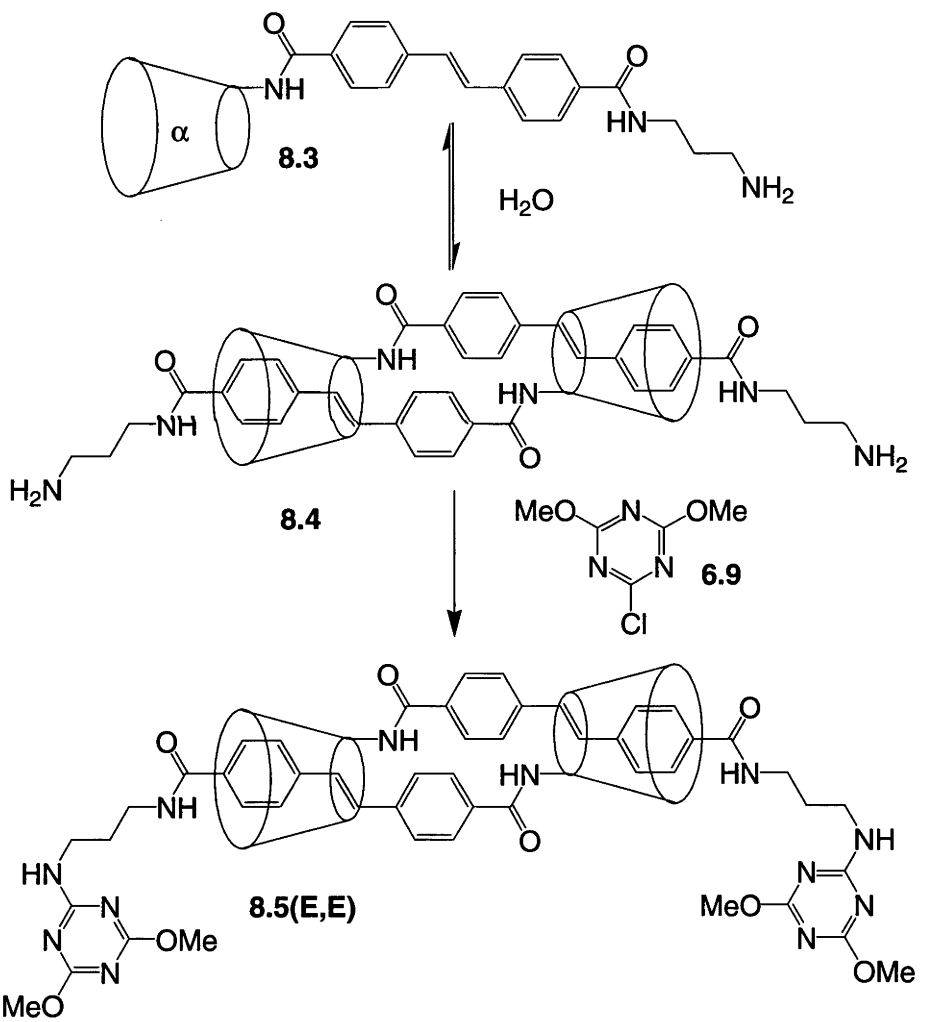

Scheme 8.2. Formation of the hermaphroditic [2]-rotaxane **8.5(E,E)**.

1D and 2D NMR spectroscopy was used to determine that the product isolated was the hermaphroditic [2]-rotaxane **8.5(E,E)**. The experiments were performed in d_4-methanol to prove that the product **8.5(E,E)** is a [2]-rotaxane. Because this solvent does not favour CD inclusion complexes, only the ROESY 2D NMR experiment of a mechanically interlocked [2]-rotaxane shows NOE interactions between the signals of CD and axle protons. Otherwise complexes dissociate under these conditions.

The ROESY contour plot of the hermaphroditic [2]-rotaxane **8.5(E,E)** is shown in Figure 8.1. The aromatic signals of the stilbene unit are shown on the x-axis of the contour plot while the signals of the CD protons are shown on the y-axis. The contour plot shows NOE interactions between the signals of the CD and aromatic protons. The ^{1}H NMR spectrum of the hermaphroditic [2]-rotaxane **8.5(E,E)** shows six sharp stilbene proton signals meaning the molecule is symmetrical. An acyclic hermaphroditic [2]-rotaxane would result in twice the number of stilbene proton signals due to the protons of the two stilbenes being inequivalent. The mass spectrum of the hermaphroditic [2]-rotaxane **8.5(E,E)** showed an ion of *m/z* 2836.3 which indicates the formation of a dimer. The hermaphroditic [2]-rotaxane **8.5(E,E)** is therefore a mechanically interlocked cyclic dimer.

Although it was shown that the hermaphroditic [2]-rotaxane is a cyclic dimer, the full assignment of the NMR signals was not practical as solubility limitations in methanol limited their intensity. A 2D NMR study of the hermaphroditic [2]-rotaxane **8.5(E,E)** was therefore conducted in D_2O which improved the solubility and the signal strength enabling the assignment to be undertaken. Since the formation of the mechanically interlocked cyclic dimer **8.5(E,E)** was shown in d_4-methanol, D_2O could be used as an alternative solvent to complete the 2D NMR assignment.

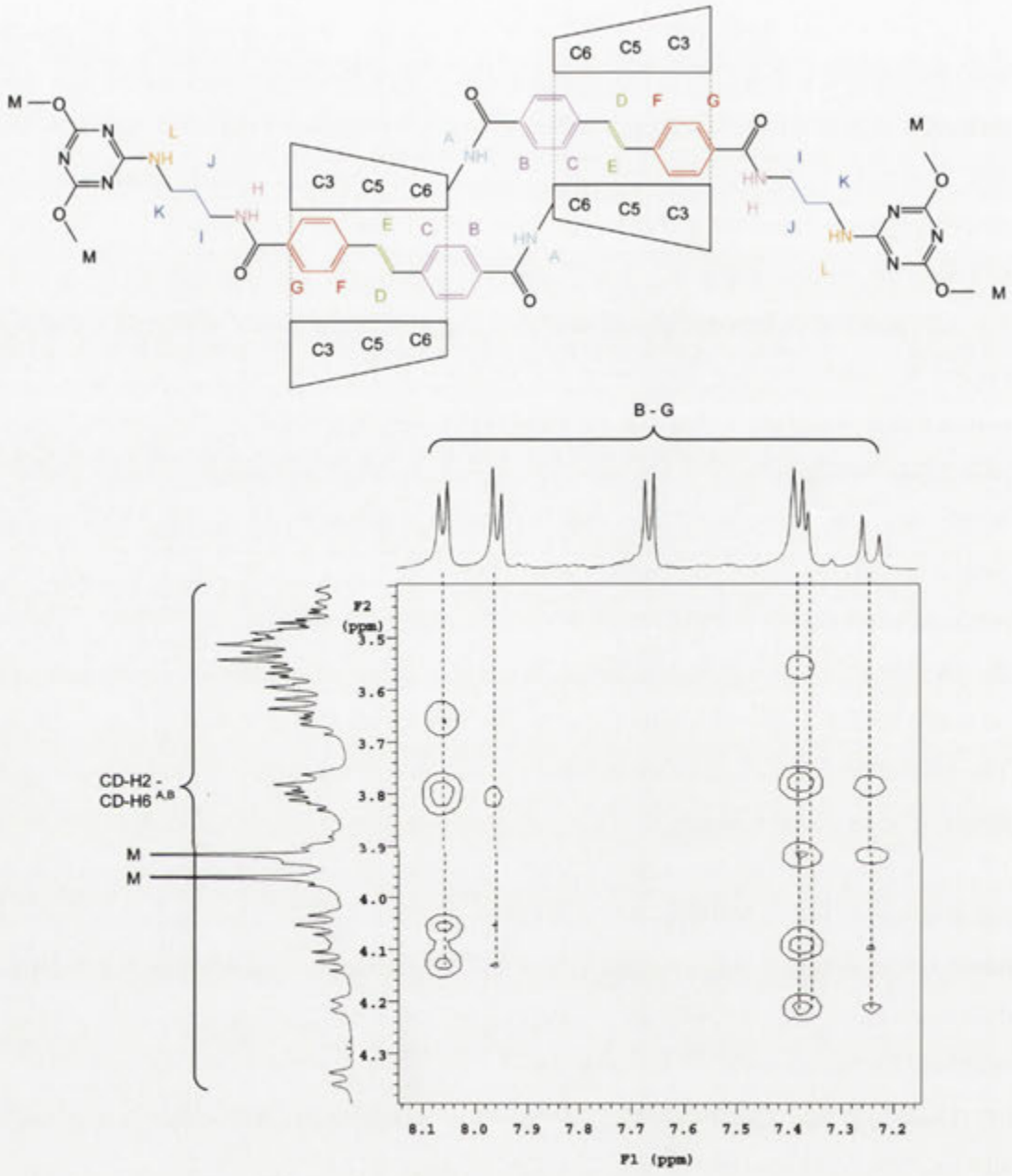

Figure 8.1. A section of the 500 MHz ROESY spectrum of the hermaphroditic [2]-rotaxane **8.5(E,E)** in d_4-methanol at 25 °C of the region where crosspeaks are observed between aromatic and cyclodextrin proton signals.

The ^{1}H NMR spectrum of the hermaphroditic [2]-rotaxane **8.5(E,E)** in D_2O is complex, but by using a combination of TOCSY, HMQC and ROESY 2D NMR spectroscopy, in a procedure similar to the literature,[77] most of the signals can be assigned. The signals are labelled as in the previous chapters with the addition that the glucopyranose unit to which the signals of the protons belong can also be assigned. The

glucopyranose units lose their symmetrical nature due to the substitution of one of the primary hydroxyl groups. The unit that incurred a substitution is labelled as glucopyranose unit A while the remaining units are labelled B to F in a clockwise direction looking at the primary face of the CD.

Each of the signals for the CD protons was assigned with their chemical shifts shown in Table 8.1.

	Glucopyranose Unit					
CD-H	A	B	C	D	E	F
1	5.11	5.15	5.04	4.94	5.17	5.16
2	3.64	3.67	3.63	3.52	3.65	3.71
3	3.59	3.89	3.92	3.50	3.84	3.99
4	3.47	3.74	3.78	3.53	3.61	3.90
5	3.70	3.96	3.98	3.48	3.84	4.12
6	3.06	-	-	-	-	-
6'	4.52	-	-	-	-	-

Table 8.1. Chemical shifts (ppm) of the CD of the hermaphroditic [2]-rotaxane **8.5(E,E)**.

For the assignment of the signals of the hermaphroditic [2]-rotaxane **8.5(E,E)**, the signals of the CD-H1 protons can be identified from the ^{1}H NMR spectrum as they characteristically appear further upfield. Using TOCSY NMR spectroscopy, through bond interactions arise as crosspeaks between the signals of nearby protons. Using this method the signals of the protons that belong to each individual glucopyranose unit can be determined. By increasing the mixing time for the TOCSY experiment, interacting protons located through greater numbers of bonds can be detected.

The TOCSY NMR spectrum of the hermaphroditic [2]-rotaxane **8.5(E,E)** with a mixing time of 30 ms is shown in Figure 8.2. The signals of the CD-H1 protons that characteristically appear furthest downfield are found in the region of 4.9-5.2 ppm. At this short mixing time, observable crosspeaks can only be seen with the signals of the CD-H2 protons.

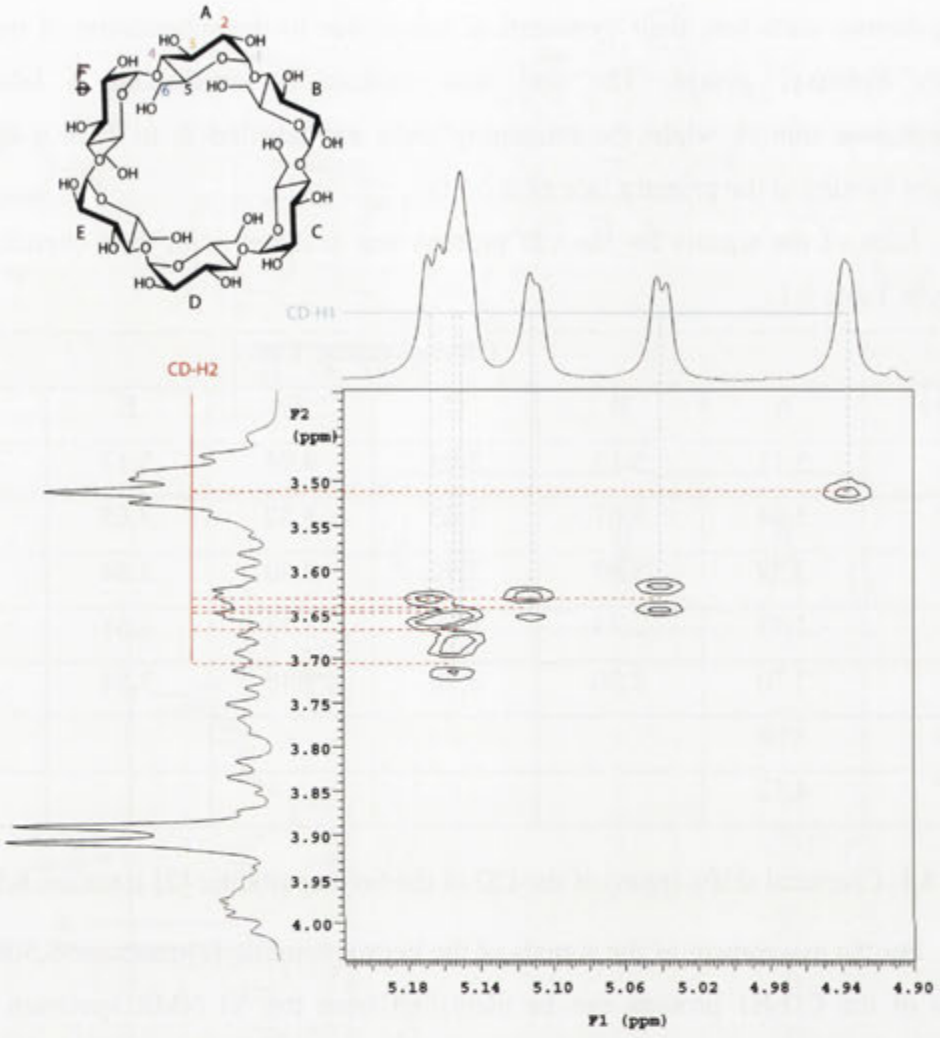

Figure 8.2. A section of the 500 MHz TOCSY spectrum of the hermaphroditic [2]-rotaxane **8.5(E,E)** in D_2O at 25 °C with a mixing time of 30 ms of the region where crosspeaks are observed between cyclodextrin proton signals.

The TOCSY contour plot of the hermaphroditic [2]-rotaxane **8.5(E,E)** with a mixing time of 55 ms is shown in Figure 8.3. By increasing the mixing time, TOCSY interactions between the signals of the CD-H1 protons and those of the CD-H2 and CD-H3 protons can be observed.

The TOCSY contour plot of the hermaphroditic [2]-rotaxane **8.5(E,E)** with a mixing time of 80 ms is shown in Figure 8.4. From the contour plot, through bond interactions between the signals of the CD-H1 and CD-H4 protons are observable. Although the contour plot in Figure 8.4 labels the glucopyranose unit to which each set of signals belongs, at this point in the assignment the information obtained is insufficient to

distinguish between the glucopyranose units. Instead this was established later but is illustrated here for clarity. Since the mixing time of 80 ms is the longest mixing time allowed for use on the NMR spectrometer, the signals of the CD-H5 and CD-H6 protons could not be identified from their interactions with the CD-H1 protons. The use of a TOCSY contour plot with an increased mixing time was not essential, however, for the complete assignment of the signals of the CD.

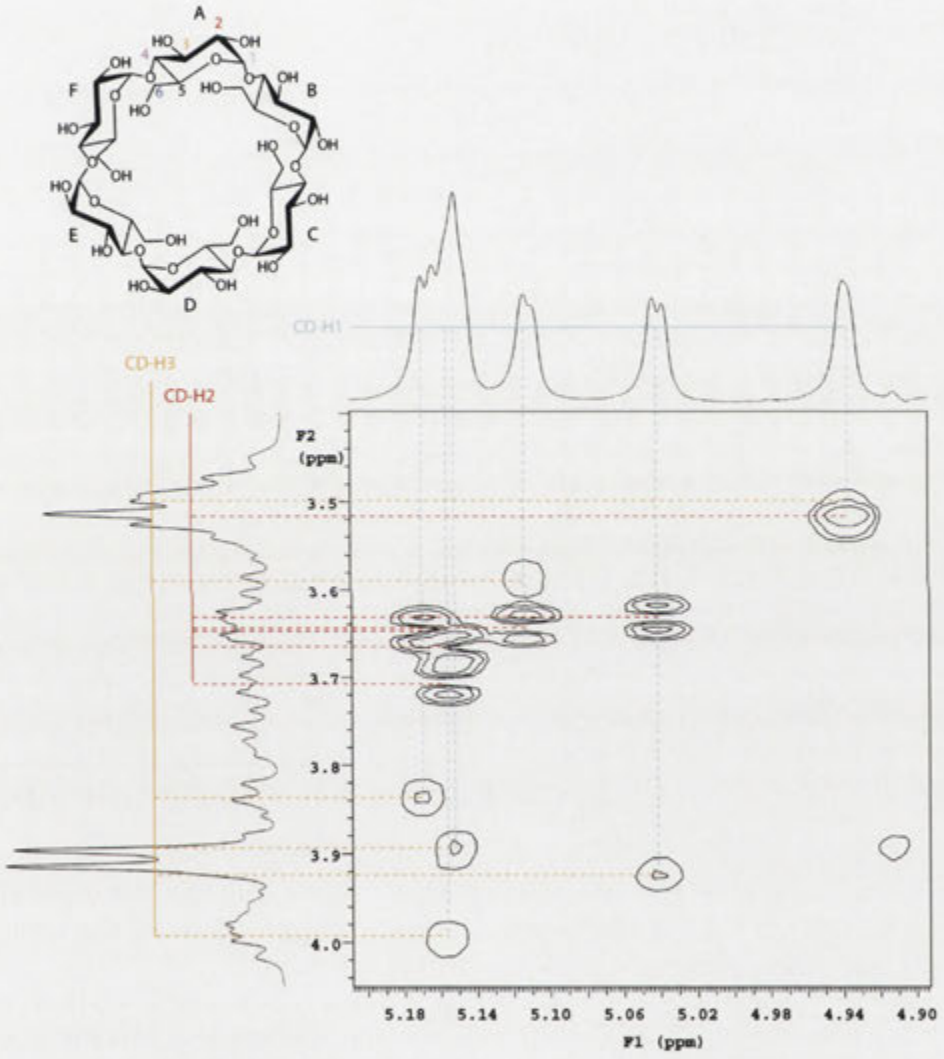

Figure 8.3. A section of the 500 MHz TOCSY spectrum of the hermaphroditic [2]-rotaxane **8.5(E,E)** in D_2O at 25 °C with a mixing time of 55 ms of the region where crosspeaks are observed between cyclodextrin proton signals.

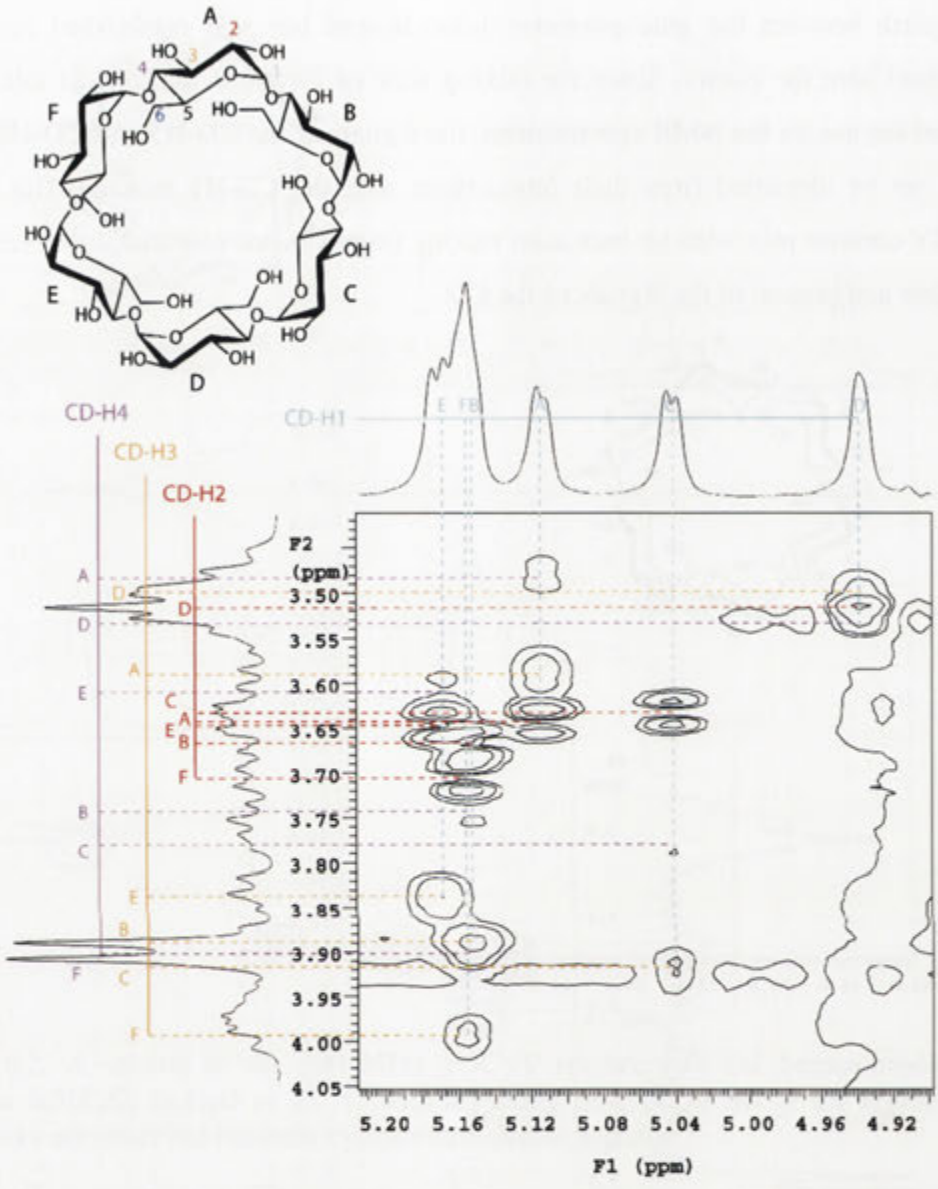

Figure 8.4. A section of the 500 MHz TOCSY spectrum of the hermaphroditic [2]-rotaxane **8.5(E,E)** in D_2O at 25 °C with a mixing time of 80 ms of the region where crosspeaks are observed between cyclodextrin proton signals.

To enable the signals of the CD to be assigned to their respective glucopyranose units, the signals of one of the units first had to be identified. Using a g-HMQC experiment, the signals of the protons CD-H6^{A}-A and CD-H6^{B}-A are able to be determined. The contour plot of the g-HMQC spectrum is shown in Figure 8.5. Because the primary hydroxyl of the A glucopyranose unit has been substituted with an amino group and allowed to react to form an amide, the signal of the nearby carbon CD-C6 is

moved upfield to around 43.8 ppm. The contour plot of the heteronuclear experiment shows the signals of the coupled protons CD-H6^{A}-A and CD-H6^{B}-B at 3.06 and 4.52 ppm.

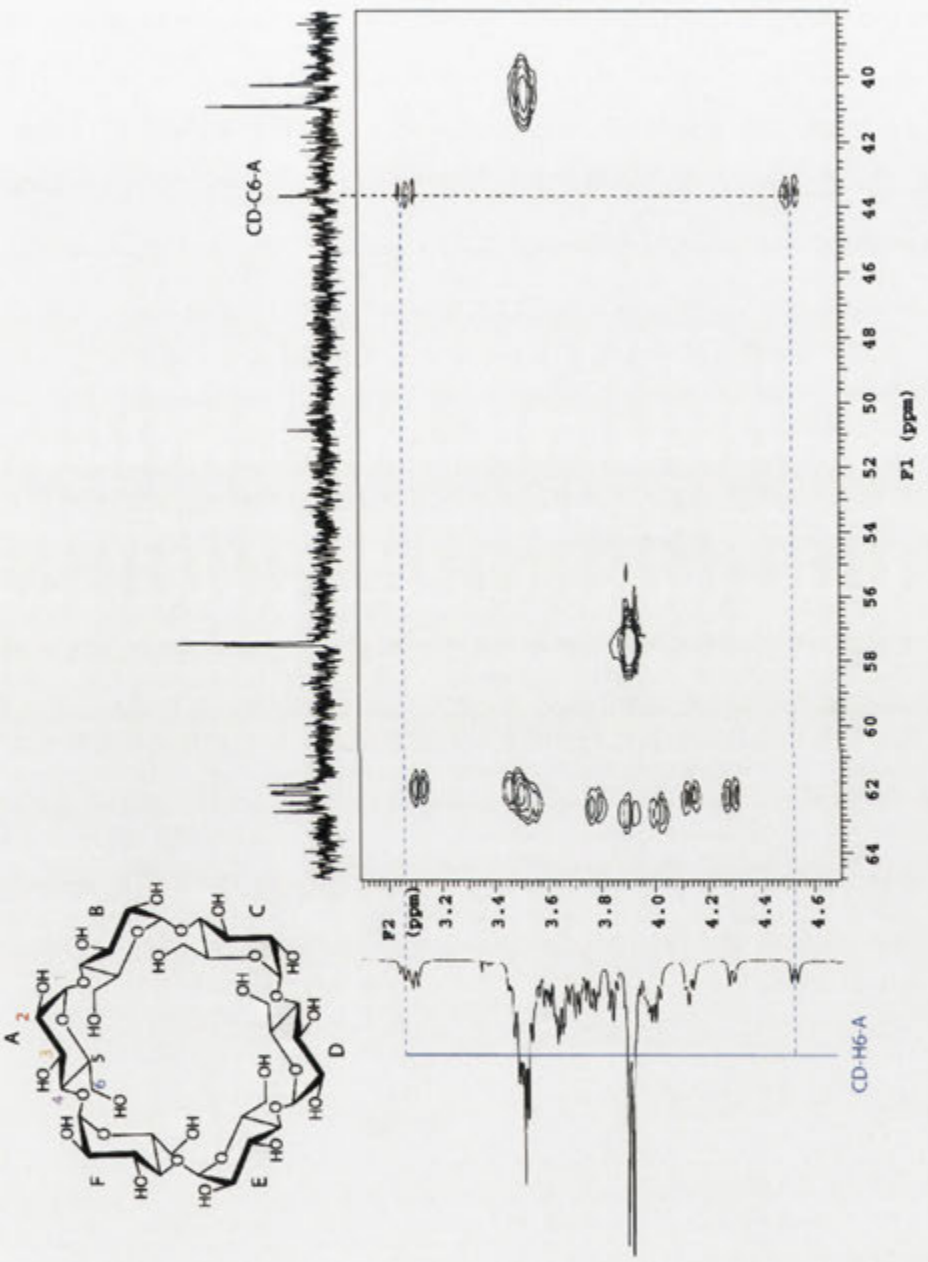

Figure 8.5. A section of the 600 MHz g-HMQC spectrum of the hermaphroditic [2]-rotaxane **8.5(E,E)** in D_2O at 25 °C of the region where crosspeaks are observed between cyclodextrin proton and carbon signals.

With the identification of the signals of the protons CD-H6^{A}-A and CD-H6^{B}-A, short range TOCSY interactions were used to identify the CD-H4-A signal. As the CD-

H1 to CD-H4 signals of each of the glucopyranose units were determined above, the entire assignment of the signals of the A glucopyranose unit was therefore possible. A section of the TOCSY contour plot with a mixing time of 30 ms of the hermaphroditic [2]-rotaxane **8.5(E,E)** is shown in Figure 8.6. The plot shows interactions between the signals of the CD-H6^{A}-A and CD-H6^{B}-A protons and that of the proton CD-H5-A. The signal of the proton CD-H5-A also shows an interaction with that of the CD-H4-A proton. The signals of the protons CD-H1-A to CD-H3-A were then assigned using the TOCSY spectrum as shown in Figure 8.4.

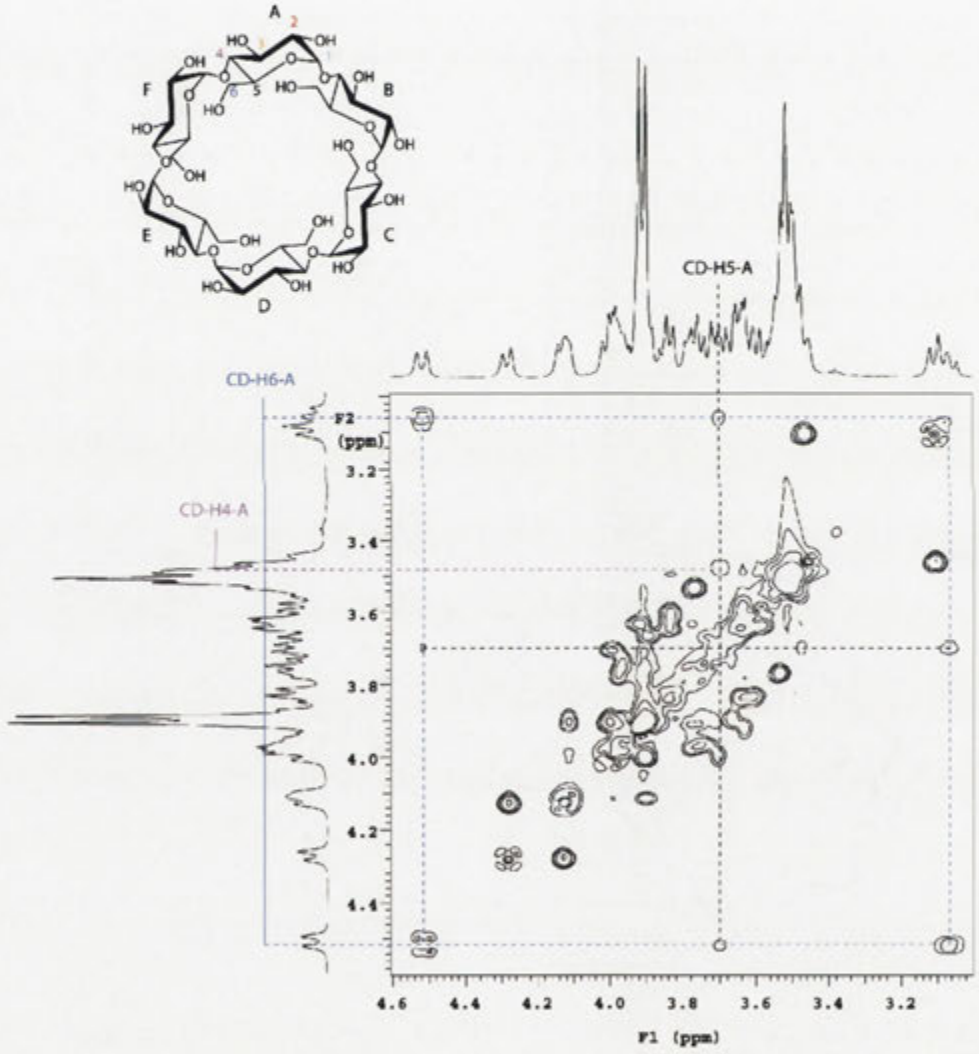

Figure 8.6. A section of the 500 MHz TOCSY spectrum of the hermaphroditic [2]-rotaxane **8.5(E,E)** in D_2O at 25 °C with a mixing time of 30 ms of the region where crosspeaks are observed between cyclodextrin proton signals.

From the complete assignment of the signals of the A glucopyranose unit, the ROESY contour plot of the CD region can be used to identify each of the signals for the remaining glucopyranose units. The assignment of the signals of the glucopyranose units is possible because the signal of the proton CD-H1 of one glucopyranose unit should show interactions with the signal of the proton CD-H4 of its neighbouring glucopyranose unit. A section of the ROESY contour plot of the hermaphroditic [2]-rotaxane **8.5(E,E)** is shown in Figure 8.7. The signal of the proton CD-H1-A shows an NOE interaction with that of the proton CD-H4-B enabling the signals of the CD-H1 to CD-H4 protons of the B glucopyranose unit to be assigned using the TOCSY contour plot shown in Figure 8.4. Further ROESY interactions between the signals of the protons CD-H1 and CD-H4 of the remaining glucopyranose units enable each of the glucopyranose signals to be assigned as shown in Figure 8.4.

At this point in the assignment, the signals of the protons CD-H1 to CD-H4 were assigned to the glucopyranose unit to which they belong. To identify the signals of the protons CD-H5, the TOCSY contour plot was again used. A section of the TOCSY contour plot which used a mixing time of 30 ms is shown in Figure 8.8. The signals of the CD-H4 protons of the A to F glucopyranose units show interactions with the signals of the protons CD-H5. The assignment is limited to the signals of the CD-H5 protons as interactions were not observed with the signals of the CD-H6 protons. The assignment of the CD-H6 protons is not important, however, as the ROESY interactions with the signals of the annular protons CD-H3 and CD-H5 are sufficient to determine where the CDs are located with respect to the axles of the hermaphroditic [2]-rotaxane **8.5(E,E)**.

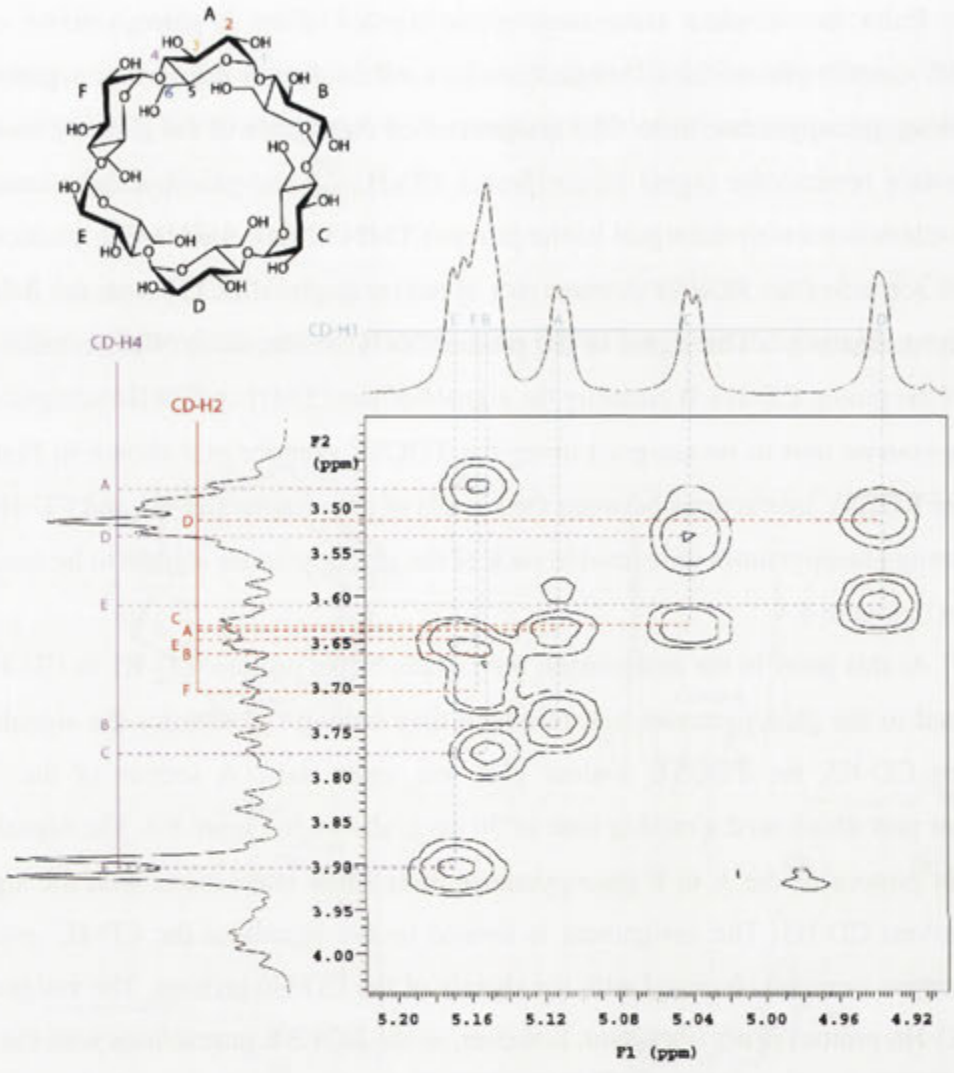

Figure 8.7. A section of the 500 MHz ROESY spectrum of the hermaphroditic [2]-rotaxane **8.5(E,E)** in D_2O at 25 °C of the region where crosspeaks are observed between cyclodextrin proton signals.

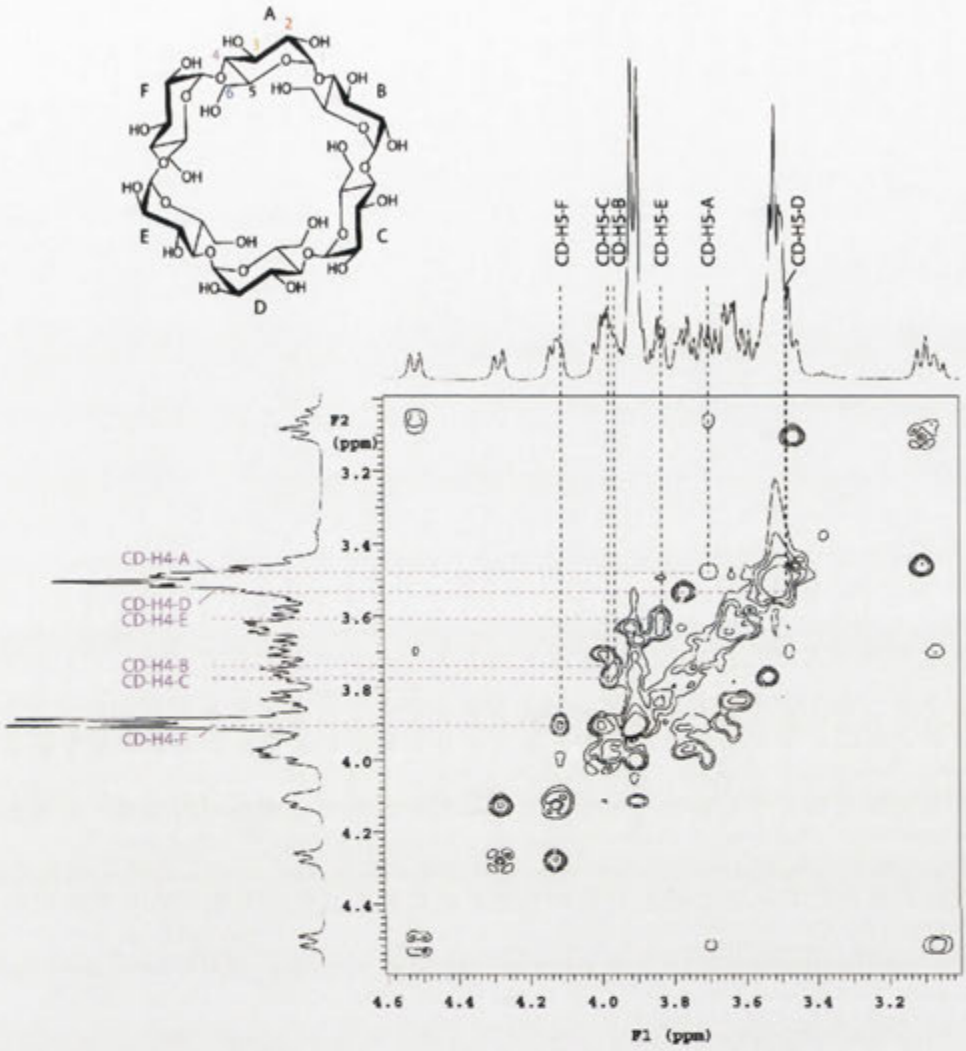

Figure 8.8. A section of the 500 MHz TOCSY spectrum of the hermaphroditic [2]-rotaxane **8.5(E,E)** in D_2O at 25 °C with a mixing time of 30 ms of the region where crosspeaks are observed between cyclodextrin proton signals.

The ROESY contour plot of the aromatic region of the hermaphroditic [2]-rotaxane **8.5(E,E)** is shown in Figure 8.9. The assignment of the signals of the stilbene unit of the axle was carried out as explained in Chapter 2. Interactions with the signals of the olefinic protons D and E allow the stilbene resonances to be assigned as shown in Figure 8.9.

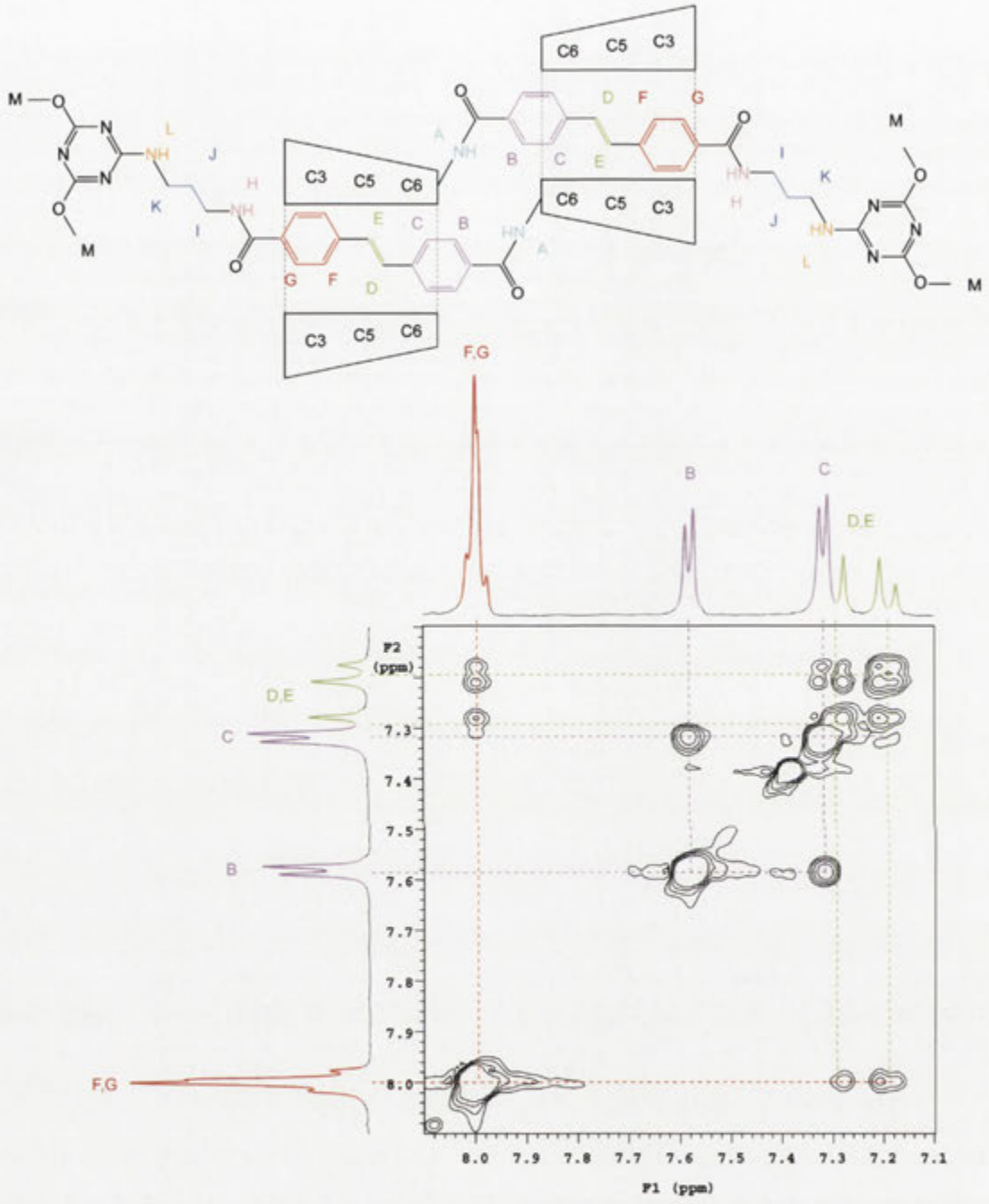

Figure 8.9. A section of the 500 MHz ROESY spectrum of the hermaphroditic [2]-rotaxane **8.5(E,E)** in D_2O at 25 °C of the region where crosspeaks are observed between aromatic proton signals.

In the ROESY contour plot in Figure 8.10, interactions between the signals of the CD and stilbene protons are observed. Interpreting these interactions allows the location of the CDs with respect to the axles of the hermaphroditic [2]-rotaxane **8.5(E,E)** to be

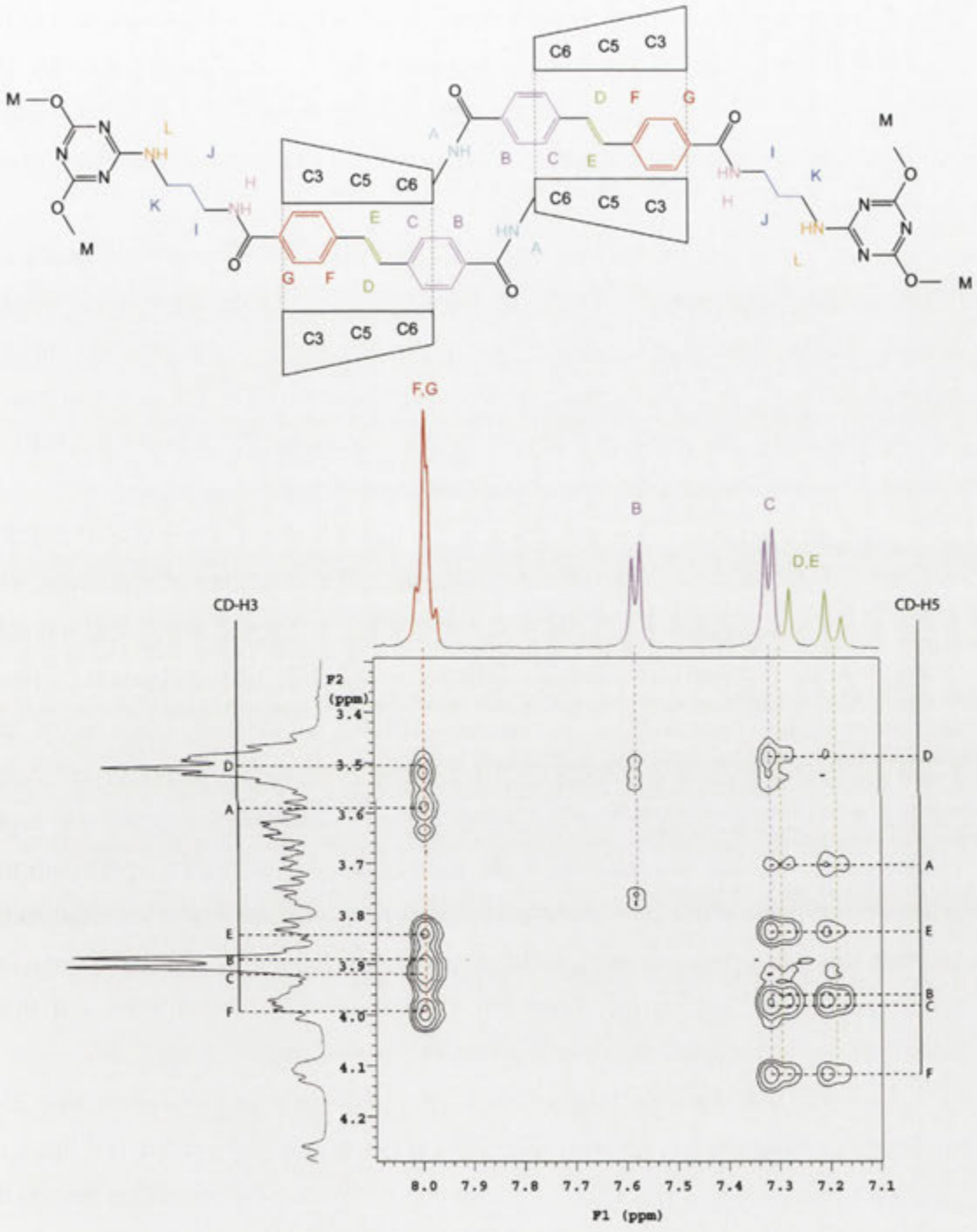

Figure 8.10. A section of the 500 MHz ROESY spectrum of the hermaphroditic [2]-rotaxane **8.5(E,E)** in D_2O at 25 °C of the region where crosspeaks are observed between aromatic and cyclodextrin proton signals.

determined. The signals of the stilbene protons C, D and E show interactions with each of the six signals of the CD-H5 protons placing the C, D and E protons centrally within the

CD. The signals of the F and G protons show strong NOE interactions with each of the six CD-H3 protons placing the F and G protons at the secondary face of the CD. The signal of the B aromatic protons shows some minor interactions with what are most likely the signals of the protons CD-H6 thus placing the B protons at the primary face of the CD.

The structure of the hermaphroditic [2]-rotaxane **8.5(E,E)** as a result of the 2D NMR assignment is therefore shown in Figure 8.10. As in the case of the similar hermaphroditic [2]-rotaxane **3.4** synthesised by Cieslinski,[80] the stilbenes of the hermaphroditic [2]-rotaxane **8.5(E,E)** are included within the CDs. The next step was to test the ability for the *trans*-stilbenes of the hermaphroditic [2]-rotaxane **8.5(E,E)** to isomerise upon irradiation with light of a particular wavelength.

Before commencing the photolysis on the hermaphroditic [2]-rotaxane **8.5(E,E)**, the required irradiation wavelength was determined from its UV/visible spectrum. The UV/visible spectrum of a 9.88×10^{-6} M solution of the hermaphroditic [2]-rotaxane **8.5(E,E)** in MQ H_2O was recorded and is shown as the black line in Figure 8.11. From the spectrum the λ_{max} at 333 nm can be attributed to the *trans*-stilbenes of the hermaphroditic [2]-rotaxane **8.5(E,E)**. In the earlier isomerisation of the [2]-rotaxanes **7.1**, **7.2**, **7.6** and **7.7**, the *cis*-stilbene appeared to have an absorbance near 265 nm. Light of wavelength 350 nm was chosen for the photolysis study as at this wavelength the absorption of light by the *cis*-stilbene units and their isomerisation was expected to be less than that for the *trans*-isomers. Light of wavelength 254 nm was used to reverse the isomerisation. At 254 nm, the absorption of light by the *trans*-stilbenes and their isomerisation was expected to be less than that for the *cis*-isomers.

For the isomerisations, irradiation with 350 nm light before irradiation with 254 nm light was designated to be one cycle. The cycle was repeated another two times to establish a trend for the reversibility of the isomerisation using the percentage amount of the hermaphroditic [2]-rotaxanes **8.5(E,E)** determined using HPLC.

As a result of the irradiation of the hermaphroditic [2]-rotaxane **8.5(E,E)** with light of wavelength 350 nm for one minute, the *trans,cis*-isomer **8.5(E,Z)** is apparently formed. The expected structure of the *trans,cis*-isomer **8.5(E,Z)** is shown in Scheme 8.3. The *trans,trans*-isomer **8.5(E,E)** was reformed following the irradiation with light of

wavelength 254 nm for one minute. From the HPLC analysis the new product **8.5(E,Z)** has a maximum absorbance at 333 nm and is therefore likely to contain a *trans*-stilbene unit. There is also an increase in the absorbance of the new product **8.5(E,Z)** below 290 nm resulting from the formation of the *cis*-stilbene unit. These changes in the UV/visible spectral profile are consistent with those observed in the UV/visible spectra shown in Figure 8.11 upon 350 nm irradiation. The change in the spectral profile therefore indicates that the product formed is the *trans,cis*-isomer **8.5(E,Z)** and must be an intermediate in the complete isomerisation of the hermaphroditic [2]-rotaxane **8.5(E,E)**.

The reversibility of the isomerisation was then determined from the graph of the percentage amount of the hermaphroditic [2]-rotaxane **8.5(E,E)** before and after irradiation. This graph is shown in Figure 8.12 and depicts the consumption of the hermaphroditic [2]-rotaxane **8.5(E,E)** upon irradiation with 350 nm. It also shows the reformation of the hermaphroditic [2]-rotaxane **8.5(E,E)** after 254 nm irradiation. At a glance it could be thought that a substantial portion of the *trans,trans*-isomer **8.5(E,E)** decomposed during the first cycle. After the second and third cycles, however, the amount of material further lost is very minor. The initial drop in the amount of the recovered *trans,trans*-isomer **8.5(E,E)** can therefore be attributed to the establishment of an equilibrium with the *trans,cis*-isomer **8.5(E,Z)**. Thus it was established that the interconversion between the *trans,trans*-isomer **8.5(E,E)** and the *trans,cis*-isomer **8.5(E,Z)** is reversible.

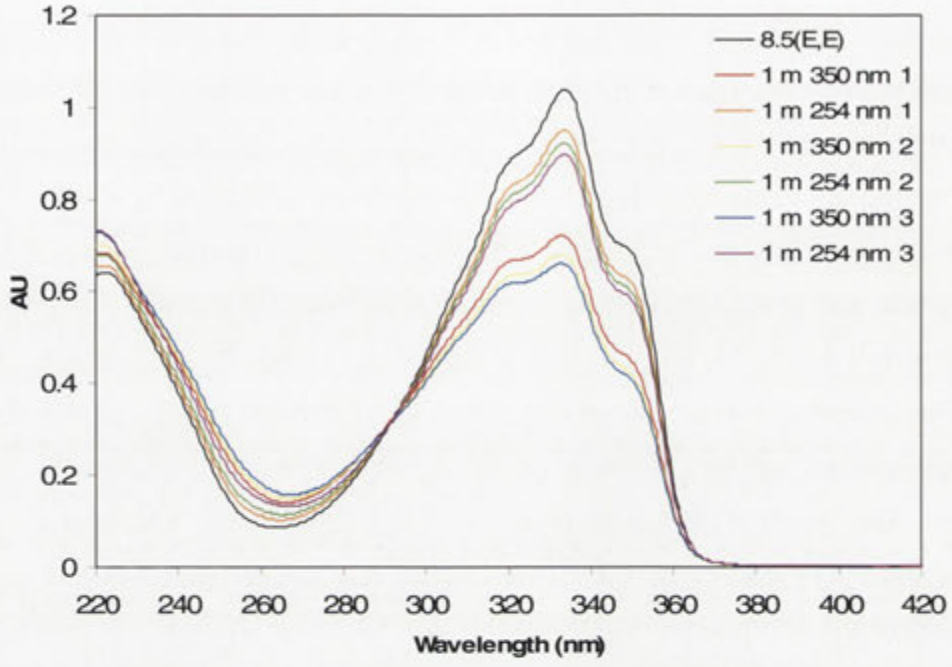

Figure 8.11. UV/visible spectra of a solution of the hermaphroditic [2]-rotaxane **8.5(E,E)** [9.88×10^{-6} M] in MQ H_2O and after exposure to 350 nm and 254 nm light.

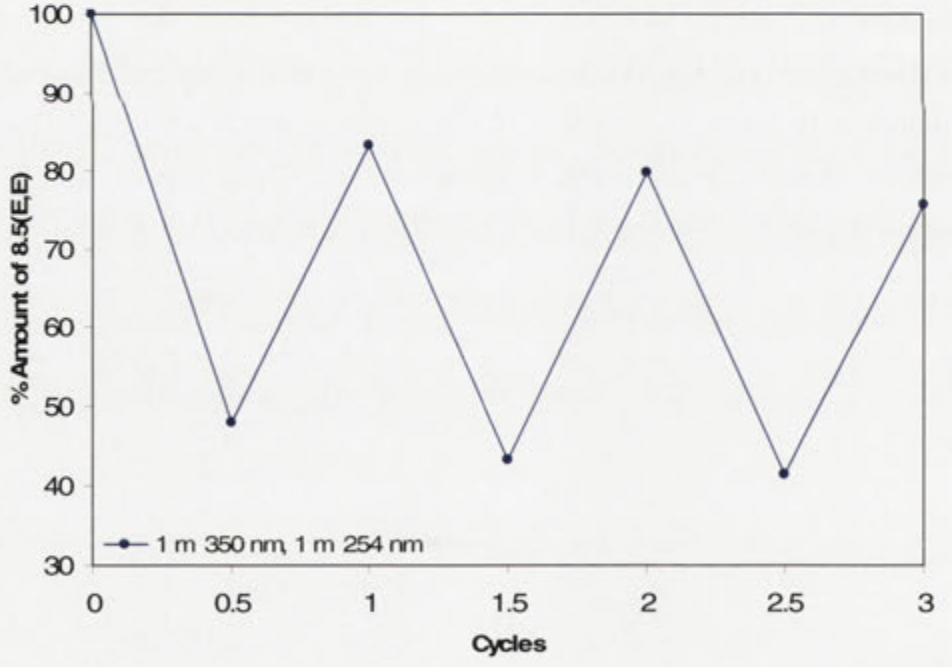

Figure 8.12. Percentage remaining of the hermaphroditic [2]-rotaxane **8.5(E,E)** [9.88×10^{-6} M] in MQ H_2O after various irradiations. One cycle as indicated on the graph denotes irradiation with 350 nm light before irradiation with 254 nm light.

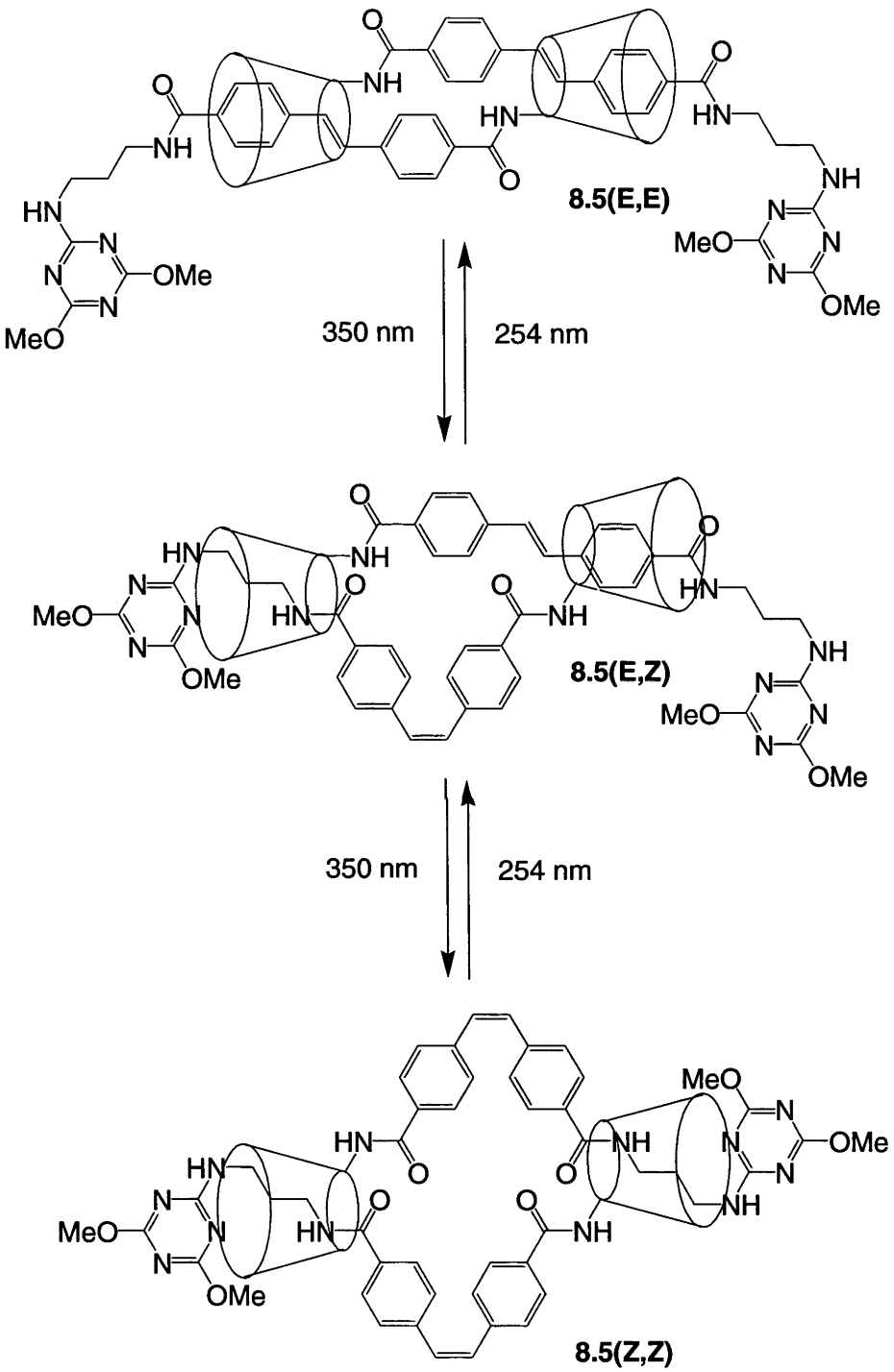

Scheme 8.3. Proposed behaviour of the hermaphroditic [2]-rotaxane **8.5(E,E)**.

Each of the stilbene units of the hermaphroditic [2]-rotaxane **8.5(E,E)** was assumed not to isomerise at the same time. The time length for the 350 nm irradiation

was therefore increased to ten minutes to isomerise both stilbene units to form the *cis,cis*-isomer **8.5(Z,Z)**. The 254 nm irradiation time length was retained and the reaction was monitored again by HPLC and UV/visible spectroscopy.

Increasing the time length of the 350 nm irradiation of the hermaphroditic [2]-rotaxane **8.5(E,E)** was successful in the formation of the *cis,cis*-isomer **8.5(Z,Z)**. From the HPLC analysis, a new product is formed that shows an absorbance below 270 nm corresponding to the formation of a *cis*-stilbene. The new product also does not show any absorbance at 333 nm indicating the absence of any *trans*-stilbene. These changes in the UV/visible profile are consistent with those observed in the UV/visible spectra of the isomerisation shown in Figure 8.13. Also evident from the HPLC traces was the formation of the intermediate **8.5(E,Z)** determined above. The UV/visible profile of the new product therefore indicates that the *cis,cis*-isomer **8.5(Z,Z)** was formed via the *trans,cis* intermediate **8.5(E,Z)** from the isomerisation of the hermaphroditic [2]-rotaxane **8.5(E,E)**.

The reversibility of the isomerisation was then determined from the graph of the percentage amount of the hermaphroditic [2]-rotaxane **8.5(E,E)** before and after irradiation. This graph is shown in Figure 8.14 and depicts the consumption of the hermaphroditic [2]-rotaxane **8.5(E,E)** upon irradiation with 350 nm light. It also shows the reformation of the hermaphroditic [2]-rotaxane **8.5(E,E)** after 254 nm irradiation. Again there was a significant amount of the *trans,trans*-isomer **8.5(E,E)** not reformed after the initial irradiation with 254 nm light. After the second and third irradiation cycles the amount of the *trans,trans*-isomer **8.5(E,E)** material lost is a lot less. The initial drop in the amount of the recovered *trans,trans*-isomer **8.5(E,E)** can therefore be attributed to the establishment of a equilibrium between the isomers. Thus it was established that the interconversion between the *trans,trans*-isomer **8.5(E,E)**, the *trans,cis*-isomer **8.5(E,Z)** and the *cis,cis*-isomer **8.5(Z,Z)** is reversible.

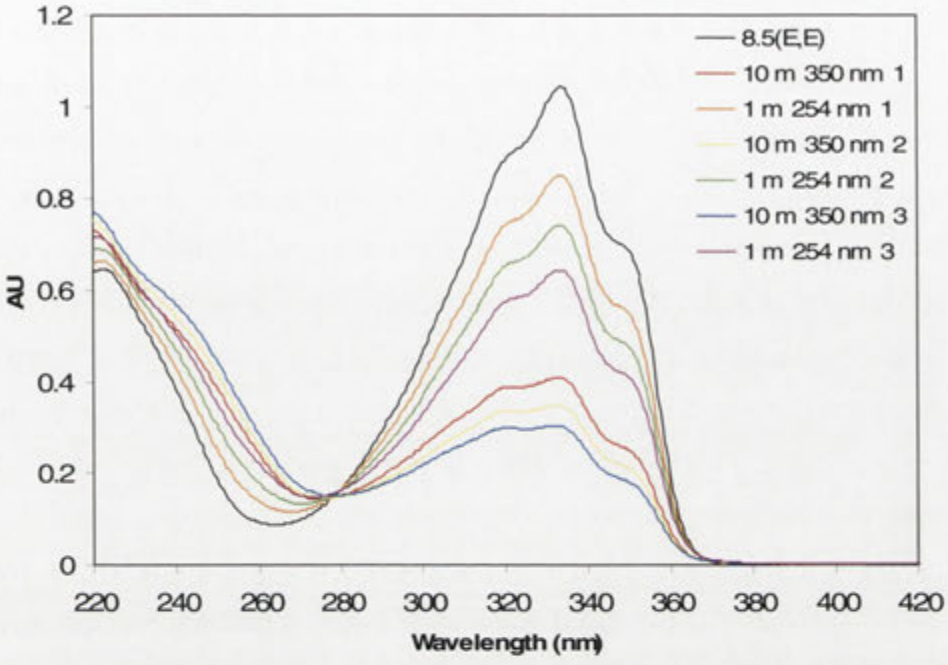

Figure 8.13. UV/visible spectra of a solution of the hermaphroditic [2]-rotaxane **8.5(E,E)** [9.88×10^{-6} M] in MQ H_2O and after exposure to 350 nm and 254 nm light.

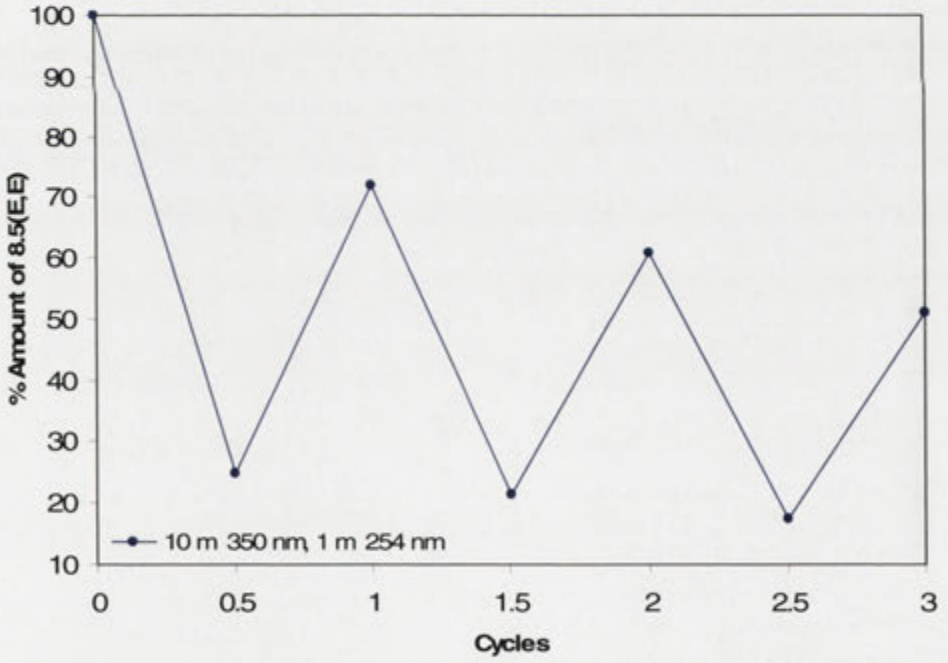

Figure 8.14. Percentage remaining of the hermaphroditic [2]-rotaxane **8.5(E,E)** [9.88×10^{-6} M] in MQ H_2O after various irradiations. One cycle as indicated on the graph denotes irradiation with 350 nm light before irradiation with 254 nm light.

It was anticipated that isomerisation to the *cis,cis*-isomer **8.5(E,E)** and the *trans,cis*-isomer **8.5(E,Z)** would cause the CDs to shuttle over the stilbenes. 2D NMR spectroscopy was therefore sought to determine the location of the CDs in the *cis,cis*-isomer **8.5(E,E)** and the *trans,cis*-isomer **8.5(E,Z)**. Due to the low yield of the formation of the hermaphroditic [2]-rotaxane **8.5(E,E)**, it was impractical to isolate each of the isomers **8.5(E,Z)** and **8.5(Z,Z)** for individual characterisation. A mixture of the isomers were therefore analysed by 2D NMR spectroscopy. Monitoring by HPLC, a dilute solution of the hermaphroditic [2]-rotaxane **8.5(E,E)** was irradiated with 350 nm light. After three minutes it was determined that a maximum amount of the *trans,cis*-isomer **8.5(E,Z)** was formed. The isomerisation mixture was then subjected to NMR spectroscopy.

The ^{1}H NMR spectrum of the hermaphroditic [2]-rotaxane **8.5(E,E)** and the spectrum of the solution after irradiation is shown in Figure 8.15. From the spectra of the irradiated sample, new signals arise in the aromatic region near the original signals of the *trans,trans*-isomer **8.5(E,E)** protons. From the HPLC monitoring of the isomerisation, a peak believed to correspond to the *trans,cis*-isomer **8.5(E,Z)** appeared. The ^{1}H NMR spectrum of the *trans,cis*-isomer **8.5(E,Z)** was anticipated to show double the number of signals due to the lack of symmetry related to the two different stilbenes. The number of signals observed in the spectrum also implies the formation of the *trans,cis*-isomer **8.5(E,Z)**.

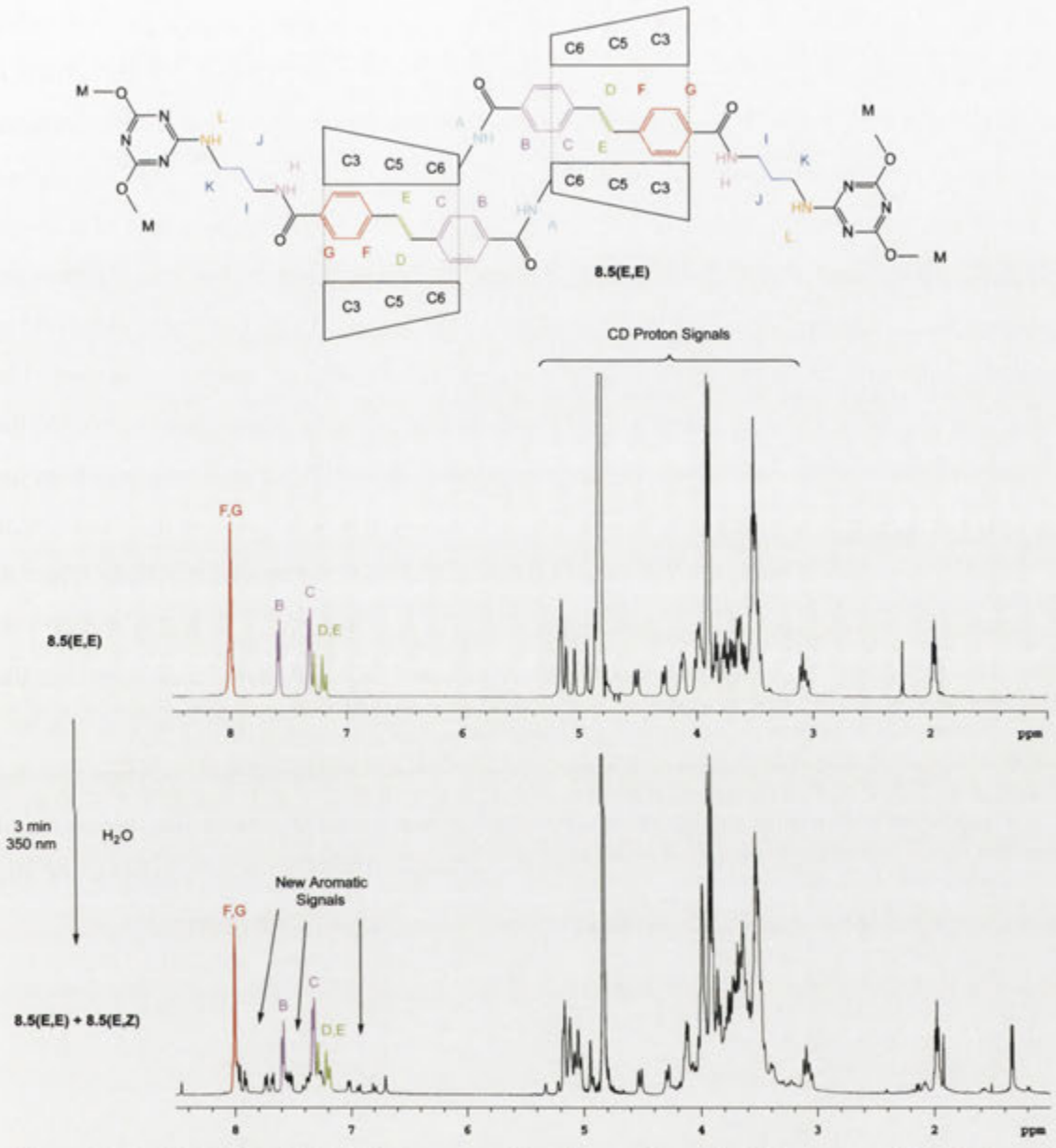

Figure 8.15. 500 MHz ^{1}H NMR spectra of the hermaphroditic [2]-rotaxane **8.5(E,E)** and an isomerisation mixture of the *trans,trans*-isomer **8.5(E,E)** and the *trans,cis*-isomer **8.5(E,Z)** in D_2O at 25 °C.

The signals of the *trans,cis*-isomer **8.5(E,Z)** were assigned using the DQCOSY and ROESY contour plots shown in Figures 8.16 and 8.17. As shown in the figures the signals are differentiated according to which stilbene unit they belong to and whether they are olefinic or aromatic signals. The signals belonging to the protons of the previously assigned *trans,trans*-isomer **8.5(E,E)** are shown as the blue signals. The

purple signals are identifiable as belonging to the protons of a *cis*-stilbene. The two olefinic signals 2-O at 6.79 ppm and 6.94 ppm were identified through their coupling constants. The two olefinic signals 2-O have a coupling constant of 12 Hz which is characteristic of a *cis*-alkene bond. The signals coloured green belong to a *trans*-stilbene and were identified by locating one of the signals of the olefinic protons 3-O. The signals of the olefinic protons 3-O have a coupling constant of 16 Hz characteristic of a *trans*-alkene bond. The fourth stilbene unit in red was able to be assigned but its conformation was not determined. The signal of the protons 4-O arises as a singlet and was identified as olefinic through its interactions with the signals of two sets of aromatic protons. The olefinic protons 4-O are likely to be *cis* orientated as Cieslinski[80] previously identified the signal of the olefinic protons of the hermaphroditic CD **5.2(Z)** to be a singlet. From the ^{1}H NMR spectrum the signals of the green *trans*-stilbene and the purple *cis*-stilbene protons integrate 1:1 and must therefore belong to the *trans,cis*-isomer **8.5(E,Z)**. The full structure is of the *cis*-stilbene unit coloured red is unknown but is probably the *cis,cis*-isomer **8.5(Z,Z)**. The formation of the *cis,cis*-isomer **8.5(Z,Z)** would account for the observation of only one set of stilbene proton signals due to the symmetry of that species.

After analysing the 2D NMR spectra of the isomerisation mixture of the hermaphroditic [2]-rotaxane **8.5(E,E)**, the signals were thus assigned for three sets of stilbenes. It was impractical, however, to determine the exact conformations of the isomers **8.5(E,Z)** and **8.5(Z,Z)** due to their low concentration in the mixture.

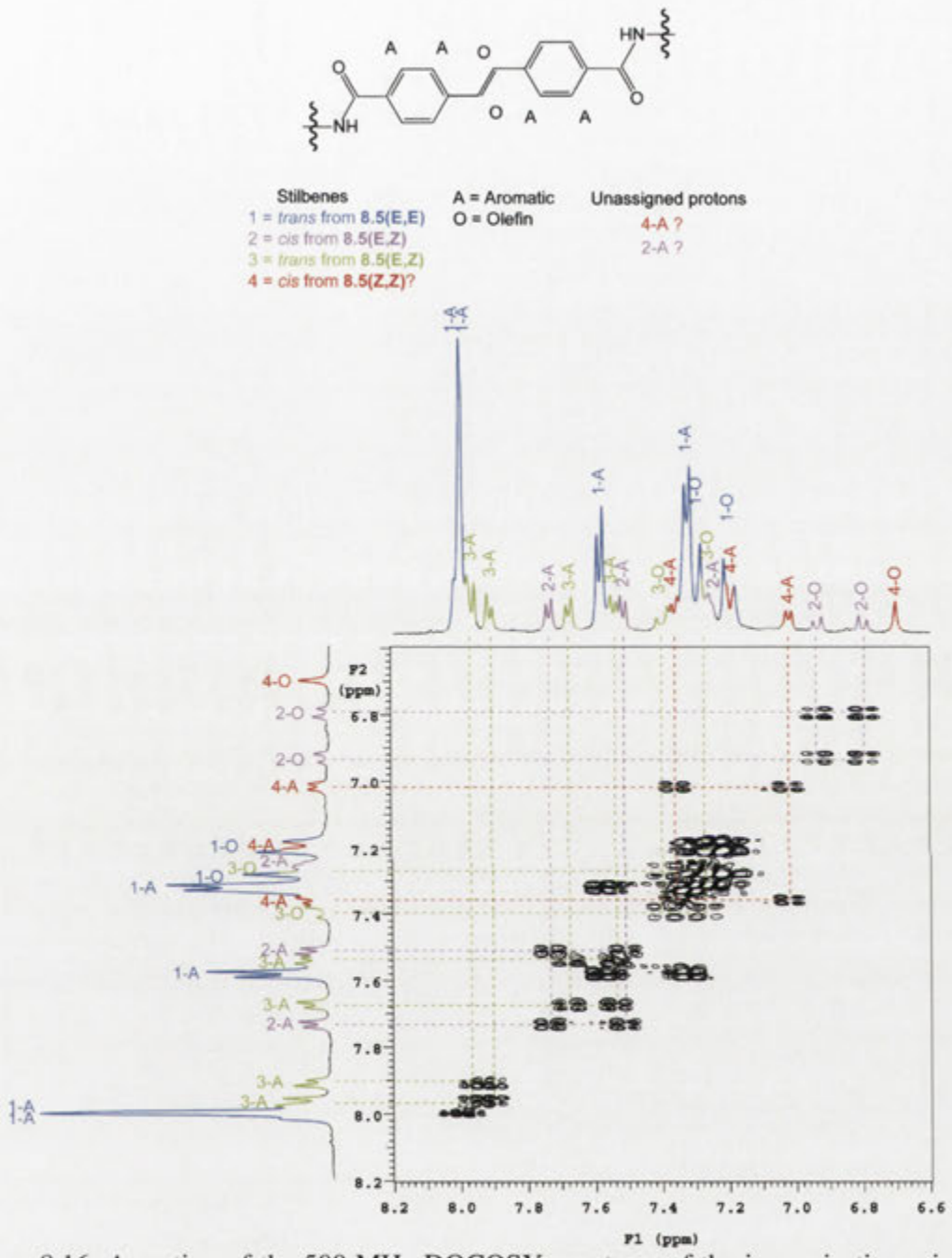

Figure 8.16. A section of the 500 MHz DQCOSY spectrum of the isomerisation mixture of the *trans,trans*-isomer **8.5(E,E)** in D_2O at 25 °C of the region where crosspeaks are observed between aromatic proton signals.

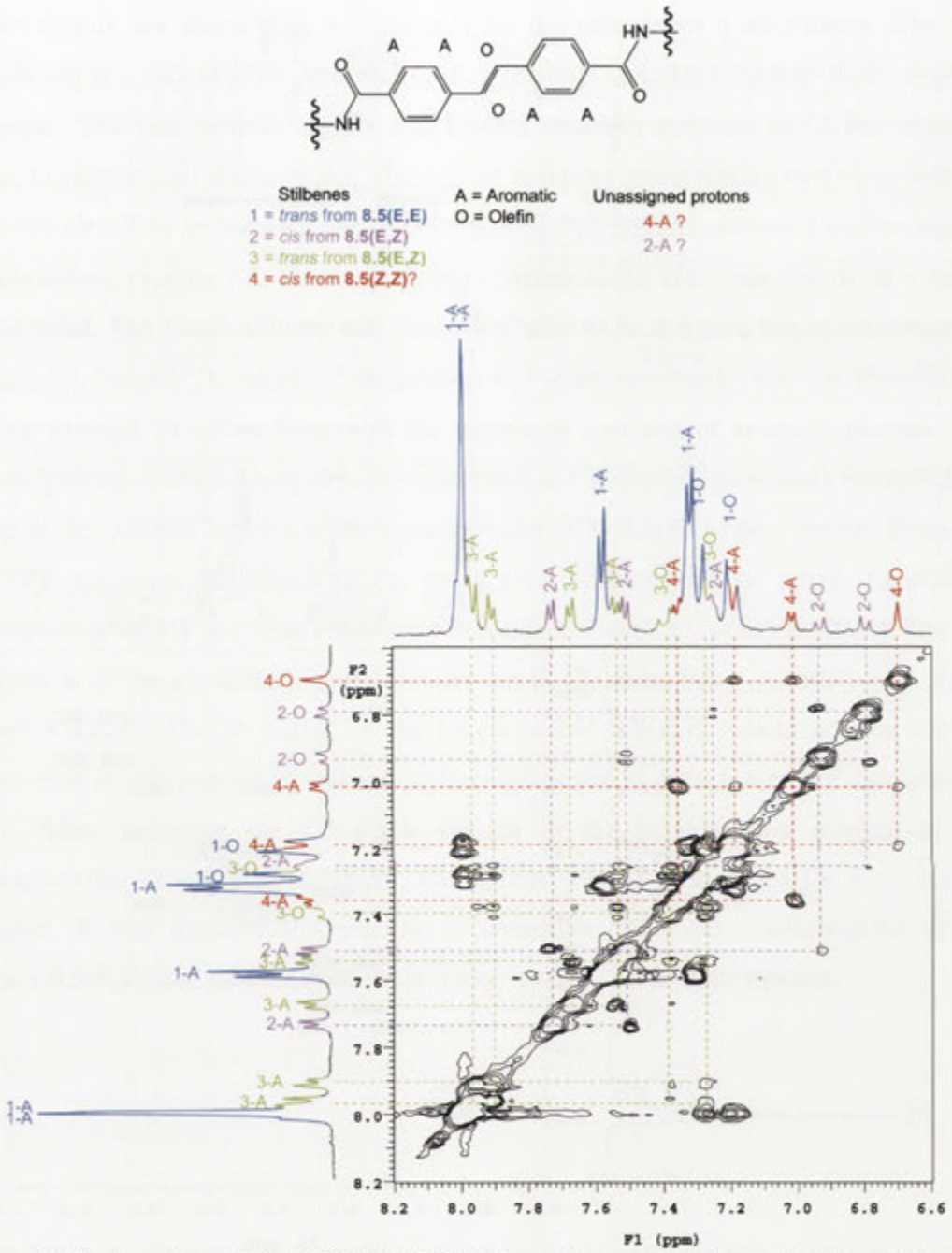

Figure 8.17. A section of the 500 MHz ROESY spectrum of the isomerisation mixture of the *trans,trans*-isomer **8.5(E,E)** in D_2O at 25 °C of the region where crosspeaks are observed between aromatic proton signals.

In conclusion, the hermaphroditic [2]-rotaxane **8.5(E,E)** was synthesised using the triazine-based blocking reagent **6.9**. The CD resides over the stilbene unit of each of the monomers to form a cyclic dimer. The structure of the hermaphroditic [2]-rotaxane **8.5(E,E)** after 2D NMR assignment is shown in Figure 8.10. After irradiation of the

hermaphroditic [2]-rotaxane **8.5(E,E)** with 350 nm light, the *trans,cis*-isomer **8.5(E,Z)** formed. Irradiation for a longer period of time formed the *cis,cis*-isomer **8.5(Z,Z)**. In the isomerisation of the [2]-rotaxanes **7.1** and **7.2** to their *cis*-isomers **7.1(Z)** and **7.2(Z)**, the CD shuttled from their stilbene units. It is therefore very likely that the formation of *cis*-stilbenes of the hermaphroditic [2]-rotaxane **8.5(Z,Z)** causes the CDs to shuttle to the alkyl chain but this has not been unambiguously determined. The irradiation of the isomer mixture with 254 nm light reformed the hermaphroditic [2]-rotaxane **8.5(E,E)**. In viewing the structures of the isomers of the hermaphroditic [2]-rotaxanes **8.5(E,E)**, **8.5(E,Z)** and **8.5(Z,Z)** shown in Scheme 8.3, the length of the molecule likely contracts upon the isomerisation of the stilbene units. This system could therefore be viewed as photochemically reversible molecular muscle.

Chapter 9: Conclusions and Future Directions

From the work described in this thesis, various structures have been made using CDs and stilbene units. Through the isomerisation of these stilbene units these structures have been shown to introduce function in what can be seen as CD based molecular devices. The isomerisation of the stilbene of the hermaphroditic CD **5.5(E)** was shown to alter its transport capabilities with the organic dye **5.8**. Also, the ditopic CD [2]-rotaxanes **7.1**, **7.2**, **7.6** and **7.7** and the hermaphroditic CD [2]-rotaxane **8.5(E,E)** were constructed. Upon the isomerisation of their stilbene units the CDs were propelled to other parts of the molecule. The [2]-rotaxanes **7.1**, **7.2**, **7.6** and **7.7** can be viewed as molecular shuttles while the hermaphroditic CD [2]-rotaxane **8.5(E,E)** can be viewed as a molecular muscle. It can therefore be concluded that the use of CDs in conjunction with stilbene units can provide the basis of a variety of molecular devices.

As a result of the research conducted there are many future directions possible for the continuation of this project. In Chapter 6, the synthesis of the [2]-rotaxanes **6.7** and **6.8** was described and entailed the use of triazine groups. The synthesis of the [2]-rotaxanes **6.7** and **6.8** was achieved in a two step procedure. The first step formed the [2]-rotaxane **6.7** before reaction with the amine **6.4** to form the [2]-rotaxane **6.8**. A different reactive group could be attached to the [2]-rotaxane **6.7** in the formation of CD [2]-rotaxane polymers.

In Chapter 5, the acetamides **5.5(E)** and **5.5(Z)** were able to transport the dye **5.8** along an HPLC column. The *cis*-isomer **5.5(Z)**, however, was more efficient in the transport of the dye **5.8**. The isomerisation of the *trans*-isomer **5.5(E)** to the *cis*-isomer **5.5(Z)** had fulfilled the purpose of a machine to do work for the transport of the dye **5.8** through a HPLC column. From Chapter 7, the isomerisation of the stilbenes of the [2]-rotaxanes **7.1**, **7.2**, **7.6** and **7.7** caused the CD to shuttle from the stilbene unit. By attaching the CD and one of the blocking groups to external objects as shown in Scheme 9.1, the energy of the movement may be harnessed.

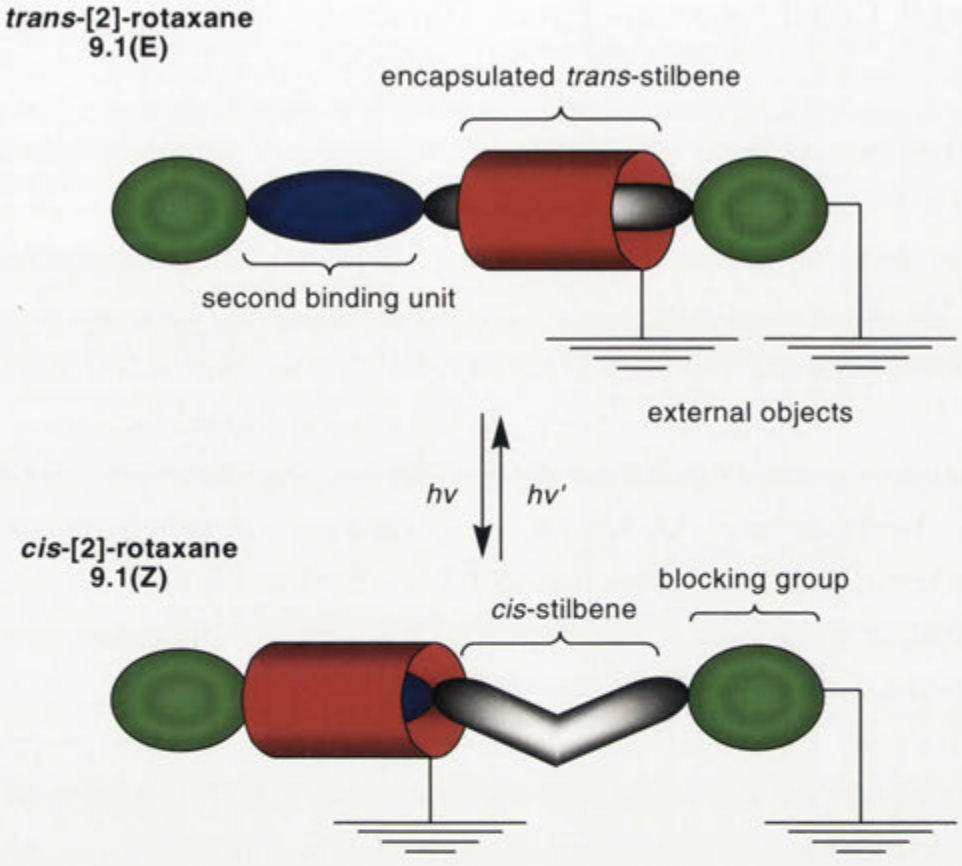

Scheme 9.1. Expected photochemical isomerisation of the stilbene unit of a *trans*-stilbene based [2]-rotaxane **9.1(E)** to produce its *cis*-isomer **9.1(Z)** that would cause the cyclodextrin to shuttle to the second cyclodextrin binding unit. The CD and one of the blocking groups are attached to external objects.

In Chapter 8, the stilbenes of the hermaphroditic CD [2]-rotaxane **8.5(E,E)** were isomerised to form the *cis,cis*-isomer **8.5(Z,Z)**. The change in conformation of the stilbene units would cause the overall length of the molecule to contract in what can be seen as a molecular muscle. If each of the blocking groups was attached to an external object as shown in Scheme 9.2, the energy of the movement may be harnessed. If the two step triazine blocking strategy was used as it was done in the formation of the [2]-rotaxane **6.8**, hermaphroditic [2]-rotaxane polymers may be formed. These polymers would be photochemically contractable and extendable.

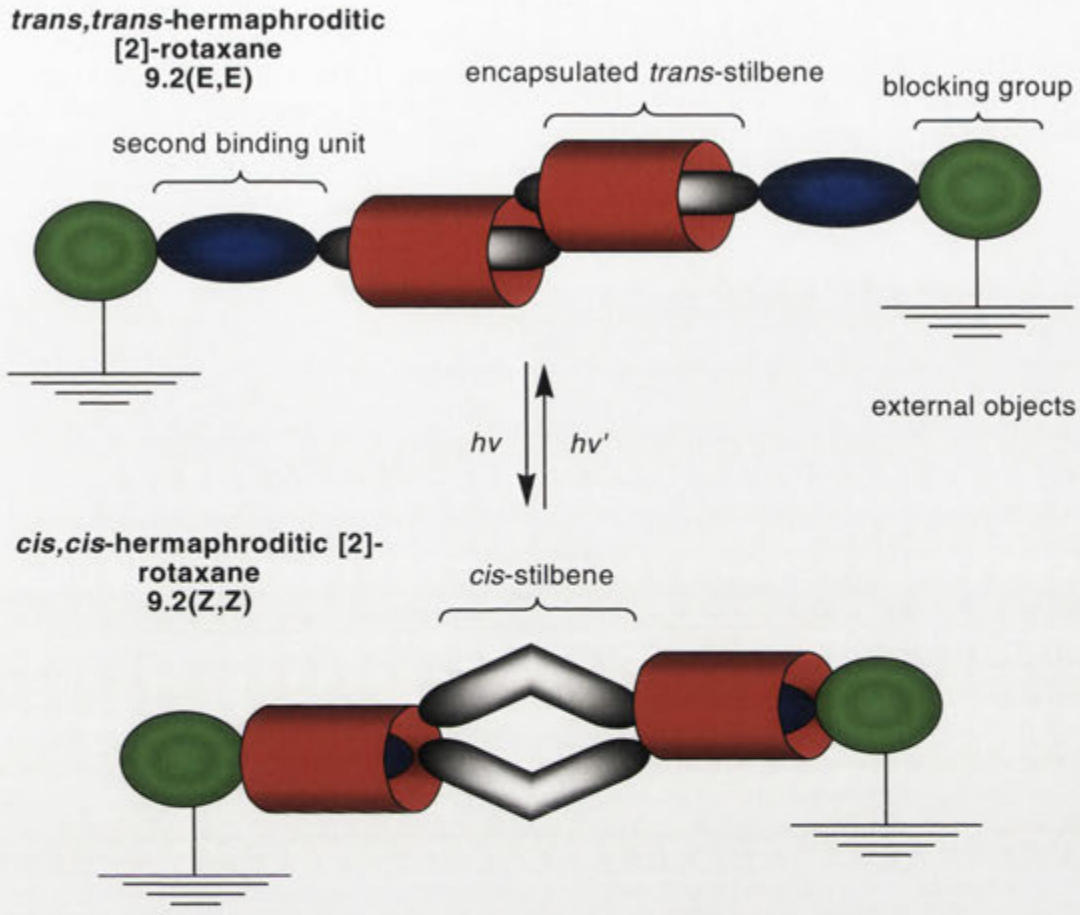

Scheme 9.2. Expected photochemical isomerisation of the stilbene units of the *trans,trans*-hermaphroditic [2]-rotaxane **9.2(E,E)** to produce its *cis,cis*-isomer **9.2(Z,Z)** that would cause the cyclodextrins to shuttle to the second cyclodextrin binding units. The CD and one of the blocking groups are attached to external objects.

Chapter 10: Experimental

General

^{1}H NMR spectroscopy and 2D NMR spectroscopy were conducted using a Varian Mercury 300 spectrometer operating at 300 MHz, a Varian Inova 300 spectrometer operating at 300 MHz, a Varian Inova 500 spectrometer operating at 500 MHz, or a Varian Inova 600 spectrometer operating at 600 MHz. ^{13}C NMR was conducted on either a Varian Mercury 300 spectrometer operating at 75 MHz, a Varian Inova 300 spectrometer operating at 75 MHz, or a Varian Inova 500 spectrometer operating at 125 MHz. The δ_H and δ_C values are reported in parts per million (ppm), while the J values are given in hertz (Hz). d_4-Methanol with an isotopic purity of 99.8% was purchased from Apollo Scientific LTD. D_2O with an isotopic purity of 99.75% and d_6-DMSO with an isotopic purity of 99.8% was purchased from Cambridge Isotope Laboratories Inc. d_4-Methanol was referenced at δ = 3.31 for ^{1}H and 39.5 for ^{13}C NMR spectroscopy. d_6-DMSO was referenced at δ= 2.50 for ^{1}H and 49.5 for ^{13}C NMR spectroscopy. When D_2O was used, 3-(trimethylsilyl)-3,3,2,2-tetradeuteropropionic acid sodium salt (d_4-TSP) was used as an external standard.

Low and high resolution electron impact (EI) mass spectra were determined using a Micromass VG AutoSpec M mass spectrometer. Low resolution electrospray ionisation (ESI) mass spectrometry was conducted using a Micromass-Waters LC-ZMD single quadrupole liquid chromatograph mass spectrometer. High resolution ESI mass spectrometry was carried out on a Bruker Apex 4.7T FTICR mass spectrometer. Matrix-assisted laser desorption-ionisation time-of-flight (MALDI-TOF) mass spectrometry was conducted on a Bruker OmniFlex instrument. Mass spectral data are reported as a mass-to-charge ratio (m/z).

Elemental analyses were performed by the Australian National University microanalytical service based at the Research School of Chemistry.

Thin layer chromatography (TLC) was carried out using aluminium backed 0.2 mm thick silica gel 60 F254 plates purchased from Merck. The mobile phases used

included *n*-butanol-ethanol-water (5:4:3 v/v/v) or *i*-propanol-ethanol-water-acetic acid (5:4:3:2 v/v/v/v). TLC plates were visualised with a 254 nm UV lamp and by treatment with a naphthalene-1,3-diol solution (0.1% w/v) in ethanol:water:H_2SO_4 (200:157:43 v/v/v). The R_f values are reported relative to the solvent front, αCD (**1.15**) or the starting material.

Analytical and semi-preparative high performance liquid chromatography (HPLC) was performed with a Waters 2695 Separation Module with a Waters 2996 Photodiode Array Detector running with Empower Pro Empower 2 software. Semi-preparative and preparative HPLC was performed with a Waters 600 Controller with a Waters 717 plus Autosampler and a Waters 2996 Photodiode Array Detector running with Empower Pro Empower 2 software. All separations were collected with a Waters Fraction Collector III.

UV/visible studies were conducted using a Shimadzu UV-2450 UV/visible spectrophotometer with a Shimadzu CPS-temperature controller running with UV Probe Version 2.10 software.

A Luzchem photoreactor was used to irradiate samples in conjunction with UV-A fluorescent lamps (for 350 nm irradiation) and UV-C fluorescent lamps (for 254 nm irradiation). A 400-1000W Oriel Research Arc Lamp with a 1000W Hg(Xe) OF source and a 370 nm Oriel filter was also used to irradiate samples.

Melting points were determined using a Reichert hot-stage microscope and were not corrected.

αCD (**1.15**) was acquired from the Nihon Shokuhin Kako Co. Japan in 99.1% purity and was dried over P_2O_5 under reduced pressure to constant weight. The Diaion HP-20 resin was purchased from Supelco, PA. All other starting materials, solvents and reagents were purchased from Aldrich, Ajax, Auspep, BDH, Fluka, Labscan, Lancaster, Merck or Unilab. HPLC solvents were purchased from J. T. Baker and MilliQ H_2O was purified using either a MilliQ reagent system or an ELGA system.

Experimental for Chapter 2

4-(*N*-(tert-Butoxycarbonyl)amino)phenylacetic acid (2.9)

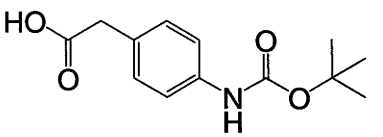

2.9

Method: From the amino acid **2.8** (1.000 g, 6.62 mmol), the carbamate **2.9** was produced according to the reaction conditions stated by Gibbs *et al.*,[69] and worked up according to the procedure of Jacobson *et al.*,[70] to produce a colourless powder. The crude material was used in the following reaction without further purification. For characterisation purposes a small portion of the crude material was recrystallised from EtOH/0.1% aq. citric acid to form colourless needles.

Yield: 1.102 g, 66%.

Melting point: 155-158 °C, lit.[69-72] 141.5-142.5, 153-154, 197-198 °C.

Mass spectrum: m/z (EI) 251.1 ($M^{+\cdot}$).

^{1}H NMR: δ_H(300 MHz; d_6-DMSO) 12.25 (1 H, s, COOH), 9.29 (1 H, s, ArNHCO), 7.37 (2 H, d, *J* 8.4, CH=CH), 7.12 (2 H, d, *J* 8.4, CH=CH), 3.46 (2 H, s, $COCH_2Ar$), 1.47 (9 H, s, $C(CH_3)_3$).

(*E*)-(4-(*N*-(tert-Butoxycarbonyl)amino)phenylacetamido)-4'-aminostilbene (2.10)

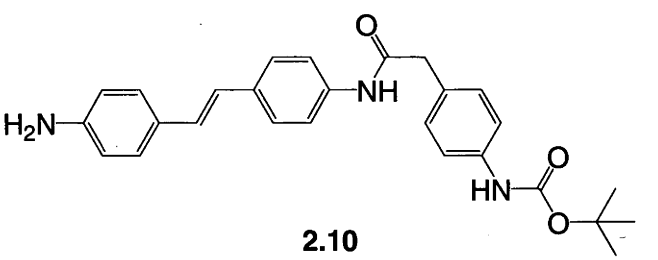

2.10

Method: Under an atmosphere of nitrogen, the carbamate **2.9** (0.500 g, 1.99 mmol), the stilbene **1.30** (1.255 g, 5.97 mmol) and BOP (1.319 g, 2.58 mmol) were dissolved in

anhydrous DMF (10 cm^3). TEA (1 cm^3, 7.17 mmol) was then added and the mixture was stirred for two days. The reaction mixture was then subjected to preparative HPLC with the desired fractions combined and concentrated under reduced pressure. The residue was then recrystallised from aqueous ethanol to give the carbamate **2.10** as a light brown powder.

Yield: 0.385 g, 44%.

Melting point: 203-205 °C.

Mass spectrum: m/z (ESI) 444.0 (M^+ + H).

^{1}H NMR: δ_H(500 MHz; d_4-methanol) 7.51 (2 H, d, *J* 8.0, CH=CH), 7.42 (2 H, d, *J* 8.0, CH=CH), 7.36 (2 H, d, *J* 8.0, CH=CH), 7.29 (2 H, d, *J* 8.0, CH=CH), 7.26 (2 H, d, *J* 8.0, CH=CH), 6.98 (1 H, d, *J* 16.0, CH=CH), 6.87 (1 H, d, *J* 16.0, CH=CH), 6.69 (2 H, d, *J* 8.0, CH=CH), 3.61 (2 H, s, $COCH_2Ar$), 1.51 (9 H, s, $C(CH_3)_3$).

^{13}C NMR: δ_C(125 MHz; d_4-methanol) 173.3, 156.2, 149.6, 140.3, 139.3, 136.6, 131.8, 131.3, 130.2, 129.8, 129.4, 128.2, 125.7, 122.2, 120.8, 117.3, 44.9 and 29.6.

Elemental analysis: Found: C, 72.87; H, 6.20; N, 9.57. $C_{27}H_{29}N_3O_3$ requires C, 73.11; H, 6.59; N, 9.47%.

HPLC: t_R 14.2 min (column: YMC-PACK ODS-AQ, 250 × 20 mm with YMC-Guardpack ODS-AQ, 50 × 20 mm; H_2O/MeCN gradient).

Time (min)	Flow (cm^3min^{-1})	H_2O (%)	MeCN (%)
0	10	50	50
15	10	0	100
17	10	0	100
18	10	50	50
20	10	50	50

(*E*)-4-(4-Aminophenylacetamido)-4'-aminostilbene (2.11)

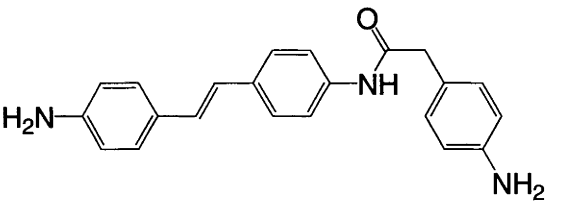

2.11

Method: To a stirring suspension of the carbamate **2.10** (0.300 g, 0.68 mmol) in DCM (50 cm^3), TFA (2 cm^3, 25.9 mmol) was added drop wise to produce a dark red solution. After 4 hours the solvent was removed and the residue suspended in water (100 cm^3). The suspension was washed with diethyl ether (30 cm^3) before being adjusted to pH 12 with 5 M NaOH to produce a yellow precipitate. The mixture was extracted with EtOAc (4 × 100 cm^3), dried over anhydrous $MgSO_4$ and concentrated under reduced pressure to afford the diamine **2.11** as a yellow powder which was carried over into the next procedure without further purification.

Yield: 0.203 g, 87%.

Melting Point: 189-191 °C.

Mass spectrum: m/z (HI-RES EI) Found: 343.1687 ($M^{+\cdot}$. $C_{22}H_{21}N_3O$). Calculated: 343.1685.

^{1}H NMR: δ_H(300 MHz; d_6-DMSO) 7.55 (2 H, d, *J* 8.4, CH=CH), 7.41 (2 H, d, *J* 8.4, CH=CH), 7.24 (2 H, d, *J* 8.4, CH=CH), 6.97 (2 H, d, *J* 8.4, CH=CH), 6.90 (1 H, d, *J* 16.5, CH=CH), 6.81 (1 H, d, *J* 16.5, CH=CH), 6.54 (2 H, d, *J* 8.4, CH=CH), 6.50 (2 H, d, *J* 8.4, CH=CH), 5.26 (2 H, s, $ArNH_2$), 4.93 (2 H, s, $ArNH_2$), 3.40 (2 H, s, $COCH_2Ar$).

^{13}C NMR: δ_C(125 MHz; d_6-DMSO) 169.8, 148.5, 147.2, 137.9, 132.9, 129.5, 127.7, 127.4, 126.0, 124.9, 122.8, 122.4, 119.1, 113.9, 42.7 and 28.1.

[(*E*)-4-(4-(2,4,6-trinitrophenylamino)phenylacetamido)-4'-(2,4,6-trinitrophenylamino)stilbene]-[α-cyclodextrin]-[2]-[rotaxanes] (2.12 and 2.13)

Method: The diamine **2.11** and αCD (**1.15**) ~~was~~ were suspended in a 0.2 M carbonate buffer (pH 10.0, 200 cm^3) and stirred at room temperature for 24 hours. The trinitrophenyl

blocking reagent **1.31** was added and the reaction mixture was stirred for three days. The reaction mixture was then washed with diethyl ether (100 cm^3) and filtered. The filtrate was applied to a Diaion HP-20 column (300 mm × 20 mm). The column was flushed with MQ H_2O until no unreacted αCD (**1.15**) was detected by TLC. The column was then flushed with methanol until all of the reacted αCD (**1.15**) was removed as detected by TLC. The solvent was removed under pressure and the crude product was dissolved in DMF and subjected to preparative reverse-phase HPLC. Fractions containing the [2]-rotaxanes **2.12** and **2.13** were isolated and lyophilised as red powders.

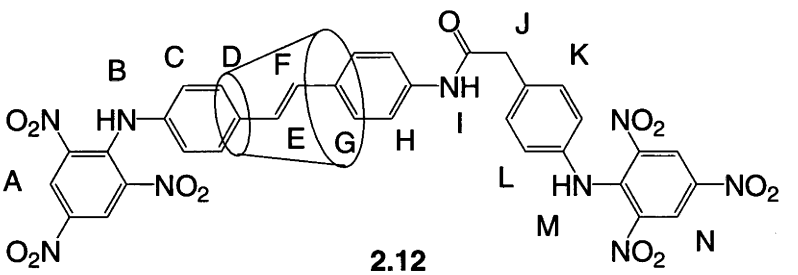

2.12

Yield: 0.023 g, 2.2%.

TLC: (5:4:3 v/v/v *n*-butanol-ethanol-water) R_f 0.72 (relative to the solvent front), 1.64 (relative to αCD (**1.15**)).

Melting point: 296 °C (dec.).

Mass spectrum: m/z (ESI) 1736.4 (M^-).

^{1}H NMR: δ_H(500 MHz; d_6-DMSO) 10.22 (1 H, s, **I**), 8.88 (4 H, s, **A** and **N**), 7.73 (2 H, d, *J* 8.0, **G**), 7.61 (2 H, d, *J* 8.0, **H**), 7.30 (2 H, d, *J* 8.0, **K**), 7.12-7.04 (6 H, m, **C**, **D** and **L**), 7.01 (1 H, d, *J* 16.0, **F**), 6.81 (1 H, d, *J* 16.0, **E**), 5.47-5.42 (6 H, m, CD-OH2), 5.27 (6 H, s, CD-OH3), 4.76-4.72 (6 H, m, CD-H1), 4.37-4.33 (6 H, m, CD-OH6), 3.69 (2 H, s, **J**), 3.68-3.60 (12 H, m, CD-H5 and CD-H3), 3.60-3.54 (6 H, m, CD-$H6^{A,B}$), 3.48-3.42 (6 H, m, CD-H4), 3.40-3.30 (6 H, m, CD-$H6^{A,B}$), 3.24-3.18 (6 H, m, CD-H2).

^{13}C NMR: δ_C(125 MHz; d_6-DMSO) 168.9, 137.0-139.0 (br), 130.2, 127.6, 126.5-127.5 (br), 126.0, 120.0-121.0 (br), 119.1, 111.4, 102.1, 81.7, 73.2, 72.1, 71.8, 59.1 and 42.5.

Elemental analysis: (Found: C, 42.64; H, 5.45; N, 6.55. $C_{70}H_{83}N_9O_{43}.13H_2O$ requires C, 42.62; H, 5.57; N, 6.39%).

HPLC: t_R 45.9 min (column: YMC-PACK ODS-AQ, 250 × 20 mm; 25% aq. MeCN; flow rate: 10.0 cm^3min^{-1}).

UV/visible spectrum: λ_{max} = 230 nm, ε_{230} = 38660.5 $M^{-1}cm^{-1}$; λ_{max} = 337.5 nm, $\varepsilon_{337.5}$ = 34769.7 $M^{-1}cm^{-1}$; λ_{max} = 392.5 nm, $\varepsilon_{392.5}$ = 32286.1 $M^{-1}cm^{-1}$.

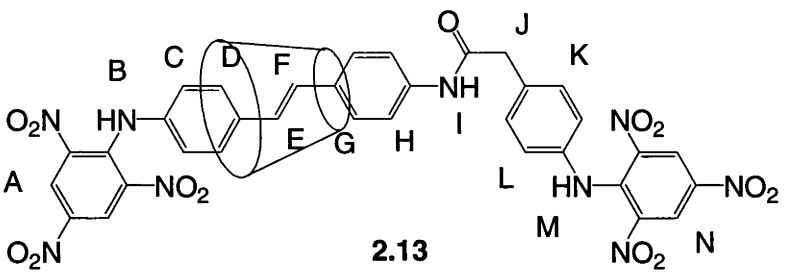

2.13

Yield: 0.021 g, 2.1%.

TLC: (5:4:3 v/v/v *n*-butanol-ethanol-water) R_f 0.71 (relative to the solvent front), 1.61 (relative to αCD (**1.15**)).

Melting point: 294 °C (dec.).

Mass spectrum: m/z (HI-RES ESI) Found: 1760.4464 (M^+ + Na. $C_{70}H_{83}N_9O_{35}$). Calculated: 1760.4482.

^{1}H NMR: δ_H(500 MHz; d_6-DMSO) 10.24 (1 H, s, **I**), 8.94 (4 H, m, **A** and **N**), 7.76-7.68 (2 H, m, **D**), 7.60 (2 H, d, *J* 7.5, **H**), 7.27 (2 H, d, *J* 7.5, **K**), 7.20-7.12 (4 H, m, **C** and **G**), 7.10-7.04 (2 H, m, **L**), 6.97 (1 H, d, *J* 16.0, **E**), 6.88 (1 H, d, *J* 16.0, **F**), 5.22-5.18 (6 H, m, CD-OH2), 5.18-5.14 (6 H, m, CD-OH3), 4.77-4.74 (6 H, m, CD-H1), 4.44-4.38 (6 H, m, CD-OH6), 3.70-3.64 (14 H, m, **J**, CD-H3 and CD-H5), 3.58-3.52 (6 H, m, CD-H6^{A,B}), 3.47-3.42 (6 H, m, CD-H4), 3.28-3.18 (6 H, m, CD-H6^{A,B} and CD-H2).

^{13}C NMR: δ_C(125 MHz; d_6-DMSO) 138.0-139.0 (br), 130.2, 126.0-128.0 (br), 120.0-121.0 (br), 118.5, 111.4, 102.1, 81.5, 73.2, 72.3, 71.7, 59.2 and 42.3.

Elemental analysis: (Found: C, 43.69; H, 5.26; N, 6.32. $C_{70}H_{83}N_9O_{35}.10H_2O$ requires C, 43.82; H, 5.41; N, 6.57%).

HPLC: t_R 48.8 min (column: YMC-PACK ODS-AQ, 250 × 20 mm; 25% aq. MeCN; flow rate: 10.0 cm^3min^{-1}).

UV/visible spectrum: λ_{max} = 231 nm, ε_{231} = 26056.3 $M^{-1}cm^{-1}$; λ_{max} = 337.5 nm, $\varepsilon_{337.5}$ = 13782.6 $M^{-1}cm^{-1}$; λ_{max} = 394 nm, ε_{394} = 23151.4 $M^{-1}cm^{-1}$.

Experimental for Chapter 3

Attempted Photochemical Isomerisation of the [2]-rotaxanes 2.12 and 2.13

The [2]-rotaxane **2.12** (0.0021 g, 0.0012 mmol) was made up to a concentration of 2.42×10^{-5} M in MQ H_2O (50 cm^3). The [2]-rotaxane **2.13** (0.00079 g, 0.00045 mmol) was made up to a concentration of 2.27×10^{-5} M in MQ H_2O (20 cm^3). The [2]-rotaxanes **2.12** and **2.13** were analysed for their molar responses using analytical reverse-phase HPLC for a 10 µl injection. Their absorbance was analysed using a UV/visible spectrophotometer. 3 cm^3 aliquots of the solutions were then sealed in a 10 mm i.d. quartz tube and irradiated with ten 350 nm UV-A lamps for 24 hours in a photolysis reactor. At time periods during the irradiation, an aliquot of the solutions ~~were~~ was subjected to HPLC while the UV/visible spectra were once again recorded. The solution was then sealed and irradiated with ten 254 nm UV-C lamps for 15 minutes. The UV/visible spectra of the solutions were recorded and an aliquot of the solutions ~~were~~ was subjected to HPLC.

Attempted Acid-Base Controlled Shuttling of the [2]-rotaxane 2.12

The [2]-rotaxane **2.12** (0.0055 g, 0.0032 mmol) was made up to a concentration of 6.33×10^{-3} M in d_4-methanol (0.5 cm^3) in an NMR spectroscopy tube. The solution was then adjusted to a pD of 3.6 with 0.5 M DCl as determined using a micro combination pH electrode. A ^1H NMR experiment was then performed on the solution. The pD of the solution was then elevated by the addition of 0.5 M NaOD. At pDs of 5.5, 6.6, 7.2, 8.1, 9.9, 10.3, 10.9 and 11.3 the ^1H NMR spectrum was recorded for the solution.

(*E*)-*N*-(6^A-Deoxy-α-cyclodextrin-6^A-yl)aminocarbonyl-4-(3-propionamido)-4'-aminostilbene (3.7)

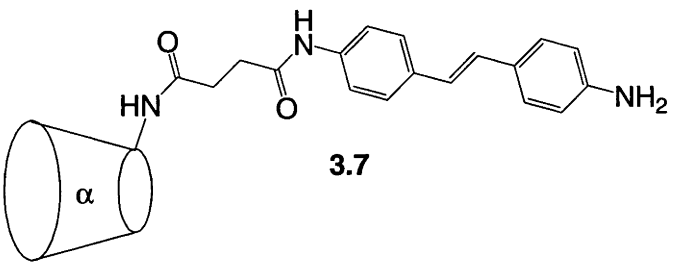

3.7

Method: Under an atmosphere of nitrogen, the succinic acid **3.6** (0.300 g, 0.279 mmol), the stilbene **1.30** (0.177 g, 0.839 mmol) and DMT-MM (0.232 g, 0.839 mmol) were dissolved in anhydrous DMF (5 cm^3). TEA (0.8 cm^3, 5.59 mmol) was then added and the mixture was stirred for two days. The reaction mixture was precipitated with acetone (20 cm^3). The precipitate was collected by centrifugation and resuspended in acetone (3 × 20 cm^3). The precipitate was recollected by centrifugation, dissolved in MQ H_2O (200 cm^3) and subjected to a Diaion HP-20 column (300 mm × 20 mm). The column was then flushed with MQ H_2O (1 dm^3). The column was then eluted with MQ H_2O-methanol gradient. The fractions (35-65% methanol) containing the hermaphroditic CD **3.7** were combined, concentrated under reduced pressure and lyophilised.

Yield: 0.181 g, 51%.

Mass spectrum: m/z (ESI) 1264.2 (M^+ + H).

Attempted synthesis of the [(*E*)-*N*-(6^A-Deoxy-α-cyclodextrin-6^A-yl)aminocarbonyl-4-(3-propionamido)-4'-(2,4,6-trinitrophenylamino)stilbene]-[c2]-[daisy chain] (3.9)

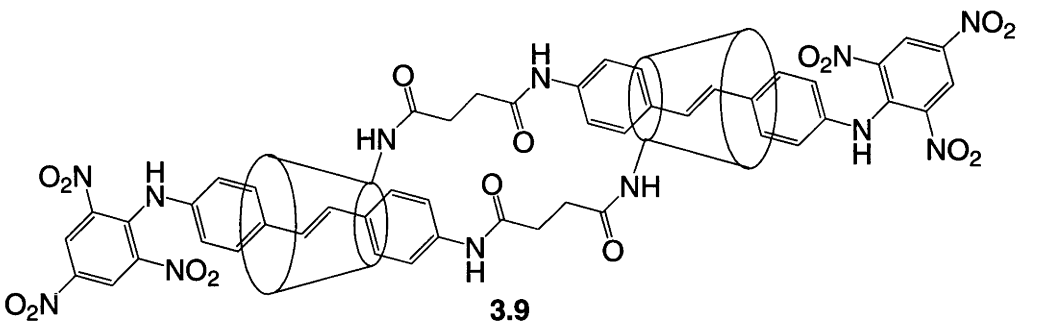

3.9

Method: The hermaphroditic CD **3.7** (0.181 g, 0.143 mmol) was suspended in a 0.2 M carbonate buffer (pH 10.0, 20 cm^3) and stirred at room temperature for 24 hours. The trinitrophenyl blocking reagent **1.31** was added and the reaction mixture was stirred for four days. The reaction mixture was then washed with diethyl ether (200 cm^3) and the aqueous layer was concentrated under reduced pressure. The red residue was dissolved in DMF and a trace amount of the hermaphroditic [2]-rotaxane **3.9** was obtained through semi-preparative reverse-phase HPLC.

Mass spectrum: m/z (MALDI) 2972.8 (M^+ + Na).

Experimental for Chapter 4

(*E*)-4,4'-Diacrylamidostilbene (4.2)

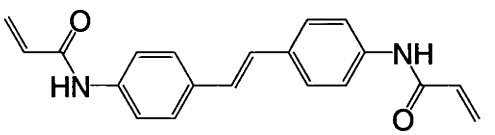

4.2

Method: To a stirring solution of the stilbene **1.30** (0.100 g, 0.476 mmol) in DMF (5 cm^3) and TEA (1 cm^3, 7.17 mmol), the acid chloride **4.1** (0.430 g, 4.751 mmol) was added. The reaction mixture was stirred for three days before being precipitated with acetone (100 cm^3). The resultant suspension was centrifuged and the supernatant was decanted and precipitated with H_2O (100 cm^3). The resultant suspension was subjected to centrifugation and the supernatant was discarded. The precipitation with H_2O and centrifugation was repeated a further two times. The residual solvent was removed *in vacuo* to give the title compound as a yellow powder.

Yield: 0.107 g, 71%.

Melting point: >300 °C.

Mass spectrum: m/z (HI-RES ESI) Found: 317.1296 ($(M - H)^-$. $C_{20}H_{18}N_2O_2$). Calculated: 317.1290.

^{1}H NMR: δ_H(300 MHz; d_6-DMSO) 10.23 (2 H, s, CONHAr), 7.68 (4 H, d, *J* 8.4, CH=CH), 7.54 (4 H, d, *J* 8.4, CH=CH), 7.12 (2 H, CH=CH), 6.45 (2 H, dd, *J* 17.1 and 9.9, $CH=CH_2$), 6.27 (2 H, dd, *J* 17.1 and 2.1, $CH=CH_2$), 5.76 (2 H, dd, *J* 9.9 and 2.1, $CH=CH_2$).

Attempted synthesis of the [(*E*)-4,4'-Bis(3-mesitylisoxazolin-5-ylamido)stilbene]-[α-cyclodextrin]-[2]-[rotaxane] (4.4)

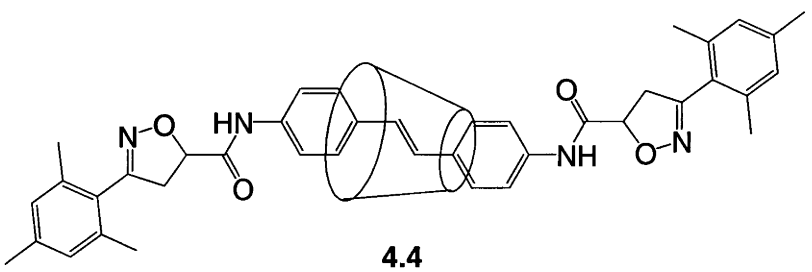

4.4

Method: The stilbene **4.2** (0.100 g, 0.314 mmol) was suspended in a solution of αCD (**1.15**) (1.527 g, 1.570 mmol) and MQ H_2O (100 cm^3) and stirred for 24 hours. The nitrile oxide **4.3** (0.111 g, 0.690 mmol) was then added to the suspension and the stirring was continued. After three days the precipitate was filtered and the filtrate was applied to a Diaion HP-20 column (300 mm × 20 mm). The column was flushed with MQ H_2O until no unreacted αCD (**1.15**) was detected by TLC. The column was then flushed with methanol until all of the remaining products on the column had been removed. The solvent was removed under pressure and the crude product was dissolved in DMF and subjected to preparative reverse-phase HPLC.

(*E*)-4-Amino-4'-(α-cyclodextrin-6^A-yl)stilbene (4.6)

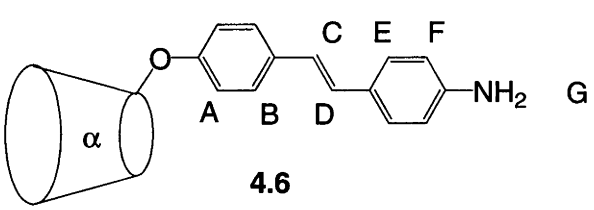

4.6

Method: The tosylate **1.19** (1.000 g, 0.877 mmol), 4-aminohydroxystilbene (0.563 g, 2.662 mmol) and potassium carbonate (1.226 g, 8.773 mmol) were dissolved in anhydrous DMF (30 cm^3) under an atmosphere of nitrogen. The reaction mixture was heated at 80 °C and stirred for 2 days. The reaction mixture was allowed to cool to room temperature and was precipitated with acetone (100 cm^3). The precipitate was collected

by centrifugation and resuspended in acetone (3 × 100 cm^3). The precipitate was recollected by centrifugation, dissolved in MQ H_2O and subjected to a Diaion HP-20 column (300 mm × 20 mm). The column was then flushed with MQ H_2O (1 dm^3). The column was then eluted with MQ H_2O-methanol gradient. The fractions (20-65% methanol) containing the hermaphroditic CD **4.6** were combined, concentrated under reduced pressure and lyophilised. The solid was dissolved in MQ H_2O/DMF and subjected to preparative reverse-phase HPLC. Fractions containing the title product **4.6** were isolated and lyophilised to give a light brown coloured powder.

Yield: 0.267 g, 26%.

TLC: (5:4:3 v/v/v *n*-butanol-ethanol-water) R_f 0.51 (relative to the solvent front), 1.00 (relative to αCD tosylate (**1.19**)).

Melting point: 267 °C (dec.).

Mass spectrum: m/z (HI-RES ESI) Found: 1166.4168 (M^+ + H. $C_{50}H_{71}NO_{30}$). Calculated: 1166.4139

^{1}H NMR: δ_H(500 MHz; D_2O) 7.67 (2 H, d, *J* 8.0, **E**), 7.19 (2 H, d, *J* 8.0, **B**), 7.01 (2 H, d, *J* 8.0, **F**), 6.91 (1 H, d, *J* 16.5, **D**), 6.74 (1 H, d, *J* 16.5, **C**), 6.68 (2 H, d, *J* 8.0, **A**), 4.91-5.15 (6 H, m, CD-H1), 3.25-4.35 (36 H, m, CD-H2, CD-H3, CD-H4, CD-H5, CD-$H6^{A,B}$).

HPLC: t_R 12.6 min (column: YMC-PACK ODS-AQ, 250 × 20 mm; 25% aq. MeCN; flow rate: 10.0 cm^3min^{-1}).

(*E*)-4-Acrylamido-4'-(α-cyclodextrin-6^A-yl)stilbene (4.7)

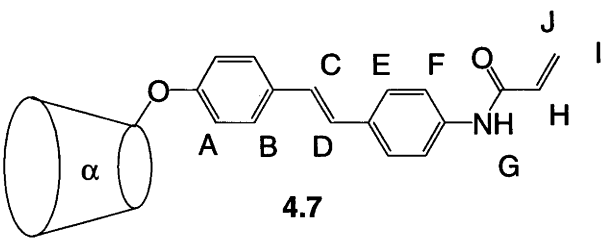

4.7

Method: To a stirring solution of the hermaphroditic CD **4.6** (0.267 g, 0.229 mmol) and TEA (0.717 g, 7.085 mmol) in MQ H_2O (25 cm^3), the acid chloride **4.1** (0.207 g, 2.285 mmol) was added. The reaction mixture was stirred for 16 hours then subjected to

preparative reverse-phase HPLC. Fractions containing the hermaphroditic CD **4.7** were isolated and lyophilised to give a colourless powder.

Yield: 0.232 g, 83%.

TLC: (5:4:3 v/v/v *n*-butanol-ethanol-water) R_f 0.61 (relative to the solvent front), 1.15 (relative to the hermaphroditic CD **4.6**).

Melting point: 232 °C (dec.).

Mass spectrum: m/z (HI-RES ESI) Found: 1242.4003 (M^+ + Na. $C_{53}H_{73}NO_{31}$). Calculated: 1242.4064.

^{1}H NMR: δ_H(500 MHz; D_2O) 7.69 (2 H, d, *J* 8.0, **E** or **F**), 7.62 (2 H, d, *J* 8.0, **E** or **F**), 7.08 (2 H, d, *J* 8.0, **B**), 6.84 (2 H, d, *J* 16.0, **C** or **D**), 6.77 (2 H, d, *J* 16.0, **C** or **D**), 6.56 (2 H, s, *J* 8.0, **A**), 6.34 (1 H, dd, *J* 10.0 and 17.0, **H**), 6.24 (1 H, apparent d, *J* 17.0, **J**), 5.76 (1 H, apparent d, *J* 10.0, **I**), 5.00-4.75 (6 H, CD-H1), 4.20-3.04 (36 H, CD-H2, CD-H3, CD-H4, CD-H5 and CD-H6^{A,B}).

^{13}C NMR: δ_C(125 MHz; d_6-DMSO) 163.0, 158.1, 138.1, 132.8, 131.9, 129.8, 127.5, 126.9, 126.6, 125.7, 119.4, 114.7, 102.2, 102.0, 101.8, 82.3, 82.1, 73.3, 72.1, 69.6, 66.7 and 60.0.

Elemental analysis: (Found: C, 47.64; H, 6.32; N, 0.92. $C_{53}H_{73}NO_{31}.6H_2O$ requires C, 47.93; H, 6.45; N, 1.05%).

HPLC: t_R 10.4 min (column: YMC-PACK ODS-AQ, 250 × 20 mm; 30% aq. MeCN; flow rate: 10.0 cm^3min^{-1}).

Attempted synthesis of the [(*E*)-4-(3-Mesitylisoxazolin-5-ylamido)-4'-(α-cyclodextrin-6^{A}-yl)stilbene]-[c2]-[daisy chain] (4.9)

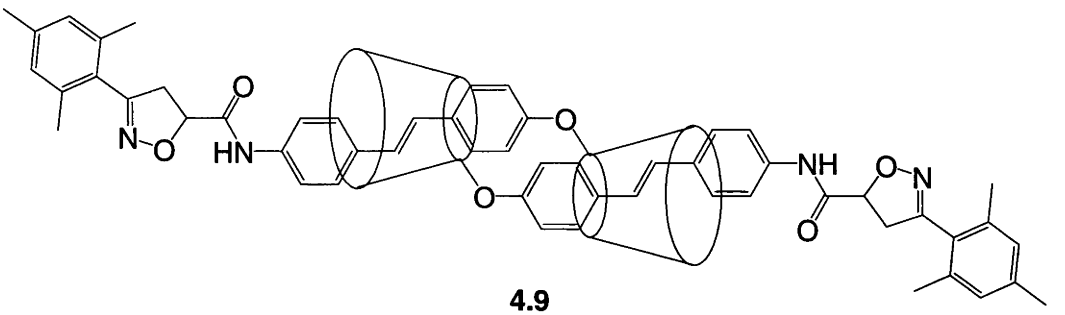

4.9

Method: The acrylamide **4.7** (0.100 g, 0.082 mmol) was dissolved in MQ H_2O (10 cm^3) and stirred for 24 hours. A solution of the nitrile oxide **4.3** (0.017 g, 0.172 mmol) in DMF (0.1 cm^3) was then added dropwise over several minutes to produce a white suspension and the stirring was continued. After six days the nitrile oxide **4.3** appeared by TLC to be completely consumed. A further amount of the nitrile oxide **4.3** (0.012 g, 0.074 mmol) dissolved in DMF (0.1 cm^3) was added dropwise to the reaction vessel and the suspension was stirred for another three days. After this time period there was none of the acrylamide **4.7** present in the suspension by TLC. DMF (5 cm^3) was added to the reaction to dissolve the white suspension and it was subjected to preparative reverse-phase HPLC.

Experimental for Chapter 5

(*E*)-4-Acetamido-4'-(α-cyclodextrin-6^{A}-yl)stilbene (5.5(E))

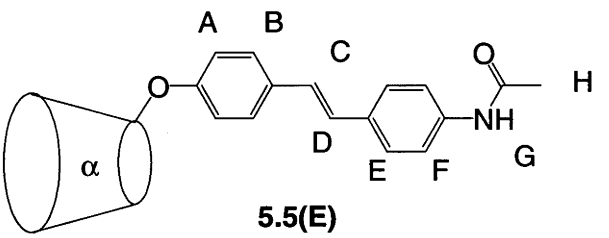

5.5(E)

Method: To a stirring solution of the hermaphroditic CD **4.6** (0.145 g, 0.124 mmol) and TEA (0.013 g, 0.248 mmol) in MQ H_2O (20 cm^3), the anhydride **5.4** (0.013 g, 0.248 mmol) was added. The reaction mixture was stirred for 3 days then subjected to semi-preparative reverse-phase HPLC. Fractions containing the hermaphroditic CD **5.5(E)** were combined and lyophilised to give a colourless powder.

Yield: 0.079 g, 53%.

TLC: (5:4:3 v/v/v *n*-butanol-ethanol-water) R_f 0.53 (relative to the solvent front), 1.50 (relative to αCD (**1.15**)).

Melting point: 245 °C (dec.).

Mass spectrum: m/z (ESI) 1208.1 (M^+ + H).

^{1}H NMR: δ_H(500 MHz; D_2O) 7.82 (2 H, d, *J* 8.0, **E**), 7.67 (2 H, d, *J* 8.0, **F**), 7.23 (2 H, d, *J* 8.0, **B**), 7.00 (1 H, d, *J* 16.0, **C** or **D**), 6.92 (1 H, d, *J* 16.0, **C** or **D**), 6.71 (2 H, d, *J* 8.0, **A**), 5.16-4.91 (6 H, CD-H1), 4.34-3.18 (36 H, CD-H2, CD-H3, CD-H4, CD-H5 and CD-H6^{A,B}), 2.22 (3 H, s, **H**).

^{13}C NMR: δ_C(125 MHz; D_2O) 175.7, 160.8, 140.2, 135.7, 131.3, 130.2, 129.8, 128.5, 124.0, 117.6, 105.3, 105.1, 104.5, 104.2, 85.3, 84.4, 84.3, 83.8, 83.4, 76.6, 76.5, 76.3, 76.2, 76.1, 75.8, 74.6, 72.7, 69.3, 63.1, 63.0, 62.5, 62.0 and 25.9.

Elemental analysis: (Found: C, 47.72; H, 6.37; N, 0.97. $C_{52}H_{73}NO_{31}.6H_2O$ requires C, 47.45; H, 6.51; N, 1.06%).

HPLC: t_R 22.8 min (column: YMC-PACK ODS-AQ, 250 × 10 mm; H_2O/MeCN gradient).

Time (min)	Flow (cm^3min^{-1})	H_2O (%)	MeCN (%)
0	3	90	10
25	3	65	35
26	3	90	10
30	3	90	10

UV/visible spectrum: λ_{max} = 233.5 nm, $\varepsilon_{233.5}$ = 9000 $M^{-1}cm^{-1}$; λ_{max} = 338 nm, ε_{338} = 27160 $M^{-1}cm^{-1}$.

(Z)-4-Acetamido-4'-(α-cyclodextrin-6^A-yl)stilbene (5.5(Z))

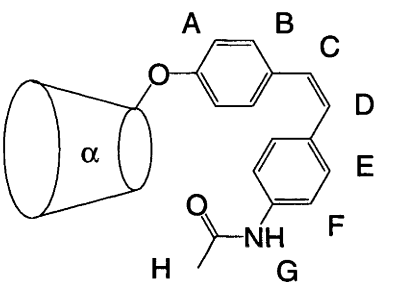

5.5(Z)

Method: The acetamide **5.5(E)** was dissolved in MQ H_2O (660 cm^3) and placed in a 1 dm^3 quartz round bottom flask. The mixture was then irradiated with light of wavelength 350 nm (10 lamps) for five minutes. The reaction mixture was then lyophilised, dissolved in 25% aqueous MeCN and subjected to semi-preparative reverse-phase HPLC. Fractions containing the acetamide **5.5(Z)** were combined and lyophilised to give a colourless powder.

Yield: 0.008 g, 40%.

TLC: (5:4:3 v/v/v *n*-butanol-ethanol-water) R_f 0.59 (relative to the solvent front), 1.69 (relative to αCD (**1.15**)).

Melting point: 244 °C (dec.).

Mass spectrum: m/z (HI-RES ESI) Found: 1208.4195 (M^+ + H, $C_{52}H_{73}NO_{31}$). Calculated: 1208.4244

^{1}H NMR: δ_H(500 MHz; D_2O) 7.28 (2 H, d, *J* 7.5, **E** or **F**), 7.24 (2 H, d, *J* 7.5, **E** or **F**), 7.20 (2 H, d, *J* 7.5, **B**), 6.83 (2 H, d, *J* 7.5, **C** or **D**), 6.59 (1 H, d, *J* 12.0, **C** or **D**), 6.55 (1 H, d, *J* 12.0, **C** or **D**), 5.10-5.00 (6 H, CD-H1), 4.38-3.55 (36 H, CD-H2, CD-H3, CD-H4, CD-H5 and CD-H6^{A,B}), 2.14 (3 H, s, **H**).

^{13}C NMR: δ_C(125 MHz; d_4-methanol/D_2O) 173.3, 159.1, 138.2, 135.4, 131.9, 130.8, 129.9, 121.8, 115.8, 103.7, 103.5, 103.3, 83.5, 83.2, 82.9, 82.6, 75.4, 75.3, 75.2, 73.8, 73.6, 73.5, 72.0, 68.7, 61.8, 61.6 and 24.4.

Elemental analysis: (Found: C, 43.87; H, 6.56; N, 0.98. $C_{52}H_{73}NO_{31}.12H_2O$ requires C, 43.85; H, 6.86; N, 0.98%).

HPLC: t_R 25.9 min (column: YMC-PACK ODS-AQ, 250 × 10 mm; H_2O/MeCN gradient).

Time (min)	Flow (cm^3min^{-1})	H_2O (%)	MeCN (%)
0	3	90	10
25	3	65	35
26	3	90	10
30	3	90	10

UV/visible spectrum: λ_{max} = 192 nm, ε_{192} = 38269.2 $M^{-1}cm^{-1}$; λ_{max} = 236 nm, ε_{338} = 15384.6 $M^{-1}cm^{-1}$, λ_{max} = 297.5 nm, $\varepsilon_{297.5}$ = 12756.4 $M^{-1}cm^{-1}$.

Photochemical interconversion between the acetamides 5.5(E) and 5.5(Z)

5.5(E)

The acetamide **5.5(E)** (0.0015 g, 0.0012 mmol) was made up to a concentration of 2.50 × 10^{-5} M in MQ H_2O (50 cm^3). The acetamide **5.5(E)** solution was analysed for its molar response using analytical reverse-phase HPLC for a 10 μl injection and its absorbance using UV/visible spectrophotometer. A 1 cm^3 aliquot of the solution was then sealed in a quartz UV/visible cell and irradiated with ten 350 nm UV-A lamps for two minutes in a photolysis reactor. An aliquot of the solution was then subjected to HPLC while the absorbance was once again recorded. The solution was again resealed and irradiated with

ten 254 nm UV-C lamps for two minutes. The UV/visible spectrum of the solution was recorded and an aliquot of the solution was subjected to HPLC.

5.5(Z)

The acetamide **5.5(Z)** (0.001 g, 0.00083 mmol) was made up to a concentration of 1.56×10^{-5} M in MQ H_2O (50 cm^3). The solution was analysed before and after each irradiation using UV/visible spectroscopy and analytical reverse-phase HPLC as for the acetamide **5.5(E)**. The only difference was that the solution was irradiated with ten 254 nm UV-C lamps for one minute in a photolysis reactor before being irradiated with ten 350 nm UV-A lamps for one minute.

HPLC: **5.5(Z)** t_R 17.7 min, **5.5(E)** t_R 20.5 min, (column: YMC-PACK ODS-AQ, 250 × 4.6 mm; H_2O/MeCN gradient).

Time (min)	Flow (cm^3min^{-1})	H_2O (%)	MeCN (%)
0	1	90	10
25	1	65	35
26	1	90	10
30	1	90	10

Transport Assay

0.05 mol dm^{-3} Borax Buffer – pH 9.0

Sodium tetraborate (76.284 g, 200 mmol) was dissolved in Milli-Q H_2O (4 dm^3) and concentrated hydrochloric acid was added dropwise to adjust the solution to pH 9.

Methyl Orange Solutions

To 0.05 mol dm^{-3} borax buffer (1 dm^3), methyl orange (**5.8**) (0.0164 g, 0.501 mmol) was added and the mixture sonicated until dissolved. Aliquots of 250, 100, 20, and 4 cm^3 of the stock solution were removed and made up to 500 cm^3 with 0.05 mol dm^{-3} borax buffer to produce concentrations of 2.5×10^{-5}, 1×10^{-5}, 2×10^{-6}, and 4×10^{-7} M respectively.

CD Solutions

Each of the CDs **1.15**, **5.5(E)** and **5.5(Z)** (0.001 mmol) were made up to 1 cm^3 with 0.05 mol dm^{-3} borax buffer to produce a solution of concentration 1×10^{-3} M.

HPLC Procedure

The transport coefficients for the CDs **1.15**, **5.5(E)** and **5.5(Z)** were obtained using the Hummel and Dryer method,[88] as adapted by Croft *et al.*[89] The 4×10^{-7} M methyl orange (**5.8**) solution was pumped through a Waters carbohydrate analysis HPLC column (25 °C) operating at a flow rate of 0.9 cm^3 min^{-1}, monitoring at an absorbance of 450 nm. The CD **1.15**, **5.5(E)** or **5.5(Z)** (20 μl) was then injected. The molar amount of the dye **5.8** transported by the CD was then determined by comparing the areas of the negative peaks with a blank injection of borate buffer. The injection of the CDs **1.15**, **5.5(E)** and **5.5(Z)** were then repeated for each of the methyl orange (**5.8**) solutions described above. Plotting the molar ratio ($\bar{r}$) of guest bound to host injected against $\bar{r}$/[guest] in a Scatchard plot[90] enabled the transport coefficient (K) for each of the CDs **1.15**, **5.5(E)** and **5.5(Z)** for the dye **5.8** to be determined.

Experimental for Chapter 6

[(*E*)-4,4'-Bis(3-chloro-5-methoxy-2,4,6-triazinylamino)stilbene]-[α-cyclodextrin]-[2]-[rotaxane] (6.7)

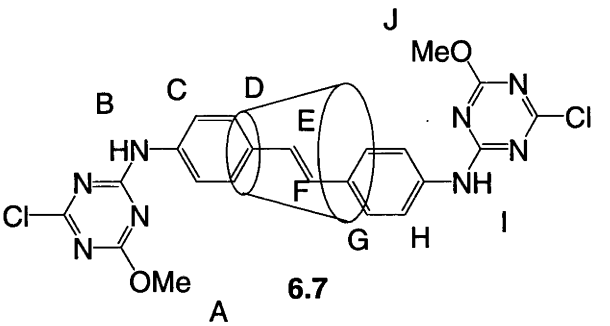

6.7

Method: To a stirred solution of αCD (**1.15**) (0.694 g, 0.713 mmol) in MQ-H_2O (80 cm^3), TEA was added unit the pH of the solution reached 9. The stilbene **1.30** (0.050 g, 0.238 mmol) was then added and the resultant suspension was stirred for two hours. The triazine **6.6** was added and the stirring was continued for another 17 hours. The reaction mixture was washed with EtOAc (3 × 50 cm^3) and lyophilsed. The crude material was dissolved in 25% aqueous MeCN and subjected to preparative HPLC. The [2]-rotaxane **6.7** was obtained after lyophilisation as a colourless powder.

Yield: 0.069 g, 19.8%.

TLC: (5:4:3 v/v/v *n*-butanol-ethanol-water) R_f 0.69 (relative to the solvent front), 1.79 (relative to αCD (**1.15**)).

Melting point: 265 °C (dec.).

Mass spectrum: m/z (ESI) 1491.5 (M^+ + Na).

^{1}H NMR: δ_H(500 MHz; d_6-DMSO) 10.81 (1 H, s, **B**), 10.62 (1 H, s, **I**), 7.80 (2 H, d, *J* 7.5, **G**), 7.76 (2 H, d, *J* 7.5, **H**), 7.71 (2 H, d, *J* 7.5, **C**), 7.27 (2 H, d, *J* 7.5, **D**), 7.02 (1 H, d, *J* 16.5, **F**), 6.83 (1 H, d, *J* 16.5, **E**), 4.75 (6 H, d, *J* 2.5, CD-H1), 4.04 (3 H, s, **J**), 4.00 (3 H, s, **A**), 3.56-3.69 (18 H, m, CD-H6^{A,B}, CD-H3, CD-H5), 3.43 (6 H, apparent t, *J* 4.0, CD-H4), 3.29 (6 H, apparent d, *J* 6.0, CD-H6^{A,B}), 3.23 (6 H, dd, *J* 3.0 and 12.5, CD-H2).

Elemental analysis: (Found: C, 42.87; H, 5.69; N, 6.61. $C_{58}H_{78}Cl_2N_8O_{32}.9H_2O$ requires C, 42.68; H, 5.93; N, 6.86%).

HPLC: t_R 10.8 min (column: YMC-PACK ODS-AQ, 250 × 20 mm; 13% aq. MeCN; flow rate: 10.0 cm^3min^{-1}).

[(*E*)-4,4'-Bis(3-anilino-5-methoxy-2,4,6-triazinylamino)stilbene]-[α-cyclodextrin]-[2]-[rotaxane] (6.8)

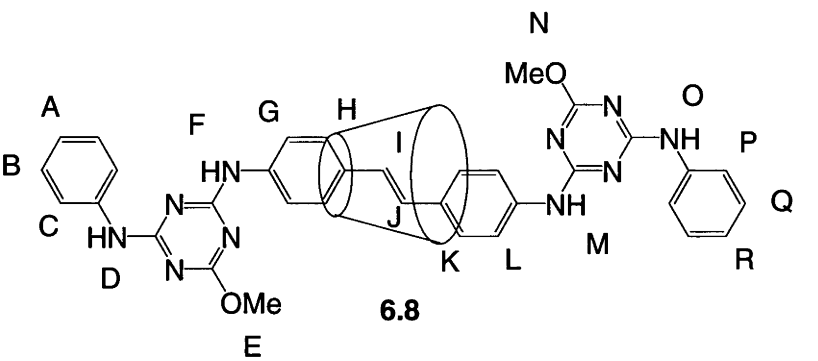

6.8

Method: To a stirring solution of the [2]-rotaxane **6.7** (0.030 g, 0.020 mmol) in MQ-H_2O/MeCN (50:50, 10 cm^3), TEA was added unit the pH of the solution reached 9. The amine **1.30** (0.019 g, 0.204 mmol) was then added and the reaction mixture was stirred at 50 °C for three hours. The reaction mixture was then subjected to preparative HPLC. The [2]-rotaxane **6.8** was obtained after lyophilisation as a colourless powder.

Yield: 0.011 g, 33.4%.

TLC: (5:4:3 v/v/v *n*-butanol-ethanol-water) R_f 0.74 (relative to the solvent front), 2.08 (relative to αCD (**1.15**)).

Mass spectrum: m/z (HI-RES ESI) Found: 1583.5780 (M^+ + H, $C_{70}H_{90}N_{10}O_{32}$). Calculated: 1583.5800.

^{1}H NMR: δ_H(500 MHz; d_6-DMSO) 9.81 (1 H, s, **F**), 9.71 (1 H, s, **M**), 9.47 (2 H, s, **D** and **O**), 7.83 (4 H, d, *J* 7.5, **C** and **P**), 7.75-7.80 (6 H, m, **G**, **K** and **L**), 7.31 (4 H, t, *J* 7.5, **B** and **Q**), 7.16 (2 H, unresolved, **H**), 7.00 (2 H, t, *J* 7.5, **A** and **R**), 6.88 (2 H, unresolved, **I** and **J**), 5.44 (6 H, s, CD-OH2), 5.31 (6 H, s, CD-OH3), 4.77 (6 H, d, *J* 3.0, CD-H1), 4.45 (6H, apparent t, *J* 5.0, CD-OH6), 3.94 (6 H, s, **E** and **N**), 3.70-3.73 (12 H, m, CD-H3 and CD-H5), 3.61 (6 H, unresolved, CD-$H6^{A,B}$), 3.47 (6 H, apparent t, *J* 4.0, CD-H4), 3.32 (6 H, unresolved, CD-$H6^{A,B}$), 3.26 (6 H, unresolved, CD-H2).

^{13}C NMR: δ_H(500 MHz; d_6-DMSO) 170.8, 164.9, 128.5, 125.7, 120.1, 102.1, 81.6, 73.2, 72.2, 71.8, 59.2 and 54.0. (not all signals resolved due to broadness)

Elemental analysis: (Found: C, 46.74; H, 6.45; N, 7.52. $C_{70}H_{90}N_{10}O_{32}.12H_2O$ requires C, 46.72; H, 6.38; N, 7.78%).

HPLC: t_R 18.9 min (column: YMC-PACK ODS-AQ, 250 × 20 mm; 23% aq. MeCN; flow rate: 10.0 cm^3min^{-1}).

[(*E*)-4,4'-Bis(3,5-dimethoxy-2,4,6-triazinylamino)stilbene]-[α-cyclodextrin]-[2]-[rotaxane] (6.10)

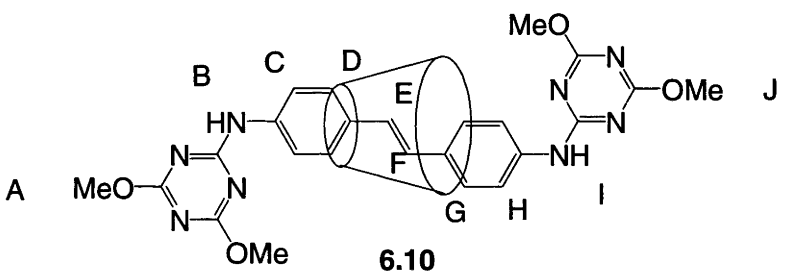

6.10

Method: To a stirred solution of αCD (**1.15**) (0.694 g, 0.713 mmol) in MQ-H_2O (80 cm^3), TEA was added until the pH of the solution reached 9. The stilbene **1.30** (0.050 g, 0.238 mmol) was then added and the resultant suspension was stirred for two hours. The triazine **6.9** was added and the stirring was continued for another 17 hours. The reaction mixture was washed with EtOAc (3 × 50 cm^3) and lyophilised. The crude material was dissolved in 25% aqueous MeCN and subjected to preparative HPLC. The [2]-rotaxane **6.10** was obtained after lyophilisation as a colourless powder.

Yield: 0.017 g, 4.8%.

TLC: (5:4:3 v/v/v *n*-butanol-ethanol-water) R_f 0.55 (relative to the solvent front), 1.15 (relative to αCD (**1.15**)).

Melting point: 264 °C (dec.).

Mass spectrum: m/z (ESI) 1462.2 (M^+ + H).

^{1}H NMR: δ_H(500 MHz; d_6-DMSO) 10.23 (1 H, s, **B**), 9.94 (1 H, s, **I**), 7.75-7.78 (4 H, m, **G** and **H**), 7.74 (2 H, d, *J* 8.0, **C**), 7.22 (2 H, d, *J* 8.0, **D**), 6.98 (1 H, d, *J* 16.0, **F**), 6.79 (1 H, d, *J* 16.0, **E**), 5.42 (6 H, s, CD-OH2), 5.28 (6 H, s, CD-OH3), 4.75 (6 H, d, *J* 2.5, CD-

H1), 4.41 (6 H, apparent t, *J* 5.5, CD-OH6), 3.88-3.98 (12 H, m, **A** and **J**), 3.70 (6 H, apparent d, *J* 9.5, CD-H5), 3.65 (6 H, apparent t, *J* 9.0, CD-H3), 3.59 (6 H, unresolved, CD-H6^{A,B}), 3.43 (6 H, apparent t, *J* 9.0, CD-H4), 3.30 (6 H, unresolved, CD-H6^{A,B}), 3.24 (6 H, unresolved, CD-H2).

^{13}C NMR: δ_C(125 MHz; d_6-DMSO) 54.2-55.8 (br), 61.0, 71.8, 72.1, 73.2, 81.7, 102.1, 119.7, 120.1, 125.2, 125.8, 127.3, 127.5, 131.0, 131.4, 133.5, 137.7, 138.0, 165.7, 165.8 and 171.8-173.0 (br)

Elemental analysis: (Found: C, 43.70; H, 6.13; N, 6.60. $C_{60}H_{84}N_8O_{34}.10H_2O$ requires C, 43.90; H, 6.39; N, 6.83%).

HPLC: t_R 13.6 min (column: YMC-PACK ODS-AQ, 250 × 20 mm; 10% aq. MeCN; flow rate: 10.0 cm^3min^{-1}).

Experimental for Chapter 7

[(*E*)-4-(4-(3,5-dimethoxy-2,4,6-triazinylamino)phenylacetamido)-4'-(3,5-dimethoxy-2,4,6-triazinylamino)stilbene]-[α-cyclodextrin]-[2]-[rotaxanes] (7.1 and 7.2)

Method: To a stirred solution of αCD (**1.15**) (4.250 g, 4.370 mmol) in MQ H_2O (300 cm^3), the diamine **2.11** (0.300 g, 0.874 mmol) was added and the resultant suspension was stirred for 24 hours. The triazine **6.9** was added and the stirring was continued for another 3 days. The precipitate was filtered and the residue was extracted with MQ H_2O (3 × 100 cm^3). The combined filrate was then subjected to Diaion HP-20 column (300 mm × 20 mm). The column was flushed with MQ H_2O until no unreacted αCD (**1.15**) was detected by TLC. The column was then flushed with methanol until all of the reacted αCD (**1.15**) was removed as detected by TLC. The solvent was reduced under pressure and the crude product was dissolved in MeOH and subjected to preparative reverse-phase HPLC. Fractions containing the [2]-rotaxanes **7.1** and **7.2** were isolated and lyophilised as colourless powders.

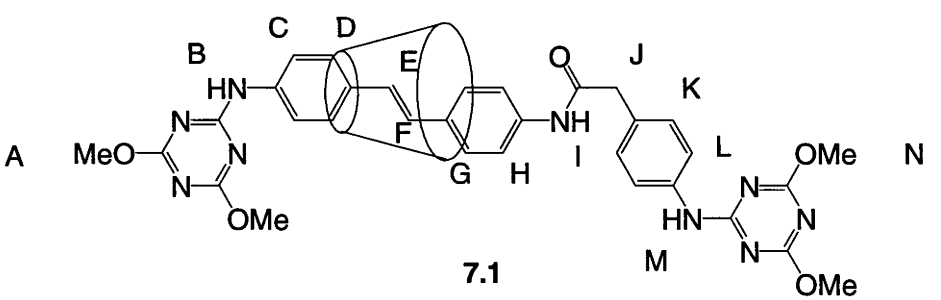

7.1

Yield: 0.047 g, 3.4%.

TLC: (5:4:3 v/v/v *n*-butanol-ethanol-water) R_f 0.64 (relative to the solvent front), 1.56 (relative to αCD (**1.15**)).

Melting point: 255 °C (dec.).

Mass spectrum: m/z (ESI) 1594.5 (M^+ + H).

^{1}H NMR: δ_H(500 MHz; d_6-DMSO) 10.26-10.22 (2 H, m, **B** and **I**), 10.07 (1 H, s, **M**), 7.73 (4 H, m, **C** and **G**), 7.65 (2 H, d, *J* 8.0, **L**), 7.62 (2 H, d, *J* 8.0, **H**), 7.32 (2 H, d, *J* 8.0, **K**), 7.18 (2 H, d, *J* 8.0, **D**), 7.01 (1 H, d, *J* 16.0, **F**), 6.85 (1 H, d, *J* 16.0, **E**), 5.44 (6 H,

unresolved, CD-OH2), 5.27 (6 H, unresolved, CD-OH3), 4.75 (6 H, unresolved, CD-H1), 4.40 (6 H, unresolved, CD-OH6), 3.95-3.90 (12 H, m, **A** and **N**), 3.70-3.62 (14 H, m, CD-H3, CD-H5 and **J**), 3.43 (6 H, unresolved, CD-H6^{A,B}), 3.43 (6 H, t, *J* 8.5, CD-H4), 3.28-3.20 (12 H, m, CD-H2 and CD-H6^{A,B}).

^{13}C NMR: δ_C(125 MHz; d_6-DMSO) 171.8, 169.2, 166.0, 165.8, 138.0, 137.3, 132.0, 130.9, 130.7, 129.5, 127.4, 125.8, 125.2, 120.6, 119.6, 119.2, 102.1, 81.7, 73.3, 72.1, 71.6, 59.2, 54.5 and 42.6.

Elemental analysis: (Found: C, 47.56; H, 5.99; N, 7.44. $C_{68}H_{91}N_9O_{35}.7H_2O$ requires C, 47.47; H, 6.15; N, 7.33%).

HPLC: t_R 13.1 min (column: YMC-PACK ODS-AQ, 250 × 20 mm with YMC-Guardpack ODS-AQ, 50 × 20 mm; 20% aq. MeCN; flow rate: 10.0 cm^{3}min^{-1}).

UV/visible spectrum: λ_{max} = 196 nm, ε_{196} = 63348.3 M^{-1}cm^{-1}; λ_{max} = 235 nm, ε_{235} = 21452.4 M^{-1}cm^{-1}; λ_{max} = 266 nm, ε_{266} = 22726.8 M^{-1}cm^{-1}; λ_{max} = 345.5 nm, $\varepsilon_{345.5}$ = 42108.3 M^{-1}cm^{-1}.

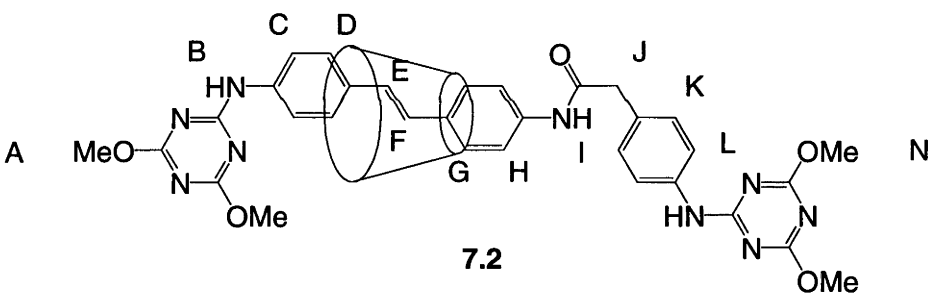

7.2

Yield: 0.018 g, 1.3%.

TLC: (5:4:3 v/v/v *n*-butanol-ethanol-water) R_f 0.63 (relative to the solvent front), 1.54 (relative to αCD (**1.15**)).

Melting point: 276 °C (dec.).

Mass spectrum: m/z (ESI) 1594.5 (M^+ + H).

^{1}H NMR: δ_H(500 MHz; d_6-DMSO) 10.23 (1 H, s, **I**), 10.08 (1H, s, **M**), 9.94 (1 H, s, **B**), 7.79-7.73 (4 H, m, **C** and **D**), 7.66 (2 H, d, *J* 8.0, **L**), 7.59 (2 H, d, *J* 8.0, **H**), 7.30 (2 H, d, *J* 8.0, **K**), 7.18 (2 H, d, *J* 8.0, **G**), 6.96 (1 H, d, *J* 16.0, **E**), 6.77 (1 H, d, *J* 16.0, **F**), 5.40 (6 H, unresolved, CD-OH2), 5.27 (6 H, unresolved, CD-OH3), 4.74 (6 H, unresolved, CD-H1), 4.41 (6 H, t, *J* 5.0, CD-OH6), 3.98 (3 H, s, **A**), 3.90 (9 H, s, **A** and **N**), 3.68 (6 H, d, *J*

9.5, CD-H5), 3.66-3.61 (8 H, m, CD-H3 and **J**), 3.57 (6 H, unresolved, CD-H6^{A,B}), 3.42 (6 H, t, *J* 9.0, CD-H4), 3.27 (6 H, unresolved, CD-H6^{A,B}), 3.22 (6 H, unresolved, CD-H2).

^{13}C NMR: δ_C(125 MHz; d_6-DMSO) 171.8, 169.2, 166.0, 165.7, 138.4, 137.7, 137.4, 131.4, 131.2, 130.5, 129.4, 127.5, 127.2, 125.9, 125.2, 120.5, 120.0, 118.5, 102.1, 81.7, 73.2, 72.1, 71.7, 59.2, 54.5 and 42.7.

Elemental analysis: (Found: C, 46.56; H, 6.04; N, 6.98. $C_{68}H_{91}N_9O_{35}.9H_2O$ requires C, 46.49; H, 6.25; N, 7.18%).

HPLC: t_R 19.3 min (column: YMC-PACK ODS-AQ, 250 × 20 mm with YMC-Guardpack ODS-AQ, 50 × 20 mm; 20% aq. MeCN; flow rate: 10.0 cm^{3}min^{-1}).

UV/visible spectrum: λ_{max} = 198 nm, ε_{198} = 57029.4 M^{-1}cm^{-1}; λ_{max} = 237 nm, ε_{237} = 19062.9 M^{-1}cm^{-1}; λ_{max} = 267 nm, ε_{267} = 20549.7 M^{-1}cm^{-1}; λ_{max} = 346 nm, ε_{346} = 36692.1 M^{-1}cm^{-1}.

(*E*)-4-(3-(*N*-(tert-Butoxycarbonyl)amino)propionamido)-4'-aminostilbene (7.4)

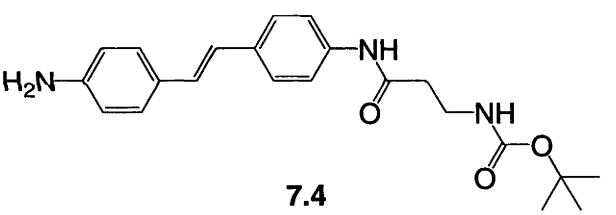

7.4

Method: Under an atmosphere of nitrogen, the carbamate **7.3** (0.500 g, 2.64 mmol), the stilbene **1.30** (1.667 g, 5.97 mmol) and BOP (1.753 g, 3.96 mmol) were dissolved in anhydrous DMF (10 cm^3). TEA (2 cm^3, 14.34 mmol) was then added and the mixture was stirred for three days. The reaction mixture was then subjected to preparative HPLC with the desired fractions combined and concentrated under reduced pressure. The residue was then recrystallised from aqueous ethanol to give the carbamate **7.4** as a light brown powder.

Yield: 0.708 g, 70%.

Melting point: 193-195 °C.

Mass spectrum: m/z (EI) 381.2 (M$^{+\cdot}$).

^{1}H NMR: δ_H(300 MHz; d_6-DMSO) 9.94 (1 H, s, CONHAr), 7.55 (2 H, d, *J* 8.4, CH=CH), 7.41 (2 H, d, *J* 8.4, CH=CH), 7.24 (2 H, d, *J* 8.4, CH=CH), 6.96 (1 H, d, *J* 16.2, CH=CH), 6.88 (1 H, t, *J* 5.1, $CONHCH_2$), 6.82 (1 H, d, *J* 16.2, CH=CH), 6.54 (2 H, d, *J* 8.4, CH=CH), 5.27 (2 H, s, NH_2Ar), 3.21 (2 H, dd, *J* 13.2 and 6.9, CH_2CH_2NH), 2.47 (2 H, unresolved, $COCH_2CH_2$), 1.38 (9 H, s, $C(CH_3)_3$),

^{13}C NMR: δ_C(75 MHz; d_6-DMSO) 169.2, 155.6, 148.5, 137.7, 132.9, 127.7, 127.4, 126.0, 124.9, 122.5, 119.2, 113.9, 77.6, 36.8, 36.5 and 28.3.

Elemental analysis: Found: C, 68.95; H, 7.25; N, 10.82. $C_{22}H_{27}N_3O_3$ requires C, 69.27; H, 7.13; N, 11.02%.

HPLC: t_R 14.5 min (column: YMC-PACK ODS-AQ, 250 × 20 mm with YMC-Guardpack ODS-AQ, 50 × 20 mm; 45% aq. MeCN; flow rate: 10.0 cm^3min^{-1}).

(*E*)-4-(3-Aminopropionamido)-4'-aminostilbene (7.5)

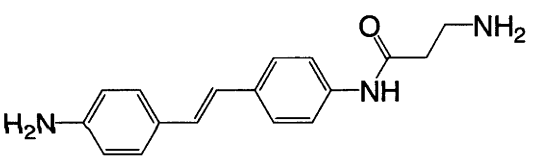

7.5

Method: To a stirring suspension of the carbamate **7.4** (0.700 g, 1.94 mmol) in DCM (250 cm^3), TFA (5 cm^3, 64.8 mmol) was added drop wise to produce a dark red solution. After 4 hours the solvent was removed and the residue was suspended in water (250 cm^3). The suspension was washed with diethyl ether (50 cm^3) before being adjusted to pH 12 with 5 M NaOH to produce a yellow precipitate. The mixture was extracted with EtOAc (5 × 100 cm^3), dried over anhydrous $MgSO_4$ and concentrated under reduced pressure to afford the diamine **7.5** as a yellow powder which was carried over into the next procedure without further purification.

Yield: 0.445 g, 88%.

Melting Point: 179-181 °C.

Mass spectrum: m/z (HI-RES EI) Found: 281.1526 ($M^{+\cdot}$. $C_{17}H_{19}N_3O$). Calculated: 281.1528.

^{1}H NMR: δ_H(500 MHz; d_6-DMSO) 10.07 (1 H, s, CONHAr), 7.55 (2 H, d, *J* 8.5, CH=CH), 7.42 (2 H, d, *J* 8.5, CH=CH), 7.24 (2 H, d, *J* 8.5, CH=CH), 6.95 (2 H, d, *J* 16.0, CH=CH), 6.82 (2 H, d, *J* 16.0, CH=CH), 6.54 (2 H, d, *J* 8.5, CH=CH), 5.27 (2 H, s, NH_2Ar), 2.87 (2 H, t, *J* 6.5, $CH_2CH_2NH_2$), 2.42 (2 H, t, *J* 6.5, $COCH_2CH_2$), (NH_2 signal hidden under H_2O peak at 3.33).

^{13}C NMR: δ_C(125 MHz; d_6-DMSO) 170.1, 148.5, 137.7, 132.8, 127.7, 127.3, 126.0, 124.9, 122.4, 119.2, 113.9 and 37.7.

[(*E*)-4-(3-(3,5-dimethoxy-2,4,6-triazinylamino)propionamido)-4'-(3,5-dimethoxy-2,4,6-triazinylamino)stilbene]-[α-cyclodextrin]-[2]-[rotaxanes] (7.6 and 7.7)

Method: To a stirred solution of αCD (**1.15**) (3.720 g, 3.826 mmol) in 0.012 M $NaHCO_3$ (250 cm^3), the diamine **7.5** (0.200 g, 0.765 mmol) was added and the resultant suspension was stirred for 24 hours. The triazine **6.9** was added and the stirring was continued for another 3 days. The precipitate was filtered and the residue was extracted with MQ H_2O (3 × 100 cm^3). The combined filtrate was then subjected to Diaion HP-20 column (300 mm × 20 mm). The column was flushed with MQ H_2O until no unreacted αCD (**1.15**) was detected by TLC. The column was then flushed with methanol until all of the reacted αCD (**1.15**) was removed as detected by TLC. The solvent was reduced under pressure and the crude product was dissolved in MeOH and subjected to preparative reverse-phase HPLC. Fractions containing the [2]-rotaxanes **7.6** and **7.7** were isolated and lyophilised as colourless powders.

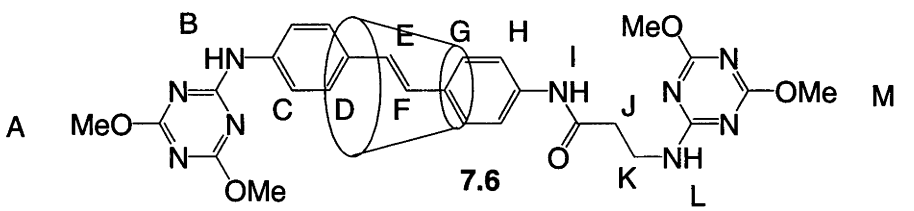

7.6

Yield: 0.0047 g, 0.4%.

TLC: (5:4:3 v/v/v *n*-butanol-ethanol-water) R_f 0.49 (relative to the solvent front), 1.48 (relative to αCD (**1.15**)).

Mass spectrum: m/z (HI-RES ESI) Found: 1532.5528 (M^+ + H, $C_{63}H_{90}N_9O_{35}$). Calculated: 1532.5539.

^{1}H NMR: δ_H(500 MHz; d_6-DMSO) 10.07 (1 H, s, **I**), 9.97 (1 H, s, **B**), 7.96 (1 H, unresolved, **L**), 7.75 (4 H, apparent s, **C** and **D**), 7.60 (2 H, d, *J* 8.0, **H**), 7.19 (2 H, d, *J* 8.0, **G**), 6.96 (1 H, d, *J* 16.5, **E**), 6.77 (1 H, d, *J* 16.5, **F**), 5.60-5.30 (12 H, m, CD-OH2 and CD-OH3), 4.74 (6 H, d, *J* 3.0, CD-H1), 4.43 (6 H, unresolved, CD-OH6), 3.98 (3 H, s, **A** or **M**), 3.89 (3 H, s, **A** or **M**), 3.86 (3 H, s, **A** or **M**), 3.81 (3 H, s, **A** or **M**), 3.69 (6 H, unresolved, CD-H5), 3.65 (6 H, unresolved, CD-H3), 3.60-3.55 (8 H, m, CD-H6^{A,B} and **K**), 3.42 (unresolved, CD-H4), 3.27 (6 H, unresolved, CD-H6^{A,B}), 3.22 (6 H, unresolved, CD-H2), 2.64 (2 H, t, *J* 6.5, **J**).

HPLC: t_R 32.1 min (column: YMC-PACK ODS-AQ, 250 × 20 mm with YMC-Guardpack ODS-AQ, 50 × 20 mm; 10% aq. MeCN; flow rate: 10.0 cm^3min^{-1}).

UV/visible spectrum: λ_{max} = 348 nm, ε_{348} = 9909.9 $M^{-1}cm^{-1}$.

Note: insufficient material for microanalysis or ^{13}C NMR.

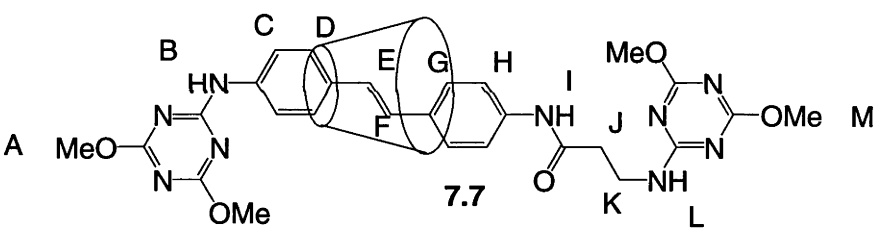

7.7

Yield: 0.020 g, 1.7%.

TLC: (5:4:3 v/v/v *n*-butanol-ethanol-water) R_f 0.50 (relative to the solvent front), 1.51 (relative to αCD (**1.15**)).

Melting point: 288 °C (dec.).

Mass spectrum: m/z (ESI) 1532.6 (M^+ + H).

^{1}H NMR: δ_H(500 MHz; d_6-DMSO) 10.24 (1 H, s, **B**), 10.07 (1 H, s, **I**), 8.03 (1 H, t, *J* 5.0, **L**), 7.76-7.70 (4 H, m, **C** and **G**), 7.63 (2 H, d, *J* 8.0, **H**), 7.18 (2 H, d, *J* 8.0, **D**), 7.00 (1 H, d, *J* 16.5, **E**), 6.84 (1 H, d, *J* 16.5, **F**), 5.47 (6 H, unresolved, CD-OH2), 5.26 (6 H, unresolved, CD-OH3), 4.75 (6 H, d, *J* 3.0, CD-H1), 4.41 (6 H, unresolved, CD-OH6), 3.98-3.89 (6 H, m, **A** or **M**), 3.87 (3 H, s, **A** or **M**), 3.81 (3 H, s, **A** or **M**), 3.71-3.62 (12

H, m, CD-H5 and CD-H3), 3.60-3.52 (8 H, m, CD-H6^{A,B} and **K**), 3.43 (6 H, t, *J* 9.0, CD-H4), 3.28-3.21 (12 H, m, CD-H6^{A,B} and CD-H2), 2.67 (2 H, t, *J* 6.5, **J**).

^{13}C NMR: δ_C(125 MHz; d_4-methanol) 173.7, 173.2, 172.4, 169.3, 167.7, 139.9, 139.2, 134.4, 132.8, 129.2, 129.0, 128.3, 127.8, 122.2, 122.0, 104.0, 83.2, 75.1, 73.9, 73.7, 61.5, 55.2, 38.4 and 37.5.

Elemental analysis: (Found: C, 44.04; H, 6.36; N, 7.09. $C_{63}H_{89}N_9O_{35}.10H_2O$ requires C, 44.18; H, 6.42; N, 7.36%).

HPLC: t_R 37.6 min (column: YMC-PACK ODS-AQ, 250 × 20 mm with YMC-Guardpack ODS-AQ, 50 × 20 mm; 10% aq. MeCN; flow rate: 10.0 cm^3min^{-1}).

UV/visible spectrum: λ_{max} = 346 nm, ε_{346} = 14132.7 $M^{-1}cm^{-1}$.

Photochemical isomerisation of the [2]-rotaxanes 7.1, 7.2, 7.6 and 7.7

Solutions

The [2]-rotaxane **7.1** (0.0006 g, 0.00038 mmol) was made up to a concentration of 1.51 × 10^{-5} M in MQ H_2O (25 cm^3). The [2]-rotaxane **7.2** (0.0015 g, 0.00094 mmol) was made up to a concentration of 1.88 × 10^{-5} M in MQ H_2O (50 cm^3). The [2]-rotaxane **7.6** (0.0034 g, 0.0022 mmol) was made up to a concentration of 2.22 × 10^{-5} M in MQ H_2O (100 cm^3). The [2]-rotaxane **7.7** (0.0015 g, 0.00098 mmol) was made up to a concentration of 1.96 × 10^{-5} M in MQ H_2O (50 cm^3).

350 nm and 254 nm irradiation

Each of the solutions of the [2]-rotaxanes **7.1**, **7.2**, **7.6** and **7.7** were analysed for their molar responses using analytical reverse-phase HPLC for a 10 μl injection and its absorbance using UV/visible spectrophotometer. A 1 cm^3 aliquot of the solutions were then sealed in quartz UV/visible cells and irradiated with ten 350 nm UV-A lamps for 30 seconds in a photolysis reactor. Aliquots of the irradiated solutions were then subjected to HPLC while the absorbances were once again recorded. The solutions were again resealed and irradiated with ten 254 nm UV-C lamps for 30 seconds. The UV/visible spectra of the solutions were recorded and aliquots of the solutions were subjected to

HPLC. The cycle of irradiation with 350nm and 254 nm light was then repeated a further two times.

370 nm and 254 nm irradiation

A 1 cm^3 aliquot of the solutions of the were sealed in 13 mm pyrex tubes and irradiated with light of wavelength 370 nm. The [2]-rotaxane **7.1** was irradiated for 45 minutes while its orientational isomer **7.2** was irradiated for 20 minutes. The [2]-rotaxanes **7.6** and **7.7** were irradiated for 30 minutes. Aliquots of the irradiated solutions were then subjected to HPLC while the absorbances were once again recorded. The solutions were again resealed and irradiated with four 254 nm UV-C lamps. The [2]-rotaxane **7.1** was irradiated for two minutes while the [2]-rotaxanes **7.2**, **7.6** and **7.7** were irradiated for one minute. The UV/visible spectra of the solutions were recorded and aliquots of the solutions were subjected to HPLC. The cycle of irradiation with 370nm and 254 nm light was then repeated a further two times.

HPLC: **7.1** t_R 6.5 min, (column: YMC-PACK ODS-AQ, 250 × 4.6 mm; H_2O/MeCN gradient).

Time (min)	Flow (cm^3min^{-1})	H_2O (%)	MeCN (%)
0	1	95	5
10	1	0	100
11	1	95	5
15	1	95	5

HPLC: **7.2** t_R 3.5 min, (column: YMC-PACK ODS-AQ, 250 × 4.6 mm; 25% aq. MeCN; flow rate: 1.0 cm^3min^{-1}).

HPLC: **7.6** t_R 2.6 min, **7.7** t_R 2.6 min, (column: YMC-PACK ODS-AQ, 250 × 4.6 mm; 30% aq. MeCN; flow rate: 1.0 cm^3min^{-1}).

[(*Z*)-4-(4-(3,5-dimethoxy-2,4,6-triazinylamino)phenylacetamido)-4'-(3,5-dimethoxy-2,4,6-triazinylamino)stilbene]-[α-cyclodextrin]-[2]-[rotaxane] (7.1(Z))

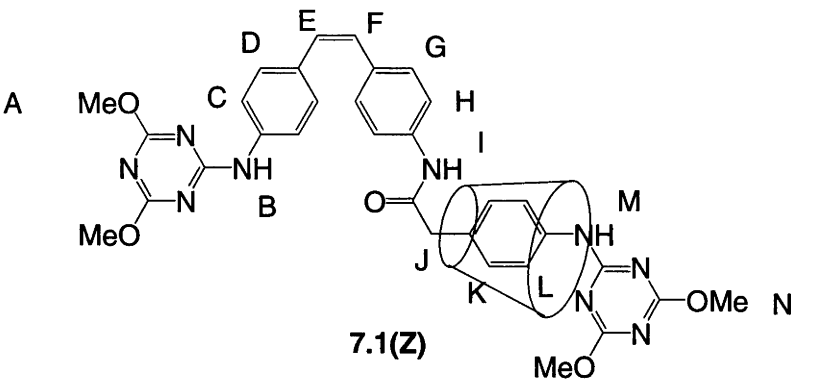

7.1(Z)

Method: The [2]-rotaxane **7.1** (0.040 g, 0.025 mmol) was dissolved in MQ H_2O (500 cm^3) and placed in a 1 dm^3 quartz round bottom flask. The mixture was then irradiated with light of wavelength 350 nm (10 lamps) for three minutes. The reaction mixture was then lyophilised, dissolved in 25% aqueous MeCN and subjected to semi-preparative reverse-phase HPLC. Fractions containing the [2]-rotaxane **7.1(Z)** were combined and lyophilised to give a colourless powder.

Yield: 0.0043 g, 11%.

TLC: (5:4:3 v/v/v *n*-butanol-ethanol-water) R_f 0.65 (relative to the solvent front), 1.67 (relative to αCD (**1.15**)).

^{1}H NMR: δ_H(500 MHz; d_6-DMSO) 7.64 (2 H, d, *J* 8.0, **L**), 7.62 (2 H, d, *J* 8.0, **C**), 7.48-7.42 (4 H, m, **H** and **K**), 7.29 (2 H, d, *J* 8.0, **D**), 7.22 (2 H, d, *J* 8.0, **G**), 6.52 (1 H, d, *J* 12.5, **E** or **F**), 6.48 (1 H, d, *J* 12.5, **E** or **F**), 4.76 (6 H, d, *J* 2.5, CD-H1), 3.92 (6 H, s, **N**), 3.89 (6 H, s, **A**), 3.79 (6 H, d, *J* 9.5, CD-H5), 3.74-3.66 (8 H, m, **J** and CD-H5), 3.60 (6 H, d, *J* 11.0, CD-H6^{A,B}), 3.44 (unresolved, CD-H4), 3.35 (unresolved, CD-H6^{A,B}), 3.24 (6 H, d, *J* 9.5, CD-H2).

HPLC: t_R 8.4 min (column: YMC-PACK ODS-AQ, 250 × 10 mm; H_2O/MeCN gradient).

Time (min)	Flow (cm^3min^{-1})	H_2O (%)	MeCN (%)
0	3	70	30
10	3	70	30
15	3	0	100
16	3	70	30
20	3	70	30

[(Z)-4-(4-(3,5-dimethoxy-2,4,6-triazinylamino)phenylacetamido)-4'-(3,5-dimethoxy-2,4,6-triazinylamino)stilbene]-[α-cyclodextrin]-[2]-[rotaxane] (7.2(Z))

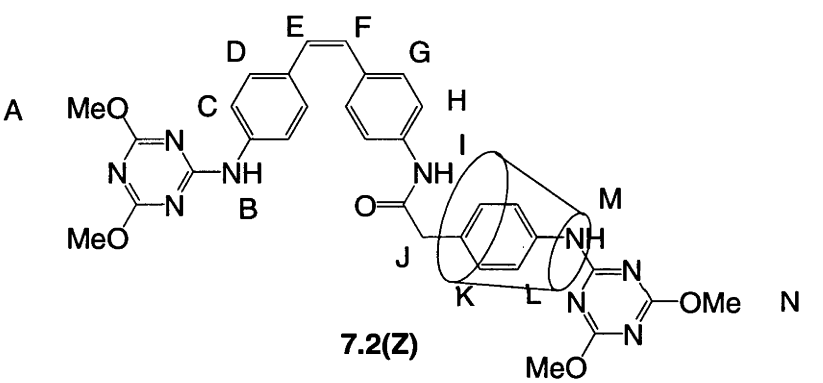

7.2(Z)

Method: The [2]-rotaxane **7.2** (0.015 g, 0.0094 mmol) was dissolved in MQ H_2O (500 cm^3) and placed in a 1 dm^3 quartz round bottom flask. The mixture was then irradiated with light of wavelength 350 nm (10 lamps) for three minutes. The reaction mixture was then lyophilised, dissolved in 25% aqueous MeCN and subjected to semi-preparative reverse-phase HPLC. Fractions containing the [2]-rotaxane **7.2(Z)** were combined and lyophilised to give a colourless powder.

Yield: 0.0055 g, 37%.

TLC: (5:4:3 v/v/v *n*-butanol-ethanol-water) R_f 0.63 (relative to the solvent front), 1.61 (relative to αCD (**1.15**)).

^{1}H NMR: δ_H(500 MHz; d_6-DMSO) 7.68-7.56 (6 H, m, **C**, **H** and **L**), 7.37 (2 H, d, *J* 8.0, **K**), 7.26-7.16 (4 H, m, **D** and **G**), 6.52-6.44 (2 H, m, **E** and **F**), 4.74 (6 H, d, *J* 3.0, CD-H1), 3.89 (9 H, s, **A** and **N**), 3.84 (3 H, s, **A** or **N**), 3.82-3.76 (8 H, m, **J** and CD-H5), 3.66

(6 H, t, *J* 9.0, CD-H5), 3.59 (6 H, d, *J* 11.5, CD-H6^{A,B}), 3.42 (unresolved, CD-H4), 3.35 (unresolved, CD-H6^{A,B}), 3.21 (6 H, dd, *J* 9.5 and 3.0, CD-H2).

HPLC: t_R 12.6 min (column: YMC-PACK ODS-AQ, 250 × 10 mm; H_2O/MeCN gradient).

Time (min)	Flow (cm^3min^{-1})	H_2O (%)	MeCN (%)
0	3	70	30
10	3	70	30
15	3	0	100
16	3	70	30
20	3	70	30

Experimental for Chapter 8

[(*E*)-*N*-(6^{A}-Deoxy-α-cyclodextrin-6^{A}-yl)-4-aminocarbonyl-4'-(3-(3,5-dimethoxy-2,4,6-triazinylamino)propionamido)stilbene]-[c2]-[daisy chain] (8.5(E,E))

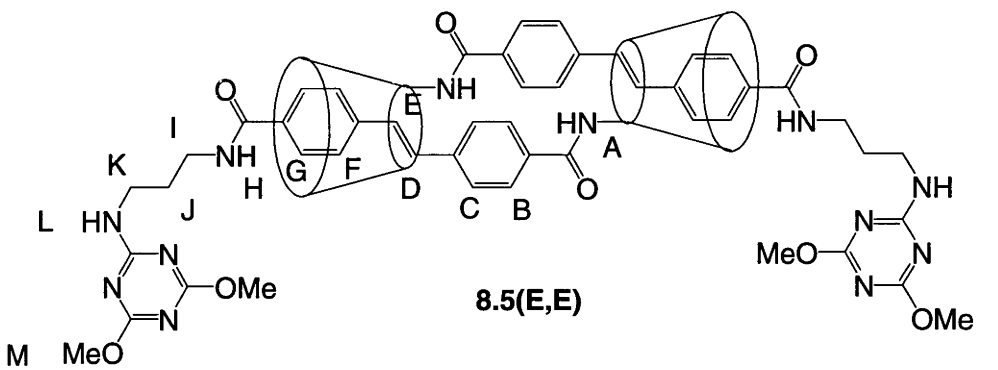

Method: The hermaphroditic CD **8.3** (0.100 g, 0.078 mmol) was dissolved in MQ H_2O (10 cm^3) and stirred for 24 hours. The triazine **6.9** (0.015 g, 0.086 mmol) was added and the resulting suspension was stirred. After two days the reaction was deemed incomplete by TLC. A further equivalent of the triazine **6.9** (0.014 g, 0.0078 mmol) was added and the suspension was stirred for a further three days. The solvent was then removed by lyophilisation. The resultant colourless powder was dissolved in MQ H_2O/MeCN and subjected to semi-preparative reverse-phase HPLC. Fractions containing the hermaphroditic [2]-rotaxane **8.5(E,E)** were isolated and lyophilised as a colourless powder.

Yield: 0.014 g, 12%.

TLC: (5:4:3:2 v/v/v *i*-propanol-ethanol-water-acetic acid) R_f 0.41 (relative to the solvent front), 0.76 (relative to αCD (**1.15**)).

Melting point: 239 °C (dec.).

Mass spectrum: m/z (ESI) 2836.3 (M^+ + H).

^{1}H NMR: δ_H(500 MHz; D_2O) 8.02-7.97 (8 H, m, **F** and **G**), 7.58 (4 H, d, *J* 8.0, **B**), 7.32 (4 H, d, *J* 8.0, **C**), 7.29 (2 H, d, *J* 16.5, **D** or **E**), 7.19 (2 H, d, *J* 16.5, **D** or **E**), 5.18-4.92 (12 H, m, CD-H1), 4.53-3.01 (92 H, m, CD-H2, CD-H3, CD-H4, CD-H5, CD-H6^{A,B}, **I**, **K**, **M**), 1.97 (4 H, p, *J* 6.5, **J**).

Detailed ^{1}H NMR assignment is shown in Chapter 8.

^{13}C NMR: δ_C(125 MHz; d_6-DMSO) 174.9, 174.3, 172.6, 171.0, 170.2, 141.5, 141.1, 137.4, 135.7, 132.6, 131.7, 131.3, 130.4, 130.1, 128.6, 105.3, 105.0, 104.9, 104.7, 87.2, 84.2, 84.0, 83.9, 83.7, 76.6, 76.5, 76.4, 76.3, 75.5, 75.3, 75.1, 74.6, 74.5, 74.4, 62.9, 62.6, 62.3, 62.1, 57.7, 57.6, 43.7, 40.9, 40.2, 33.1 and 31.0.

Elemental analysis: (Found: C, 47.07; H, 6.26; N, 5.15. $C_{120}H_{168}N_{12}O_{66}.13H_2O$ requires C, 46.96; H, 6.37; N, 5.48%).

HPLC: t_R 10.3 min (column: YMC-PACK ODS-AQ, 250 × 10 mm; H_2O/MeCN gradient).

Time (min)	Flow (cm^3min^{-1})	H_2O (%)	MeCN (%)
0	3	85	15
15	3	85	15
25	3	0	100
30	3	0	100
31	3	85	15
40	3	85	15

UV/visible spectrum: λ_{max} = 222.5 nm, $\varepsilon_{222.5}$ = 64979.8 $M^{-1}cm^{-1}$; λ_{max} = 333.5 nm, $\varepsilon_{333.5}$ = 105161.9 $M^{-1}cm^{-1}$.

Photochemical isomerisation of the hermaphroditic [2]-rotaxane 8.5(E,E)

The hermaphroditic [2]-rotaxane **8.5(E,E)** (0.0007 g, 0.00025 mmol) was made up to a concentration of 9.88 × 10^{-6} M in MQ H_2O (25 cm^3). The molar response for the hermaphroditic [2]-rotaxane **8.5(E,E)** was analysed using analytical reverse-phase HPLC for a 10 μl injection and its absorbance using UV/visible spectrophotometer. A 1 cm^3 aliquot of the solution was then sealed in a quartz UV/visible cell and irradiated with ten 350 nm UV-A lamps for one minute in a photolysis reactor. An aliquot of the irradiated solution was then subjected to HPLC while the absorbance was once again recorded. The solution was again resealed and irradiated with ten 254 nm UV-C lamps for one minute.

The UV/visible spectrum of the solution was recorded and an aliquot of the solution was subjected to HPLC. The cycle of irradiation with 350nm and 254 nm light was then repeated a further two times. The photochemical isomerisation was then repeated as described above. The only change was the time length of the 350 nm irradiation which was increased to ten minutes.

HPLC: **8.5(E,E)** t_R 6.2 min, (column: YMC-PACK ODS-AQ, 250 × 4.6 mm; 15% aq. MeCN; flow rate: 1.0 cm^3min^{-1}).

References

(1) Wolf, K. L., Frahm, H., Harms, H. *Z. Phys. Chem. Abt.* **1937**, *B 36*, 17.

(2) Wolf, K. L., Dunken, H., Merkel, K. *ibid.* **1940**, *46*, 287.

(3) Wolf, K. L., Wolff, R. *Angew. Chem.* **1949**, *61*, 191.

(4) Lehn, J.-M. *Angew. Chem. Int. Ed. Engl.* **1988**, *27*, 89.

(5) Lehn, J.-M. *Comprehensive Supramolecular Chemistry, Foreword*; Elsevier Science Ltd.: Oxford, 1996.

(6) Lehn, J.-M. *Pure & Appl. Chem.* **1978**, *50*, 871.

(7) Schalley, C. A. *J. Phys. Org. Chem.* **2004**, *17*, 967.

(8) Philp, D., Stoddart, J. F. *Angew. Chem. Int. Ed. Engl.* **1996**, *35*, 1154.

(9) Nakashima, N., Kawabuchi, A., Murakami, H. *J. Inclusion Phenom. Macro. Chem.* **1998**, *32*, 363.

(10) Wenz, G., Wolf, F., Wagner, M., Kubik, S. *New. J. Chem.* **1993**, *17*, 729.

(11) Ogino, H. *New. J. Chem.* **1993**, *17*, 683.

(12) Schill, G., Zollenkopf, H. *Lieb. Ann. Chem.* **1969**, *721*, 53.

(13) Frisch, H. L., Wasserman, E. *J. Am. Chem. Soc.* **1961**, *83*, 3789.

(14) Wenz, G. *Angew. Chem. Int. Ed. Engl.* **1994**, *33*, 803.

(15) Amabilino, D. B., Stoddart, J. F. *Chem. Rev.* **1995**, *95*, 2725.

(16) Nepogodiev, S. A., Stoddart, J. F. *Chem. Rev.* **1998**, *98*, 1959.

(17) Harrison, I. T., Harrison, S. *J. Am. Chem. Soc.* **1967**, *89*, 5723.

(18) Chambron, J.-C., Heitz, V., Sauvage, J-P. *J. Am. Chem. Soc.* **1993**, *115*, 12378.

(19) Diederich, F., Dietrich-Buchecker, C., Nierengarten, J-F., Sauvage, J-P. *J. Chem. Soc., Chem. Commun.* **1995**, 781.

(20) Cardenas, D. J., Gavina, P., Sauvage, J-P. *Chem. Commun.* **1996**, 1915.

(21) Cardenas, D. J., Gavina, P., Sauvage, J-P. *J. Am. Chem. Soc.* **1997**, *119*, 2656.

(22) Spencer, N., Stoddart, J. F. *J. Am. Chem. Soc.* **1991**, *113*, 5131.

(23) Collier, C. P., Jeppensen, J. O., Luo, Y., Perkins, J., Wong, E. W., Heath, J. R., Stoddart, J. F. *J. Am. Chem. Soc.* **2001**, *123*, 12632.

(24) Jeppenson, J. O., Vignon, S. A., Stoddart, J. F. *Chem. Eur. J.* **2003**, *9*, 4611.

(25) Tseng, H.-R., Vignon, S. A., Stoddart, J. F. *Angew. Chem. Int. Ed. Engl.* **2003**, *42*, 1491.

(26) Dichtel, W. R., Miljanic, O. S., Spruell, J. M., Heath, J. R., Stoddart, J. F. *J. Am. Chem. Soc.* **2006**, *128*, 10388.

(27) Lane, A. S., Leigh, D. A., Murphy, A. *J. Am. Chem. Soc.* **1997**, *119*, 11092.

(28) Gatti, F. G., Leigh, D. A., Nepogodiev, S. A., Slawin, A. M. Z., Teat, S. J., Wong, J. K. Y. *J. Am. Chem. Soc.* **2001**, *123*, 5983.

(29) Asakawa, M., Brancato, G., Fanti, M., Leigh, D. A., Shimizu, T., Slawin, A. M. Z., Wong, J. K. Y., Zerbetto, F., Zhang, S. *J. Am. Chem. Soc.* **2002**, *124*, 2939.

(30) Da Ros, T., Guldi, D. M., Morales, A. F., Leigh, D. A., Prato, M., Turco, R. *Org. Lett.* **2003**, *5*, 689.

(31) Altieri, A., Gatti, F. G., Kay, E. R., Leigh, D. A., Martel, D., Paolucci, F., Slawin, A. M. Z., Wong, J. K. Y. *J. Am. Chem. Soc.* **2003**, *125*, 8644.

(32) Altieri, A., Bottari, G., Dehez, F., Leigh, D. A., Wong, J. K. Y., Zerbetto, F. *Angew. Chem. Int. Ed. Engl.* **2003**, *42*, 2296.

(33) Keavaney, C. M., Leigh, D. A. *Angew. Chem. Int. Ed. Engl.* **2004**, *43*, 1222.

(34) Jimenez, M. C., Dietrich-Buchecker, C., Sauvage, J-P., De Cian, A. *Angew. Chem. Int. Ed. Engl.* **2000**, *39*, 1295.

(35) Yamada, T., Fukuhara, G., Kaneda, T. *Chem. Lett.* **2003**, *32*, 534.

(36) Fukuhara, G., Fujimoto, T., Kaneda, T. *Chem. Lett.* **2003**, *32*, 536.

(37) Ashton, P. R., Baxter, I., Cantrill, S. J., Fyfe, M. C. T., Glink, P. T., Stoddart, J. F., White, A. J. P., Williams, D. J. *Angew. Chem. Int. Ed. Engl.* **1998**, *37*, 1294.

(38) Kaneda, T., Yamada, T., Fujimoto, T., Sakata, Y. *Chem. Lett.* **2001**, 1264.

(39) Onagi, H., Easton, C. J., Lincoln, S. F. *Org. Lett.* **2001**, *3*, 1041.

(40) Jimenez, M. C., Dietrich-Buchecker, C., Sauvage, J-P. *Angew. Chem. Int. Ed. Engl.* **2000**, *39*, 3284.

(41) Balzani, V., Credi, A., Silvi, S., Venturi, M. *Chem. Soc. Rev.* **2006**, *35*, 1135.

(42) Colasson, B. X., Dietrich-Buchecker, C., Jimenez-Molero, M. C., Sauvage, J-P. *J. Phys. Org. Chem.* **2002**, *15*, 476.

(43) Villiers, A. *Compt. Rend.* **1891**, *112*, 536.

(44) Freudenberg, K., Blomquist, G., Ewald, L., Soff, K. *Ber. Dtsch. Chem. Ges.* **1936**, *69*, 1258.

(45) Harata, K. *Comprehensive Supramolecular Chemistry, Volume 3: Cyclodextrins, Chapter 9: Crystallographic Studies*; Elsevier Science Ltd.: Oxford, 1996.

(46) Saenger, W., Jacob, J., Gessler, K., Steiner, T., Hoffmann, D.,Sanbe, H., Koizumi, K., Smith, S. M., Takaha, T. *Chem. Rev.* **1998**, *98*, 1787.

(47) Harata, K. *Chem. Rev.* **1998**, *98*, 1803.

(48) Szejtli, J. *Comprehensive Supramolecular Chemistry, Volume 3: Cyclodextrins, Chapter 2: Chemistry, Physical and Biological Properties of Cyclodextrins*; Elsevier Science Ltd.: Oxford, 1996.

(49) Easton, C. J., Lincoln, S. F. *Modified Cyclodextrin: Scaffolds and Templates for Supramolecular Chemistry*; Imperial College Press: London, 1999.

(50) Pringsheim, H. *Chemistry of the Saccharides*; McGraw-Hill: New York, 1932.

(51) Pringsheim, H. *A Comprehensive Survey of Starch Chemistry*; Chemical Catelog Co.: New York, 1928.

(52) Szejtli, J. *Comprehensive Supramolecular Chemistry, Volume 3: Cyclodextrins, Chapter 5: Inclusion of Guest Molecules, Selectivity and Molecular Recognition by Cyclodextrins*; Elsevier Science Ltd.: Oxford, 1996.

(53) Khan, A. R., Forgo, P., Stine, K. J., D'Souza, V. T. *Chem. Rev.* **1998**, *98*, 1977.

(54) Melton, L. D., Slessor, K. N. *Carbohyd. Res.* **1971**, *18*, 29.

(55) Hamasaki, K., Ikeda, H., Nakamura, A., Ueno, A., Toda, F., Suzuki, I., Osa, T. *J. Am. Chem. Soc.* **1993**, *115*, 5035.

(56) Brown, S. E., Coates, J. H., Coghlan, D. R., Easton, C. J., van Eyk, S. J., Janowski, W., Lepore, A., Lincoln, S. F., Luo, Y., May, B. L., Schiesser, D. S., Wang, P., Williams, M. L. *Aust. J. Chem.* **1993**, *46*, 953.

(57) Onagi, H. Ph.D Thesis, The Australian National University, 2002.

(58) Macartney, D. H. *J. Chem. Soc., Perkin Trans. 2* **1996**, 2775.

(59) Ashton, P. R., Philip, D., Reddington, M. V., Slawin, A. M. Z., Spencer, N., Stoddart, J. F., Williams, D. J. *J. Chem. Soc., Chem. Commun.* **1991**, 1680.

(60) Ogino, H. *J. Am. Chem. Soc.* **1981**, *103*, 1303.

(61) Ogino, H., Ohata, K. *Inorg. Chem.* **1984**, *23*, 3312.

(62) Harada, A., Li, J., Kamachi, M. *Chem. Commun.* **1997**, 1413.

(63) Wenz, G., von der Bay, E., Schmidt, L. *Angew. Chem. Int. Ed. Engl.* **1992**, *31*, 783.

(64) Wenz, G., Han, B-H., Muller, A. *Chem. Rev.* **2006**, *106*, 782.

(65) Easton, C. J., Lincoln, S. F., Meyer, A. G., Onagi, H. *J. Chem. Soc., Perkin Trans. 1* **1999**, 2501.

(66) Meier, H. *Angew. Chem. Int. Ed. Engl.* **1992**, *31*, 1399.

(67) Stainer, C. A., Alderman, S. J., Claridge, T. D. W., Anderson, H. L. *Angew. Chem. Int. Ed. Engl.* **2002**, *41*, 1769.

(68) Rekharsky, M. V., Inoue, Y. *Chem. Rev.* **1998**, *98*, 1875.

(69) Gibbs, R. A., Benkovic, P. A., Janda, K. D., Lerner, R. A., Benkovic, S. J. *J. Am. Chem. Soc.* **1992**, *114*, 3528.

(70) Jacobson, K. A., Barone, S., Kammula, U., Stiles, G. L. *J. Med. Chem.* **1989**, *32*, 1043.

(71) Hoffmann, K., Finn, F. M., Kiso, Y. *J. Am. Chem. Soc.* **1978**, *100*, 3585.

(72) Rai, R., Katzenellenbogen, J. A. *J. Med. Chem.* **1992**, *35*, 4150.

(73) Isnin, R., Kaifer, A. E. *J. Am. Chem. Soc.* **1991**, *113*, 8188.

(74) Buston, J. E. H., Young, J. R., Anderson, H. L. *Chem. Commun.* **2000**, 905.

(75) Park, J. W., Song, H. J. *Org. Lett.* **2004**, *6*, 4869.

(76) Lambert, J. B., Shurvell, H. F., Lightner, D. A., Cooks, R. G. *Organic Structural Spectroscopy*; Prentice Hall: Upper Saddle River, New Jersey, 1998.

(77) Schneider, H.-J., Hacket, F., Rudiger, V. *Chem. Rev.* **1998**, *98*, 1755.

(78) Ashton, P. R., Ballardini, R., Balzani, V., Baxter, I., Credi, A., Fyfe, M. C. T., Gandolfi, T., Gomez-Lopez, M., Martinez-Diaz, M-V., Piersanti, A., Spencer, N., Stoddart, J. F., Venturi, M., White, A. J. P., Williams, D. J. *J. Am. Chem. Soc.* **1998**, *120*, 11932.

(79) Maran, F., Severin, M. G., Vianello, E. *Tetrahedron Lett.* **1990**, *31*, 7523.

(80) Cieslinski, M. M. Ph.D Thesis, The Australian National University, 2005.

(81) Huisgen, R. *Angew. Chem. Int. Ed. Engl.* **1963**, *2*, 565.

(82) Clayden, J., Greeves, N., Warren, S., Wothers, P. *Organic Chemistry*; Oxford University Press, 2001.

(83) Grundmann, C., Dean, J. *Angew. Chem. Int. Ed. Engl.* **1964**, *3*, 585.

(84) Liu, K.-C., Shelton, B. R., Howe, R. K. *J. Org. Chem.* **1980**, *45*, 3916.

(85) Meyer, A. G., Easton, C. J., Lincoln, S. F., Simpson, G. W. *Chem. Commun.* **1997**, 1517.

(86) Meyer, A. G., Easton, C. J., Lincoln, S. F., Simpson, G. W. *J. Org. Chem.* **1998**, *63*, 9069.

(87) Coulston, R. Honours Thesis, The Australian National University, 2005.

(88) Hummel, J. P., Dreyer, W. J. *Biochim. Biophys. Acta* **1962**, *63*, 530.

(89) Croft, A. K., Easton, C. J., Lincoln, S. F., May, B. L., Papageorgiou, J. *Aust. J. Chem.* **1997**, *50*, 857.

(90) Scatchard, G., Ann, N. Y. *Acad. Sci.* **1949**, *51*, 660.

(91) Matsui, Y., Mochida, K. *Bull. Chem. Soc. Jpn.* **1978**, *51*, 673.

(92) Hersey, A., Robinson, B. H. *J. Chem. Soc. Faraday Trans. 1* **1984**, *80*, 2039.

(93) Buvari, A., Barcza, L. *J. Incl. Phenom. Mol. Recog. Chem.* **1989**, *7*, 313.

(94) Abu-Shamleh, H. M. M. Sc. Thesis, Yarmouk University, 1990.

(95) Tawarah, K. M., Wazwaz, A. A. *J. Chem. Soc. Faraday Trans.* **1993**, *89*, 1729.

(96) Kunitake, M., Kotoo, K., Manabe, O., Muramatsu, T., Nakashima, N. *Chem. Lett.* **1993**, 1033.